# THE EFFECTS AND CAUSES OF OXIDATIVE AGING OF COMPACTED ASPHALT MIXTURES

WEN YONG

Ph.D

The Hong Kong Polytechnic University

2018

The Hong Kong Polytechnic University

Department of Civil and Environmental Engineering

# The Effects and Causes of Oxidative Aging of Compacted Asphalt Mixtures

WEN Yong

A Thesis Submitted in Partial Fulfilment of the Requirements for

the Degree of Doctor of Philosophy

September 2017

# CERTIFICATE OF ORIGINALITY

I hereby declare that this thesis is my own work and that, to the best of my knowledge and belief, it reproduces no material previously published or written, nor material that has been accepted for the award of any other degree or diploma, except where due acknowledgement has been made in the text.

_______________ (Sign)

WEN Yong (Name of student)

# ABSTRACT

Asphalt mixture is a widely used material for the construction of road, airfield, and parking lot pavements. Asphalt binder in asphalt mixture is subjected to oxidative aging, which causes asphalt to become stiffer and more brittle and leads to higher asphalt stress that makes the pavement more susceptible to cracking under a given deformation. Existing studies mainly focus on the aging-related issues of asphalt binder *per se.* It remains unclear how asphalt binder aging drives the mechanical property changes of asphalt mixtures and what factors affect asphalt binder aging in asphalt mixtures.

The overall goal of this research is to (1) quantify the relationships between the aging-induced chemical and physical changes of recovered asphalt binder and the property changes of compacted asphalt mixture, and (2) identify the key factors that affect the aging of asphalt binder in asphalt mixtures. The overall research goal consists of four specific objectives: (1) Development of a new method to simulate the long-term aging for compacted asphalt mixtures, (2) Quantification of the relationship between the aging of asphalt binders and asphalt mixtures, (3) Determination of the oxygen transport efficiency and possible oxygen consumption of asphalt mixtures, and (4) Identification of critical factors that affect the aging susceptibility of asphalt binders in compacted asphalt mixtures.

To achieve the research objectives, two new pieces of equipment were developed. One piece of equipment was developed to more realistically simulate the long-term aging of compacted asphalt mixtures. The newly developed equipment was subsequently used to age a variety of compacted asphalt mixture types. The dynamic modulus values of compacted asphalt mixtures at different aging states were tested. Based on the results, the quantitative relationship between the rheological properties of asphalt binder and the dynamic modulus of compacted asphalt mixtures were examined. The other new piece of equipment was developed to measure the oxygen diffusion and consumption coefficients of compacted asphalt mixtures, along with test procedures for making the measurements. The methods to calculate the oxygen diffusion and consumption coefficients of compacted asphalt mixtures were also assessed. The relationship between oxygen diffusion coefficients and mixtures' volumetric parameters were examined.

The following major findings are made through this research. (1) The newly developed aging method can efficiently simulate the long-term aging of compacted asphalt mixtures without impairing the integrity of the mixtures during the aging process. (2) The dynamic modulus values of compacted asphalt mixtures are well related to the aging states of asphalt binders. (3) The accuracy and robustness of six models for predicting the dynamic modulus of compacted asphalt mixtures vary with mixture types and aging states, and the Improved Hirsch's Model has higher accuracy and robustness in predicting the dynamic modulus of compacted asphalt mixtures for different asphalt mixture types. (4) It is feasible to use the developed apparatus and test procedure to measure the oxygen diffusion coefficients of compacted asphalt mixtures. Additionally, oxygen consumption can be neglected at room temperature. (5) Oxygen diffusion coefficients of compacted asphalt mixtures vary greatly and are affected by the volumetric characteristics of the compacted asphalt mixtures. (6) The oxygen diffusion coefficient provides a good indication of the aging susceptibility of compacted asphalt mixtures.

It is believed that this study contributes to the body of knowledge in pavement

engineering by having developed new methods and gained new insights into compacted asphalt mixture aging. The findings will also have significant implications for pavement engineering practices.

# ACKNOWLEDGMENTS

I would like to express heartfelt gratitude to my supervisor Dr. Yuhong Wang for his valuable guidance, continuous support, and encouragement throughout the past years. I am so fortunate to have such a kind and knowledgeable supervisor, who has been wholeheartedly committed to guiding my Ph.D. study. Under his supervision, my academic competence and critical and logical thinking skills have been greatly improved.

I am very grateful to Shenzhen Water Engineering Testing Co., Ltd for providing a place for storing the aging equipment. I would also like to express my gratitude to Mr. Junwei Xie for helping me communicate with the manufacturer. Meanwhile, I am also indebted to Dr. L.W., Cheung, and Mr. C.K., Chau for providing the experimental materials that were used in my experiments. Special thanks to two senior technicians, C.F., Cheung and Y.M. Harry, Lai in the mechanic workshop of the Department of Civil and Environmental Engineering at the Hong Kong Polytechnic University. They helped me manufacture the diffusion apparatus according to the design. I also want to express my thanks to three laboratory technicians, Mr. W.K Wong, Mr. M.C Choi, and Mr. W.L. Wong, for their technical support. Whenever I encountered problems in laboratory work, they would kindly help me solve the problems.

Thanks to my friends and colleagues for supporting and encouraging me in the past several years. Special thanks to Dr. Dan Chong, Dr. Bing Zhang, Ms. Ling Chen, Mr. Kecheng Zhao, Mr. Shicong Mo, Ms. Mengqi Xiao, and Mr. Kinming Chan. They made my Ph.D. study more colorful and enjoyable.

Lastly, but most importantly, I owe my deepest gratitude to my parents for their support

and love. All my gratitude goes to my wife, Danli Li, for her love, company, and support throughout the entire process.

# TABLE OF CONTENTS

## CHAPTER 4. THE COMPARISON OF ACCELERATED AGING TREATMENT METHODS TO SIMULATE THE LONG-TERM AGING OF COMPACTED ASPHALT MIXTURE ................................................ 55

## CHAPTER 5. THE RELATIONSHIP BETWEEN THE RHEOLOGICAL AND CHEMICAL PROPERTIES OF RECOVERED ASPHALT.............. 73

## CHAPTER 6. EFFECT OF OXIDATIVE AGING ON THE DYNAMIC MODULUS OF COMPACTED ASPHALT MIXTURE........................................... 89

# LIST OF FIGURES

## LIST OF TABLES

# CHAPTER 1. INTRODUCTION

## 1.1 **Background**

Asphalt was first used as a road building material in Babylon circa 615 BCE [1]. To date, the Asphalt Institute and Eurobitume estimate that the total global production of asphalt is 87 million tons per year, and approximately 85% of the production is used in various asphalt pavement constructions [2]. This can be attributed to the advantageous properties of asphalt pavements, such as lower construction cost, smoother surface, greater durability, and quieter driving conditions. By 2007, Europe had paved 3.2 million km of asphalt pavement, accounting for approximately 90% of roads in the entire road network [3]. In Hong Kong, of the over 2,100 km of road, approximately three-quarters had been paved with asphalt pavement materials by 2016 [4].

However, asphalt as an organic material is subjected to oxidative aging that causes asphalt to become stiffer and more brittle, leading to higher stresses in asphalt binder and making asphalt pavement more susceptible to cracking under a given deformation [5, 6]. The main long-term aging mechanism of asphalt binders in pavements is oxidative aging. Researchers have studied asphalt oxidative aging for nearly one hundred years [7]. These studies have been conducted from the following aspects:

(1) Developing methods to simulate asphalt binder aging in the laboratory to aging state in the field as closely as possible.

(2) Evaluating the effect of aging on the chemical and mechanical properties of asphalt binders.

(3) Predicting the distribution of aging state of asphalt binders as a function of time and

depth in field pavement as accurately as possible.

There are numerous aging methods to simulate the oxidative aging of asphalt binders, loose asphalt mixtures, compacted asphalt mixtures in the laboratory [7]. These methods often adopt a high temperature and/or a high pressure to accelerate the aging process. For example, the current standardized long-term aging methods are to place asphalt binder in a pressure aging vessel at 90°C, 100°C or 110°C for 20 hours or to place a compacted asphalt mixture in an oven at 85°C for five days. Moreover, existing studies have mainly focused on the aging-related issues of asphalt binder *per se.* A comprehensive literature review by Glover et al. [8, 9] suggests that research considering oxygen transport into hot-mix asphalt (HMA) mixture and asphalt binder in the mixture is “practically nonexistent.” This finding is echoed by another comprehensive review by Petersen [10], who believes that “The pragmatic importance of differential oxidative age hardening as a function of pavement depth to pavement service life, … is self-evident.” and more understanding is demanded in this critical area.

Existing studies on the aging of compacted asphalt mixtures are mainly based on experiences gained from the field. Early studies suggest that the oxidative aging of asphalt binders in field pavement primarily occurs at the pavement surface (less than 40 mm from the surface) [11, 12]. This finding has a significant influence on pavement research and practices and has been incorporated in the global aging model for the Mechanistic-Empirical Pavement Design Guide (MEPDG) [8]. However, more recent studies in Texas, USA, suggest that asphalt aging may penetrate into deeper HMA pavement layers [13]. Using binder test data obtained at various times from a heavily trafficked 36-year-old HMA pavement, a study in Hong Kong examined the evolution of asphalt binder aging as well as variations in aging severity with pavement depth. The study also found that asphalt binders in deeper pavements also became severely aged.

The aging susceptibility of asphalt binder in asphalt pavement is essentially governed by pavement temperature and oxygen concentration in the pavement [14]. One easily conceivable approach to assessing the aging susceptibility of a compacted asphalt mixture is to examine its total air void content [8]. Although the total air void content provides some indication of the oxygen accessibility of asphalt binder, it does not provide information on the connectivity of the air voids. After all, oxygen diffuses much more slowly through asphalt binder and aggregate than through interconnected air void channels. Recently, a research team led by Glover [8] made several investigations on this issue. For instance, an oxygen transport and reaction model for asphalt mixtures was developed, in which oxygen was modeled to be transported through air void channels and diffused into asphalt shells, and the average air void size and distance between adjacent pores were used to predict binder oxidation. Although the existing studies on oxygen transport and diffusion at the microscopic level have helped to gain insights into asphalt binder aging in asphalt mixtures, these studies have relied on X-ray computed tomography (CT) images to examine air void characteristics and consequently have several limitations. First, the resolution of CT images is usually inadequate to detect small air voids and air void channels. Second, computer programs for accurately calculating air void content and connectivity need to be improved. Third, many pavement practitioners lack access to a CT facility. Therefore, this technology cannot be used to assess the aging susceptibility of compacted asphalt mixtures. In addition, other existing studies have mainly focused on the determination of oxygen diffusion and reaction coefficients based on asphalt binder aging in the laboratory.

## 1.2 **Problem statement**

To accelerate compacted asphalt mixture aging in the laboratory, high temperatures and/or high pressures are frequently used in ongoing studies. However, there are two major limitations of these aging methods. First, many researchers did not take the drain-down of asphalt binder into account during the development of the aging method for compacted asphalt mixtures; drain-down may occur at temperatures higher than the softening point of an asphalt binder [15]. Hence, it is necessary to develop an aging method that simulates the actual aging process as closely as possible based on the above considerations. Second, the accelerated aging methods at high temperatures are inconsistent with the actual aging process that occurs in the field as the aging mechanism of asphalt binder at high temperatures is different with that at low temperatures [10, 16]. Moreover, very limited studies have been conducted to examine the effect of oxidative binder aging at low temperatures on the mechanical property changes of asphalt mixtures. It remains unclear how asphalt binder aging realistically drives the mechanical property changes of asphalt mixtures.

Previous studies utilized various indexes to characterize the aging susceptibility of asphalt binder in asphalt pavement [17-19]. However, two critical parameters, oxygen diffusion and reaction coefficients in asphalt pavement, were not taken into account. These parameters represent how fast oxygen diffuses into asphalt pavement and how much oxygen is consumed during the diffusion process. To my best knowledge, no published study has been made to determine the oxygen diffusion and consumption coefficients of compacted asphalt mixtures.

## 1.3 **Objectives**

The objectives of this study are as follows:

(1) Development of a new method to simulate the long-term aging of compacted asphalt mixtures.

(2) Quantification of the relationship between aging of asphalt binder and asphalt mixture.

(3) Determination of the oxygen diffusion and possible consumption coefficients of compacted asphalt mixtures.

(4) Identification of key factors that affect the aging susceptibility of asphalt binder in the compacted asphalt mixtures.

## 1.4 **Outline of the Dissertation**

This dissertation consists of eight chapters. In Chapter 1, a general background is presented followed by a description of the current limitations of oxidative aging of asphalt and then main objectives. Chapter 2 presents a literature review on the aging mechanisms of asphalt binder and asphalt mixture, artificial aging methods, aging indicators, and oxidation models. Chapter 3 describes research methodologies and experimental methods. Chapter 4 compares four different aging protocols by using an oven and a customized autoclave and then determines a new long-term aging method for compacted asphalt mixtures. Chapter 5 validates a new micro-extraction and recovery method for extracting and recovering asphalt binder from microcores; and then investigates the relationship between rheological and chemical properties of recovered asphalt binder. Chapter 6 discusses the effect of the oxidative aging on the dynamic modulus of compacted asphalt mixtures. This chapter also evaluates the effect of the oxidative aging on the accuracy and robustness of six predictive models for dynamic modulus of compacted asphalt mixtures. In Chapter 7, oxygen diffusion coefficients of compacted asphalt mixtures are determined based on the oxygen concentrations changes with time, measured by using a customized diffusion apparatus. The predictive model of oxygen diffusion coefficient for compacted asphalt mixture is then developed. Finally, Chapter 8 summarizes the major conclusions of this dissertation and provides some recommendations.

# CHAPTER 2. LITERATURE REVIEW

## 2.1 **Asphalt binder aging**

### 2.1.1 Aging mechanism of asphalt binder

Asphalt is subjected to oxidative aging that causes asphalt to become stiffer and more brittle, leading to higher stresses in the asphalt binder and making asphalt pavement more susceptible to cracking under a given deformation[5, 6]. Asphalt aging has been studied for nearly one hundred years by researchers [7]; it is one of the major research fields in pavement engineering. The aging mechanisms of asphalt binder can be classified into four types [20]：

a. Oxidation；

b. Evaporation of volatiles；

c. Exudative evaporation；

d. Steric or physical hardening.

*Oxidation*

Johansson [21] states that oxidation is the most probable cause of asphalt aging, and is an irreversible chemical reaction between the components of asphalt and atmospheric oxygen. The reaction results in the changes of oxygen-containing functional groups in asphalt, such as sulfoxide (oxidation of sulfide), carboxylic acid, ketone, and dicarboxylic anhydride [22-25].

Corbett and Mertz investigated a road in Michigan after 18 years of service, concluding that oxidation had an influence on the weight variation of aromatic, resin, and asphaltene and had no significant loss of the saturate fraction [26]. Farcas further found that aromatic fractions decrease, first becoming resins and then asphaltene [27]. This process is due to oxygen functional groups forming in the asphalt molecules, resulting in the decrease in resins and aromatic fractions and increase in asphaltene fractions [28-31].

*Evaporation of volatiles*

Volatile components in asphalt evaporate during the processes of mixing, transport, and paving [32]. Zupanic and Baselice reported three main sources of asphalt volatility [33]:

(1) Existing molecules in asphalt,

(2) Newly synthesized molecules through reaction between oxygen and existing molecules in asphalt,

(3) Newly generated molecules through thermal cracking of existing molecules

During the production, storage, transport, and paving procedures, asphalt is exposed to high temperature at which light asphalt fractions begin to evaporate quickly. More specifically, when asphalt contacts with aggregate at or above 150℃ , aromatic fractions rapidly evaporate, while the weight of asphaltenes can increase by 1-4% [27]. This is the reason why fume and steam are observed during these stages. In addition， the evaporation causes the loss of the light components in asphalt that, in turn, increases the viscosity of the asphalt binder and makes it stiffer. It was found that the asphalt viscosity would be increased by 150-400% during these procedures [34, 35].

*Exudative evaporation*

Exudative evaporation is also an irreversible process that oily components in asphalt exude into mineral aggregates, resulting in the hardening of asphalt binder [36, 37]. Although exudative evaporation is not a major contributor to asphalt hardening, it also results in the compositional changes of asphalt and affects the asphalt properties [38].

*Steric or physical hardening*

Steric hardening, also called physical hardening, is a reversible process [21]. Steric hardening leads to the increases in viscosity and slight volume contraction due to the slow crystallization of waxes in asphaltene fractions at room temperature [28]. The viscosity of asphalt binder returns to its original value as storage temperature increases to 70°C [39].

### 2.1.2 Factors affecting asphalt aging

Asphalt binder aging has been widely studied for many years. Traxler (1963) summarized 15 different factors that affect asphalt aging, as listed in Table 2.1. It shows that asphalt aging is highly dependent on temperature, time, oxygen concentration and sunlight.

Table 2.1 Factors affecting asphalt aging [30]

| | Influenced by | | | | | Occurring | |
|---|---|---|---|---|---|---|---|
| | Time | Heat | oxygen | sunlight | Beta and rays | At the surface | In the mixture |
| Oxidation (in dark) | √ | √ | √ | | | √ | |
| Photo-oxidation (direct light) | √ | √ | √ | √ | | √ | |
| Volatilisation | √ | √ | | | | √ | √ |
| Photo-oxidation (reflected light) | √ | √ | √ | √ | | √ | |
| Photochemical (direct light) | √ | √ | | √ | | √ | |
| Photochemical (reflected light) | √ | √ | | √ | | √ | √ |
| Polymerization | √ | √ | | | | √ | √ |
| Steric or physical | √ | √ | | | | √ | √ |
| Exudation of oils | √ | √ | | | | √ | |
| Changes in nuclear energy | √ | √ | | | √ | √ | √ |
| Action by water | √ | √ | √ | √ | | √ | |
| Absorption by solid | √ | √ | | | | √ | √ |
| Absorption of components at a solid surface | √ | √ | | | | √ | |
| Chemical reactions | √ | √ | | | | √ | √ |

|  | Influenced by |  |  |  |  | Occurring |  |
|---|---|---|---|---|---|---|---|
|  | Time | Heat | oxygen | sunlight | Beta and rays | At the surface | In the mixture |
| Microbiological deterioration | √ | √ | √ |  |  | √ | √ |

### 2.1.3 Effect of aging on chemical composition changes of asphalt binder

Two approaches are usually used to describe the chemical composition changes of asphalt binder:

1) Multiple-phase system (traditional approach)

This approach is explained by using four functional groups (saturates, aromatics, resins, and asphaltenes). The asphalt is defined as a semi-solid phase in which asphaltenes are covered by a protective layer of resin dispersing in a liquid phase consisting of aromatics and saturates [6]. The schematic diagram of asphalt is shown in Figure 2.1. During the oxidative aging process, non-polar fractions decrease and form polar fractions followed by asphaltenes; while saturates are considered to be essentially unchanged due to its low chemical reactivity, as shown in Figure 2.2 [30, 31, 40]. Siddiqui and Ali further found that the formation rate of asphaltene was linear with increasing aging time, and the asphaltene contents increased by 6-7% in 340 minutes at 163°C. This pattern was also observed with the asphalt extracted and recovered from an field pavement which had serviced for 90 months under southern French climate [41].

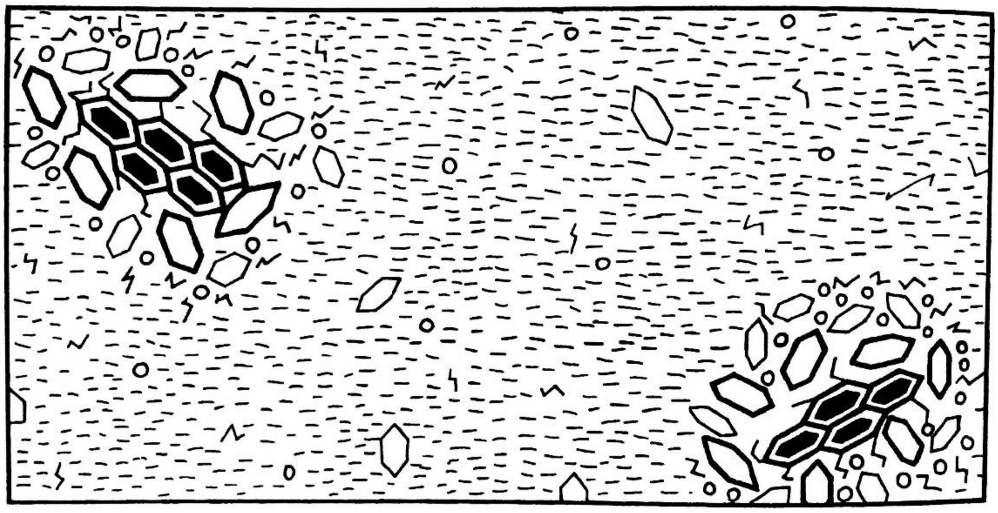

(a) Sol-type

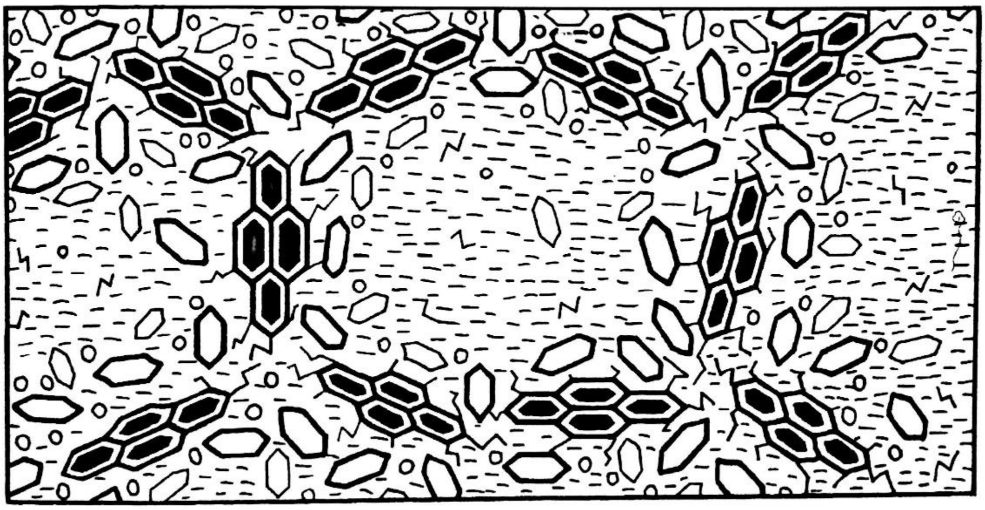

(b) Gel-type

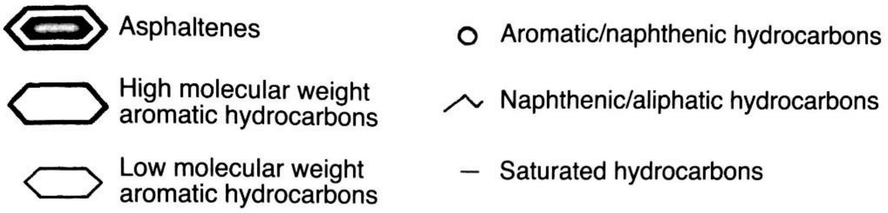

Figure 2.1 Schematic representation of (a) sol-type asphalt; and (b) gel-type asphalt [42]

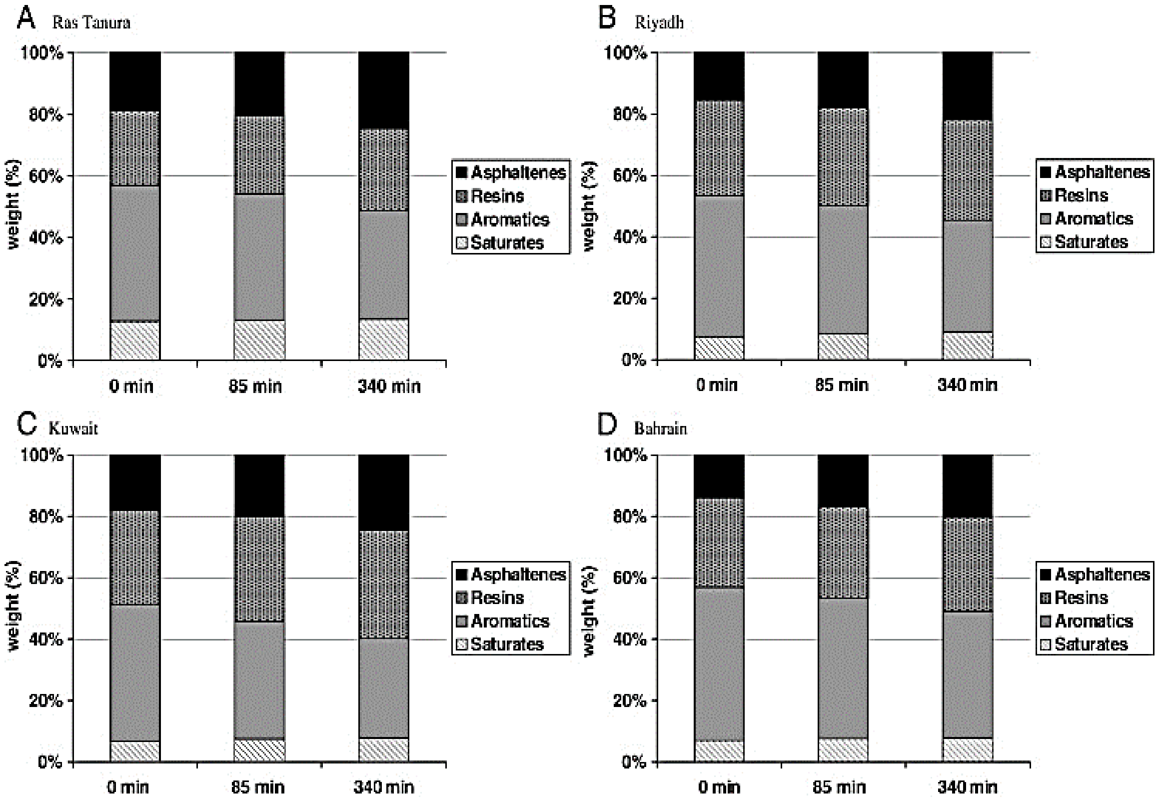

Figure 2.2 SARA fractions for various asphalt before and after RTFOT aging for 85 min and 340 min [31]

2) Single-phase system (SHRP approach)

In SHRP A-367 report, asphalt is defined to be a continuous and homogeneous material consisting of organic molecules that are composed primarily of carbon and hydrogen. In addition, the majority of molecules contain one or more heteroatoms, such as nitrogen, sulfur, oxygen, and a trace amount of metal (e.g., vanadium, and nickel) [22]. During the oxidative aging process, molecules in asphalt binder react with oxygen and form carbonyl species, which further form larger and more complex molecules.

Since the 1960s, many studies have been conducted to identify and characterize polar and heteroatom-containing functional groups related to oxidation [23-25, 43, 44]. Two general conclusions of these studies are that ketone and sulfoxide are two major oxidation products, and anhydrides and carboxylic acids are also discovered but in small amounts, as shown in Figure 2.3 and Table 2.2.

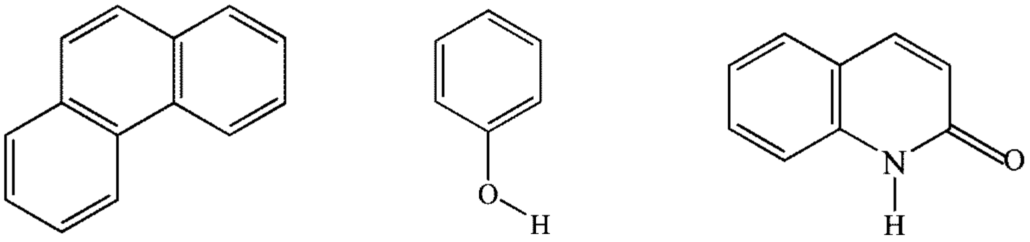

Polynuclear aromatic (1) Phenolic (1) 2-quinolone type (1)

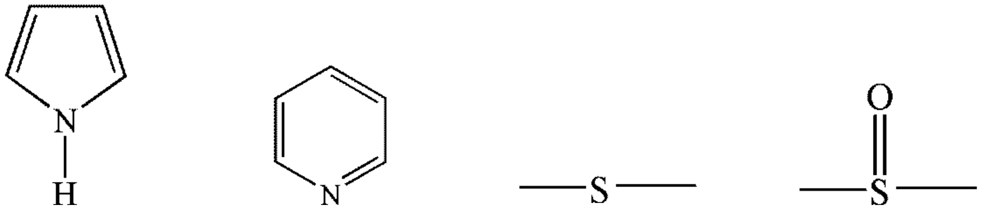

Pyrrolic (1) Pyridinic (1) Sulfide (1) sulfoxide (2)

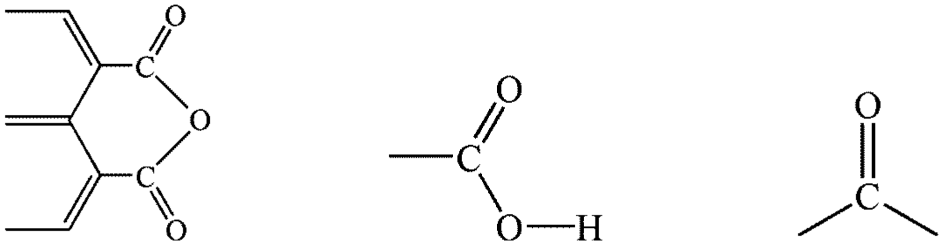

Anhydride (2) Carboxylic acid (1,2) Ketone (2)

***Note: (1) Naturally occurring; (2) Formed on oxidative aging***

Figure 2.3 Chemical functional groups in asphalt molecules initially present or formed on oxidative aging [45]

Table 2.2 Chemical functional groups formed in asphalt during oxidative aging [45]

| Type of asphalt | Source of asphalt | Concentration (mol/L) | | | | Average hardening index[2] |
|---|---|---|---|---|---|---|
| | | Ketones | Anhydrides[1] | Carboxylic acids | Sulfoxides | |
| B-2959 | Mexican | 0.50 | 0.014 | 0.008 | 0.30 | 38.0 |
| B-3036 | Arkansas Louisiana | 0.55 | 0.015 | 0.005 | 0.29 | 27.0 |
| B-3051 | Bosan | 0.58 | 0.020 | 0.009 | 0.29 | 132.0 |
| B-3602 | California | 0.77 | 0.043 | 0.005 | 0.18 | 30.0 |

***Note: [1]Naturally occurring acids have been subtracted from report value.***

***[2]Ration of viscosity after oxidative aging to viscosity before oxidative aging.***

Peterson (1998) simulated asphalt binder aging at 130℃ in the laboratory and found that the chemical composition of asphalt increased as aging time increased, as shown in Figure 2.4. Note that ketones and sulfoxides rapidly formed during the initial stage of oxidation. However, formation rates of ketones and sulfoxides became slower over aging time, especially for sulfoxides. This trend is highly consistent with Branthaver's findings [22].

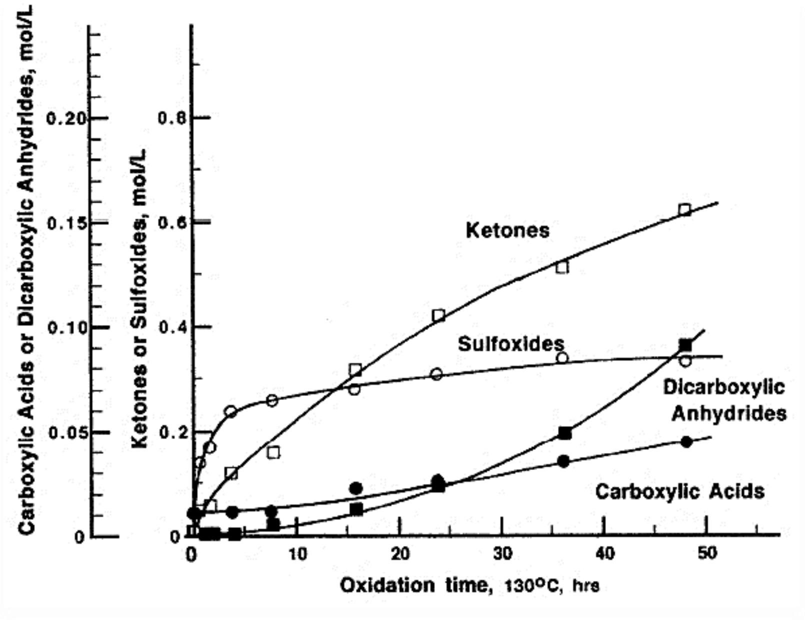

Figure 2.4 Oxidation products vs. oxidation time for Boscan asphalt at 130℃ [46]

As previously stated, ketones and sulfoxides are two major oxidation products. Therefore, formation mechanisms of ketones and sulfoxides were investigated by Petersen's team [47, 48] and Mill and Tse [43]

For the formation mechanism of ketones, Deorrence *et al.* (1974) provided strong evidence that the ketone is generated at the benzylic carbon position (the first carbon of an alkyl chain attached to an aromatic ring). More precisely, the lone hydrogen attached to the carbon adjacent to the aromatic ring on the tertiary benzylic carbon is very reactive and is easily removed during the oxidation process. Mill and Tse (1990) further found that a majority of benzylic hydrogen belong to tertiary (methine) types. The carbon-hydrogen bond in the tertiary (methine) types is orders of magnitude more reactive than unbranched aliphatic hydrocarbons.

For the formation of sulfoxides, Peterson *et al.* (1981) found that sulfoxides result from the oxidation of organic sulfide on many asphalt molecules. More specifically, the sulfide forms sulfoxides by the reaction with hydroperoxide intermediates from the oxidation of asphalt hydrocarbons. Although sulfoxides are rapidly formed during the oxidation process, it is thermally unstable [5]. Moreover, sulfoxides content depends on not only the initial sulfur content in asphalt but also the oxygen diffusion rate in the asphalt [5].

### 2.1.4 Effect of aging on physical properties of asphalt binder

As mentioned in the previous section, aging leads to the decrease in aromatic content and subsequently increase in resin and asphaltene contents. Furthermore, asphaltene content has a significant effect on the physical property change of asphalt. The higher asphaltene content is, the harder and more viscous the asphalt is. It represents a lower penetration, higher softening point, lower ductility, higher viscosity, and, usually, higher penetration index (*PI)* [29]. These phenomena are caused by that oxygen reacts with asphalt molecules, subsequently forming carbonyl compounds, which further lead to the larger and more complex molecules that would make asphalt to be harder and less flexible [29]. In other words, the tendency that asphalt becomes harden is caused by the multiple impacts including polymerization, volatilization, photochemical action, oxidation, and photo-oxidation [30].

Ishai (1996) investigated the effect of aging temperature on the penetration values of asphalt by using thin film oven test (TFOT), as indicated in Figure 2.5. Note that the penetration values rapidly decreased as aging time increased, especially in the initial stage of the aging process. The similar tendency was found by Francken [49]. In SHRP program, eight asphalts were adapted to simulate oxidative aging in the pressure vessel at 2.07 MPa [22]. The dynamic shear viscosity was measured at 60℃ as a function of aging time, as shown in Figure 2.6. It is apparent that dynamic shear viscosity rapidly increased in the first 50 hours and then increased at a nearly constant rate. Moreover, the trend of dynamic shear viscosity in the long-term aging stage is quite similar for eight types of asphalt.

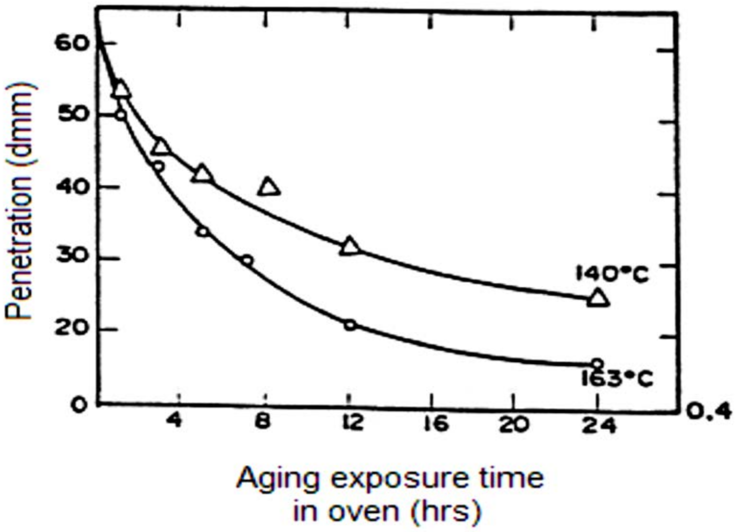

Figure 2.5 Penetration value vs. aging time [41]

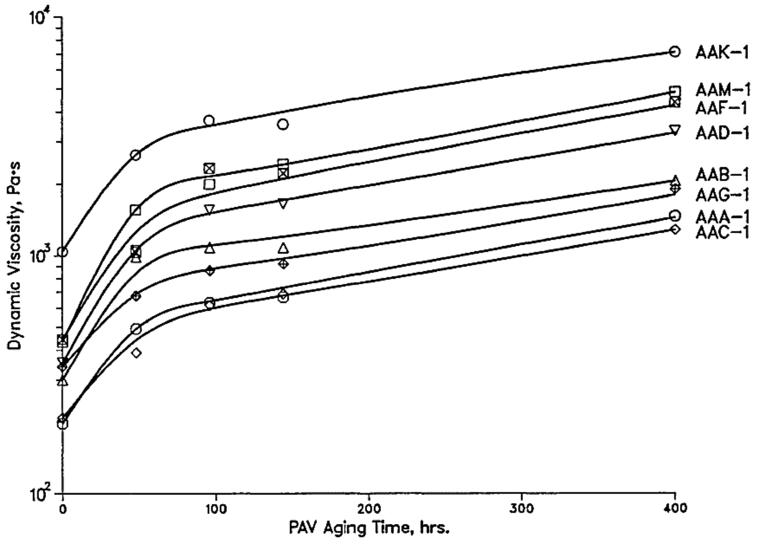

Figure 2.6 The relationship between dynamic viscosity at 60℃ and Pair void aging time [22]

### 2.1.5 Summary

During the processes of storage, mixing, transport, and paving, asphalt binder is exposed to high temperatures. As a result, asphalt binder rapidly oxidizes. In service, asphalt binder is further aged due to the acceleration of oxygen, pavement temperature, and UV light, while oily components in asphalt binder exude into aggregate.

The mechanism of asphalt aging can be briefly summarized that several molecular groups in asphalt binder react with oxygen at high temperatures, atmospheric oxygen, high pressures, and UV light, and chemical compositions in asphalt are changed during the reaction process. More specifically, asphalt binder aging results in decreasing in aromatic content and subsequently increasing in resin content, and finally rising in asphaltene content. These changes further lead to a harder asphalt binder, which shows a lower penetration, higher softening point, lower ductility, higher viscosity, and, usually, higher *PI.*

## 2.2 **Aging of asphalt mixture in asphalt pavement**

### 2.2.1 Oxidation of asphalt pavement

The aging process of asphalt mixture can be divided into two stages: short- and long-term aging.

(1) Short-term aging

Short-term aging mainly occurs during the stages of mixing, transport, and paving due to high temperatures. In these stages, the asphalt is rapidly aged, especially in the mixing stage. When hot asphalt binder blends with hotter aggregates and then coats on the surface of aggregates with a thin film (usually 5-15 μm), the lightweight fractions volatile (evaporation), and some oil components exude into the aggregate (exudative hardening), while some functional groups in asphalt react with oxygen. Similarly, these processes continue at a slower rate during the storage, transport, and paving stages.

(2) Long-term aging

Long-term aging mainly occurs in the service life of asphalt pavement although the aging rate is slower compared with short-term aging. External air supplies enough fresh oxygen for the oxidative aging of asphalt binder. UV radiation raises energy levels which result in carbon-carbon chains breaking and reacting with oxygen [29]. When cracks and interconnected air paths appear in asphalt pavement, air can penetrate into a deeper pavement layer and causes oxidative aging of asphalt binder in the deeper layer of asphalt pavement. Also, it is believed that the upper 10 μm of asphalt binder below the exposed surface, which results in the photo-oxidation and the formation of the skin with 4-5 μm thick on the surface of asphalt binder [29]. The skin can hinder oxygen from penetrating into a deeper layer of asphalt binder, but the oxidative material is soluble in rainwater and can be washed away with rainwater, leading to the exposure of fresh asphalt [50].

### 2.2.2 Factors affecting asphalt aging in asphalt mixture

During the mixing, transport, and paving processes, asphalt binder is subject to high temperatures for a relatively short time and is then aged at relatively low temperatures for a longer period. In these stages, asphalt rapidly oxidizes to a certain extent, and the aging rate of asphalt binder in field pavement is highly dependent on pavement temperature [29]. In service, air void content, pavement service life, and film thickness of asphalt binder also affect the rate and degree of asphalt aging [42, 51, 52]. Besides these factors, pavement depth, nature of aggregate, filler, and aggregate gradation also have a direct influence on asphalt aging [51, 53-55]. These factors are detailed as follows:

1. Pavement temperature

As previously mentioned, asphalt binder is exposed to high temperatures during mixing, transport and paving stages. The existing studies reported that penetration values of asphalt binder decreased by 30% during the mixing process [42]. Whiteoak and Fordyce [56] also found that oxidative aging of asphalt binder was a function of temperature, as shown in Figure 2.7. In service, aging rate of asphalt binder is also highly dependent on temperature profile within the pavement [29]. This influence can be divided into two different types. On the one hand, high pavement temperatures in summer accelerate oxidative aging of asphalt binder in the pavement. On the other hand, the oxidative rate might significantly slow down due to the immobilization of reactive components in asphalt at low temperatures, and this phenomenon was found and proven by Coons and Wright. It is because that most of reactive components containing in polar aromatic fractions reduce due to the oxidation, resulting in inactivation of the polar aromatic fractions. At lower oxidation temperatures (about 60°C or less), oxidation tends to quench; and oxidation nearly ceases when temperatures are lower than the quenching level [10].

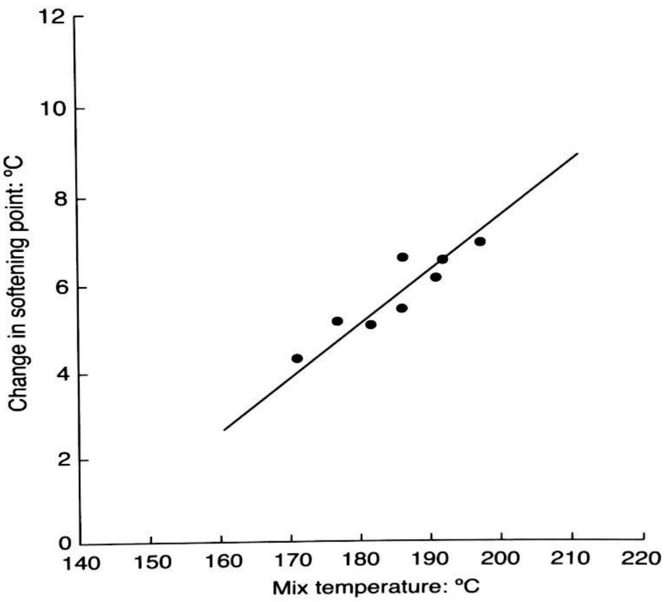

Figure 2.7 Effect of mixing temperature on softening point [56]

2. Pavement service life

The asphalt binder rapidly oxidizes and hardens during mixing and paving processes followed by being aged at a slow rate in service life. Coons and Wright [55] extracted and recovered asphalt binders after being serviced for various periods from four months to 13 years, and measured viscosities of the asphalt binders at 25°C (see Figure 2.8). It is apparent from the figure that relative viscosities increased as the service time increased. Similarly, Lubbers (1985) continually tracked and surveyed the changes of penetration, softening point, and PI over service life, as shown in Figure 2.9. Note that penetration values of the asphalt binders rapidly dropped to 25 dmm after seven years of service while PI values of the binders at surface increased to above 3. As a result, a significant conclusion can be drawn that asphalt aging in pavement is also a function of pavement service life.

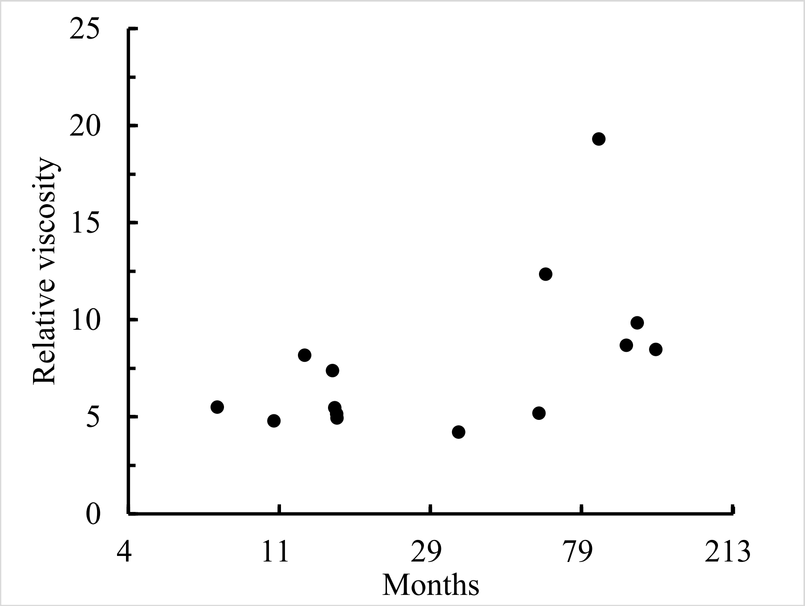

Figure 2.8 Relative viscosity versus service time

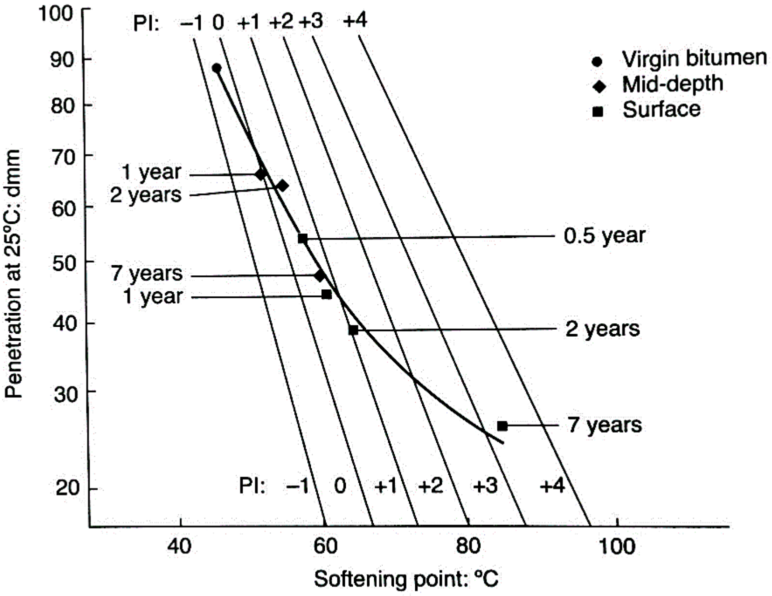

Figure 2.9 Hardening of asphalt at the surface and mid-depth of an asphalt pavement [52]

3. Film thickness of asphalt binder

The film thickness of asphalt binder also plays a crucial role in the oxidative aging of asphalt binder since oxidation is a chemical process as a function of oxygen diffusion rate [6]. Moreover, the thinner film thickness is believed to result in faster oxidative aging since oxygen is easier to penetrate into the thinner film and then react with asphalt in service, as shown in Figure 2.10 [57, 58]. Blokker and Doorn (1959) found that the oxidative aging at high temperatures only occurred in the 4 μm of depth below the surface of asphalt binder film [59]. Therefore, it was suggested that the minimum binder film thickness should be between 6 μm and 8μm for the sake of safety [60].

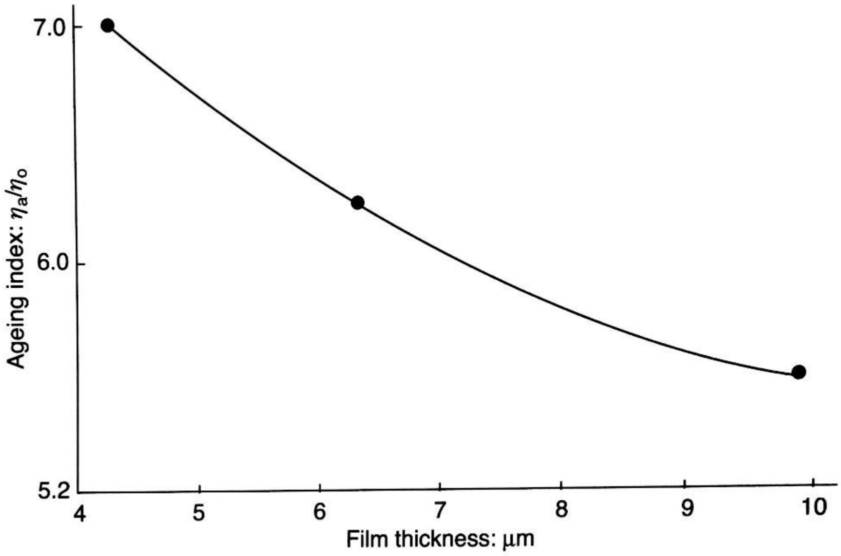

Figure 2.10 Effect of film thickness on the aging index [58]

4. Air void content

Air void content is considered to be the major factor affecting asphalt aging in field pavement [29]. It is evident that higher air void improves the probability that fresh air permeates into the deeper layer of asphalt pavement. The effect of air void content on asphalt binder oxidative aging in asphalt pavement was reported in 1970 [61]. There was the best correlation between air void content and the age hardening of asphalt binder in the pavement based on extensive data collected from 53 asphalt pavements after 11-13 years of service. It is evident from the data that the age hardening of the recovered binder increased by 13 times with increasing air void content from 4% to 10%. In 1985, Lubbers also found the similar trend by using the asphalt binder recovered from a 5-years-old asphalt pavement, as shown in Figure 2.11. Note that hardening of the asphalt binder rarely occurred when air void content was less than 5%. However, the penetration values of the asphalt binder rapidly decreased from 70 dmm to 25 dmm or less when air void contents were greater than 9%. Based on these previous studies, a conclusion can be drawn that the oxidative aging is also a function of air void content in the field.

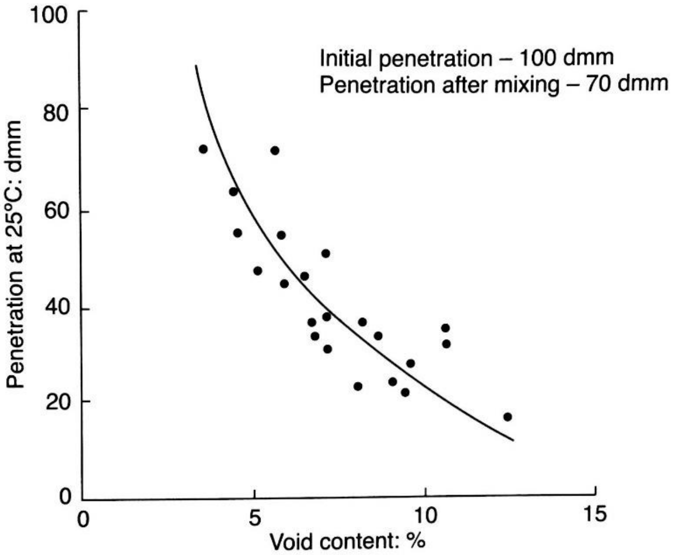

Figure 2.11 The effect of air void on the penetration (@ 25℃ ) of the binder on the road [52]

5. Pavement depth

It is intuitively apparent that the oxidative rate of asphalt binder on the surface of asphalt pavement is faster than that in the deeper layers. This is because that UV light and fresh air directly contact with asphalt binder on the surface and then accelerate the oxidation of the asphalt binder. For asphalt binder in deeper layers of asphalt pavement, fresh air is hard to permeate into a deeper layer, thereby the oxidative rate of asphalt binder in the deeper layer extremely is slow. However, there is a controversial issue on how deep oxidative aging could happen below the surface layer of asphalt pavement. Coons and Wright investigated the aging states of asphalt binders extracted and recovered from several asphalt pavements after various years of service and reported that asphalt binder aging happened in the top 3.75 cm of asphalt pavements. Besides, the aging state of asphalt binder did not change as service life increase [55]. Furthermore, this finding was adopted by latest MEPDG software [62]. However, some other studies revealed the different findings. These studies are summarized in Table 2.3. One possible reason for this phenomenon is that actual situation of the pavements is various each other. To be more specific, pavement loads in the past are not as heavy as today, or these pavement conditions are different from each other.

Table 2.3 The asphalt binder aging with depth of pavement and time in existing literature

| Aging Situation | Data source | Reference |
|---|---|---|
| Aging diminished within the top 2.5 to 3.9 cm of pavement surface | Material master database from various studies | [11] |
| Oxidation penetrated up to 1.5 cm below the surface layer | | [12] |
| Pavements oxidize at uniform rates with depth | Texas, U.S. | [13, 63] |
| Aging initially decreases with pavement depth but increases towards the pavement bottom | Texas and Minnesota, U.S. | [64] |
| Asphalt pavement oxidize at road base | Hong Kong | [14] |

6. Nature of mineral aggregate

The effect of the nature of mineral aggregate on the oxidative aging of asphalt binder can be classified into two types [53]. On the one hand, mineral aggregates promote the oxidation of saturates and naphthalene aromatics. On the other hand, mineral aggregates hinder mineral compositions to react with oxygen at the mineral surface since the mineral aggregates highly absorb the polar fractions in asphalt. The rates and levels of chemical reactions between aggregates and asphalt binders are various with the type of asphalt binder and surface charge of aggregate [6]. For example, quartzite presented the greatest catalytic influence in oxidative aging [65], while limestone had the smallest catalytic effect in oxidative aging [42, 53].

7. Filler

The filler is an extender of asphalt binder, which could greatly affect pavement performance [54]. The effect of filler on oxidation varies with its particle size, type, nature, and concentration in the mixture [66]. According to the study [67], filler also has a dual role in the oxidative aging: 1) To promote oxidative aging or side reaction (e.g., dehydration and polymerization); 2) To reduce oxidative aging by hindering the oxygen diffusion in asphalt binder. The specific response between filler and asphalt is dependent on the types and natures of filler and asphalt [66-68]. For example, Bianchetto et al. reported that the use of hydrated lime and calcium carbonate as fillers improved the aging resistance of asphalt binder [69].

### 2.2.3 Effect of asphalt binder aging on the properties of asphalt pavement

As previously discussed, oxidation leads to a significant increase in both viscous and elastic properties in service life [34, 70]. Oxidative aging causes asphalt binder stiffer and more brittle and further leads to pavement embrittlement and the reduction of performance and service life of asphalt pavement [5, 6]. During these periods, fatigue cracking and thermal cracking are two common failures [5, 34, 35]. To be more specific, Fatigue cracking is considered to be attributed to repeated traffic loading; oxidation also plays an important role. In addition, many previous studies also found that there was a positive correlation between ductility value of asphalt binder and cracking failure of asphalt pavement [71-76]. Moreover, some studies found that ductility values (@15.0℃ ) ranging from 2 cm to 3 cm could correspond to a critical level for age-related cracking in the field [72, 74, 75].

### 2.2.4 Summary

Asphalt binder aging in asphalt pavement can be divided into two categories, short- and long-term aging. Short-term aging mainly occurs during the stages of storage, mixing, transport, and paving. During these processes, asphalt binder rapidly oxidizes to a certain extent, especially in the mixing stage. Long-term aging mainly occurs in the service life of asphalt pavement although the aging rate is slower compared with that in short-term aging. It can be contributed to the fact that asphalt binder aging results in the skin formation on the surface of asphalt binder. This skin hinders oxygen from penetrating into a deeper layer of asphalt pavement. In service, air void content, pavement temperature, service life, and the film thickness of the asphalt play major roles in the rate and degree of asphalt aging. Besides these factors, pavement depth, nature of aggregate, filler, and aggregate gradation also influence asphalt binder aging in asphalt pavement. The asphalt binder aging in asphalt pavement also makes the binder stiffer and more brittle and further causes pavement embrittlement in asphalt pavement, resulting in the reduction of performance and service life.

## 2.3 **Aging indicators**

### 2.3.1 Aging indicators for asphalt binders

As previously stated, the oxidation influences the rheological and chemical properties of asphalt binders. Aging indicators are utilized to quantify the aging of asphalt binders over aging time. For the aging indicators of asphalt binders, they can be divided into two major categories, rheological and chemical indicators. These indicators are summarized in Table 2.4.

Table 2.4 Summary of aging indicators for asphalt binders

| Type | Aging indicators | Equations | Reference |
|---|---|---|---|
| Rheology | Retained penetration (%) | $\frac{\text{Penetration of aged binder}}{\text{Penetration of unaged binder}} \times 100$ | [77] |
| | Increase in softening point (°C) | $\Delta T_{R\&B} = T_{aged} - T_{unaged}$ | [77] |

| Type | Aging indicators | Equations | Reference |
|---|---|---|---|
| | Mass loss during short-term aging (%) | $\frac{M_{unaged}\text{-}M_{aged}}{M_{unaged}} \times 100$ | [77] |
| | Aging index / Viscosity ratio | $\frac{\eta_{aged}}{\eta_{unaged}}$ | [22] |
| | Complex modulus and phase angle | $\frac{G^*_{aged}}{G^*_{unaged}}$ or $\frac{\delta_{aged}}{\delta_{unaged}}$ or $\frac{(G^* \sin\delta)_{aged}}{(G^* \sin\delta)_{unaged}}$ | [78, 79] |
| | Rheological index *R* | $\Delta G^* = G^*_{glassy} - G^*_{at\ cross\ over\ f}$ | [80] |
| Chemical | Gaestel index (*IC*) | $IC = \frac{\text{Asphaltenes+Saturates}}{\text{Aromatics+Resins}}$ | [41] |
| | Change of carbonyl, sulfoxide, aromatic, aliphatic, and ketones area (infra-red spectra test) | C=O peak in 1700 cm$^{-1}$;<br>S=O peak in around 1000 cm$^{-1}$;<br>Ketone in 1800-1600 cm$^{-1}$ region | [81, 82] |
| | Aging index based on band area ratio | Aromatic index: $A_{1600}/\sum A$;<br>Aliphatic index: $A_{1460} + A_{1376}/\sum A$;<br>Carbonyl index: $A_{1700}/\sum A$;<br>Sulphoxide index: $A_{1030}/\sum A$<br>$\sum A = A_{1700} + A_{1600} + A_{1460} + A_{1376} + A_{1030} + A_{864} + A_{814} + A_{743} + A_{724} + A_{(2953,\ 2923,\ 2862)}$ | [83] |
| | Change in molecular weight distribution (GPC test) | Large molecular size portion | [41] |

### 2.3.2 Aging indicators for asphalt mixtures

Some aging indicators for asphalt mixture are listed in Table 2.5.

Table 2.5 Summary of aging indicators for asphalt mixtures

| Aging indicators | Equation | Reference |
|---|---|---|
| Resilient modulus ratio (%) | $\frac{E_{after\ aging}}{E_{before\ aging}} \times 100$ | [84] |
| Ductility index (DI) | $\frac{\text{Slope of a creep curve for aged mixture}}{\text{Slope of a creep curve for unaged mixture}}$ | [85] |

### 2.3.3 Summary

As previously mentioned, asphalt binder aging influences its physical and chemical properties. Hence, researchers proposed different aging indicators to characterize aging states of asphalt binders.

## 2.4 **Simulation of asphalt mixture aging**

It is understood that field aging is a complicated process and affected by many factors, such as environmental factors (i.e., temperature, UV light, and moisture), material properties, and mixture types. However, natural aging is pretty time-consuming. Hence, a general solution is to accelerate asphalt mixture aging at high temperatures and/or high pressure in the laboratory. Similarly, some aging methods for asphalt mixtures are summarized in Table 2.6.

Table 2.6 Summary of laboratory aging methods for asphalt mixtures

| Test method | Short-term aging | Long-term aging | Reference |
|---|---|---|---|
| Ottawa sand mixture | 50×50 $mm^2$ cylinders; various periods at 163℃ | | [86] |
| Production aging | Loose material; 8 h, 16 h, 24 h, and 36 h at 135℃ | | [87] |
| Bitutest protocol | Loose material; 2 h at 135℃ | | [88] |
| Oven aging procedure | 25×40 mm specimens; 5 h at 150℃ | | [89] |
| Ottawa sand mixtures | 1200 h at 60℃ | | [90] |
| Short-term oven aging | 4 d or 7 d at 100℃ | | [91] |
| Long-term aging | | Compacted specimens; 5 h at 163℃ | [92] |
| Long-term aging | | Compacted specimens; 2 d at 60℃ followed by 5 d at 107℃ | [87] |

| Test method | Short-term aging | Long-term aging | Reference |
|---|---|---|---|
| Long-term aging | | Compacted specimens with and without ultraviolet; 90 d at 60℃ | [93] |
| Long-term aging | | Loose mixture in sealed tin; 16 h at 160℃ | [94] |
| Bitutest protocol | | Compacted specimens; 5 d at 85℃ | [37] |
| Semi-compacted sand mixtures | | 1000 h at 60℃ | [95] |
| Long-term aging | | Compacted specimens at 0.5 mm of water; 1 d, 2 d, 4 d, 6 d, and 10 d at 60℃ | [85] |
| Long-term aging | | Compacted specimens; 5 to 10 d at 60℃ and 0.7 MPa of air pressure | [87] |
| Oregon mixtures | | Compacted specimens; 0 d, 1 d, 2 d, 3 d, and 5 d at 60℃ and 0.7 MPa of air pressure | [96] |
| SHRP low-pressure oxidation (LPO) | | Compacted specimens; 5 d at 60℃ or 85℃ and oxygen condition (1.9 l/min) | [84] |
| Modified SHAP long-term oven aging (LTOA) | | Compacted specimens; up to 25 d at 60℃ and air condition (3.0 l/min) | [97] |
| Pair void mixtures | | Compacted specimens; 72 h at 100℃ and 2.07 MPa of air pressure | [98] |
| Liverpool University method | | Marshall cores of Porous Asphalt; 21 d at 163℃ | [99] |
| SHRP (LTOA) | Loose material; 2-4 h at 135℃ with stirring. | Compacted specimens; 5 days at 85℃ | [84] |
| Beams aging | 4×25×4 cm beam; 8 h at 70℃ | 4×25×4 cm beam; 20 d at 60℃ | [100] |
| RILEM TG5 method | Loose material; 4 h at 135℃ | Loose material; 7-9 d at 85℃ | [101] |
| Belgian Road Research Centre method | Loose material (3 cm thickness); 1.5 h at 135℃ | Loose material (3 cm thickness); 14 d at 60℃ | [102] |

As shown in Table 2.6, aging methods for short- and long-term aging can be classified into two types according to the form of asphalt mixtures: loose, and compacted asphalt mixture aging. Moreover, there is one trend that most studies chose aging temperature below 100℃ for long-term aging since the temperature of 100°C is considered to be a transition temperature between aging mechanisms [103]. The oxidative rate of asphalt binder doubles for each 10°C increase when aging temperature is over 100℃ . Another trend is that higher temperature was usually applied for short-term aging while lower temperatures and high pressures were typically implemented in long-term aging.

## 2.5 **The oxidation model of asphalt binder**

### 2.5.1 The oxidative rate model

The oxidative rate is dependent on the types of asphalt binders due to the difference in activation energies and first jump characteristics. The oxidative rate at a given time can be expressed as a function of concentrations of reactive compounds in asphalt [104-106]. However, the reaction order concerning an oxygen concentration is various with the types of asphalt binders [107].

Many researchers [59, 108-111] usually assumed the first order and can be expressed in Eq. (2.1).

$$\frac{dP}{dt} = -kBC \tag{2.1}$$

where $P$ is the concentration of reaction products (or some parameter related to it, such as a log of viscosity or the carbonyl concentration), $B$ is the concentration of oxidative products, $C$ is the oxygen concentration, and $k$ is the rate constant at a given temperature.

Eq. (2.1) can predict an exponentially decreasing or approximately linear rate, but it does not satisfactorily describe the overall reaction [112]. The other disadvantage is that $B$ cannot be calculated and must be estimated. Therefore, Herrington [112] assumed that overall reaction could be approximated as the sum of two concurrent reactions, one 'fast' and one 'slow.' Moreover, the equation was proposed and given in Eq. (2.2). Compared with Eq. (2.1), Eq. (2.2) accurately predicted the formation of oxidation products at high pressures and in solutions where diffusion effect was not significant.

$$\frac{dP}{dt} = k_f B_f C + k_s B_s C \tag{2.2}$$

where $k_f$ and $k_s$ are the rate constants for the fast and slow reactions respectively, $B_f$ and $B_s$ are the concentration of reactive asphalt species in the fast and slow reaction respectively, and $C$ is the oxygen concentration.

Glover et al. proposed a new oxidation rate model which was different with previous models. The model is a typical first-order and zero-order aging kinetic model based on infrared (IR) results [9]. The equations are expressed in Eqs. (2.3) and (2.4).

$$C_p = M \times (1 - e^{-k_1 \times t}) + k_2 \times t \tag{2.3}$$

$$S_p = M \times (1 - e^{-k_1 \times t}) + k_2 \times t \tag{2.4}$$

where $C_p$ and $S_p$ are the carbonyl and sulfoxide peak heights in IR spectrum, respectively, $k_1$ and $k_2$ are the reaction constants for the fast reaction (first order) and constant reaction (zero order) respectively, and $M$ is the total carbonyl (or sulfoxide) produced in the fast reaction. The typical Arrhenius equation is used to plot the relationship between reaction constants ($k_1$ and $k_2$) and the reciprocal of absolute aging temperatures.

To sum up, the reaction constant is an important parameter that has a pronounced effect on oxidation rate of asphalt binder. Moreover, the parameter can be calculated by using

Arrhenius equation that proposed by Svante Arrhenius in 1889, as expressed in Eq. (2.5).

$$K_t = A \times e^{-E_a/(RT)} \tag{2.5}$$

where: $K_t$ is the rate constant of chemical reaction at temperature $T$, $A$ is the constant (frequency factor), $E_a$ is the activation energy, $R$ is the gas constant, 8.314 J/(K•mol), and $T$ is absolute temperature (°K).

Several studies found that the formation of carbonyl compounds resulted from the oxidative aging of asphalt binder [23-25, 113]. This influence varies with the types of asphalt binder. For each asphalt binder, there was a linear correlation between CA growth and total oxygen increase. Therefore, Lau et al. adopted the standard Arrhenius equation to characterize the carbonyl formation rate [25]. Later, Liu et al. found carbonyl formation rate as a function of temperature and pressure and then modified the standard Arrhenius equation, as given in Eq. (2.6) [106].

$$r_{CA} = A \times P^{\alpha} \times e^{-E_a/(RT)} \tag{2.6}$$

where $r_{CA}$ is the carbonyl formation rate, P is the oxygen pressure, and $\alpha$ is the reaction order with respect to oxygen pressure.

### 2.5.2 Oxygen diffusion and reaction model

In practice, the oxidation process of asphalt binder can be divided into two interlinked steps: 1) oxygen from atmosphere diffuses into the pavement through the interconnected path, and 2) oxygen penetrates into and then reacts with asphalt binder coated on the surface of aggregates. To understand the oxidative aging of asphalt binder, researchers have developed various oxidation models to predict oxygen diffusion and reaction in asphalt pavement. These studies can be classified into two categories: one type only considered the effect of oxygen diffusion into asphalt binder, and the other type considered the effect of oxygen diffusion and consumption (reaction) during the diffusion process. It found that the diffusion of low molecular weight organic components was a function of deformation response and temperature, and the expression is given in Eq. (2.7).

$$\log(D/RT) = A + B\log\alpha_T \tag{2.7}$$

where *D* is the diffusion coefficient, *A* and *B* are constants, *T* is the absolute temperature, and $\log\alpha_T$ is the shifting factor which can be identified with the change of $\log\eta$ ($\eta$ is the measured viscosity) with temperature for asphalt. Later, Dickinson [109] modified the Fujita's equation by replacing $\alpha_T$ with $\eta$.

Periasamy [114] proposed an electrodynamic balance single particle method to characterize oxygen diffusion by directly measuring mass changes of asphalt binder, as expressed in Eq. (2.8). However, the diffusion model did not consider oxygen consumption, and the results also did not represent a good relationship between temperatures and diffusion coefficients.

$$\frac{M_t}{M_\infty} = \frac{4}{L}\sqrt{Dt/\pi} \tag{2.8}$$

where $M_t$ and $M_\infty$ are the oxygen mass absorbed at time *t* and at infinite time by the particle coated with asphalt sample respectively, *t* is the time, *L* is the thickness of the asphalt film on the particle, and *D* is the diffusion coefficient of oxygen in the thin asphalt film.

For the field oxidation of asphalt binder, oxygen reacts with active components in asphalt binder coated on the surface of aggregates. Therefore, oxygen consumption was taken into account so that the oxidation model made a more accurate prediction of oxidation for asphalt binder in asphalt pavement.

Bird et al. developed a mathematical equation to explain oxygen diffusion and reaction, as expressed in Eq. (2.9) [115].

$$\frac{\partial C_{O_2}}{\partial t} = -\nabla \cdot F_{O_2} - \gamma_{O_2} \tag{2.9}$$

where $C_{O_2}$ is the concentration of oxygen, t is the time, $F_{O_2}$ is the molar flux of oxygen, and $\gamma_{O_2}$ is the consumption rate of oxygen. For asphalt binder, $N_{O_2}$ can be expressed by Fick's first law of diffusion as given in Eq. (2.10).

$$F_{O_2} = -D_{O_2} \frac{\partial C_{O_2}}{\partial x} \tag{2.10}$$

where $x$ is the depth of the film, and $D_{O_2}$ is the diffusion coefficient which varies with depth because of different oxidative degree in the film.

Lunsford [116] combined Bird's equation and Fick's first law to propose a new one-dimensional diffusion and reaction model, as expressed in Eq. (2.11). The equation describes oxygen partial pressure in asphalt as a function of time, temperature, and depth below the film surface. Also, this model can obtain the oxygen diffusivity by calculating the change of oxygen partial pressure over time. However, this model did not take air void and mixture morphology into account during developing the oxidation rate model [117]. Also, this model was not sufficient to determine the oxygen diffusion coefficient and must be approached differently [118].

$$\frac{\partial P}{\partial t} = \frac{\partial \mathcal{D}_{O_2}}{\partial x} \cdot \frac{\partial P}{\partial x} + \mathcal{D}_{O_2} \cdot \frac{\partial^2 P}{\partial x^2} - \frac{cRT}{h} \cdot r_{AC} \tag{2.11}$$

where $P$ is the gas-phase oxygen partial pressure, $c$ is the constant that converts rate of carbonyl formation to rate of oxygen consumption and depends on asphalt type, ranging from $2.75\times10^{-4}$ to $4.59\times10^{-4}$ mol $O_2$/mL/CA for ten asphalts reported by Liu et al. [119], $R$ is the gas constant, $T$ is the absolute temperature, $r_{AC}$ is the carbonyl formation rate, and $h$

is the dimensionless Henry's law absorption constant, which is the function of temperature [109].

Oxygen diffusion and reaction coefficients are influenced by temperature, air void, and aggregate [120]. To be specific, small aggregate particles and absorption of asphalt binders by aggregates impair oxygen diffusion. Additionally, accessible air voids gradually decrease in service life due to traffic compaction. If the accessible air voids reduce to a very low extent, oxygen diffusion in asphalt pavement could be considered to be hindered. Therefore, an improved model of asphalt oxidation in pavement should take these factors into account.

Prapaitrakul et al. made an early attempt to model asphalt binder oxidation in asphalt pavement by using an improved model based on the surrounding cylindrical shell of an air void channel [121]. In this model, a constant oxygen partial pressure of 0.2 atm was adopted for all air voids, and mono-disperse air void distribution and the same air void content at each pavement layer. Moreover, the concept of effective diffusivity was adopted to replace the diffusivity in Eq. (2.11). The effective diffusivity $(D_e)$ is a function of actual oxygen diffusivity in asphalt binder, asphalt volume fraction $(\varepsilon)$, and tortuosity $(\tau)$ that account for the effect of small aggregate particles on diffusion path, as given in Eq. (2.12). This mixture binder oxidation model with the effective diffusivity was demonstrated that it could reasonably predicts the actual average aging rate for a pavement [121].

$$D_e = \mathcal{D}_{O_2} \times \frac{\varepsilon}{\tau} \tag{2.12}$$

Although the oxygen diffusion and reaction model is encouraging, there are some differences with actual conditions: 1) oxygen concentrations in actual air voids vary with time, temperature, depth, and other conditions, rather than a constant, and 2) air void contents and distribution are various in pavement rather than mono-disperse and same air void content for each pavement layer. Therefore, Han [118] determined three pavement air void properties, radius of each air void ($r$), number of air voids ($N$), and average shell distance ($r_{NFB}$) between two adjacent pores, with the aid of X-ray CT technique and imaging analysis tools. Then, by using the three air voids parameters as model inputs, the oxygen diffusion and reaction model was further adjusted. It was proved that this model was more accurate to predict asphalt aging in a newly constructed pavement.

In summary, many oxidation models had been developed based on the studies of asphalt binder oxidation in the laboratories rather than asphalt mixture or pavement. Moreover, those models did not consider oxygen consumption. In 1994, Lunsford proposed a new model considering the effect of oxygen diffusion and consumption on oxidation [116]. Later, Glover's team made some modification based on the air voids results obtained by using X-ray CT technique and imaging analysis tools and field oxidation data [122]. However, oxygen diffusivity and consumption only can be indirectly attained by calculating the change of oxygen partial pressure over time, rather than by measuring the change of oxygen concentration over time. Moreover, this oxygen diffusivity is just investigated with asphalt mortars rather than compacted asphalt mixtures. Fortunately, Aubertin and Mbonimpa [123] designed a diffusion cell (see Figure 2.12) to measure the oxygen flux parameters in soil and then to determine oxygen diffusion and reaction coefficients of soil. They provided a new approach to determine oxygen diffusion and reaction coefficients by directly measuring the changes in oxygen concentration, and these models are reviewed in detail in next section.

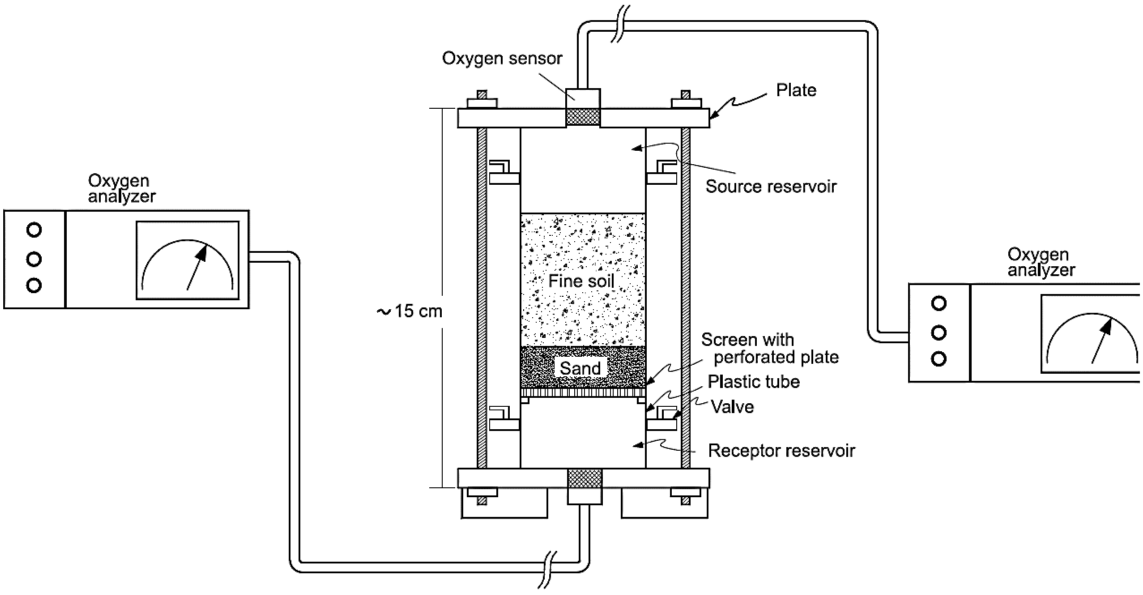

Figure 2.12 The schematic diagram of a diffusion cell (adapted from [123])

### 2.5.3 Oxygen diffusion and reaction model used in soil

This model was developed based on the Fick's first and second laws as given by Hillel [124] for one-dimensional diffusion, as expressed in Eqs. (2.13) and (2.14).

$$F(z,t) = -\theta_{eq} D^* \frac{\partial C(z,t)}{\partial z} = -D_e \frac{\partial C(z,t)}{\partial z} \tag{2.13}$$

$$\frac{\partial}{\partial \mathrm{t}}\left(\theta_{eq} C\right) = \frac{\partial}{\partial \mathrm{z}}\left(\theta_{eq} D^* \frac{\partial C}{\partial z}\right) = \frac{\partial}{\partial \mathrm{z}}\left(D_e \frac{\partial C}{\partial z}\right) \tag{2.14}$$

where $F(z,t)$ is the diffusive flux of oxygen (mol·$\mathrm{L}^{-2}$·$\mathrm{T}^{-1}$), $\theta_{eq}$ is an equivalent (diffusion) porosity ($\mathrm{L}^3$· $\mathrm{L}^{-3}$), $D^*$ and $D_e$ are the bulk and effective diffusion coefficient ($\mathrm{L}^2$·$\mathrm{T}^{-1}$, $D_e = \theta_{eq} D^*$) respectively, and $C(z,t)$ is the oxygen concentration in pores at time $t$ (T) and depth $z$ (L).

In Eqs. (2.13) and (2.14), the oxygen concentration is a function of time and depth and is related to the effective diffusion coefficient of materials. Moreover, assuming that oxygen will not be consumed or generated during diffusing through an inner material. However, reactive materials may consume oxygen during oxygen diffusion process. Hence, Crank [125] modified the Fick's second law after considering the oxygen consumption, as given in Eq.

(2.15).

$$\frac{\partial}{\partial \mathrm{t}}\left(\theta_{eq} C\right)=\frac{\partial}{\partial \mathrm{z}}\left(\theta_{eq} D^{*} \frac{\partial C}{\partial z}\right)-\theta_{eq} K_{r}^{*} C=\frac{\partial}{\partial \mathrm{z}}\left(D_{e} \frac{\partial C}{\partial z}\right)-K_{r} C \tag{2.15}$$

where $K_r^*$ and $K_r$ are the bulk and effective reaction rate coefficients, respectively ($\mathrm{T}^{-1}$, $K_r=\theta_{eq}K_r^*$).

For a particular material, the saturation degree of the water-retaining layer is considered to be constant. Therefore, $\theta_{eq}$ and $D^*$ are independent of time and depth in the internal material. Thus, Eq. (2.15) can be rewritten and expressed in Eq. (2.16)

$$\frac{\partial \mathrm{C}}{\partial \mathrm{t}}=D^{*} \frac{\partial^{2} C}{\partial z^{2}}-K_{r}^{*} C \tag{2.16}$$

Eq. (2.16) can be solved analytically but relatively simple boundary conditions in steady state [125]. Once oxygen concentration profile in the layer is obtained, and then oxygen flow can be attained with Eq. (2.13). The boundary conditions for the case of diffusion through a homogeneous layer with a thickness L are listed as follows: 1) the initial oxygen concentration throughout the material pores is zero, $C(z>0,t=0)=0$; 2) the oxygen concentration at upper interface is constant, $C(z=0,t\geq 0)=C_0$; and 3) the oxygen concentration at lower interface is zero since oxygen is rapidly consumed, $C(z\geq L,t>0)=0$.

For a reactive material, the concentration at position z can be derived using the Danckwert's moving frames [125]. According to this method, the general solution (for $K_r^*\geq 0$) of Eq. (2.16) can be rewritten in following form:

$$C(z,t)=K_r^*\int_0^t C_1(z,t')e^{-K_r^*t'}dt'+C_1(z,t)e^{-K_r^*t} \tag{2.17}$$

where $t'$ is a dummy integration variable representing time. Solving this equation leads to:

$$C(z,t)=C_0\Bigg[1-\frac{z}{L}-\frac{2}{\pi}\sum_{i=1}^{\infty}\frac{\sin(i\pi z/L)}{i}\exp\left[-\left(\frac{i^2\pi^2}{L^2}D^*+K_r^*\right)t\right]-\frac{2K_r^*}{\pi}\sum_{i=1}^{\infty}\frac{\sin(i\pi z/L)}{\frac{(i^3\pi^2D^*)}{L^2}+K_r^*}\Big\{1-$$

$$\exp\left[-\left(\frac{i^2\pi^2}{L^2}D^* + K_r^*\right)t\right]\Bigg\}\Bigg] \quad (2.18)$$

where $C_0$ is the oxygen concentration at upper surface, and $i$ is an integer.

Introducing Eq. (2.18) into Eq. (2.13) and integrating leads to the following expression for the flux at position (L):

$$F(z = L, t > 0) = F_{s,L} + 2K_r^* F_{s,L} \sum_{i=1}^{\infty}\left(\frac{(-1)^i}{\frac{(i^2\pi^2 D^*)}{L^2} + K_r^*}\right)\left\{1 - \exp\left[-\left(\frac{i^2\pi^2}{L^2}D^* + K_r^*\right)t\right]\right\} +$$

$$2\,F_{s,L}\sum_{i=1}^{\infty}(-1)^i \exp\left[-\left(\frac{i^2\pi^2}{L^2}D^* + K_r^*\right)t\right] \quad (2.19)$$

where $F_{s,L}$ is expressed by Eq. (2.20)

$$F(s, L) = \frac{C_0 D_e}{L} \quad (2.20)$$

To use these equations, two critical parameters ($D^*$ and $K_r^*$, or $D_e$ and $K_r$) are need to be determined. The actual parameters can be obtained iteratively by comparing measured and calculated curves of oxygen concentration over time, which are attained by measuring the changes of oxygen concentration in both ends of the reservoirs with diffusion cell (see Figure 2.12) designed by Aubertin and Mbonimpa [123].

### 2.5.4 Summary

To well predict asphalt binder aging with time and position, researchers developed different models to establish relationships between the properties or compounds of asphalt binders and aging conditions. Since oxidation is a major factor resulting in asphalt binder aging, the current aging models can be classified into three categories: oxygen reaction rate model, oxygen diffusion model, and oxygen diffusion and consumption model. Regarding the oxygen reaction rate models, these models were developed based on Arrhenius's equation. Some of the models considered oxygen consumption during oxygen diffusion process. For the oxygen diffusion and consumption models, the early diffusion models, which did not consider the oxygen consumption, were developed based on the studies of asphalt binder oxidation in the laboratory rather than asphalt mixture or pavement. Additionally, most of these models had been not validated by using the field oxidation data. Later, Glover's team made many modifications based on the first diffusion and reaction model proposed by Lunsford in the light of the actual air voids value obtained by using X-ray CT technique and imaging analysis tools, and field oxidation data.

Among these oxidation models, oxygen reaction rate and oxygen diffusion coefficient are crucial. Nevertheless, they cannot be determined with these existing oxidation models. Fortunately, Aubertin and Mbonimpa [123] designed a diffusion cell (see Figure 2.12) to measure the oxygen flux parameters in soil and then to determine oxygen diffusion and reaction coefficients using their models. It provides a new approach to determine oxygen diffusion and reaction coefficients by measuring the changes in oxygen concentrations of the diffusion cell.

# CHAPTER 3. RESEARCH METHODOLOGY

## 3.1 **Introduction**

This dissertation first aimed to develop a new method to simulate the long-term aging for compacted asphalt mixtures and then investigate the property changes in compacted asphalt mixtures over aging time. Based on these results, six common predictive models of dynamic modulus were examined. To further investigate aging susceptibility of compacted asphalt mixtures, an apparatus was first manufactured to determine oxygen diffusion and consumption coefficients. Then, a predictive model was developed based on the relationship between the coefficients and volumetric parameters of compacted asphalt mixtures. Therefore, this dissertation can be divided into two research topics.

(1) A new aging method was determined to simulate the long-term aging for compacted asphalt mixtures by comparing dynamic modulus values, volumetric parameters, or CT images of compacted asphalt mixtures before and after being aged. After determining aging conditions, three mixture types were chosen to evaluate the effect of the aging method on dynamic modulus of compacted asphalt mixtures, and rheological and chemical properties of recovered asphalt binders. Based on these data, accuracies and robustness of six predictive models for dynamic modulus were examined.

(2) The oxygen diffusion and possible consumption coefficients of compacted asphalt mixtures were measured, and the effects of different variables (e.g., complex shear modulus, phase angle, viscosity, and air voids) on the coefficients were analyzed. Additionally, a relationship between the coefficients and aging-related changes in the properties of compacted asphalt mixtures was investigated.

A flow diagram for the two research topics is given in Figure 3.1. Moreover, the detailed research methodologies and experimental plans are described in the following sections.

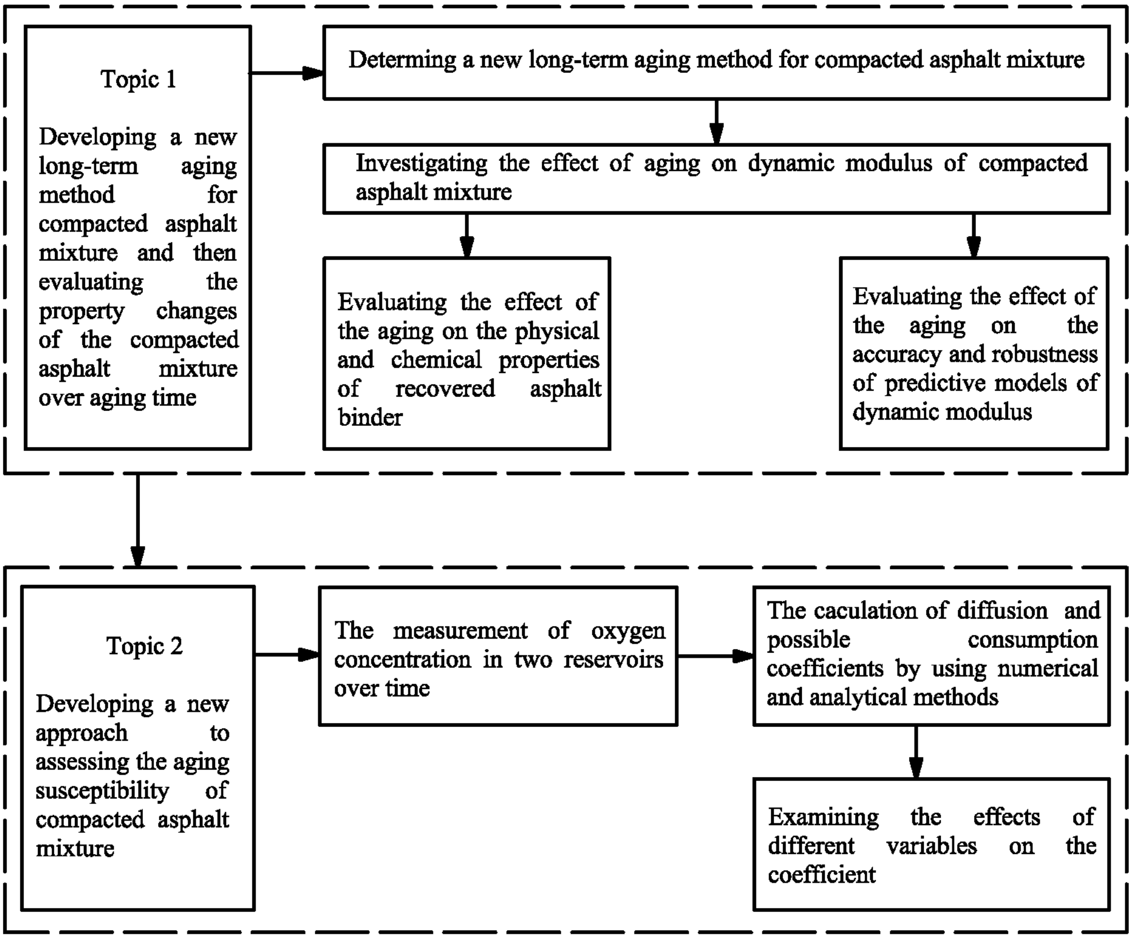

Figure 3.1 The flow diagram of two research topics

## 3.2 **Research topic 1**

The research scheme of research topic 1 is drawn in Figure 3.2. After determining a new long-term aging method for compacted asphalt mixtures, three mixture types were chosen to simulate the long-term aging by using a customized autoclave, as shown in Figure 3.3. Before and after each aging, two small cores were drilled from a control specimen to determine the aging state of compacted asphalt mixtures. The volumetric parameters of the control specimen are close to average values of those of other five specimens in the same batch. Other five specimens were utilized to conduct dynamic modulus test. After the test, all six specimens were placed in the autoclave again. Based on the dynamic modulus values obtained at different aging states, the effect of aging on the accuracies and robustness of six predictive models of dynamic modulus were investigated.

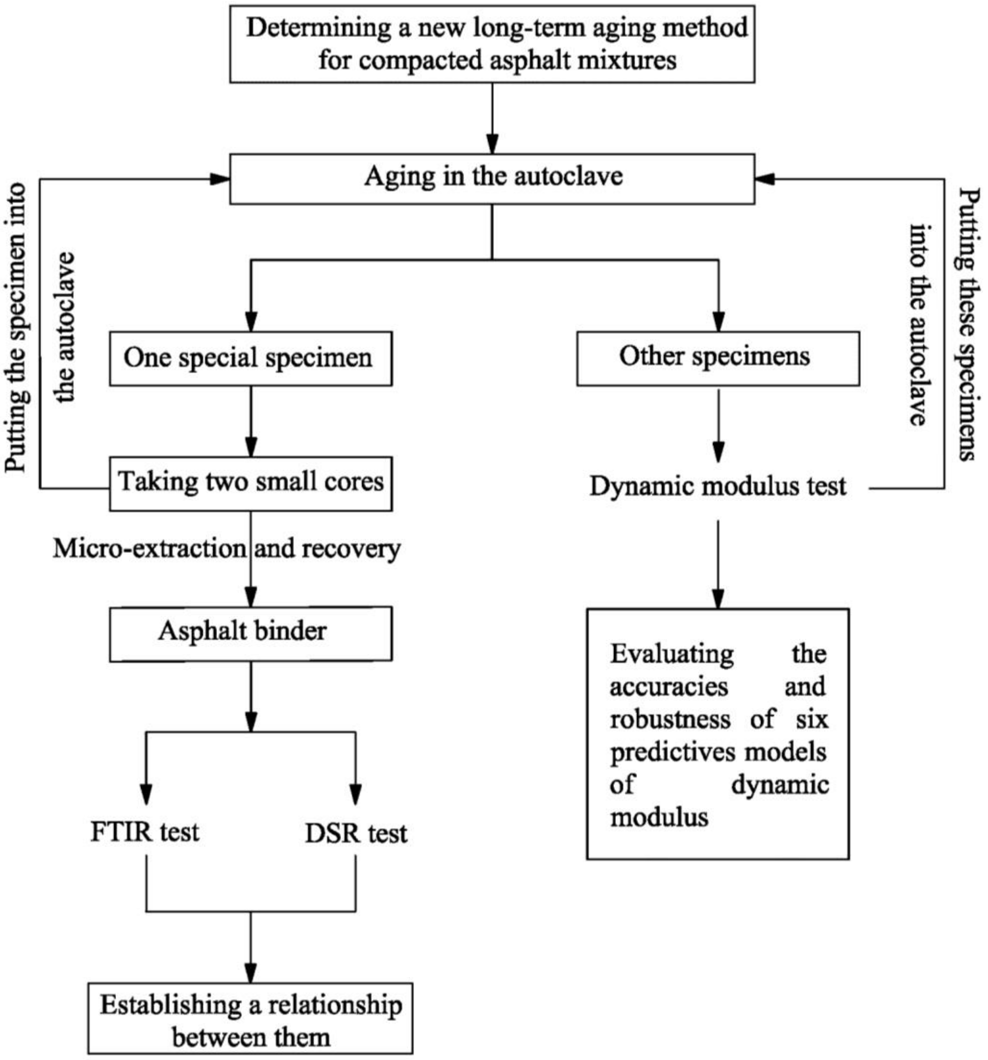

Figure 3.2 The general research scheme for research topic 1

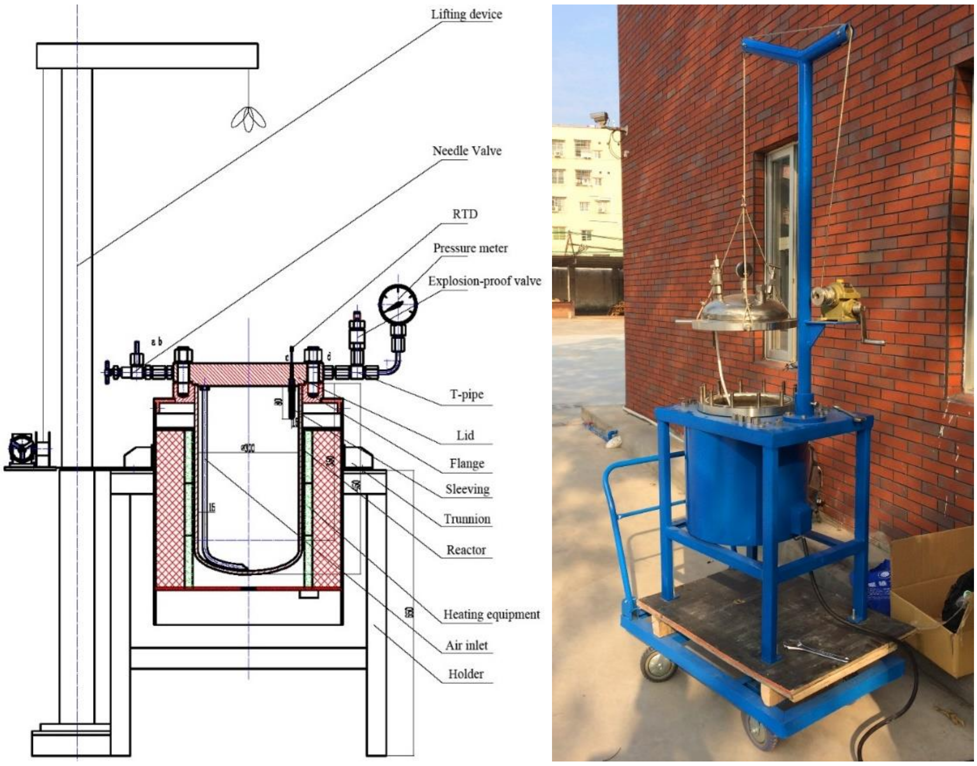

Figure 3.3 The customized autoclave used for aging compacted specimens

### 3.2.1 Artificially aging asphalt mixtures in the laboratory

As stated above, asphalt oxidation is highly dependent on temperature, time, and oxygen concentration [30]. Therefore, these three factors were major considerations during the designing stage of aging protocols. In addition, the following features of an aging apparatus should be included: large capacity, solid reliability, easy operation and maintenance, automatic temperature control, and excellent airtightness. Based on these considerations, we designed and customized an autoclave with an inner height of 45 cm and an inner diameter of 30 cm (see Figure 3.3) as an environment simulator to artificially simulate the long-term aging of compacted asphalt mixtures in the laboratory. Based on previous studies, long-term aging conditions often adopt a temperature of 60°C with or without applied pressure. Hence, this temperature was also chosen as an aging temperature. Additionally, an aging temperature of 40°C was also used because this temperature is lower than the softening point of base asphalt used in this study. Some previous studies found that the drain-down phenomenon might appear during aging process when the aging temperature is greater than softening points of asphalt binders. In addition, pure oxygen and pressure were used to accelerate aging process. The detailed aging procedure using the autoclave is described below.

(1) The autoclave is first heated to a target temperature. During this period, specimens are wrapped with elastic gauze to avoid or minimize deformation of the specimens caused by the gravity acting on the specimens heated to high temperatures for a long time, as shown in Figure 3.4. One advantage of using gauze is that gauge points can be consistently placed to eliminate the effect of the position of gauge points on dynamic modulus of specimens.

(2) When the target temperature is reached, the autoclave lid is then opened. The specimens are then placed on perforated plates inside the autoclave, as shown in Figure 3.5.

(3) Next, the autoclave lid is closed. All air valves are then opened to facilitate the flow of oxygen into the autoclave through an air pipe at the bottom of the autoclave. Thus, other gases are gradually exhausted from the autoclave as the density of oxygen is greater than that of air, as shown in Figure 3.6.

(4) After half an hour, a pure oxygen atmosphere is assumed to be inside the autoclave in this study. The valves are then closed, and these conditions are maintained for a target duration.

(5) After a target duration, the specimens are taken out from the autoclave and cooled to

room temperature for further testing.

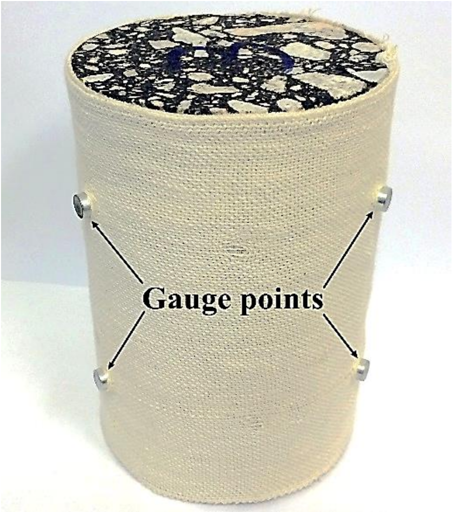

Figure 3.4 The specimen wrapped with gauze

Figure 3.5 The specimens are placed on a perforated plate

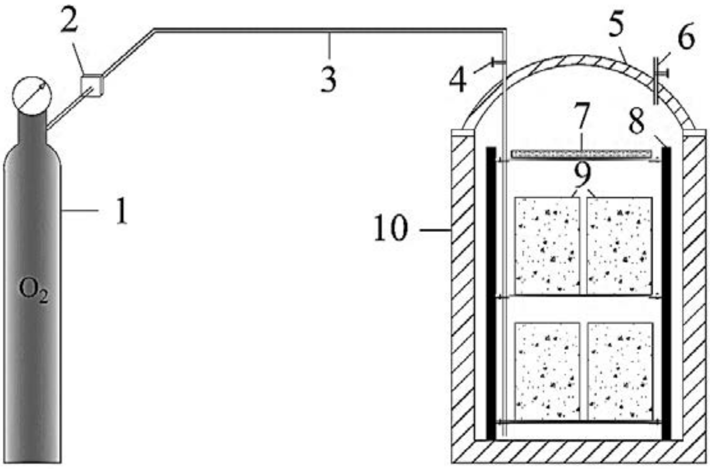

1. Oxygen cylinder; 2. Flow meter; 3. Air inlet; 4. Air valve; 5. Lid of the autoclave; 6. Air outlet; 7. The plate used to place the asphalt binder for aging; 8. The iron shelf; 9. Aged specimens; 10. Autoclave.

Figure 3.6 The schematic diagram of aging system

### 3.2.2 Micro-sampling, and micro-extraction and recovery methods

To determine the aging states of asphalt binders in compacted asphalt mixtures, one specimen was chosen as a control specimen. The volumetric and mechanical properties of the control specimen should be approximately equal to the average value of the other specimens in the same batch. The control specimen was utilized to drill small cores for determining the aging states of the specimens before and after being aged. Thus, a new micro-sampling method should be developed. In this study, a handheld diamond core drill was used to extract two small cores before and after each aging. The cores are too small to use standard extraction and recovery methods to recover asphalt binders since the standard recovery method requires distilling the solvent in a flask and a certain amount of recovered asphalt binders will adhere to the inside of the flask. Thus, asphalt could not be poured from the flask if the amount of asphalt was tiny. Therefore, an improved micro-extraction and recovery method was developed in this study.

Figure 3.7 presents the flow diagram of the micro-sampling and micro-extraction and recovery methods. Two small cores with 10 mm in diameter and approximately 75 mm in height were drilled with a handheld diamond core drill (Figure 3.8), as shown in Figure 3.9. During the drilling process, the drill bit was cooled with water to avoid further aging of asphalt binders due to the high-speed revolutions of the diamond core drill. After drilling the cores, the control specimen and cores were dried at room temperature, and the two holes in the control specimen were then filled with hot melt glue to hinder the flow of oxygen into the specimen along the holes during the next aging process, as shown in Figure 3.10. Each core was crushed into small pieces and then soaked with dichloromethane for approximately half an hour in a metal container sealed with a lid. After dissolution, the solution was decanted into centrifuge tubes, as shown in Figure 3.11. The residue in the metal container was washed several times until the solvent was clear or just straw-colored, as illustrated in Figure 3.12. The solution was then centrifuged at 3500 rpm for 20 minutes. The supernatant liquid was removed from the centrifuge tube into a clean metal container by using a syringe with a 0.45-micron filter. The solvent was then evaporated at room temperature under nitrogen and further evaporated on a hot plate under nitrogen for half an hour at 100°C, as shown in Figure 3.13. Fourier transform infrared spectroscopy (FTIR) analysis was then conducted to ensure that the solvent was completely removed.

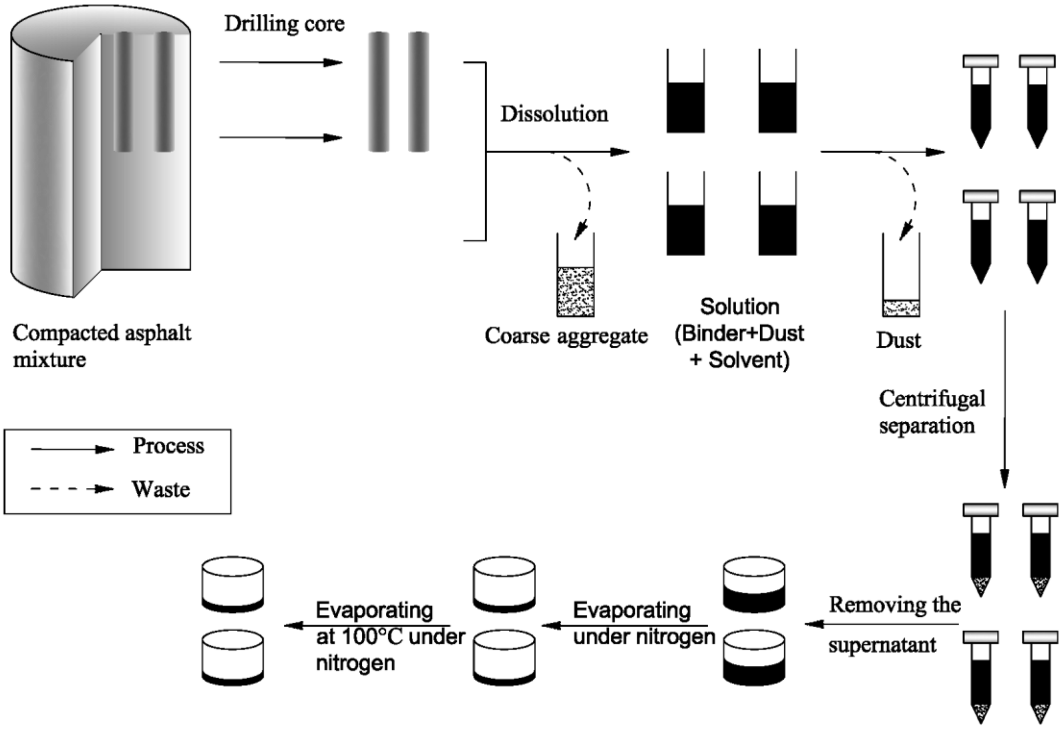

Figure 3.7 The flow diagram of the micro-sampling, and micro-extraction and recovery methods

Figure 3.8 The handheld diamond core drill

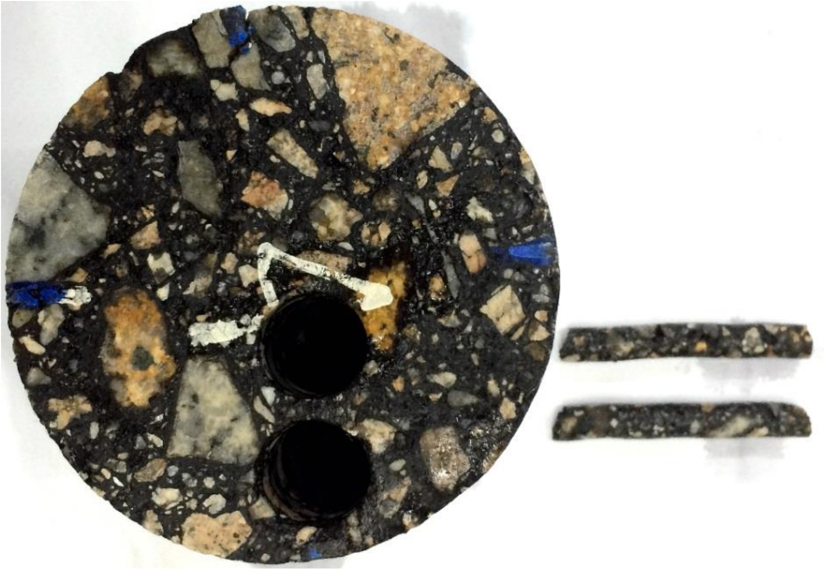

Figure 3.9 A control specimen after being drilled two small cores

Figure 3.10 The holes of the control specimen after being filled with hot melt glue

Figure 3.11 The solution was decanted into centrifuge tubes

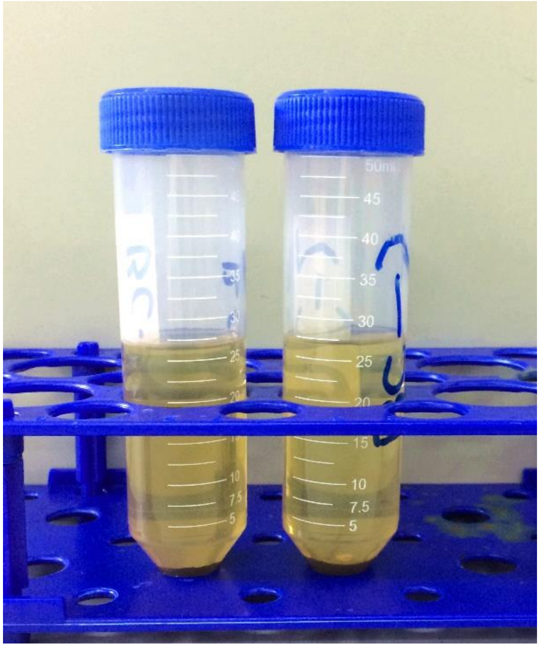

Figure 3.12 The straw-colored solution

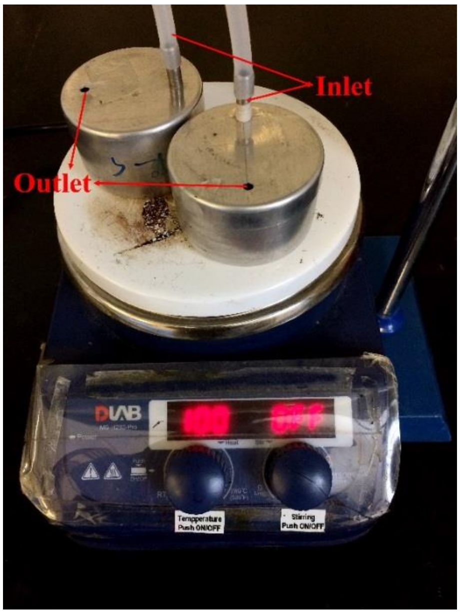

Figure 3.13 The evaporating apparatus

### 3.2.3 Evaluation of rheological and chemical properties of recovered asphalt binders

The rheological properties of recovered asphalt binders were evaluated by using the complex shear viscosity and complex shear modulus. These indicators were chosen based on the following considerations: viscosity is a good indicator of asphalt hardness, and complex shear modulus represents the elastic and viscous properties. These indicators can be directly measured with a dynamic shear rheometer (DSR) apparatus. FTIR characterized the chemical properties of recovered asphalt binders. Moreover, this study adopted the band area ratio method proposed by Lamontagne *et al.* [83]. Van den bergh found that this method can provide more information about the compositions of asphalt binders [20]. The detailed method is described below.

1) Carbonyl index: $A_{1700}/\sum A$;
2) Sulfoxide index: $A_{1030}/\sum A$.

The sum of the area that was calculated according to Lamontagne *et al.* [83], as shown in Figure 3.14.

$$\sum A = A_{1700} + A_{1600} + A_{1460} + A_{1376} + A_{1030} + A_{863} + A_{809} + A_{742} + A_{722} + A_{(2953,\ 2923,\ 2862)} \tag{3.1}$$

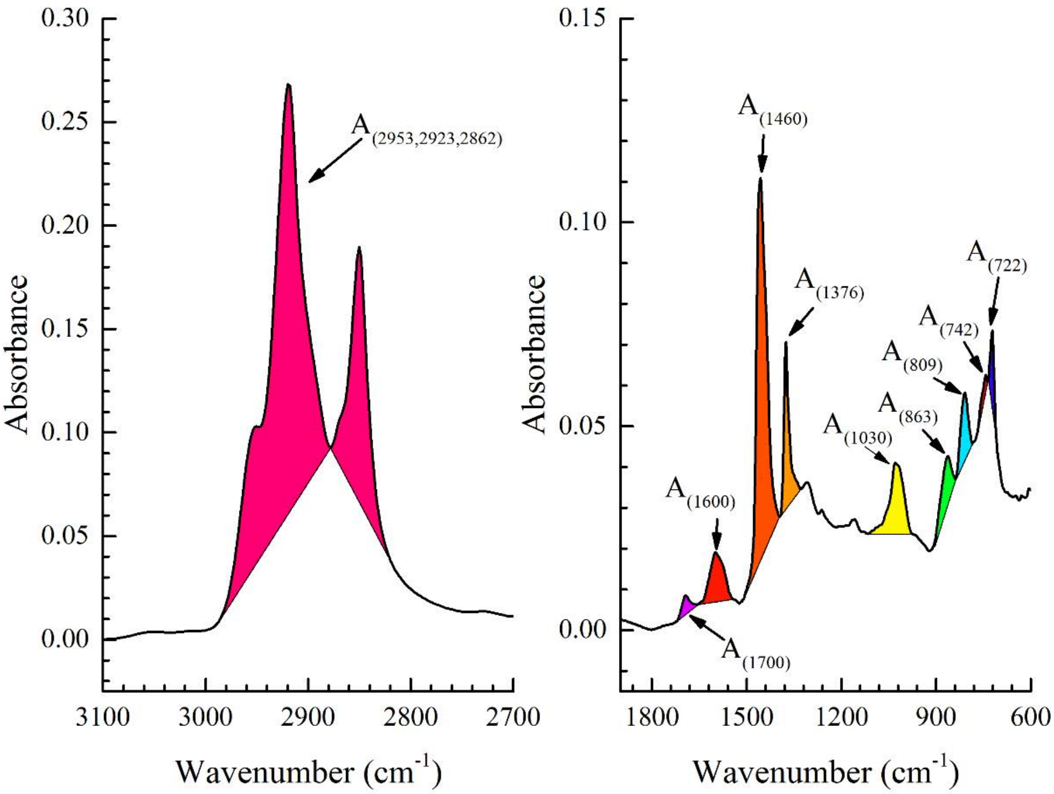

Figure 3.14 The schematic diagram of peak area calculated in this study

### 3.2.4 Evaluation of dynamic modulus of compacted asphalt mixtures

An objective of this dissertation was to assess the effect of aging on dynamic modulus of compacted asphalt mixtures with increasing aging time, so dynamic modulus test was conducted on compacted asphalt mixtures before and after being aged by using a simple performance tester (Interlaken Technology Corporation, Chaska, Minnesota, USA). Based on dynamic modulus values for the three mixture types, the effect of aging on accuracies and robustness of six common predictive models (the Witczak 1-37A, Witczak 1-40D, original Hirsch, improved Hirsch, AI-Khateeb, and 2S2P1D models) were examined.

## 3.3 **Research Topic 2**

A diffusion system was designed to measure oxygen diffusion and possible consumption coefficients of compacted asphalt mixtures, as shown in Figure 3.15. The diffusion apparatus consists of two air reservoirs and a test specimen. In the initial stage of diffusion tests, one of the air reservoirs is filled with air, while the other reservoir is filled with nitrogen. The oxygen concentrations of the two reservoirs were measured with two oxygen sensors (Southland PO2-160) and were simultaneously recorded with a Graphtec GL240 midi data logger. Then, the oxygen diffusion and possible consumption coefficients were computed by both numerical and analytical solutions. Finally, the effects of different variables (i.e., complex shear modulus, phase angle, viscosity, and air voids) on the coefficients were examined. A predictive model was then developed based on these analytical results.

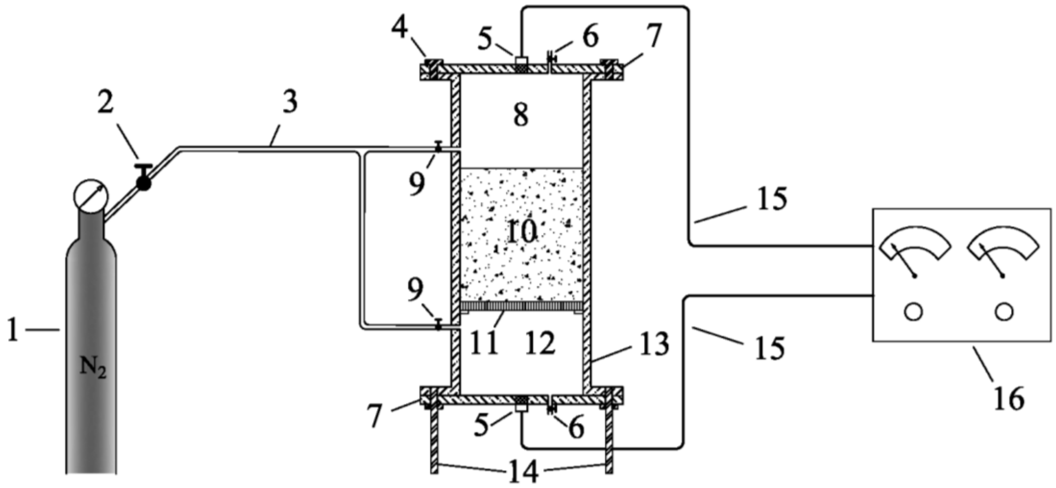

1. Nitrogen cylinder; 2. Pressure reducing valve; 3. Air tube; 4. Screw; 5. Oxygen Sensor; 6. Air outlet; 7. Lid; 8. Source reservoir; 9. Air inlet; 10. Compacted asphalt mixture; 11. Perforated plate; 12. Receptor reservoir; 13. Wall; 14. Threaded metal rod; 15. Metal wire; 16. Oxygen analyzer.

Figure 3.15 Schematic representation of a diffusion system

# CHAPTER 4. THE COMPARISON OF ACCELERATED AGING TREATMENT METHODS TO SIMULATE THE LONG-TERM AGING OF COMPACTED ASPHALT MIXTURE

## 4.1 **Introduction**

Asphalt binder aging has a significant impact on nearly all the critical performance-related properties of HMA mixture. Aged asphalt binder becomes more brittle and stiffer, and thus reduces pavement's resistance to fatigue cracking and thermal cracking [5, 6, 126]. To examine the effects of asphalt binder aging, extensive studies have been conducted to simulate the aging process in laboratory settings. The laboratory aging treatment methods may be categorized as short-term aging treatment and long-term aging treatment. The former is to simulate asphalt binder aging occurs in the processes of mixing, transportation, laying, and compaction. The latter is to simulate asphalt binder aging during the service life of the asphalt pavements. Depending on the object being treated, laboratory aging treatment methods may be divided into binder aging simulation methods and mixture aging simulation methods. The mixture aging simulation can be performed on either loose mixtures or compacted asphalt mixtures. This study is focused on the aging treatment methods for compacted asphalt mixtures to simulate long-term aging in the field. The advantage of using compacted asphalt mixtures is that the properties of the specimens (e.g., dynamic modulus) can be well compared before and after being aged.

Over the last decades, various long-term aging methods have been used, as summarized in Table 2.6. The long-term aging temperature is usually lower than 100℃ since this temperature is believed to be a transition temperature of aging mechanisms [103]. Many early studies on long-term aging were carried out in the Strategic Highway Research Program (SHRP). In the standard adopted by American Association of State Highway and Transportation Officials (AASHTO), compacted asphalt mixtures placed in an oven at 85℃ for five days to simulate long-term aging. Table 2.6 indicates that 60℃ is often chosen as long-term aging temperature. However, there are two concerns about the existing long-term aging methods. One is the integrity of compacted asphalt mixtures at elevated temperature levels. Specimens may be damaged or deformed by gravity especially the specimen is tall. Another concern is the possible flow of asphalt binder induced by gravity in asphalt mixtures at elevated temperatures higher than softening point of asphalt binders. The flow of asphalt binders at the microscopic level may change the internal air voids characteristics of asphalt mixtures. If the properties of asphalt mixtures (e.g., dynamic modulus) before and after being aged are interested, such changes in voids characteristics are not desirable.

The primary objective of this chapter was to compare accelerated aging treatment methods to simulate the long-term aging of compacted asphalt mixtures. In addition to the aging treatment methods reported in previous studies, a new treatment method is developed. The effects of the different treatment methods on asphalt mixtures are assessed by their changes in dynamic modulus, sample sizes, air voids, and images generated by X-ray CT.

## 4.2 **Materials and methods**

### 4.2.1 Materials and specimen preparation

Shell Company provided base asphalt (60/70 pen or PG64-16) used in this study, and its physical properties are listed in Table 4.1.

Table 4.1 The physical properties of the asphalt binder

| Description | Unit | Result | Method |
|---|---|---|---|
| Specific Gravity (25℃) | | 1.039 | ASTM D70 |
| Softening Point, R&B | °C | 46.2 | ASTM D36 |
| Penetration (25℃) | 0.1mm | 68 | ASTM D5 |
| Retained Penetration after TFO Test | % | >52 | ASTM D1754 |
| Flash Point | °C | >232 | ASTM D92 |
| Ductility (25℃) | cm | >100 | ASTM D113 |
| Ductility after TFO Test (25℃) | cm | >50 | ASTM D1754 |
| Viscosity (135℃，300mmHg Vac) | Pa.sec | 0.413 | ASTM D2171 |
| Wax Content | % | 1.6 | DIN 52015 |

Aggregate used in this study is granite, produced from the Lam Tei Quarry in Hong Kong. A commonly used dense-graded asphalt mixture job-mix formula (JMF) in Hong Kong is used. The aggregate gradation of the JMF is plotted in Figure 4.1. The asphalt binder content is 5.0% by mass of the total asphalt mixture, and the air voids of the specimens are 6.0±0.5%.

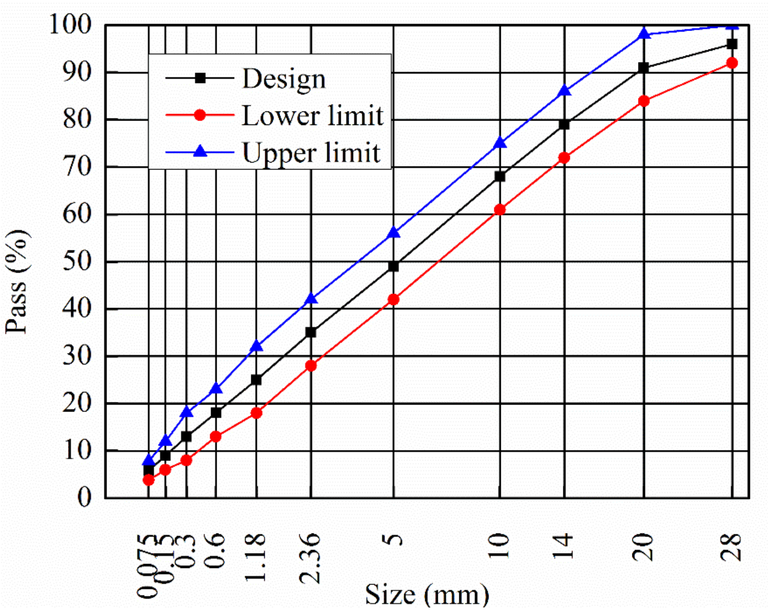

Figure 4.1 Aggregate gradation of the JMF

Specimens of 150 mm in diameter by 170 mm in height were compacted with a Gyratory compactor in accordance with AASHTO PP 60-14 and then cooled in air for about 24 h.

After that, if the specimens were not drilled and sawed immediately, they were sealed in plastic bags and stored carefully in an environmental chamber at 20℃ to minimize the aging effect. No specimen was drilled and sawed later than two weeks after they had been produced. These SGC specimens were then drilled and sawed to a diameter of 100 mm and height of 150 mm. The bulk-specific gravity and air void values of each specimen before and after being drilled and sawed were measured in accordance with AASHTO T 16-13 and T 269-14, respectively. Then, the diameter, height, and flatness, and perpendicularity of each specimen were measured to select those specimens that meet the tolerance listed in Table 1 of AASHTO PP 60-14.

### 4.2.2 Long-term aging conditions

In this chapter, specimens were divided into four groups and then aged under different aging conditions, as shown in Table 4.2. The specimens in Group 1 were placed in an oven to simulate long-term aging in accordance with AASHTO R30-02(2010). A customized autoclave was specifically designed and manufactured for this study (Figure 3.3). The autoclave is manufactured with heavy stainless steel with a heating sub-system and an automatic heating control sub-system. The maximum working temperature of the equipment is up to 200°C. The equipment also possesses a pressure-control sub-system which enables the application of pressure up to 3.0 MPa with precise control. The internal capacity of the equipment is 30 liters, which can host six specimens of 100 mm in diameter and 150 mm in height. A pressure release sub-system is also included for safety considerations.

Specimens in other groups were placed in the customized autoclave under pure oxygen environment at a lower temperature with or without applied pressures. The specific aging treatment conditions are listed in Table 4.2. The aging temperature of Group 2 was chosen to be 60°C based on previous studies [36, 87, 93, 97]. The aging temperature of 40°C was applied in the Group 3 and 4 because it is less than the softening point of asphalt binder used for this study. During the aging process, all specimens were wrapped with elastic gauze to avoid or minimize deformation caused by the gravity for a long time, as shown in Figure 3.4.

Table 4.2 The detailed aging treatment conditions

| Group No. | Temperature (°C) | Applied pressure (MPa) | Duration time (day) | Gas | Aging Apparatus |
|---|---|---|---|---|---|
| 1 | 85 | 0.0 | 5 | Air | Oven |
| 2 | 60 | 0.5 | 7 | Pure oxygen | Customized autoclave |
| 3 | 40 | 1.0 | 7 | Pure oxygen | Customized autoclave |
| 4 | 40 | 0.0 | 7<br>14<br>21<br>28 | Pure oxygen | Customized autoclave |

### 4.2.3 Dynamic modulus test

Dynamic modulus test was conducted using a simple performance tester (SPT) produced by Interlaken Technology Corporation (ITC), as shown in Figure 4.2. The test was performed at 4°C, 20°C, and 40°C and three frequencies (10 Hz, 1 Hz, and 0.1 Hz) in accordance with NCHRP Project 9-29. The test was conducted from lowest to highest temperature and from the highest frequency to the lowest frequency at a given temperature to minimize damage to specimens. During the test, the dynamic load was adjusted to obtain axial strains within the range of 75-125 $\mu\varepsilon$. To eliminate the effect of the position of strain sensors on dynamic modulus, the positions of metallic gage points on each specimen were kept the same during the entire testing and aging process, as shown in Figure 3.4.

Figure 4.2 SPT

Before dynamic modulus test, specimens were placed in an external environmental chamber to ensure temperature equilibrium as specified in Table 4.3. At the beginning of the testing, a specimen was put into the environmental chamber of apparatus. When the chamber temperature return to the testing temperature, dynamic modulus test was conducted with different numbers of cycles for various frequencies as shown in Table 4.4. During the testing process, the dynamic load was adjusted to obtain axial strains within the range 75-125 με. At a given temperature, the loading was applied from highest to lowest frequency. When all specimens had been tested at the lowest temperature, the external environmental chamber was set to the next temperature for a specific time as specified in Table 4.3.

Table 4.3 Recommended equilibrium times

| Specimen temperature (°C) | Time from room temperature (h) | Time from previous test temperature (h) |
|---|---|---|
| 4 | Overnight | Overnight |
| 20 | 1 | 3 |
| 40 | 2 | 2 |

Table 4.4 Number of cycles at different frequency

| Frequency (Hz) | Number of cycles |
|---|---|
| 10 | 100 |
| 1 | 20 |
| 0.1 | 15 |

During each testing, dynamic modulus and phase angle were recorded at each temperature for each specimen. The dynamic modulus master curves were then developed in accordance with AASHTO PP 61-13. The principle of developing dynamic modulus master curves is same as that for asphalt binder. The difference between them is the equations of shift factors and predicted dynamic modulus. The shift factors were computed using the Arrhenius equation, as expressed in Eq. (4.1).

$$\log \alpha_T = \frac{\Delta E_a}{19.14714}\left(\frac{1}{T} - \frac{1}{T_{ref}}\right) \tag{4.1}$$

where:

$\Delta E_a$ is the activation energy,

$T$ is the test temperature (°K), and

$T_{ref}$ is the reference temperature (°K).

Therefore, the reduced frequencies were then calculated using the Eq. (4.2). Also, the predicted dynamic modulus equation is a sigmoidal logistic model, as expressed in Eq. (4.3).

$$\log f_r = \log f + \frac{\Delta E_a}{19.14714}\left(\frac{1}{T} - \frac{1}{T_{ref}}\right) \tag{4.2}$$

$$\log|E^*| = \delta + \frac{(|E^*|_{max} - \delta)}{1 + e^{\beta + \gamma \log f_r}} \tag{4.3}$$

where:

$|E^*|$ is the dynamic modulus (psi),

$\delta$, $\beta$, and $\gamma$ are the fitting parameters,

$|E^*|_{max}$ is the limiting maximum asphalt mixture dynamic modulus (psi), as shown in Eq. (4.4), and

$f_r$ is the reduced frequency (Hz).

$$|E^*|_{max} = P_c\left[4.2 \times 10^6\left(1 - \frac{VMA}{100}\right) + 4.35 \times 10^5\left(\frac{VFA \times VMA}{10000}\right) + \frac{1 - P_c}{\frac{\left(1 - \frac{VMA}{100}\right)}{4.2 \times 10^6} + \frac{VMA}{4.35 \times 10^5 (VFA)}}\right] \tag{4.4}$$

where:

$VMA$ is the void in the mineral aggregate (%),

$VFA$ is the voids filled with asphalt (%), and

$$P_c = \frac{\left(20 + \frac{4.35 \times 10^5 (VFA)}{VMA}\right)^{0.58}}{650 + \left(\frac{4.35 \times 10^5 (VFA)}{VMA}\right)^{0.58}}.$$

The final form of dynamic modulus master curve equation is obtained by substituting Eq. (4.2) into Eq. (4.3).

$$\log|E^*| = \delta + \frac{(|E^*|_{max} - \delta)}{1 + e^{\beta + \gamma\left[\log f + \frac{\Delta E_a}{19.14714}\left(\frac{1}{T} - \frac{1}{T_{ref}}\right)\right]}} \tag{4.5}$$

In this study, the reference temperature was set to be 20°C (293.15°K). The initial fitting parameters of Eq. (4.5) were recommended: $\delta = 0.5, \beta = -1.0, \gamma = -0.5$, and $\Delta E_a =$

$200{,}000$. The optimization for the four parameters was performed using the Solver function in Microsoft Excel® until the squared errors between the logarithm of the average measured dynamic modulus and the average predicted dynamic modulus reached the minimum.

### 4.2.4 X-Ray CT analysis

X-ray CT was used to capture the microscopic structure of specimens. Specimens were scanned at an energy intensity of 225 kV without beam filtration. Binder content area ratio was analyzed based on the principle of intensity difference of different material in CT image. The pixels of aggregates tend to have the highest intensity value, while the pixels of air voids have the lowest value and the pixels of asphalt binder have the median values. Therefore, image thresholding method was used to separate a CT image into three phases: air voids, asphalt binder, and aggregates. Two thresholds, $(t_1,\ t_2)$, were selected as the boundaries to separate the intensity values of different phases in the CT image based on the minimization of the within-class variance. In this study, Eq. (4.6) was used to obtain the thresholds for dividing the image sections of air voids, asphalt binder and aggregates. $k \in (1,2,3)$ was used to characterize the three different phases in the asphalt mixture. $(L_{\mathrm{k}},\ U_{\mathrm{k}})$ indicates the intensity value range of pixels in each phase. The value ranges for air voids, asphalt binder and aggregates are $(0, t_1)$, $(t_1+1, t_2)$ and $(t_2+1, L-1)$, respectively. The number of intensity levels in the grayscale CT image is $L$, $i$ is the intensity level, $p_i$ is the probability of the occurrence of intensity level $i$ in the target image, and $q$ is a user-defined parameter. This method is very effective to separate air voids, aggregate and asphalt binder. Figure 4.3 presents the CT image before and after processing with thresholding method. In this figure, pink, blue, and green color represent the aggregate, asphalt binder, and air voids, respectively.

$$\sigma_w{}^2 = \sum_{k=1}^{3} \sum_{i=L_k}^{U_k} (\varpi_k)^{q-1}(i-\mu_k)^2 p_i \tag{4.6}$$

In which,

$$\varpi_k = \sum_{i=L_k}^{U_k} p_i\,, \quad k = 1,2,3 \tag{4.7}$$

$$\mu_k = \frac{1}{\varpi_k}\sum_{i=L_k}^{U_k} i p_i\,, \quad k = 1,2,3 \tag{4.8}$$

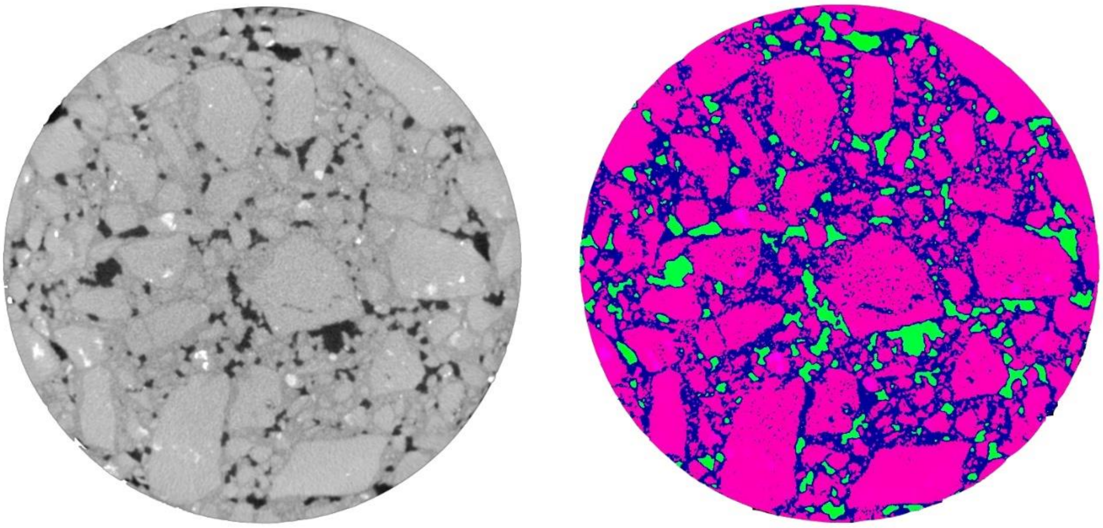
(a) (b)

Figure 4.3 The CT image before and after processing with thresholding method: (a) original image, and (b) processed image

## 4.3 **Results and discussion**

### 4.3.1 Effect of aging conditions on dynamic modulus

Using time-temperature superposition (TTS) principle, dynamic modulus master curves at a reference temperature of 20℃ were developed, as shown in Figure 4.4. The $|E^*|$ values increased with the increase of frequency. The $|E^*|$ values of aged specimens in Group 1 were significantly greater than those of unaged specimens due to asphalt aging. Compared with the $|E^*|$ value of unaged specimen at 20°C and 1 Hz, the $|E^*|$ value of aged specimen was increased by 95.3%. For Group 2 and 3, the |E*| values of aged specimens were less than those of unaged specimens. For Group 2, the difference between unaged and aged specimens at the high temperature was greater than that at the low temperature and intermediate temperatures. Overall, |*E**| values of aged specimens were decreased by 7.8% to 10.4% in comparison to unaged specimens. For Group 3, |*E**| values of aged specimens were slightly less than those of unaged specimens, decreased by 4.5-10.6% in comparison to unaged specimens. For Group 2 and 3, the confining pressure likely had an adverse effect on |*E**| values. However, |*E**| values of aged specimens in Group 2 are obviously lower than those in Group 3, even though the confining pressure in Group 2 is half of that in Group 3. It appears that both pressure and temperature play important roles in |*E**| values of compacted asphalt mixtures. Figure 4.4 (d) indicates that |*E**| values of specimens after being aged at 40°C were greater than those of unaged specimens, and they were continuously increased after each aging treatment. For example, comparing with |*E**| value of unaged specimens at 20°C and 1 Hz, |*E**| values of the specimens after being aged for 7 days, 14 days, 21 days, and 28 days were increased by 24.2%, 37.1%, 79.3%, and 101.8%, respectively. It also appears that specimens aged under pure oxygen environment at 40°C for 28 days can reach the similar aging level of specimens subjected to an aging condition of 85°C for 5 days.

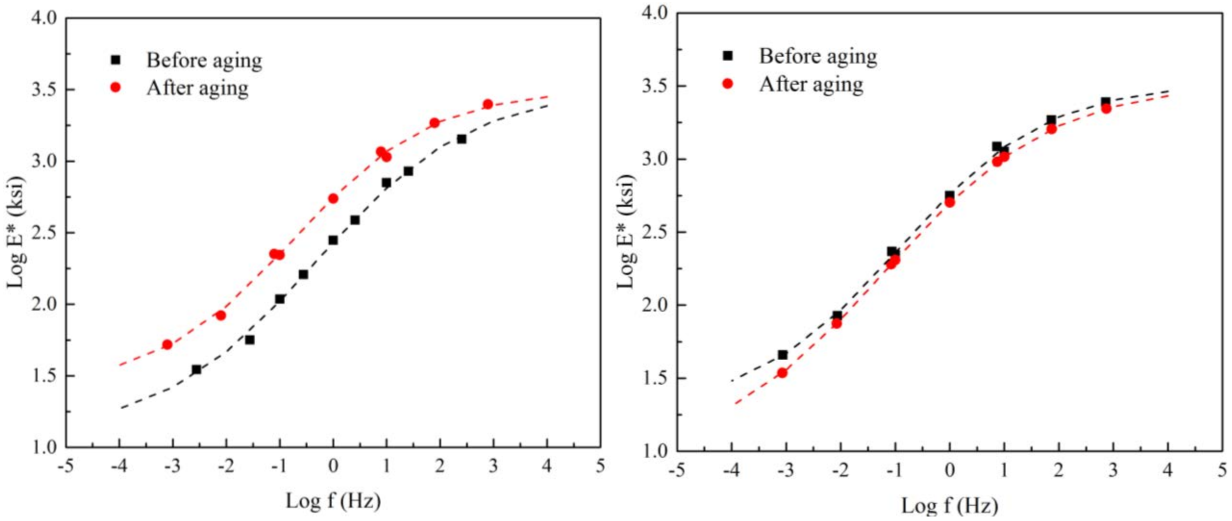

(a)

(b)

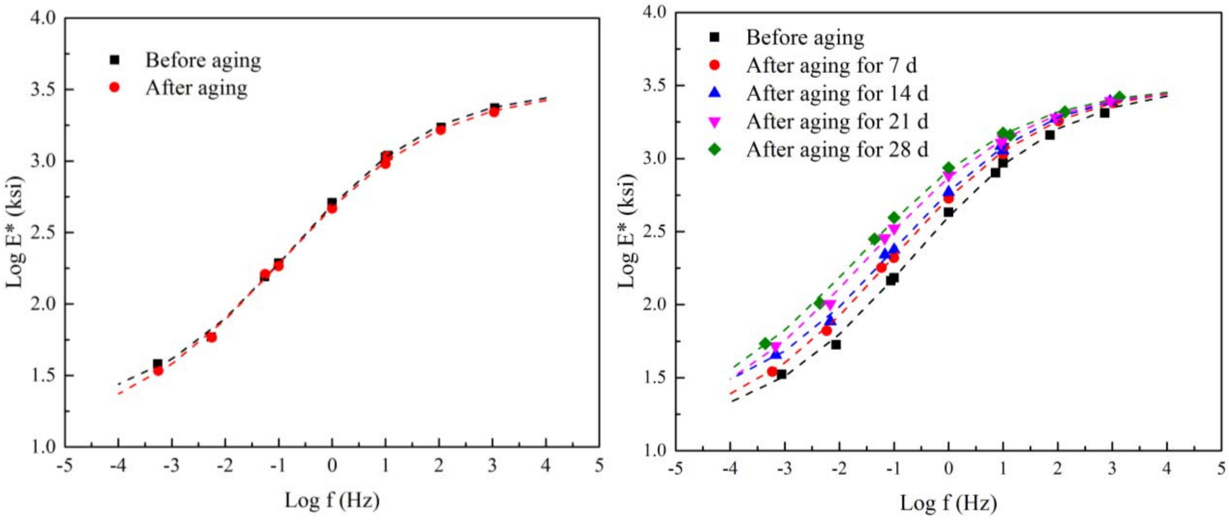

(c) (d)

Figure 4.4 Dynamic modulus master curves for four groups: (a) Group 1, (b) Group 2, (c) Group 3, and (d) Group 4

### 4.3.2 Factors influencing dynamic modulus

To examine the change in $|E^*|$ values of specimens after being aged, air voids of specimens before and after being aged were measured and calculated in accordance with AASHTO T 269-14. The following equation calculated the difference of air voids values between unaged and aged specimens. Table 4.5 lists the air voids of four groups of specimens before and after being aged.

$$V_{diff} = V_{aged} - V_{unaged} \tag{4.9}$$

where:

$V_{unaged}$ = air voids of unaged specimens,

$V_{aged}$ = air voids of aged specimens, and

$V_{diff}$ = difference of air voids between unaged and aged specimens.

Table 4.5 indicates that the air voids of aged specimens in Group 2 and 3 increased by about 1.0% compared with those of unaged specimens. It is likely due to two reasons. One is that air pressure in the autoclave is greater than that of closed pores inside the specimens in the initial of aging treatment, and thereby specimens in the autoclave are gradually compressed until the pressures between closed air voids in specimens and air in the autoclave reach a balance. After specimens are taken out from the autoclave, the pressures of the closed pores in the specimens are greater than atmospheric pressure; therefore, the volumes of specimens expand. This explanation can be verified by specimen dimension, as shown in Table 4.6. The diameter and height of specimens gradually increased over time, indicating that the pressure has a significant effect on the volume of specimens. During these processes, some micro-cracks might be generated in the specimens. In addition, asphalt binder at 60°C is softer than that at 40°C, and thus micro-cracks form more easily at high temperatures. Hence, Group 2 is more affected as compared with Group 3. Another reason is that the differential pressure might result in the transformation of closed pores to opened pores in specimens. In summary, micro-cracks and the increase of air voids are the main factors leading to a decrease in $|E^*|$ values of aged specimens in comparison with the unaged ones.

It is also shown in Table 4.5 that the air voids of aged specimens in Group 1 and 4 were slightly lower than those of unaged specimens. This is likely caused by the loading applied to the specimen during the dynamic modulus test. The trend is consistent with the research results reported by Rowe et al. [127].

Table 4.5 Air voids of four groups of specimens before and after aging

| Group No. | Air voids (%) | | | | $V_{diff}$ (%) |
|---|---|---|---|---|---|
| | Unaged specimen | | Aged specimen | | |
| | Average | Std. | Average | Std. | |
| 1 | 6.5 | 0.1 | 6.3 | 0.1 | -0.2 |
| 2 | 4.8 | 0.1 | 5.8 | 0.2 | 1.0 |
| 3 | 6.1 | 0.2 | 7.2 | 0.4 | 1.1 |
| 4[a] | 6.0 | 0.2 | 5.8 | 0.2 | -0.2 |

*Note: [a] The air void was measured for the unaged and aged specimens for seven days.*

Table 4.6 The diameter and height of specimens from Group 3 after taking them out from the autoclave

| Specimens No. | Measuring in 2 hours | | | | Measuring in 24 hours | | | | Diff. (mm) | |
|---|---|---|---|---|---|---|---|---|---|---|
| | Diameter （mm) | | Height (mm） | | Diameter （mm) | | Height (mm） | | | |
| | Average | Std. | Average | Std. | Average | Std. | Average | Std. | Diameter | Height |
| 1 | 99.35 | 0.35 | 150.95 | 0.36 | 100.15 | 0.21 | 151.88 | 0.43 | **0.80** | **0.93** |
| 2 | 99.00 | 0.27 | 152.10 | 0.29 | 99.88 | 0.31 | 153.05 | 0.23 | **0.87** | **0.95** |
| 3 | 99.10 | 0.07 | 151.73 | 0.31 | 100.00 | 0.16 | 152.63 | 0.26 | **0.90** | **0.90** |
| 4 | 99.13 | 0.13 | 151.03 | 0.43 | 100.10 | 0.21 | 152.05 | 0.56 | **0.97** | **1.02** |

### 4.3.3 X-ray CT analysis

One specimen from Group 1 and one from Group 4 were selected to examine the detailed microscopic structure before and after aging with X-ray CT. Figure 4.5 plots the asphalt binder area ratios before and after aging for the specimen in Group 1. The peak position of asphalt binder after aging was lower than that before aging, indicating that the asphalt binder tends to flow down at 85°C. There are no obvious changes for the specimen in Group 4.

CT images in the same position before and after aging were also examined manually. Several examples are shown in Figure 4.6. It can be observed that the morphologies of air voids before aging (marked with red circles) are different from those after aging. Figure 4.7 shows the CT images of Group 4 specimen in the sample position before and after aging for seven days. The morphologies of air voids before aging apparently matched very well with those after aging, indicating that the potential flow of asphalt binder at this temperature is not noticeable and hence can be safely neglected. Therefore, a method in Group 4 truly reflects the asphalt aging, without being compounded with the changes of macroscopic volumetric characteristics.

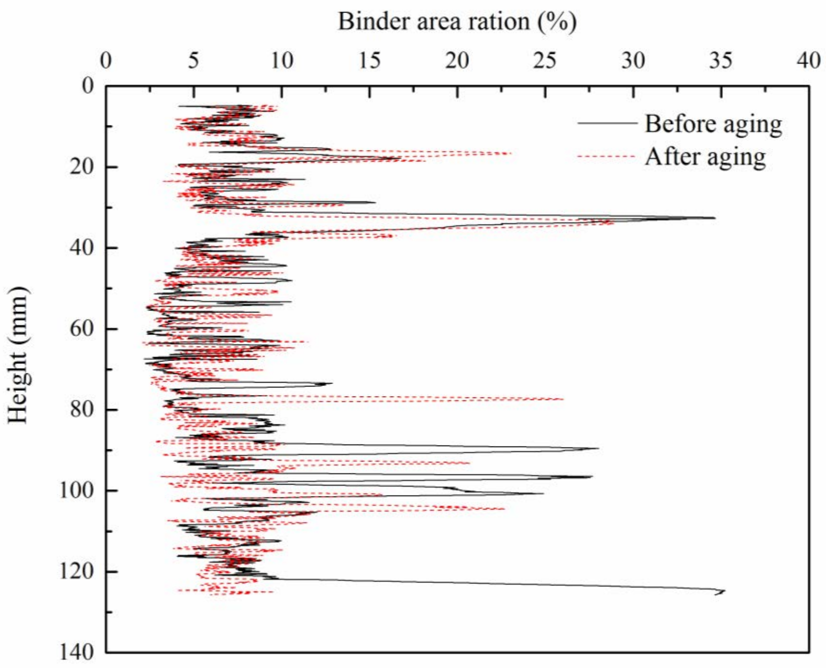

Figure 4.5 Asphalt binder contents before and after aging

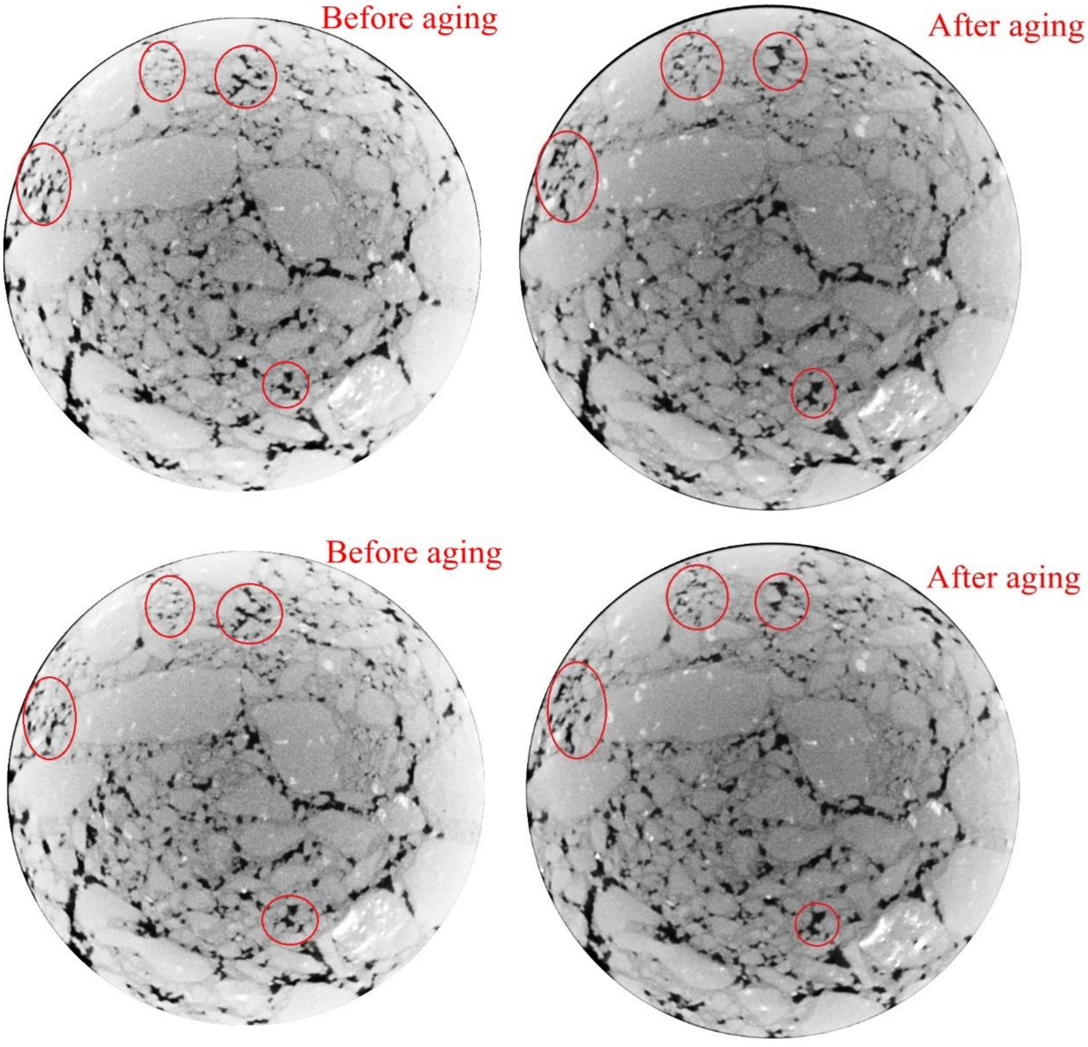

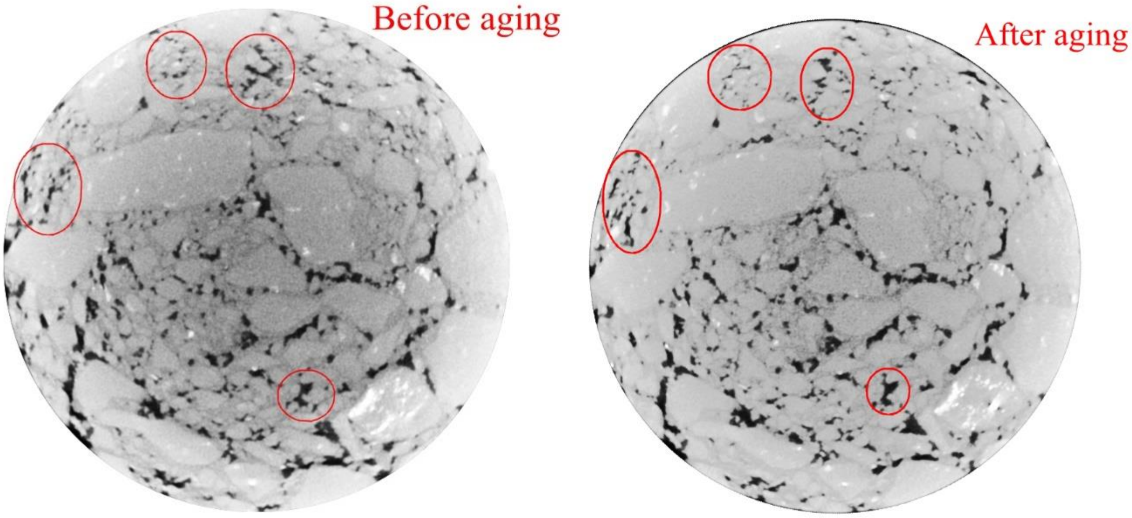

Figure 4.6 Six CT images of Group 1 before and after aging

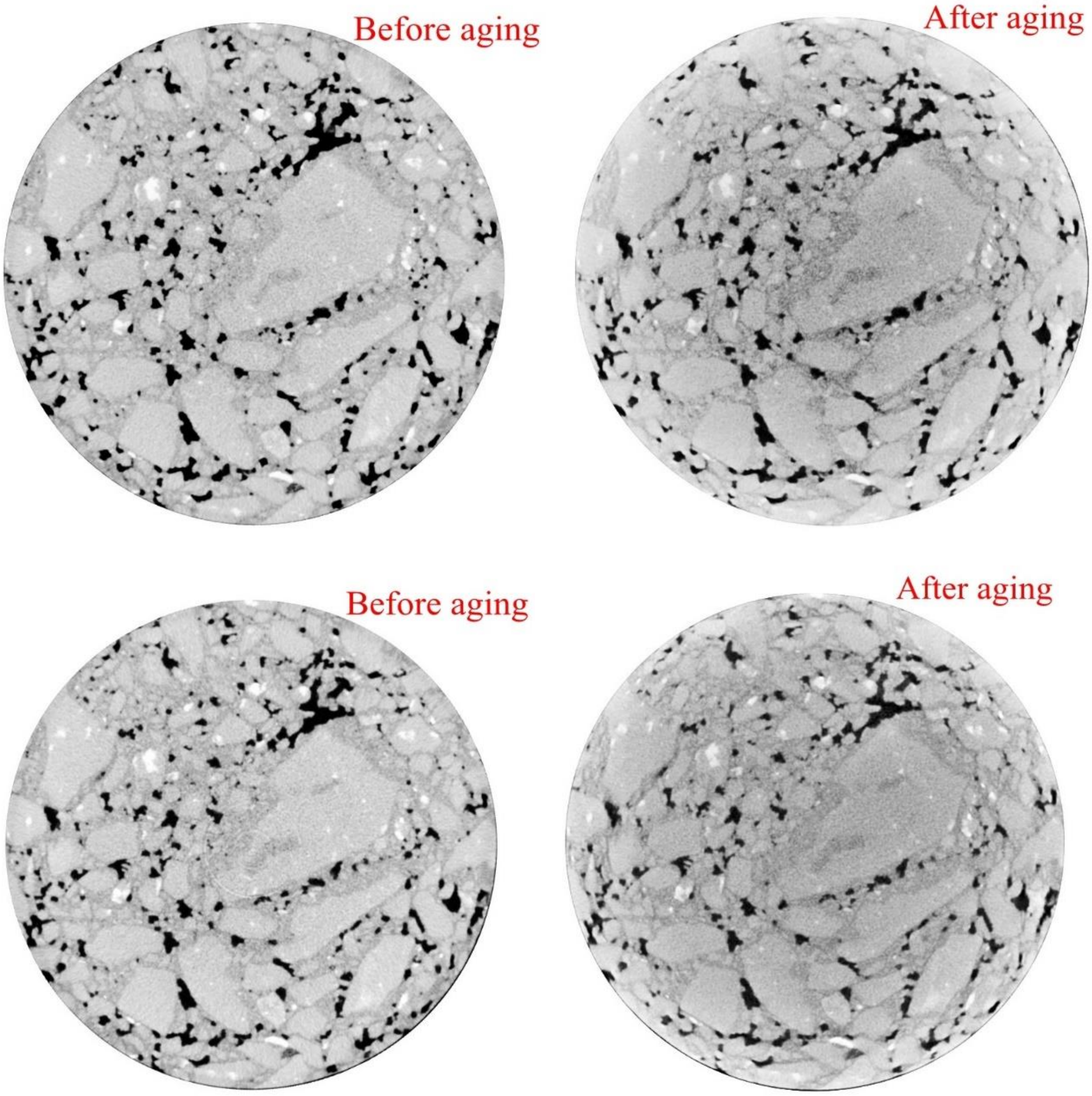

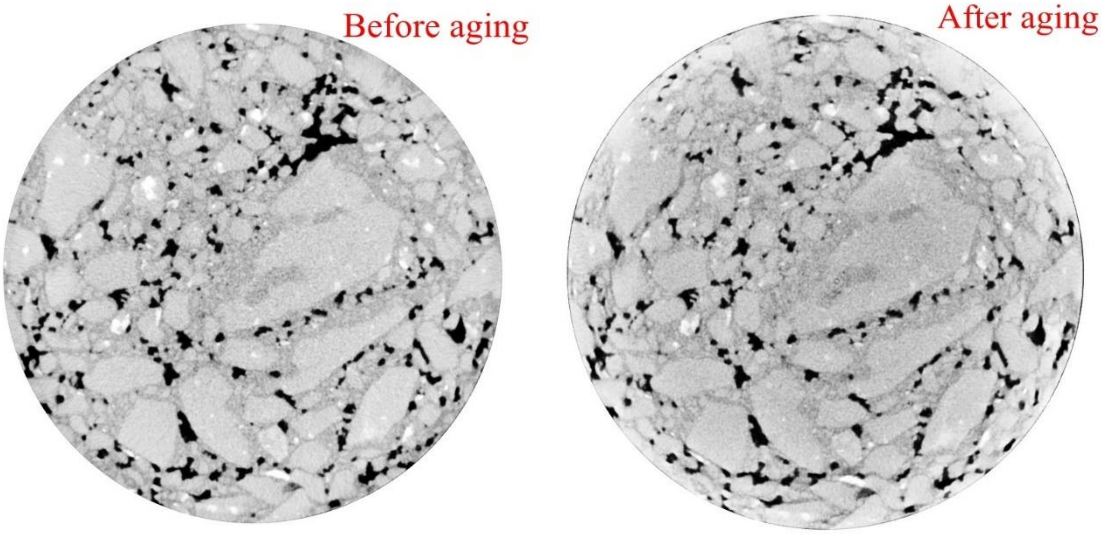

Figure 4.7 Six CT images of Group 4 before and after aging

## 4.4 **Conclusions**

Identifying a proper method to simulate the long-term aging for compacted asphalt mixtures is necessary for mechanistic-based pavement analysis and mixture design optimization. This study investigated the effect of different aging conditions on compacted asphalt mixtures. The study found that the use of air pressure to accelerate aging process damages the integrity of specimens by reducing their dynamic modulus values and negatively affecting their dimensions. The use of elevated temperature (e.g., 85°C for five days) to accelerate aging process apparently does not affect the overall integrity of compacted asphalt mixtures if specimens are laterally confined. However, X-ray CT images suggest that the internal void characteristics of specimens are subject to changes because high temperatures facilitate the flow of asphalt binders under gravity. The placement of compacted asphalt mixtures in a pure oxygen environment without applied pressure and at 40°C (below the softening point of the base asphalt) results in the best integrity of aged specimens at both the microscopic and macroscopic levels. The only concern for this process is that it takes about 28 days for specimens to reach an aging state similar to the aging state of specimens being treated at 85°C for five days.

# CHAPTER 5. THE RELATIONSHIP BETWEEN THE RHEOLOGICAL AND CHEMICAL PROPERTIES OF RECOVERED ASPHALT

## 5.1 Introduction

As an organic material, asphalt is subjected to oxidative aging that has an essential impact on nearly all critical performances of hot mix asphalt (HMA) [10]. During the process of asphalt binder oxidation, it is found that aromatic fractions decrease, first becoming resins and then asphaltene [27]. This process is due to oxygen functional groups forming in the asphalt molecules, resulting in a reduction in resins and aromatic fractions and an increase n asphaltene fractions [28-31]. The increase in asphaltene fractions has been shown to be related to the increase in asphalt viscosity [9,10]. Furthermore, the asphalt becomes stiffer and more brittle, leading to higher stresses in the asphalt, making the pavement more susceptible to cracking under a given deformation [5, 6, 14]. Moreover, Petersen provided strong evidence that ketone and sulfoxide formation are two major contributors to the increase in viscosity of asphalt binder [128, 129].

Hence, in this chapter, the rheological and chemical properties of recovered asphalt binders were evaluated by using DSR and FTIR tests. First, the new extraction method was validated by using DSR and FTIR tests. Next, the change in sulfoxides and ketones were investigated as a function of aging time, and the effect of oxidative aging on the rheological properties of the asphalt binders was then evaluated. Finally, a relationship between rheological and chemical properties of the recovered asphalt binders was analyzed.

## 5.2 Material and methods

### 5.2.1 Material

In this chapter, asphalt binder was extracted and recovered from the specimens for dynamic modulus test.

### 5.2.2 Micro-sampling, and micro-extraction and recovery methods

The micro-sampling, and micro-extraction and recovery methods are detailed in section 3.2.2.

### 5.2.3 DSR test

A frequency sweep test was performed in a controlled strain model using a DSR (Anton Paar MCR702, see Figure 5.1). All tests were conducted at various temperatures from -20°C to 40°C in 6°C intervals. As mentioned previously, there is a relationship between the loading frequencies used in the dynamic shear mode for asphalt binders and used in dynamic compression mode for asphalt mixtures. Therefore, the data was sampled at the following 13 unique frequencies: 0.016 Hz, 0.08 Hz, 0.1 Hz, 0.159 Hz, 0.251 Hz, 0.398 Hz, 0.796 Hz, 1 Hz, 1.59 Hz, 2.51 Hz, 3.98 Hz, 6.31 Hz, and 10 Hz. Furthermore, the linear viscoelastic range was determined before the frequency sweep test, which ensures that the test was performed in the range. The test utilizes 4 mm parallel plates with 1.75mm gap recommended by Western Research Institute (WRI) since extracted binders are not enough for conducting the test with 8mm parallel plates [130]. The test method with 4 mm plates requires only about 150 mg of asphalt binders to load and trim the sample. Moreover, the excellent reproducibility was found with results collected on 8mm parallel plates at low and intermediate temperatures [131].

Figure 5.1 DSR apparatus (Anton Paar MCR702)

After the test, the master curve was developed at the reference temperature of 20℃ using the time-temperature superposition principle. The shifting factor was utilized to transform the frequency at other temperatures into that at the reference temperature. The general shift factor equation is expressed in Eq. (5.1).

$$\alpha_T = \frac{f_r}{f} \tag{5.1}$$

where $\alpha_T$ is the shift factor, $f$ is the reduced frequency at a reference temperature (Hz), and $f_r$ is the tested frequency (Hz).

There are many methods to determine the shift factor. In this study, Williams, Landel, and Ferry (WLF) equation was chosen and is expressed in Eq. (5.2).

$$\log \alpha_T = \frac{-C_1(T-T_{ref})}{C_2+(T-T_{ref})} \tag{5.2}$$

where $C_1$ and $C_2$ are constant, $T$ is the tested temperature (°C), and $T_{ref}$ is the reference temperature (°C).

Combining Eqs. (5.1) and (5.2), the reduced frequencies at other tested temperatures were calculated according to Eq. (5.3).

$$\log f_r = \log f - \frac{C_1(T-T_{ref})}{C_2+(T-T_{ref})} \tag{5.3}$$

Next step was to predict complex shear modulus values with reduced frequencies by using the predictive formula which developed based on the data tested at the reference temperature. Then, the Solver function in Microsoft Excel was used to obtain the optimum values of $C_1$ and $C_2$ with non-linear least squares regression techniques. The procedure consisted of minimizing the sum of square error (SSE) between the measured data and predicted data, as shown in Eq. (5.4). When no further changes were observed, the iteration process was terminated and the final values quoted for the coefficients.

$$\text{SSE} = \sum \frac{\left(V_m - V_{pre}\right)^2}{(V_m)^2} \tag{5.4}$$

where $V_m$ is the measured value, and $V_{pre}$ is the predicted value.

### 5.2.4 FTIR-ATR test

A Bruker Tensor Π spectrometer (see Figure 5.2) was used to conduct the infrared test to ensure that the solvent had been completely removed and investigate the aging levels of recovered asphalt binders. The background check scan and sample scan (two replicates) were executed with 32 scans and a resolution of 4 $cm^{-1}$ over wavenumbers from 4000 $cm^{-1}$ to 600 $cm^{-1}$. A computer software "OPUS" was then utilized to process the Attenuated Total Refraction (ATR) interferogram into an absorption spectrum through Fourier Transformation function.

Figure 5.2 Bruker Vertex 70 FTIR spectrometer

## 5.3 **Results and discussion**

### 5.3.1 Effect of new micro-extraction and recovery method on chemical and rheological properties of the binder

As stated previously, ketones and sulfoxides are two major oxidation products. To investigate the changes in the two compounds with increasing aging time, the IR method was utilized on recovered asphalt binders of three types of asphalt mixtures, as this method is currently often used for quantitative studies of asphalt binders. The micro-extraction and recovery method was detailed in section 3.2.2. After evaporating dichloromethane from asphalt binders on a hot plate under nitrogen environment for half an hour at 100°C, the asphalt binders were first tested using an FTIR-ATR apparatus to determine whether the solvent was thoroughly evaporated under these conditions. Figure 5.3 shows the infrared spectrum of the solvent and recovered asphalt binders before and after aging. It can be seen that there were no peaks at 703 $cm^{-1}$, 731 $cm^{-1}$, and 1264 $cm^{-1}$ for the recovered asphalt binders before and after aging, indicating that the solvent had been completely removed from the asphalt binders during the extraction process.

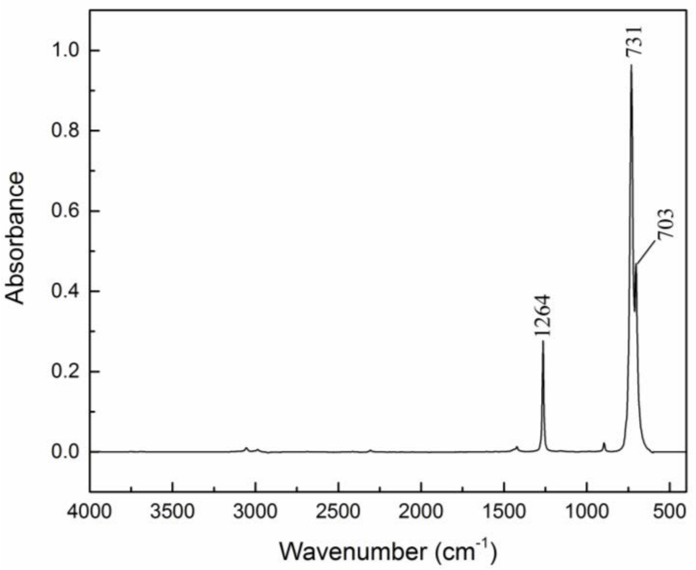

(a)

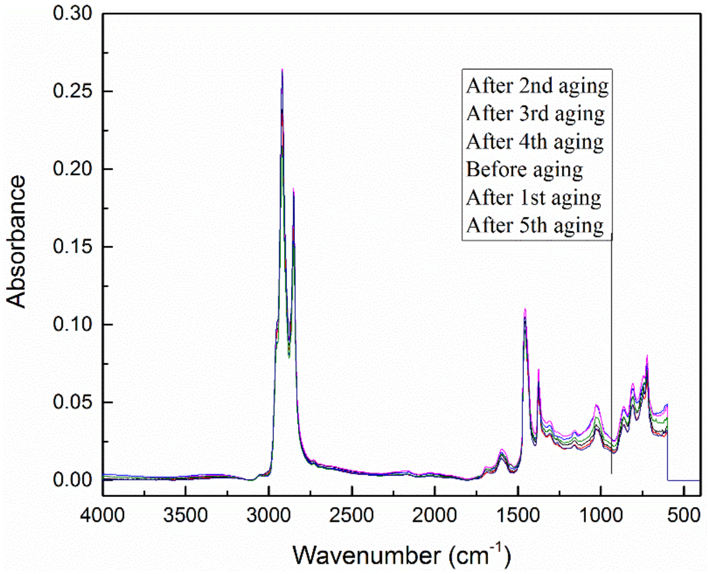

(b)

Figure 5.3 The infrared spectra of (a) the solvent (Dichloromethane), and (b) recovered asphalt binders before and after aging

The original base asphalt (60/70 pen) was utilized to examine the effect of the new micro-extraction and recovery method on the rheological properties of asphalt binders. Hence, the base asphalt was treated according to the new micro-extraction and recovery method, as shown in Figure 5.4. The master curve of the original asphalt matched well with that of the recovered asphalt, indicating that the new micro-extraction and recovery method does not influence the rheological properties of asphalt and is reliable in recovering asphalt binder from asphalt mixtures.

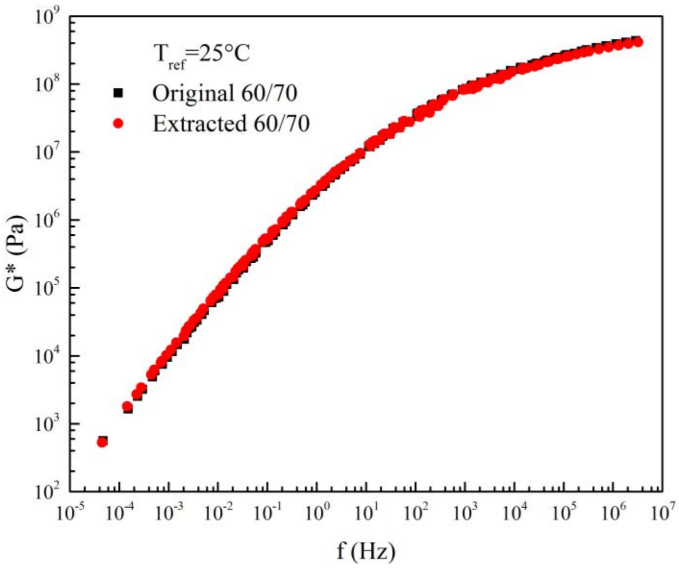

Figure 5.4 Master curves of *G** of original and recovered asphalt (60/70 pen)

Based on the results above, the new micro-extraction and recovery method described in section 3.2.2 is a viable alternative to standard drilling and extraction with the advantages as follows.

(1) The improved micro-extraction and recovery method is efficient in recovering asphalt binders from asphalt mixtures, particularly for a small amount of sample. The standard recovery method requires distilling the solvent in a flask, and a certain amount of recovered asphalt binder will adhere to the inside of the flask. Thus, it is difficult to pour the asphalt binder from the flask if its amount is small.

(2) The new micro-extraction and recovery method reduces cost by simplifying the extraction and recovery apparatus since the new method needs only a centrifuge.

### 5.3.2 Effect of testing geometry on the rheological properties of asphalt binder

The DSR test used 4 mm parallel plates with a 1.75 mm gap, recommended by WRI [130]. WRI found that there is a good match between the master curves of *G** values measured with 4 mm and 8 mm plates [130]. In this study, this relationship was verified with unaged base asphalt (60/70 pen). A frequency sweep test was conducted from 0.1 Hz to 10 Hz at temperatures ranging from -20°C to 40°C in 6°C intervals. The machine compliance was automatically adjusted through the software parameters. The resulting master curves of *G** values measured with 4 mm and 8 mm diameter plates for unaged asphalt (60/70 pen) are visualized in Figure 5.5. It is clear that the master curve of *G** values measured with 4 mm diameter plates matched well with that measured with 8 mm diameter plates, indicating that it is valid that DSR tests are conducted with 4 mm diameter plates.

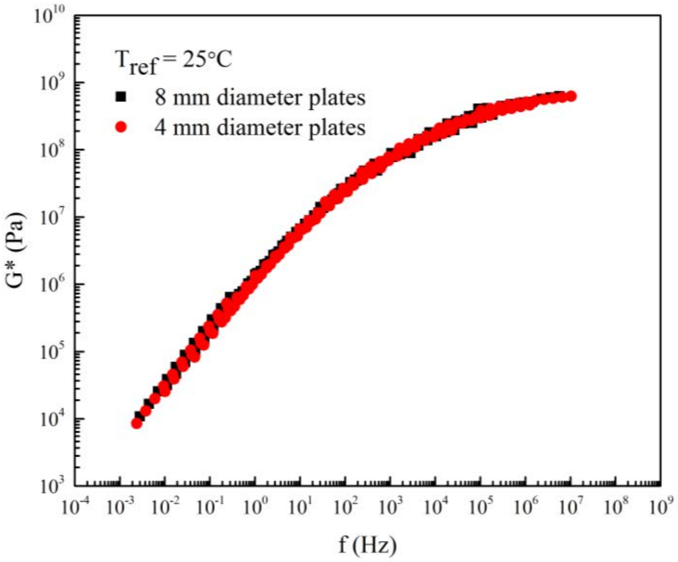

Figure 5.5 Master curves of *G**measured with 4 mm and 8mm diameter plates for unaged asphalt (60/70 pen)

### 5.3.3 Effect of asphalt mixture aging on the chemical compounds of asphalt binder

In this study, the investigation of asphalt mixture aging is carried out with recovered asphalt binders by semiquantitative analysis of the band area near 1700 $cm^{-1}$ (C=O) and 1030 $cm^{-1}$ (S=O) bonds. Asphalt binders were extracted and recovered from the mini-cores drilled from control specimens at different aging levels by using the new extraction method, and then the aging levels of asphalt binders were determined. The area ratios of ketones and sulfoxides were calculated according to the method proposed by Lamontagne *et al*. [83]. Figure 5.6 plots ketones and sulfoxides area ratios of recovered asphalt binders from WC, BC, and SMA mixtures as a function of aging time. The changes in ketones and sulfoxides occurred more quickly in the initial stage of oxidation. The rapid reaction ended before seven days of aging. After the initial oxidation spurt, the formation rates of ketones and sulfoxides slowed and became constant. In addition, the formation rate of sulfoxides was faster than that of ketones. These findings are consistent with the previous studies [10, 46]. The initial oxidation spurt is caused by reactive perhydroaromatic hydrocarbons reacting with oxygen and forming intermediate hydroperoxides, which can easily react with sulfides in asphalt binders to form sulfoxides since sulfides in asphalt binders are effective antioxidants [10, 16]. Moreover, sulfoxides formation is less sensitive to temperature change than ketones formation [16, 132]. The spurt is over when all of the reactive perhydroaromatic hydrocarbons are exhausted. Then, the ketones and sulfoxides form at a nearly constant rate. It is also noteworthy that area ratios of sulfoxides are much greater than those of ketones. This might be caused by the following two reasons: One reason is that the asphalt (60/70 pen) used in this study contains a high sulfur content and sulfur competes for hydroperoxide ketone precursors. Thus, sulfoxides are formed in greater quantities than ketones [16, 22]. Moreover, the ratios of sulfoxides to ketones formed at high oxygen concentrations are independent of oxidation temperature [16]. The other reason is that physicochemical effects prevent ketone formation at low temperatures [16]. In addition, it can be observed that the area ratios of sulfoxides and ketones were greatest for WC mixture followed by BC mixture and lastly SMA mixture, indicating that aggregate gradation has a direct effect on the aging susceptibility of compacted asphalt mixtures.

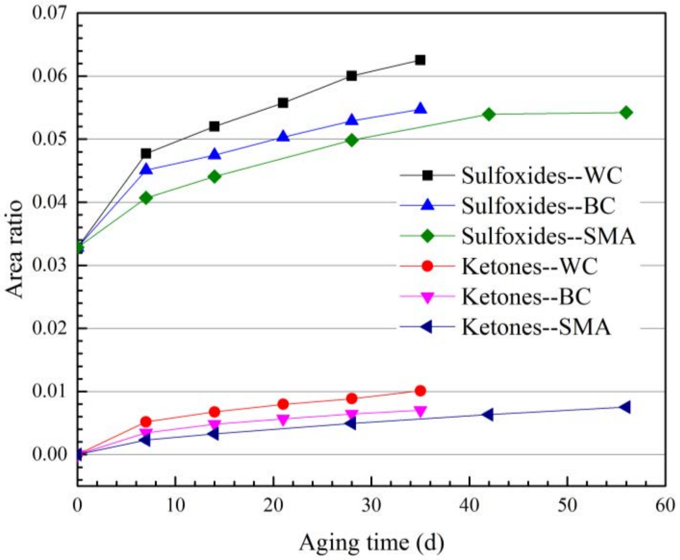

Figure 5.6 Oxidation products formed as a function of time for recovered asphalt binder in WC, BC, and SMA mixtures

### 5.3.4 Effect of asphalt mixture aging on the rheological properties of asphalt binder

The asphalt binder was extracted and recovered according to the new micro-extraction and recovery method described in section 3.2.2. Then, a frequency sweep test was conducted at various temperatures from -20°C to 40°C at 6°C intervals. The master curves of the three mixture types are shown in Figure 5.7. The complex shear modulus ($G^*$) values of the three mixture types at each aging level were similar to each other at high frequencies (or low temperatures), indicating that the aging does not have a significant effect on the rheological properties of asphalt binders in compacted asphalt mixtures at low temperatures. The $G^*$ values of recovered asphalt binder at low frequencies (or high temperatures) increased with aging time. Moreover, the difference between the $G^*$ values before and after aging increased as the testing temperature increased. In addition, the $G^*$ values of recovered asphalt binder after seven days of aging increased compared with those before aging while the $G^*$ values exhibited a slight increase with increasing aging time. This phenomenon agreed well with the trend of FTIR results. This phenomenon is caused by asphalt binder rapidly oxidizing during the initial stage of oxidation, which was followed by a slower, nearly linear oxidizing rate.

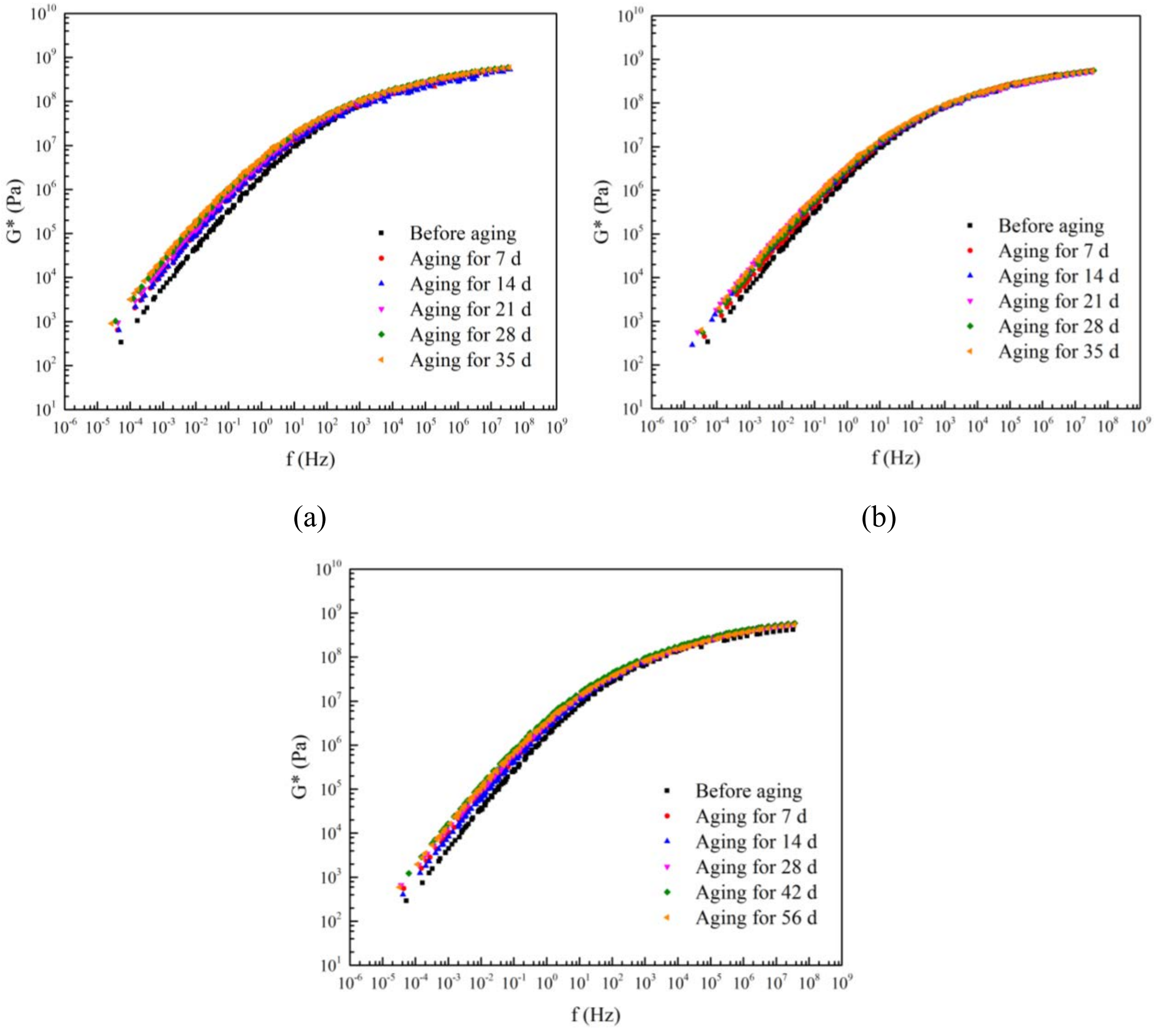

(a) (b)

(c)

Figure 5.7 The master curves of three mixture types: (a) WC, (b) BC, and (c) SMA

### 5.3.5 The relationship between functional groups and rheological properties

Earlier studies found that ketone formation was a major contributor to asphaltene formation during the oxidation period and that asphaltene was proven to increase the viscosity through oxidation [45, 106]. However, viscosity significantly increases with aging time when sulfoxides are formed in substantially greater quantities than those of ketones, especially in high-sulfur asphalt or for asphalt oxidation at low temperatures [10, 46, 129]. Petersen (2011) provided strong evidence that sulfoxide formation is also a major contributor to the increase in asphalt viscosity, since the rate of free radicals, produced by the thermal decomposition of the perhydroaromatic hydroperoxides, is immensely reduced at low temperatures [128].

The dynamic viscosity values of recovered asphalt binders were taken from the results of the frequency sweep test at 0.1 rad/s and 40ºC. The angular frequency is very low and created a near-zero shear rate. Thus, the dynamic viscosity had approximately zero shear viscosity. Figure 5.8 plots the dynamic viscosity as a function of aging time for the three types of compacted asphalt mixtures. With a logarithmic scale, the dynamic viscosity rapidly increased in the initial stage of aging which was followed by an increase at a nearly constant rate. This finding was consistent with previous studies [128, 133]. Additionally, the dynamic viscosity of WC mixture was apparently greater than those of BC and SMA, which were approximately equal, indicating that aggregate gradation has a significant effect on the aging susceptibility of compacted asphalt mixtures. This finding agreed with the results of the area ratios of sulfoxides and ketones, which were functions of aging time.

Earlier studies found that there is an apparent relationship between sulfoxides and ketones, and log viscosity [128]. The relationship was validated in this study. Figure 5.9 shows the relationship between the logarithmic dynamic viscosity and the sulfoxide and ketone formations for the three mixture types. The logarithmic dynamic viscosities had excellent linear correlations with the area ratios of sulfoxides and ketones for the three mixture types, indicated by very high $R^2$ values. It could also be found that the rapid viscosity increase is due to the sulfoxide formation of compacted asphalt mixture aging under an oxygen atmosphere at 40°C.

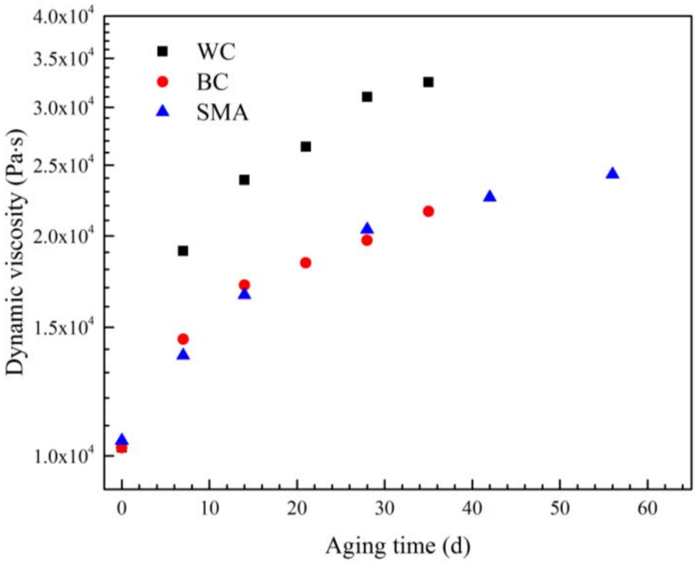

Figure 5.8 The dynamic viscosity as a function of aging time for three mixture types

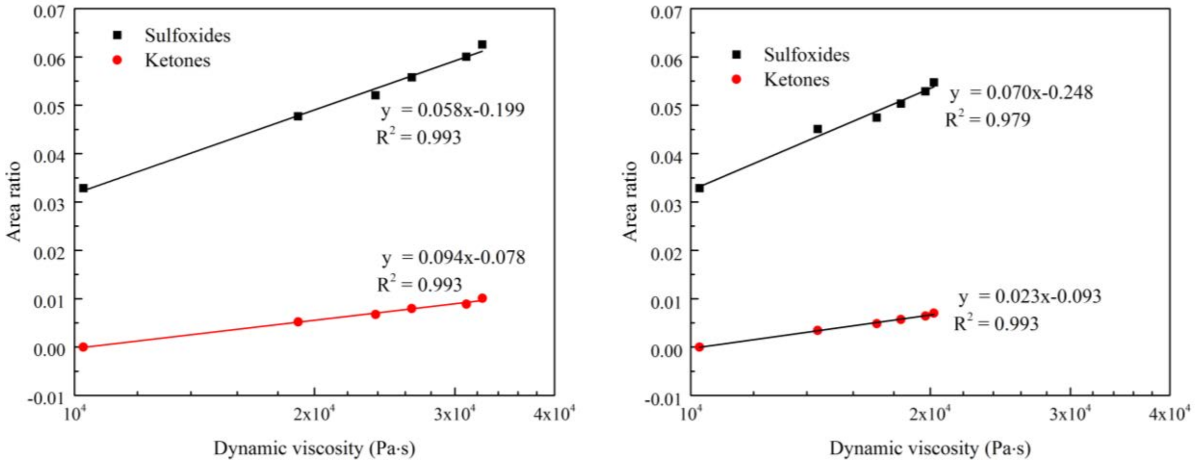

(a) (b)

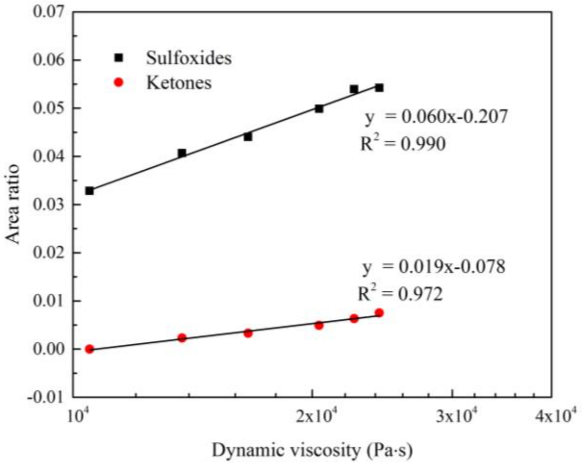

(c)

Figure 5.9 The relationship between dynamic viscosity and the formation of sulfoxides and ketones for three mixture types: (a) WC, (b) BC, and (c) SMA

## 5.4 **Summary and conclusions**

Based on the analysis presented in this chapter, the following conclusions are drawn:

(1) The new micro-extraction and recovery method is reliable in recovering asphalt binders from asphalt mixtures and does not influence the chemical and rheological properties of asphalt binders.

(2) The 4 mm diameter plates with a 1.75 mm gap are an efficient and reliable geometry to measure the rheological properties of asphalt binders, particularly for a low amount of asphalt binders, since this method requires only approximately 25 mg of asphalt binder.

(3) Sulfoxides and ketones rapidly form during the first aging cycle of compacted asphalt mixtures and then increase at a nearly constant rate. Moreover, the formation rate of sulfoxides is significantly greater than that of ketones under an oxygen atmosphere at 40ºC. In addition, aggregate gradation has a direct effect on the aging susceptibility of compacted asphalt mixtures.

(4) The increasing rates of $G^*$ values of recovered asphalt binders decrease with increasing the aging time as asphalt binders are rapidly oxidized during the initial stage of oxidation followed by a slower, nearly linear rate.

(5) The logarithmic dynamic viscosity shows the same trend with aging time as those of sulfoxide and ketone formations. Furthermore, the logarithmic dynamic viscosities have excellent linear correlations with the area ratios of sulfoxides and ketones for the three mixture types, indicated by very high $R^2$ values. In addition, it is validated that sulfoxide formation is a major contributor to viscosity increase at low temperatures.

In addition, the new micro-sampling, and micro-extraction and recovery methods include many advantages as follows.

(1) During the drilling process, the drill bit is cooled with water, so asphalt binders is not aged due to the high-speed revolutions of the diamond core drill.

(2) A small core of 10 mm diameter can be drilled to the desired depth using a handheld diamond core drill. Moreover, small holes will not damage the entire structure of asphalt pavement.

(3) Small cores can be cut into several slices to investigate the effect of pavement depth on the performance of asphalt binders.

(4) The micro-sampling method improves safety during site sampling by reducing the time that it takes to acquire the sample and not exposing the drill operator to traffic.

(5) The new micro-extraction and recovery method is efficient to recover asphalt binders from asphalt mixtures, particularly for a small amount of samples. The

standard recovery method requires distilling the solvent in a flask, and a certain amount of recovered asphalt binder will adhere to the inside of the flask. Thus, it is difficult to pour the asphalt from the flask if the amount of asphalt is small.

The new micro-sampling, and micro-extraction and recovery methods reduce cost by reducing the time required to drill cores in the field and simplifying the apparatus of extraction and recovery, as the new method requires only a centrifuge.

.

# CHAPTER 6. EFFECT OF OXIDATIVE AGING ON THE DYNAMIC MODULUS OF COMPACTED ASPHALT MIXTURE

## 6.1 Introduction

Dynamic modulus which is defined as the absolute value of the complex modulus is an important parameter in the design stage of flexible pavement. The MEPDG software uses dynamic modulus as an essential input at all three levels. Level 1 input requires the laboratory measured dynamic modulus values of compacted asphalt mixtures. However, it is not always feasible since the sample preparation, and experimental procedure will spend several days, and trained personnel are required for developing a master curve [134-136]. Moreover, the testing equipment is expensive. It is therefore essential to utilize a predictive model for estimating dynamic modulus of compacted asphalt mixtures. Several predictive models, Witczak 1-37A [137], Witczak 1-40D [138], Hirsch [139, 140], 2S2P1D [141], Al-Khateeb [142] and artificial neural network (ANN) [143] models, have been increasingly utilized for the estimation of dynamic modulus of compacted asphalt mixtures. These models mainly consist of asphalt binder properties (i.e., shear complex modulus, phase angle, and viscosity), aggregate gradation, loading frequency, or the volumetric properties of asphalt mixtures (i.e., air voids, effective asphalt binder content, voids in mineral aggregate, and voids filled with asphalt).

These models had shown high accuracies in predicting the dynamic modulus of compacted asphalt mixtures during the developing procedure, but numerous studies found that the accuracies of these models were not consistent and varied with the types and volumetric properties of asphalt mixtures [134, 135, 142-147]. For example, Witczak 1-37A model was considered more accurate at lower dynamic modulus (higher temperatures) than at lower temperatures according to Birgisson and Obulareddy's studies [134, 135]. However, other studies found that Witczak 1-37A model exhibited more accurate prediction of dynamic modulus at low and intermediate temperatures than at high temperatures [144, 148, 149]. It is therefore important to investigate the accuracies of predictive models of dynamic modulus for locally available materials.

The previous studies mainly used various aggregates, asphalt binders, and gradations in different countries and regions to investigate the accuracies of predictive models [135, 146, 150, 151]. Although dynamic modulus values in these previous studies were measured with specimens from the laboratory or the field, no published research evaluates the effect of aging level of compacted asphalt mixtures on the accuracies of the predictive models.

The objectives of this chapter were to assess the effect of aging on dynamic modulus of compacted asphalt mixtures and predictive models of dynamic modulus based on the conventional asphalt mixtures in Hong Kong.

## 6.2 **Review of the current predictive models**

The dynamic modulus is an important parameter in asphalt pavement design. However, the measurement of dynamic modulus in the laboratory is not always available because of the time-consuming process and costly equipment. Hence, the predictive models were developed to estimate the dynamic modulus of compacted asphalt mixtures in recent years. Most of them are empirical or semi-empirical and based on volumetric properties of mixture and binder characteristics. There are six common predictive models: Witczak 1-37A, Witczak 1-40D, Hirsch, AI-Khateeb, 2S2P1D, and Artificial Neural Network (ANN) models.

Since the ANN model requires a large data set and spends an amount of time to train the model, this study did not utilize this model to predict the dynamic modulus of compacted asphalt mixtures. The other models were detailed below.

### 6.2.1 Witczak 1-37A model

The original version of this model was developed by Shook et al. [152] and was further modified and refined by Fonseca and Witczak [153]. The NCHRP 1-37A model was developed in 1999 based on a combined database of the original Fonseca and Witczak model (1430 data points from 149 conventional asphalt mixtures) and an additional 1320 data points from 56 new mixtures including 34 mixtures with modified asphalt binder [137]. The model had been incorporated in earlier MEPDG version (V.0.7) and used to predict the dynamic modulus of compacted asphalt mixtures in level 2. The model is a function of aggregate gradation, air voids, effective binder content, loading frequency, and binder stiffness, as expressed in Eq. (6.1)

$$\begin{aligned}\log|E^*| &= -1.249937 + 0.029232\rho_{200} - 0.001767{\rho_{200}}^2 - 0.002841\rho_4 - 0.058097V_a \\ &- 0.802208\frac{V_{beff}}{\left(V_{beff} + V_a\right)} \\ &+ \frac{3.871977 - 0.0021\rho_4 + 0.003958\rho_{38} - 0.000017{\rho_{38}}^2 + 0.005470\rho_{34}}{1 + e^{(-0.603313 - 0.313551\log f - 0.393532\log\eta)}} \quad (6.1)\end{aligned}$$

where $|E^*|$ is the HMA dynamic modulus, $10^5$ psi; $\eta$ is the asphalt binder viscosity, $10^6$ poise; $f$ is the loading frequency, Hz; $V_a$ is the air voids in the mixture, volume %; $V_{beff}$ is the effective asphalt binder content, volume %; $\rho_{34}$ is the percentage of aggregates retained on the 3/4 inch sieve by total aggregate weight; $\rho_{38}$ is the percentage of aggregates retained on the 3/8 inch sieve by total aggregate weight; $\rho_4$ is the percentage of aggregates retained on No. 4 sieve by total aggregate weight (%); and $\rho_{200}$ is the percentage of aggregates retained on No. 200 sieve by total aggregate weight.

The extracted asphalt binders are not enough for viscosity test in the laboratory. Nevertheless, binder viscosity in Eq. (6.1) could be estimated with an empirical equation developed by Witczak and his colleagues according to Cox-Merz rule [154].

$$\eta = (|G^*|/\omega)(1/sin\delta)^{a_0+a_1\omega+a_2\omega^2} \tag{6.2}$$

where $\eta$ is the viscosity, Pa·s; $|G^*|$ is the complex modulus of asphalt binder, in shear, Pa; $\omega$ is the angular frequency, rad/s; $\delta$ is the phase angle, °; and $a_0$, $a_1$ and $a_2$ are the fitting parameters which are equal to 3.639216, 0.131373, and -0.000901, respectively.

### 6.2.2 Witczak 1-40D model

In 2006, Bari and Witczak proposed a new predictive model based on 7400 points from 346 different HMA mixtures [156]. These mixtures include different aggregate gradations, binder types (conventional, polymer modified and rubber modified), mix types (conventional unmodified and lime or rubber modified), and aging conditions (no aging, short-term aging, plant aging and field aging). Also, this model is also a function of aggregate gradation, air voids, effective binder content, loading frequency, and binder stiffness which is expressed as a function of $G^*$ and phase angle ($\delta$) instead of $\eta$ and $f$, as in the NCHRP 1-37A model. Moreover, the refined model was introduced under the NCHRP 1-40D project and then incorporated into version 1.0 of MEPDG software [138]. The new model is expressed in Eq. (6.3) [138]:

$$\log|E^*| = -0.349 + 0.754(|G^*|^{-0.0052}) \times \Big(6.65 - 0.032\rho_{200} + 0.0027{\rho_{200}}^2 + 0.011\rho_4 - 0.0001{\rho_4}^2 + 0.006\rho_{38} - 0.00014{\rho_{38}}^2 - 0.08V_a - 1.06 \times \frac{V_{beff}}{V_{beff}+V_a}\Big) +$$

$$\frac{2.558-0.032V_a+0.713\times\frac{V_{beff}}{V_{beff}+V_a}+0.0124\rho_{38}-0.0001\rho_{38}{}^2-0.009870\rho_{34}}{1+e^{(-0.7814-0.5785\log|G^*|+0.8834\log\delta)}} \quad (6.3)$$

where $|E^*|$ is the HMA dynamic modulus, psi; $|G^*|$ is the dynamic shear modulus of asphalt binder, in shear, psi; and the other variables are as defined above.

According to Bari and Witczak's finding, there was a relationship between the loading frequencies used in the dynamic shear mode for asphalt binder and used in dynamic compression mode for asphalt mixtures [155]. The relationship is given in Eq. (6.4).

$$f_c = 2\pi f_s \quad (6.4)$$

where $f_c$ and $f_s$ are the frequencies in compression mode and in shear mode, Hz, respectively.

### 6.2.3 Hirsch model

Christensen et al. developed a relatively simple model to predict $|E^*|$ values of compacted asphalt mixtures based on an existing version of the Hirsch model, which combined series and parallel elements of the phases [139]. A total of 206 observations, 18 different mixtures with eight different binders, and five different aggregates and gradations were utilized in the development of this model. The original model is given in Eq. (6.5).

$$|E^*| = P_c\left(4{,}200{,}000\left(1-\frac{VMA}{100}\right)+3|G^*|\left(\frac{VFA\times VMA}{10{,}000}\right)\right)$$
$$+(1-P_c)\Big/\left(\frac{1-\frac{VMA}{100}}{4{,}200{,}000}+\frac{VMA}{VFA\times 3|G^*|}\right) \quad (6.5)$$

$$P_c = \left(20+\frac{VFA\times 3|G^*|}{VMA}\right)^{0.58}\Big/\left(650+\left(\frac{VFA\times 3|G^*|}{VMA}\right)\right)^{0.58} \quad (6.6)$$

where $P_c$ is the contact factor; $VMA$ is the voids in mineral aggregate, in %; $VFA$ is the voids filled by asphalt, in %; and the other variables are as defined previously.

The Original Hirsch model is simpler than the Witczak models since the Original Hirsch model only utilizes three inputs ($VMA$,$VFA$, and $G^*$). Moreover, the Original Hirsch model had been verified by many researchers with generally good results [146, 156]. However, some studies found that the Original Hirsch model sometimes expressed poor accuracy [147, 157]. Therefore, Christensen presented a improved version of Hirsch model based on a database of 15 different mixtures with eight different aggregates and three different binders in 2015 [140]. The improved model considers the effect of applied strain level and aggregate specific gravity, which is expressed in terms of the aggregate modulus [140]:

$$|E^*| = P_c\left(H_6 G_{agg}^{H_7}\left(1-\frac{VMA}{100}\right)+3|G^*|\left(\frac{VFA\times VMA}{10{,}000}\right)\right) \tag{6.7}$$

where

$$P_c = H_1 + (1-H_1)\frac{\exp(H_2+H_3\ln(VFA/100\times|G^*|)+H_4 VMA/100+H_5\ln(\varepsilon))}{1+\exp(H_2+H_3\ln(VFA/100\times|G^*|)+H_4 VMA/100+H_5\ln(\varepsilon))} \tag{6.8}$$

*Note: VMA term in Equation (6.7) and (6.8) is different with the Equation (8) and (9) in the Christensen's paper [140]. The VMA term in new Hirsch model should be divided by 100 in comparison with the older Hirsch model.*

And $H_1$, $H_2$, $H_3$ … $H_7$ are coefficients fitted to the model, $G_{agg}$ is the aggregate modulus, $\varepsilon$ is the peak-to-peak strain, and other parameters are as defined previously.

### 6.2.4 2S2P1D model

The 2S2P1D (2 Springs, 2 Parabolic, and 1 Dashpot) model was developed through the generalization of the Huet-Sayegh model which consists of a linear dashpot in series with the two parabolic elements and the spring of rigidity. This model was reported that it could predict the linear viscoelastic properties of asphalt and asphalt mixtures [141, 158, 159]. The model is given Eq. (6.9) [141].

$$E^*(i\omega\tau) = E_0 + \frac{E_\infty - E_0}{1+\alpha(i\omega\tau)^{-k}+(i\omega\tau)^{-h}+(i\omega\beta\tau)^{-1}} \tag{6.9}$$

where $i$ is the complex number defined by $i^2 = -1$; $\omega$ is the pulsation, so that $\omega =$

$2\pi f$ ($f$ is the frequency); $k$ and $h$ are the exponents with 0<k<h<1; $\alpha$ is a constant; $E_0$ is the static modulus, which is the value of $E^*$ when $\omega$ tends towards zero ($\omega \rightarrow 0$), for ; $E_\infty$ is the glassy modulus, which is the value of $E^*$ when $\omega$ tends towards infinity ($\omega \rightarrow \infty$); $\beta$ is a constant, defined by $\eta = (E_\infty - E_0)\beta\tau$, $\eta$ is the Newtonian viscosity; and $\tau$ is the characteristic time, which only depends on the temperature. The $\tau$ value at temperature $T$ may be calculated by a WLF-type law:$\tau(\mathrm{T}) = \alpha_T(T)\tau_0$, where $\alpha_T(T)$ is the shift factor at temperature *T*; and $\tau_0$ is the characteristic time at a reference temperature and may be obtained by the equation: $\tau_0 = 1/f_{Cross}$, where $f_{Cross}$ is the crossover frequency at a reference temperature.

The shift factor at temperature T, $\alpha_T$, can be obtained through the WLF equation for asphalt binder.

$$\log \alpha_T = -\frac{C_1(T-T_{ref})}{C_2+T-T_{ref}} \qquad (6.10)$$

where $T_{ref}$ is the reference temperature; $C_1$ and $C_2$ are constant.

After determining the characteristic time of asphalt binder, $\tau_{binder}$, the characteristic time of asphalt mixture, $\tau_{mix}$, could be calculated with the following relation:

$$\tau_{mix}(T) = 10^\alpha \times \tau_{binder}(T) \qquad (6.11)$$

with $\mathrm{\alpha} = 2.66$ for any temperature “*T*.”

Before predicting $|E^*|$ values of compacted asphalt mixtures, the 2S2P1D model is calibrated with asphalt binder results at a reference temperature. The minimization is made at a reference temperature using the Excel Solver Tool. It comes:

Minimization of $\sum_{i=1}^{i=N}\left(\left(E_1^{exp}(\omega_i) - E_1^{pre}(\omega_i)\right)^2 + \left(E_2^{exp}(\omega_i) - E_2^{pre}(\omega_i)\right)^2\right)$ (6.12)

where $E_1^{exp}$ and $E_1^{pre}$ are respectively the real part of the experimental and predicted complex modulus. $E_2^{exp}$ and $E_2^{pre}$ are respectively the imaginary part of the experimental and predicted complex modulus.

### 6.2.5 AI-Khateeb model

AI-Khateeb et al. proposed a new model to predict $|E^*|$ values based on the findings from the Original Hirsch model [142]. This model is given as

$$|E^*| = 3\left(1 - \frac{VMA}{100}\right)\left(\frac{\left(90+10{,}000(|G^*|/VMA)\right)^{0.66}}{1{,}100+\left(900(|G^*|/VMA)\right)^{0.66}}\right)|G^*|_g \tag{6.13}$$

where $|G^*|_g$ is the dynamic shear modulus of asphalt binder at the glassy state (assumed to be 145,000 psi); and the other variables are as defined above.

Like the Hirsch model, this model was derived from the law of mixture where the material phases (aggregate, asphalt binder, and air) are arranged in a composite system in parallel. In another word, this model is a simpler expression of the Original Hirsch model. Furthermore, it should be noted that the model could avoid one of the drawbacks of Hirsch which could not accurately predict $|E^*|$ values at high temperatures or low frequencies [160].

## 6.3 **Materials and methods**

### 6.3.1 Materials and sample preparation

This study chose three mixture types typically used in Hong Kong. Two types were dense-graded mixture usually used in base and wearing course with a nominal maximum aggregate size of 28 mm and 20 mm (for short, BC and WC, respectively), respectively. One type was gap-graded (stone matrix asphalt, SMA) mixture with a nominal maximum aggregate size of 10 mm. All mixtures were produced using the base asphalt (60/70 pen) and granite.

Prior to compaction, loose mixtures were short-term aged in the forced-draft oven at

135°C for four hours in accordance with AASHTO R30. Each mixture type with seven replicates was compacted to a target air void using a gyratory compactor. These specimens in 150 mm diameter by 170 mm height were then drilled and sawed to obtain the samples of 100 mm diameter and 150 mm height, as shown in Figure 6.1. The gradations and volumetric properties of compacted asphalt mixtures are summarized in Table 6.1 and 6.2, respectively.

(a) (b)

Figure 6.1 The specimens prepared for $|E^*|$ test: (a) Before drilling and sawing, and (b) After drilling and sawing

Table 6.1 The gradation of compacted asphalt mixtures

| Sieve size (mm) | % Passing | | |
|---|---|---|---|
| | BC | WC | SMA |
| 37.5 | 100 | | |
| 28 | 96 | 100 | |
| 20 | 91 | 96.5 | |
| 14 | 79 | 89 | 100 |
| 10 | 68 | 79 | 96.5 |
| 5 | 49 | 62 | 37 |
| 2.36 | 35 | 47 | 28 |
| 1.18 | 25 | 34 | — |
| 0.6 | 18 | 25 | — |
| 0.3 | 13 | 17 | — |
| 0.15 | 9 | 12 | — |
| 0.075 | 5.8 | 7.8 | 11.5 |

Table 6.2 The volumetric parameters of compacted asphalt mixtures

| Property | BC | WC | SMA |
|---|---|---|---|
| $G_{mm}$ | 2.44 | 2.39 | 2.34 |
| $V_a$ (%) | 6.0±0.5 | 6.0±0.5 | 5.0±0.5 |
| VMA (%) | 16.1-16.7 | 17.9-18.5 | 18.8-19.8 |
| VFA (%) | 61.3-64.1 | 64.3-67.1 | 73.1-78.3 |
| Binder content (%) | 5.0 | 5.4 | 6.5 |

### 6.3.2 The long-term aging conditions

AASHTO R30 recommends that compacted specimens are placed in an oven at a temperature of 85°C for 120 h to simulate the long-term aging of compacted asphalt mixtures. However, the temperature is not suitable for unmodified asphalt binders because the binder in compacted asphalt mixtures might occur the drain-down phenomenon due to the low viscosity of the binder at the temperature higher than its softening points [6]. However, aging at low temperatures and the air is disadvantageous since specimens would take a longer time to achieve the same aging level in comparison with aging at high temperatures. Hence, in this study, the temperature of 40℃ was chosen as aging temperature since the temperature is lower than the softening points of 60/70 pen. Additionally, pure oxygen was adopted to accelerate the specimens aging. However, the current aging apparatuses could not meet the requirements of large capacity and excellent airtightness. Hence, the research team designed and ordered an autoclave with an inner height of 45 cm and an inner diameter of 30 cm (see Figure 3.3) to artificially simulate the long-term aging of compacted specimens in the laboratory. The autoclave can host six specimens of 100 mm in diameter and 150 mm in height at the same time. A pressure release sub-system is also included for safety considerations. Hence, three mixture types were chosen to simulate the long-term aging by using the autoclave. The detailed aging procedure is described in section 3.2.1. The particular aging conditions of the three mixture types are summarized in Table 6.3.

Table 6.3 The aging conditions of three types of asphalt mixtures

| Mix type | Aging temperature (°C) | Gas | Applied pressure (Pa) | Accumulated aging time (days) |
|---|---|---|---|---|
| WC | 40 | Oxygen | 0 | 7, 14, 21, 28, and 35 |
| BC | 40 | Oxygen | 0 | 7, 14, 21, 28, and 35 |
| SMA | 40 | Oxygen | 0 | 7, 14, 28, 42, and 56 |

### 6.3.3 Dynamic modulus test

The detailed $|E^*|$ test is described in section 4.2.3

### 6.3.4 DSR test

The detailed DSR test method is described in section 5.2.3.

## 6.4 **Results and discussion**

### 6.4.1 Effect of aging on $|E^*|$ values of compacted asphalt mixtures

For each type of asphalt mixtures, one of six specimens was chosen as a control sample for determining the aging state of asphalt binder. The volumetric and mechanical properties of the control specimen should be approximately equal to the average value of the other five specimens in the same batch. The other five specimens were utilized to conduct $|E^*|$ test. The average $|E*|$ values of the five specimens were then used to develop a master curve at a reference temperature of 20°C by using time-temperature superposition (TTS) principle. Figure 6.2 shows the master curves of $|E^*|$ values for three mixture types. The figure indicates that $|E^*|$ values increased with increasing aging time, and the increasing rates of $|E*|$ values decreased as aging time increased. For example, comparing with the $|E^*|$ values of unaged specimens for SMA mixture tested at 20°C and 1 Hz, the $|E^*|$ values of the specimens after being aged for 7 d, 14 d, 28 d, 42 d, and 28 d increased by 32.5%, 43.3%, 57.5%, 70.4%, and 75.2%, respectively. This trend was consistent with that of recovered asphalt binders. It is caused by that asphalt binders are rapidly oxidized in the initial stage of oxidation followed by at a slower, nearly linear rate. Besides, the increasing rates of $|E^*|$ values were varied with aggregate gradation, indicating that aggregate gradation affects the aging rates of compacted asphalt mixtures.

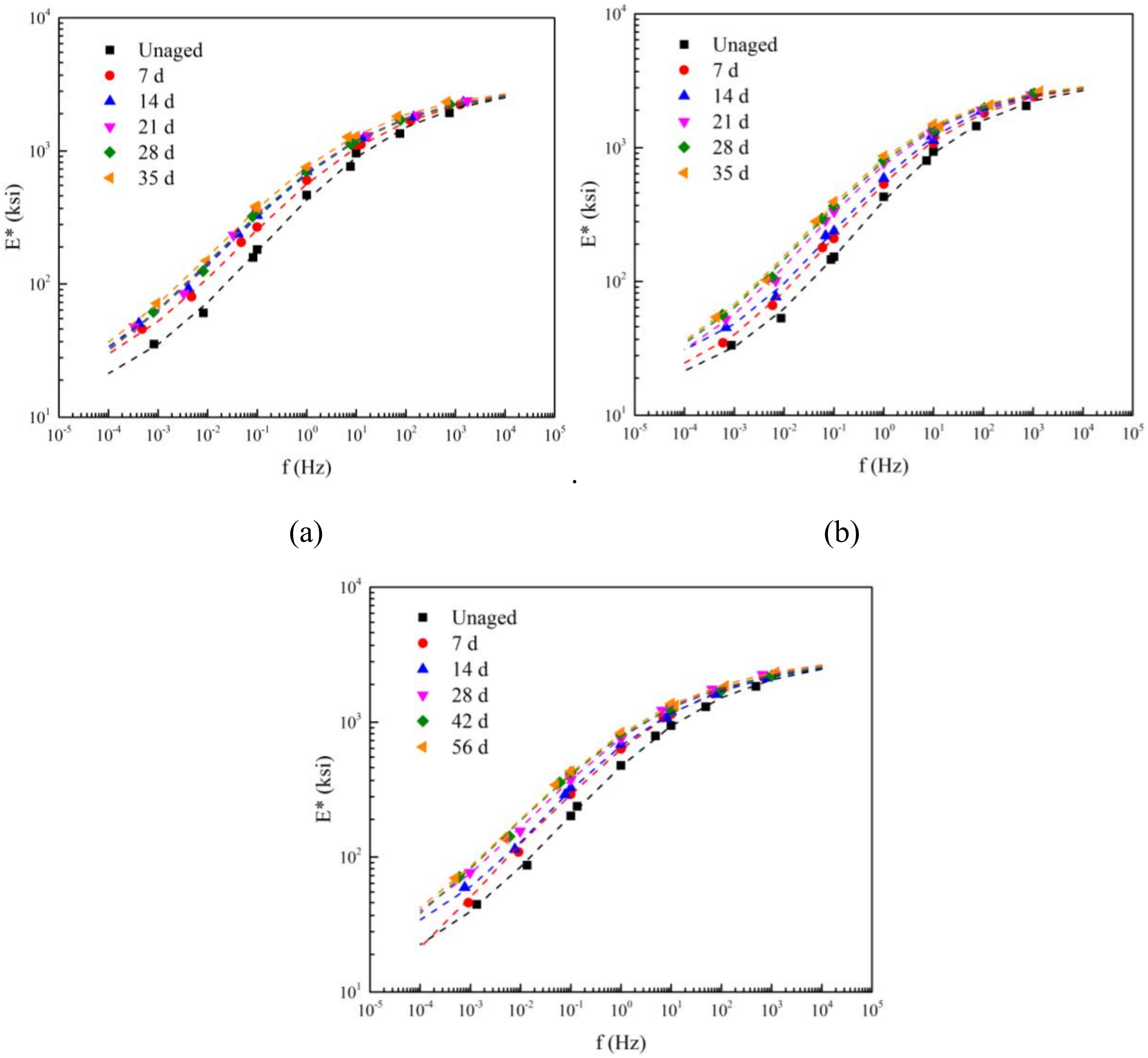

(a)

(b)

(c)

Figure 6.2 The master curves of $|E^*|$ values for the three mixture types: (a) WC, (b) BC, and (c) SMA

### 6.4.2 Comparison of measured and predicted $|E^*|$ values

In this chapter, $|G^*|$ and δ values of recovered asphalt binders were measured at the loading frequencies (0.016 Hz, 0.159 Hz, and 1.59 Hz) which are corresponded to the loading frequencies (0.1 Hz, 1 Hz, and 10 Hz) in dynamic compression mode [155]. Figure 6.3-6.5 plot the comparisons between measured and predicted $|E^*|$ values for the three mixture types. The plots were segregated by the different aging states of compacted asphalt mixtures to investigate the accuracies of six predictive models. The black dash lines shown in Figure 6.3-6.5 are the line of equality (LOE). The closer the data point is to the LOE, the higher is the accuracies of predicted values.

As can be seen from Figure 6.3-6.5, Original Hirsch, Improved Hirsch, and Al-Khateeb models underestimated $|E^*|$ values for the three mixture types over the whole temperature range. In addition, Witczak 1-37A model slightly overpredicted $|E^*|$ values at high temperatures and underestimated them at low temperatures for WC and BC mixtures. The data points in Witczak 1-40D model distributed evenly at the both sides of the LOE for WC mixture and located on the top of the LOE for BC mixture at low temperatures. It indicates that Witczak 1-40D model has a high prediction accuracy of $|E^*|$ values for WC mixture, and presents the underestimation of $|E^*|$ values at low temperatures for BC mixture. For the 2S2P1D model, it under-predicted $|E^*|$ values at high temperatures and overestimated them at low temperatures for the three mixture types blending with the base asphalt. Comparing with WC and BC mixtures, Witczak 1-37A and 1-40D models for SMA mixture significantly underpredicted and overestimated $|E^*|$ values, respectively.

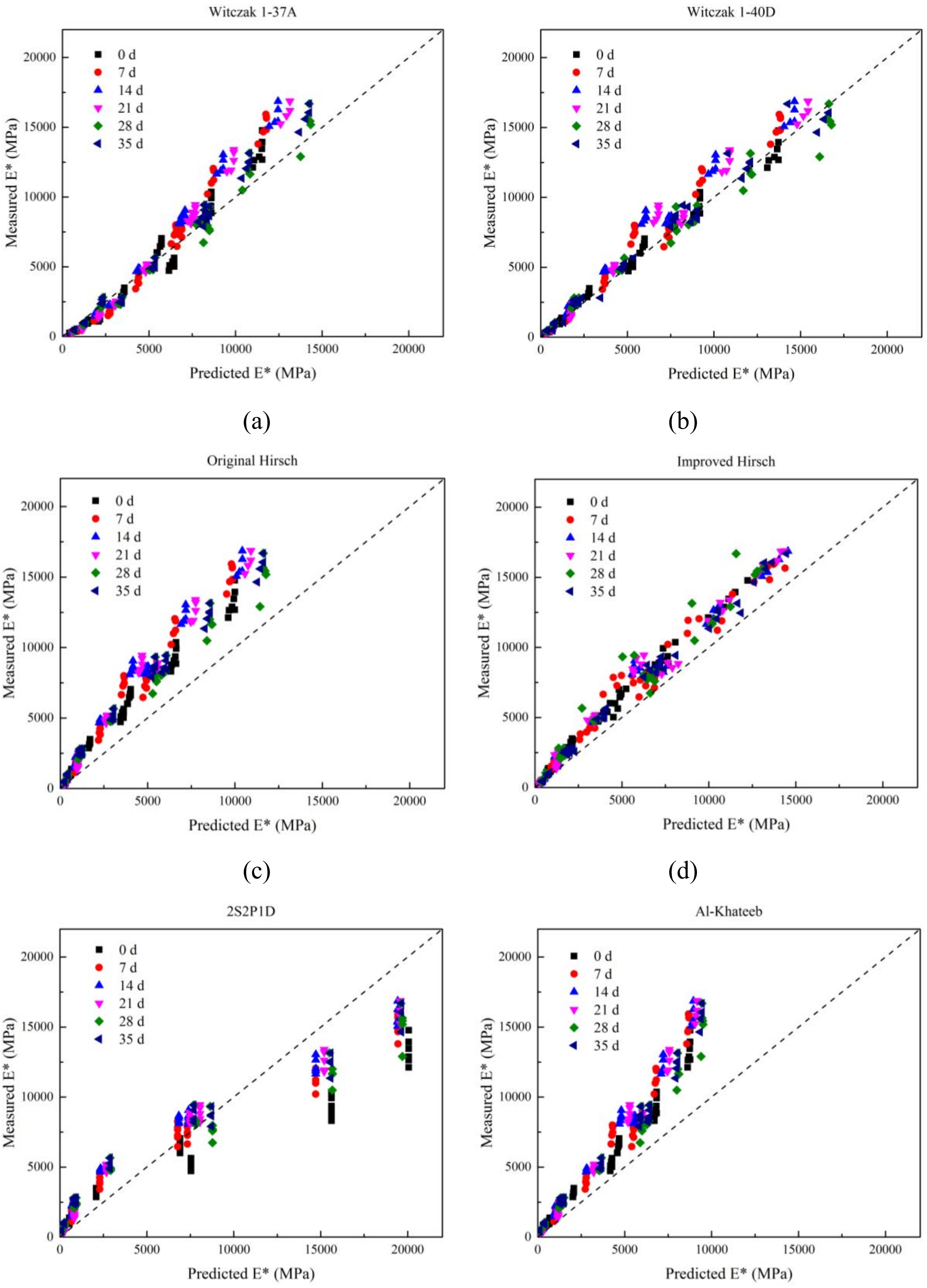

(a) (b)

(c) (d)

(e) (f)

Figure 6.3 Measured versus predicted $|E^*|$ values of WC mixture for the six predictive models: (a) Witczak 1-37A, (b) Witczak 1-40D, (c) Original Hirsch, (d) Improved Hirsch, (e) 2S2P1D, and (d) Al-Khateeb

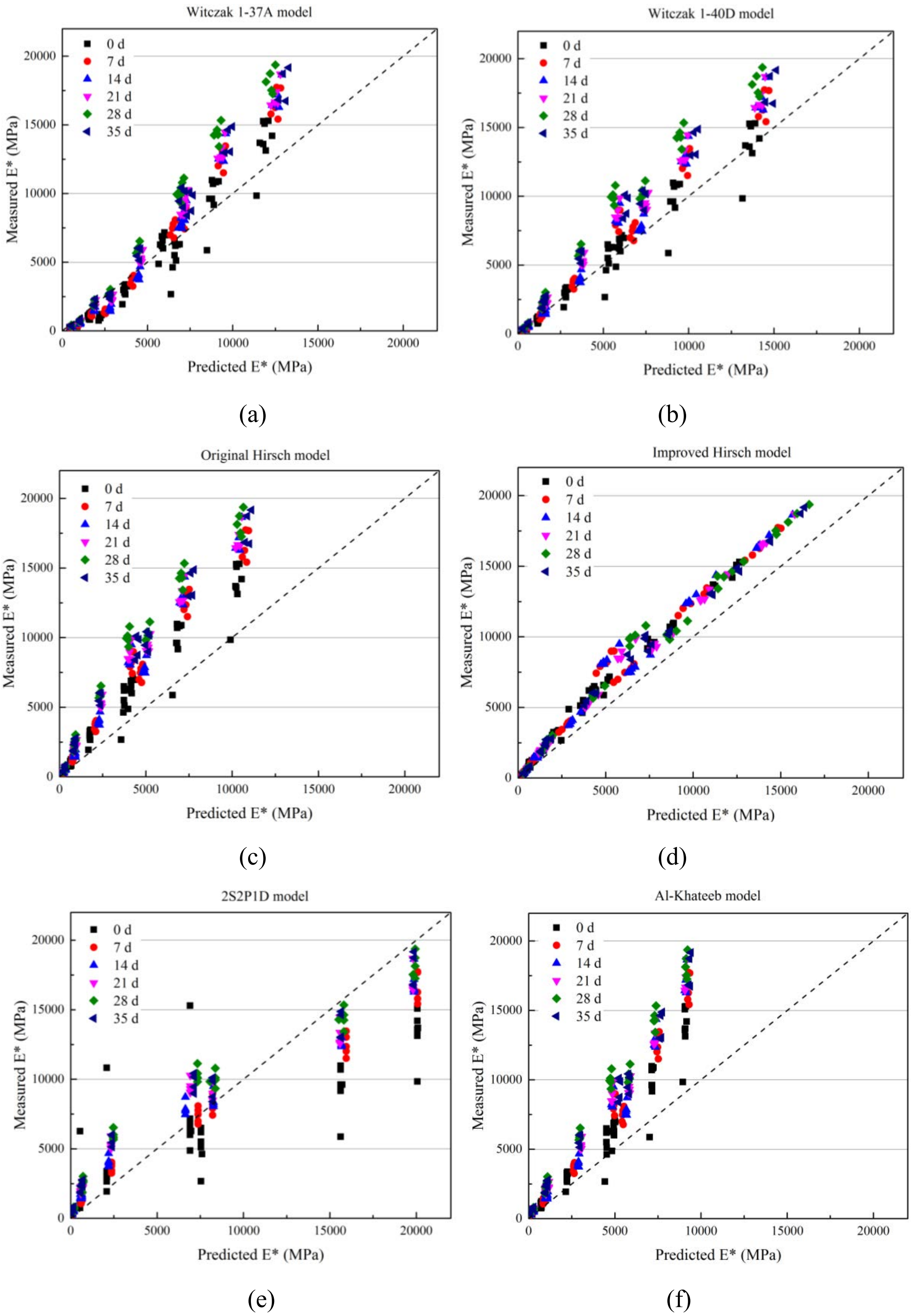

(a) (b)

(c) (d)

(e) (f)

Figure 6.4 Measured versus predicted $|E^*|$ values of BC mixture for the six predictive models: (a) Witczak 1-37A, (b) Witczak 1-40D, (c) Original Hirsch, (d) Improved Hirsch, (e) 2S2P1D, and (d) Al-Khateeb

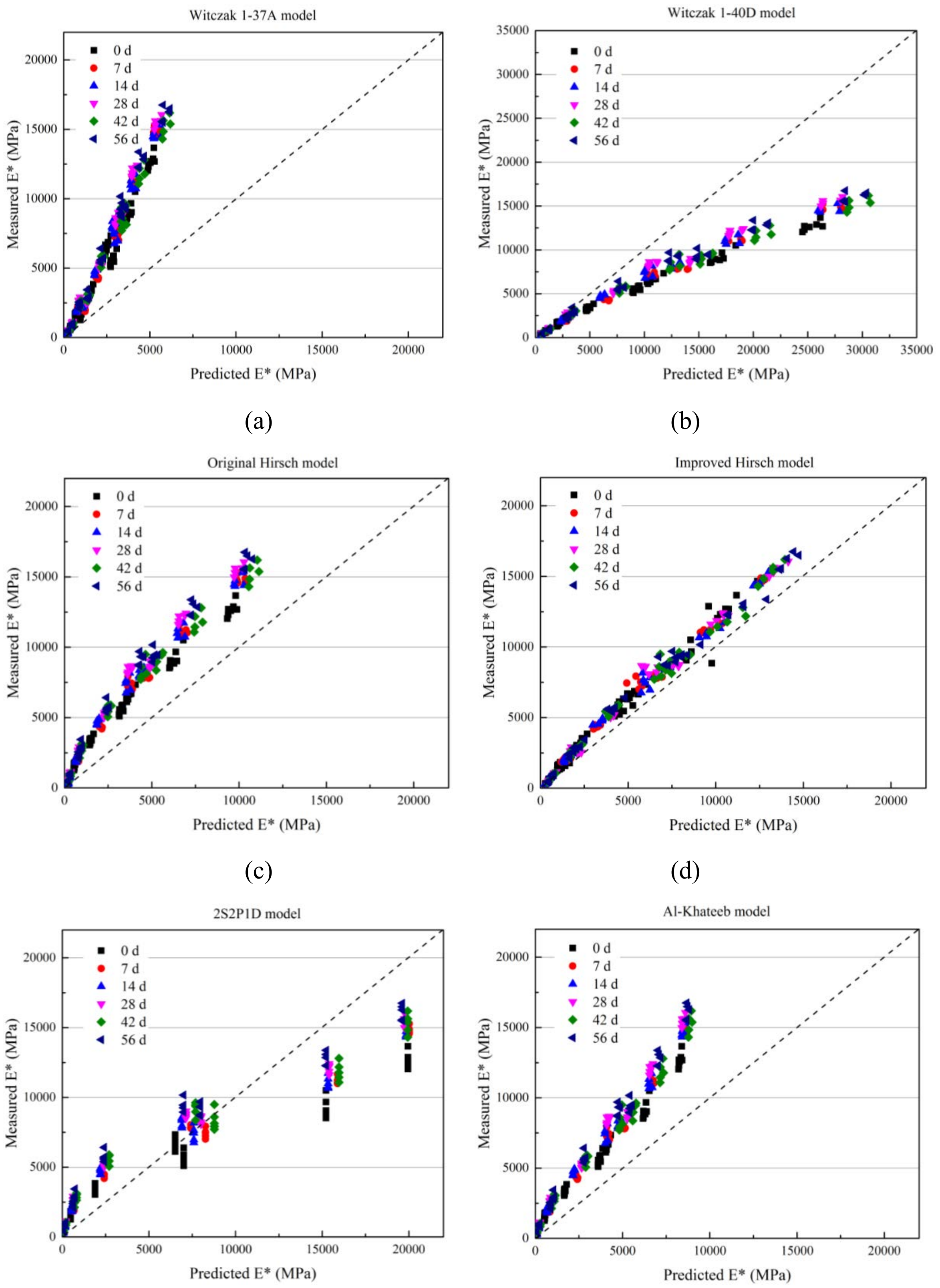

(a) (b)

(c) (d)

(e) (f)

Figure 6.5 Measured versus predicted $|E^*|$ values of SMA mixture for the six predictive models: (a) Witczak 1-37A, (b) Witczak 1-40D, (c) Original Hirsch, (d) Improved Hirsch, (e) 2S2P1D, and (d) Al-Khateeb

### 6.4.3 Statistics of the goodness-of-fit

To evaluate the goodness-of-fit of the predictive models, several statistical indicators were calculated by using Eqs. (6.14) to (6.17) [147, 161].

$$S_y = \sqrt{\frac{\sum_{i=1}^{n}\left(E_{mi}^{*} - \bar{E}_{m}^{*}\right)^2}{(n-1)}} \tag{6.14}$$

$$e_i = \left(E_{pi}^{*} - E_{mi}^{*}\right) \tag{6.15}$$

$$S_e = \sqrt{\frac{\sum_{i=1}^{n} e_i^2}{(n-p)}} \tag{6.16}$$

$$R^2 = 1 - \frac{(n-p)}{(n-1)}\left(\frac{S_e}{S_y}\right)^2 \tag{6.17}$$

where $E_m^*$ is the measured dynamic modulus, $E_p^*$ is the predicted dynamic modulus, $\bar{E}_m^*$ is the mean value of measured dynamic modulus, *n* is the size of the sample, *k* is the number of regression, $e_i$ is the error between measured and predicted values, $S_y$ is the standard deviation of the measured values $S_e$ is the standard error of estimate, and $R^2$ is the correlation coefficient.

In the data analysis, the ratio $S_e/S_y$ is utilized to evaluate the accuracy of the predictive models. Similarly, $R^2$ is a measure of the model accuracy. A $R^2$ value is close to 1 indicates that there is a good agreement between predicted and measured values. Higher $R^2$ and lower $S_e/S_y$ values, therefore, present the better performance of a model. A detailed criteria proposed by Witczak was adopted and listed in Table 6.4 [161].

Tables 6.5 to 6.7 summarize the goodness-of-fit statistics for WC, BC, and SMA mixtures at different aging states, respectively. As can be seen from the tables, the $R^2$ and $S_e/S_y$ values of WC and BC mixtures showed the similar trends with the increase of aging time for the predictive models except Improved Hirsch and 2S2P1D models. The $R^2$ values exhibited a trend of going down and then rising up while $S_e/S_y$ values showed the opposite trend. This indicates that asphalt mixture aging has a negative effect on the accuracies of these predictive models at the initial stage of aging. Moreover, the ratings of Witczak 1-37A and 1-40D models (Grade E or G) were higher than those of Original and Al-Khateeb models (Grade G or F) for WC, BC, and SMA mixtures. Improved Hirsch model had the highest $R^2$ and the least $S_e/S_y$ values, and was rated as excellent at the different aging level for the three mixture types, indicating that the model is relatively superior to the other models. For the three mixture types, the 2S2P1D model presented the better robustness for aged specimens than unaged specimens, which implies that aging could improve the robustness of the model. The tendency of the Al-Khateeb model for the three mixture types was contrary to that of the 2S2P1D model. Overall, the performance of Improved Hirsch model was the best, classified as excellent, followed by 2S2P1D model (Grade G) for the three mixture types. The grades of Witczak 1-37A and 1-40D models were the highest for WC mixture rated as Grade E, followed by BC mixture classified as Grade G and then followed by SMA mixture (Grade P or V). Besides, the best grade of Orginal Hirsch model was a "E" for WC mixture followed by BC and SMA mixtures classified as Grade F which was also the grades of the Al-Khateeb model for the three mixture types.

Some researchers found that the accuracies of the six predictive models were various at different temperatures [143, 150, 162]. The accuracies of the six predictive models, therefore, were investigated at the three testing temperatures (4°C, 20°C, and 40°C). Tables 6.5 to 6.7 summarize the goodness-of-fit statistics for WC, BC, and SMA mixtures segregated by the testing temperatures. For WC and BC mixtures, the rankings of all models were the lowest at the temperature of 4°C compared with them at the other two temperatures, but Witczak 1-

40D model exhibited a Grade G for WC mixture. It means that the predictions of the six predictive models exhibit lower robustness at low temperatures than the other temperatures. Additionally, Witczak 1-37A model showed the best ranking (Grade E and G for WC and BC mixtures, respectively) at the temperature of 20°C, and was classified as Grade F at 40°C. Witczak 1-40D model was classified as Grade E and G at 20°C and 40°C, respectively. Original Hirsch, 2S2P1D, and Al-Khateeb models were ranked as Grade F, P, and V at the three temperatures, indicating that these predictive models have a poor robustness of predicting $|E^*|$ values over the whole temperature range. It is noteworthy that Improved Hirsh model expressed a relatively higher grade (G) compared with the other models at intermediate and high temperatures. For SMA mixture, all models did not show a high rank but Improved Hirsch model (Grade G) at medium and high temperatures and Witczak 1-40 model (Grade G) at high temperatures. Singh et al. also found that Witczak models (1-37A and 1-40D), Original Hirsch, and Al-Khateeb models were inaccurate at low temperatures [147]. To summarize, Improved Hirsch shows the best prediction of $|E^*|$ values for the three types of asphalt mixtures blending with the base asphalt over the whole temperature ranges. Witczak 1-40D model also expresses the high robustness for WC and BC mixtures.

The negative $R^2$ is caused by that the standard error of estimate is greater than the standard deviation of measured values. It suggests that the model is not necessarily a good fit for the particular selected data. This situation also appeared in previous studies [143, 162, 163].

Table 6.4 The criteria for subjective classification of the goodness-of-fit statistics

| Criteria | $R^2$ | $S_e/S_y$ |
|---|---|---|
| Excellent/E | ≥0.9 | ≤0.35 |
| Good/G | 0.79-0.89 | 0.36-0.55 |
| Fair/F | 0.40-0.69 | 0.56-0.75 |
| Poor/P | 0.20-0.39 | 0.76-0.90 |
| Very Poor/V | ≤0.19 | ≥0.90 |

Table 6.5 Summary of goodness-of-fit statistics for WC mixture segregated by different aging periods

| Model | Regression coefficient | 0 d | 7 d | 14 d | 21 d | 28 d | 35 d | Overall |
|---|---|---|---|---|---|---|---|---|
| 1-37A | $R^2$ | 0.96 | 0.91 | 0.91 | 0.93 | 0.98 | 0.97 | 0.93 |
| | $S_e/S_y$ | 0.22 | 0.32 | 0.33 | 0.29 | 0.17 | 0.18 | 0.27 |
| | Rating | E | E | E | E | E | E | E |
| 1-40D | $R^2$ | 0.99 | 0.95 | 0.95 | 0.97 | 0.98 | 0.98 | 0.96 |
| | $S_e/S_y$ | 0.10 | 0.24 | 0.26 | 0.20 | 0.15 | 0.14 | 0.19 |
| | Rating | E | E | E | E | E | E | E |
| Original Hirsch | $R^2$ | 0.82 | 0.67 | 0.64 | 0.69 | 0.81 | 0.76 | 0.71 |
| | $S_e/S_y$ | 0.44 | 0.59 | 0.63 | 0.58 | 0.46 | 0.51 | 0.54 |
| | Rating | G | F | F | F | G | G | G |
| Improved Hirsch | $R^2$ | 0.93 | 0.93 | 0.94 | 0.93 | 0.91 | 0.95 | 0.91 |
| | $S_e/S_y$ | 0.30 | 0.29 | 0.29 | 0.30 | 0.36 | 0.26 | 0.30 |
| | Rating | E | E | E | E | G | E | E |
| 2S2P1D | $R^2$ | 0.49 | 0.85 | 0.89 | 0.90 | 0.81 | 0.85 | 0.77 |
| | $S_e/S_y$ | 0.76 | 0.42 | 0.37 | 0.34 | 0.48 | 0.43 | 0.49 |
| | Rating | P | G | G | E | G | G | G |
| Al-Khateeb | $R^2$ | 0.81 | 0.66 | 0.62 | 0.65 | 0.73 | 0.69 | 0.67 |
| | $S_e/S_y$ | 0.45 | 0.60 | 0.64 | 0.61 | 0.53 | 0.58 | 0.58 |
| | Rating | G | F | F | F | G | F | F |

Table 6.6 Summary of goodness-of-fit statistics for BC mixture segregated by different aging periods

| Model | Regression coefficient | 0 d | 7 d | 14 d | 21 d | 28 d | 35 d | Overall |
|---|---|---|---|---|---|---|---|---|
| 1-37A | $R^2$ | 0.93 | 0.91 | 0.89 | 0.87 | 0.79 | 0.87 | 0.85 |
| | $S_e/S_y$ | 0.28 | 0.33 | 0.36 | 0.40 | 0.51 | 0.41 | 0.39 |
| | Rating | E | E | G | G | G | G | G |
| 1-40D | $R^2$ | 0.97 | 0.94 | 0.93 | 0.89 | 0.81 | 0.89 | 0.89 |
| | $S_e/S_y$ | 0.19 | 0.27 | 0.30 | 0.36 | 0.48 | 0.37 | 0.34 |
| | Rating | E | E | E | G | G | G | G |
| Original Hirsch | $R^2$ | 0.82 | 0.71 | 0.65 | 0.56 | 0.46 | 0.57 | 0.61 |
| | $S_e/S_y$ | 0.44 | 0.56 | 0.62 | 0.69 | 0.76 | 0.68 | 0.63 |
| | Rating | G | F | F | F | P | F | F |
| Improved Hirsch | $R^2$ | 0.93 | 0.93 | 0.93 | 0.94 | 0.93 | 0.95 | 0.91 |
| | $S_e/S_y$ | 0.30 | 0.31 | 0.32 | 0.29 | 0.30 | 0.27 | 0.30 |
| | Rating | E | E | E | E | E | E | E |
| 2S2P1D | $R^2$ | 0.51 | 0.91 | 0.93 | 0.90 | 0.91 | 0.92 | 0.82 |
| | $S_e/S_y$ | 0.74 | 0.32 | 0.29 | 0.35 | 0.33 | 0.33 | 0.42 |
| | Rating | F | E | E | E | E | E | G |
| Al-Khateeb | $R^2$ | 0.80 | 0.68 | 0.63 | 0.56 | 0.46 | 0.55 | 0.60 |
| | $S_e/S_y$ | 0.45 | 0.58 | 0.63 | 0.69 | 0.76 | 0.70 | 0.64 |
| | Rating | G | F | F | F | F | F | F |

Table 6.7 Summary of goodness-of-fit statistics for SMA mixture segregated by different aging periods

| Model | Regression coefficient | 0 d | 7 d | 14 d | 28 d | 42 d | 56 d | Overall |
|---|---|---|---|---|---|---|---|---|
| 1-37A | $R^2$ | 0.31 | 0.24 | 0.22 | 0.13 | 0.19 | 0.15 | 0.23 |
| | $S_e/S_y$ | 0.88 | 0.96 | 0.98 | 1.03 | 0.99 | 1.02 | 0.89 |
| | Rating | P | V | V | V | V | V | P |
| 1-40D | $R^2$ | -0.49 | 0.03 | 0.09 | 0.20 | -0.31 | 0.08 | -0.06 |
| | $S_e/S_y$ | 1.29 | 1.09 | 1.06 | 0.99 | 1.26 | 1.06 | 1.04 |
| | Rating | V | V | V | V | V | V | V |
| Original Hirsch | $R^2$ | 0.75 | 0.66 | 0.62 | 0.54 | 0.64 | 0.55 | 0.67 |
| | $S_e/S_y$ | 0.51 | 0.60 | 0.64 | 0.71 | 0.62 | 0.70 | 0.57 |
| | Rating | G | F | F | F | F | F | F |
| Improved Hirsch | $R^2$ | 0.94 | 0.95 | 0.95 | 0.95 | 0.95 | 0.96 | 0.94 |
| | $S_e/S_y$ | 0.28 | 0.27 | 0.26 | 0.27 | 0.25 | 0.24 | 0.24 |
| | Rating | E | E | E | E | E | E | E |
| 2S2P1D | $R^2$ | 0.45 | 0.77 | 0.76 | 0.82 | 0.78 | 0.85 | 0.74 |
| | $S_e/S_y$ | 0.79 | 0.53 | 0.54 | 0.47 | 0.52 | 0.43 | 0.52 |
| | Rating | P | G | G | G | G | G | G |
| Al-Khateeb | $R^2$ | 0.71 | 0.61 | 0.58 | 0.49 | 0.57 | 0.48 | 0.63 |
| | $S_e/S_y$ | 0.55 | 0.65 | 0.67 | 0.74 | 0.68 | 0.74 | 0.61 |
| | Rating | G | F | F | F | F | F | F |

Table 6.8 Summary of goodness-of-fit statistics for WC mixture segregated by temperature

| Temperature (°C) | Regression coefficient | 1-37A | 1-40D | Original Hirsch | Improved Hirsch | 2S2P1D | Al-Khateeb |
|---|---|---|---|---|---|---|---|
| 4 | $R^2$ | 0.63 | 0.81 | -0.46 | 0.61 | -0.17 | -0.84 |
|  | $S_e/S_y$ | 0.63 | 0.46 | 1.23 | 0.67 | 1.13 | 1.38 |
|  | Rating | F | G | V | F | V | V |
| 20 | $R^2$ | 0.92 | 0.95 | 0.33 | 0.79 | 0.68 | 0.57 |
|  | $S_e/S_y$ | 0.30 | 0.22 | 0.83 | 0.49 | 0.59 | 0.66 |
|  | Rating | E | E | P | G | F | F |
| 40 | $R^2$ | 0.71 | 0.91 | 0.33 | 0.83 | -0.02 | 0.43 |
|  | $S_e/S_y$ | 0.56 | 0.32 | 0.83 | 0.45 | 1.06 | 0.77 |
|  | Rating | F | E | P | G | V | P |

Table 6.9 Summary of goodness-of-fit statistics for BC mixture segregated by temperature

| Temperature (°C) | Regression coefficient | 1-37A | 1-40D | Original Hirsch | Improved Hirsch | 2S2P1D | Al-Khateeb |
|---|---|---|---|---|---|---|---|
| 4 | $R^2$ | 0.29 | 0.47 | -0.84 | 0.62 | 0.27 | -1.06 |
|  | $S_e/S_y$ | 0.88 | 0.76 | 1.38 | 0.66 | 0.9 | 1.46 |
|  | Rating | P | P | V | F | P | V |
| 20 | $R^2$ | 0.8 | 0.81 | 0.2 | 0.86 | 0.59 | 0.47 |
|  | $S_e/S_y$ | 0.47 | 0.46 | 0.91 | 0.41 | 0.67 | 0.74 |
|  | Rating | G | G | V | G | F | F |
| 40 | $R^2$ | 0.67 | 0.86 | 0.28 | 0.76 | -0.13 | 0.37 |
|  | $S_e/S_y$ | 0.6 | 0.39 | 0.86 | 0.52 | 1.11 | 0.8 |
|  | Rating | F | G | P | G | V | P |

Table 6.10 Summary of goodness-of-fit statistics for SMA mixture segregated by temperature

| Temperature (°C) | Regression coefficient | 1-37A | 1-40D | Original Hirsch | Improved Hirsch | 2S2P1D | Al-Khateeb |
|---|---|---|---|---|---|---|---|
|  | $R^2$ | -3.66 | -5.79 | -0.77 | 0.73 | -0.47 | -1.26 |
| 4 | $S_e/S_y$ | 2.25 | 2.72 | 1.35 | 0.56 | 1.27 | 1.53 |
|  | Rating | V | V | V | F | V | V |
|  | $R^2$ | -0.66 | -0.50 | -0.08 | 0.84 | 0.49 | 0.11 |
| 20 | $S_e/S_y$ | 1.34 | 1.28 | 1.06 | 0.43 | 0.75 | 0.96 |
|  | Rating | V | V | V | G | F | V |
|  | $R^2$ | 0.00 | 0.82 | -0.29 | 0.75 | -0.56 | -0.35 |
| 40 | $S_e/S_y$ | 1.04 | 0.44 | 1.15 | 0.54 | 1.31 | 1.18 |
|  | Rating | V | G | V | G | V | V |

### 6.4.4 Residual distribution

Ideally, residuals should fluctuate in a random pattern and a small range around the center line. Figures 6.6-6.8 and Figures 6.9-6.11 plot the residuals versus corresponding predicted values, and normal probability plots of residuals of the six predictive models, respectively. As can be seen from these figures, most of the models showed the similar pattern that the variances of residuals increased as the predicted dynamic modulus rose. It indicates that the difference of the error increases as the predicted value increases. Besides, different types of asphalt mixtures exhibited various fluctuations around the zero residuals lines for various models.

For WC mixture, the residuals of unaged specimens for Witczak 1-40D, Original Hirsch, and Improved Hirsch models were less than those of aged specimens, indicating that the aging might have an adverse effect on the robustness of the three predictive models. Among these models, the residual of Improved Hirsch model for unaged specimens ranged from -

0.69 GPa to 0.89 GPa giving a span of 1.57 GPa, was the closest to the zero residual line. The trend of Witczak 1-37A model was opposite to those of the above models. The residuals of Witczak 1-37A model for aged specimens was the closest to the zero residual line compared with the other five predictive models at the same aging state. Besides, there was no significant difference between unaged and aged specimens for 2S2P1D and Al-Khateeb models. Moreover, 2S2P1D exhibited the largest fluctuation in comparison with the other models. On top of these findings, all six models except Improved Hirsch model showed the similar patterns that the variances of the residuals increased as the predicted values increased. It indicates that the error differences increase as the predicted values increase.

For BC mixture, Improved Hirsch and Witczak 1-37A models showed the similar trends with those in WC mixture. The six models for aged specimens showed the smaller amplitudes of fluctuation of residual than unaged specimens, implying that these models have the better robustness in predicting $|E^{*}|$ values of aged specimens compared with unaged specimens, and there was no difference among aged asphalt mixtures over aging time. It is also noteworthy that there were several outliers in 2S2P1D model, which is the reason why 2S2P1D model was the furthest from the zero residuals line, ranging from -4.86 GPa to 9.88 GPa.

For SMA mixture, Witczak 1-40D, Original Hirsch, and 2S2P1D models for unaged specimens expressed the smaller amplitudes of fluctuation of residuals than aged specimens while the trends of Improved Hirsch and Al-Khateeb models were contrary to those of Witczak 1-40D, Original Hirsch, and 2S2P1D models. Additionally, there was no difference between unaged and aged specimens for Witczak 1-37A model. Comparing with WC and

BC mixtures, the six models in SMA mixture showed the smaller amplitudes of fluctuation, indicating that the six models have the better robustness of predicting of $|E^*|$ values for SMA mixture. The Al-Khateeb model exhibited the best performance on it. For example, the residual spans of unaged WC and BC mixtures were 3.55 GPa and 6.48 GPa respectively, which were greater than the span of 2.65 GPa for unaged SMA mixture.

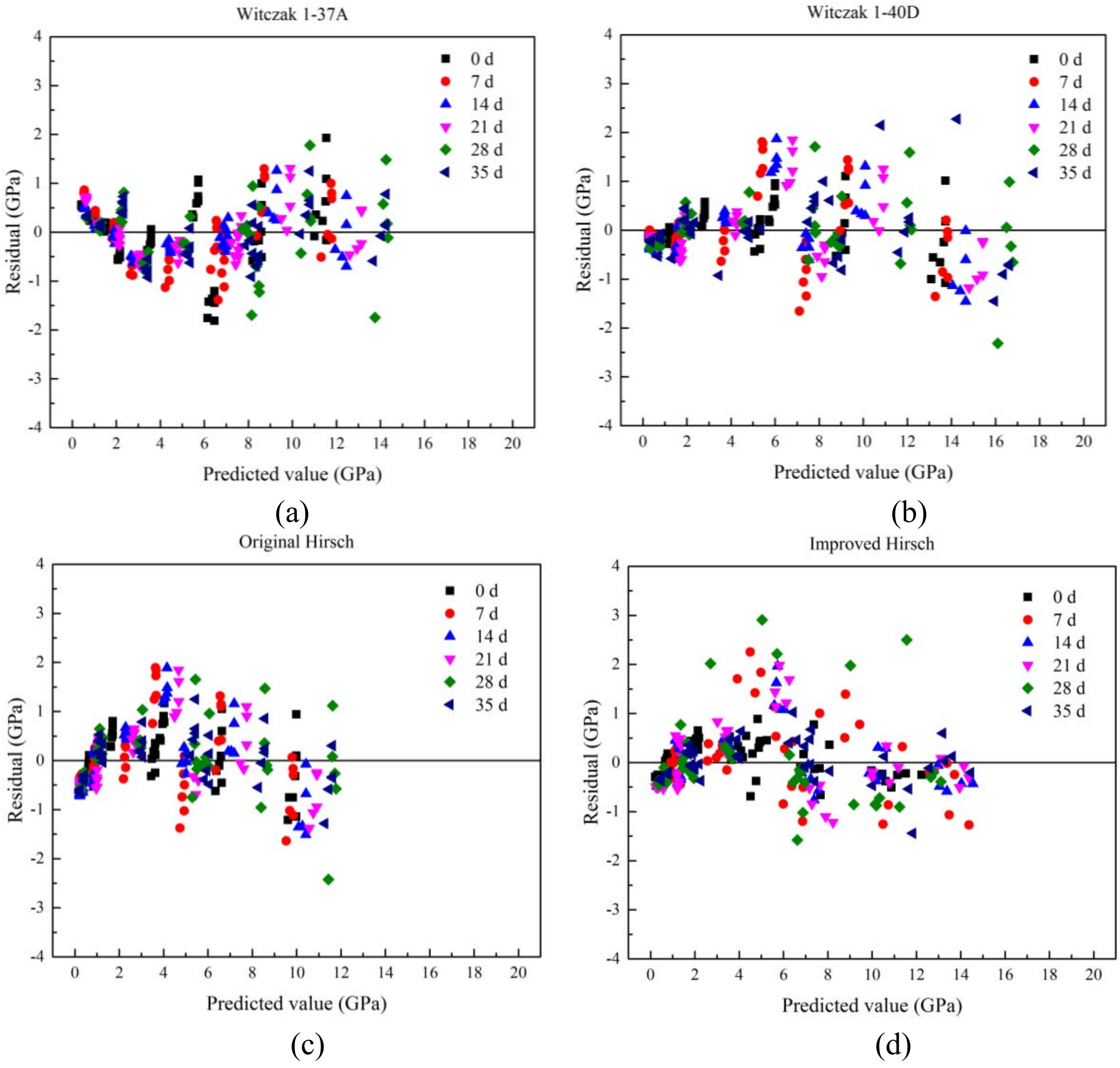

(a) (b)

(c) (d)

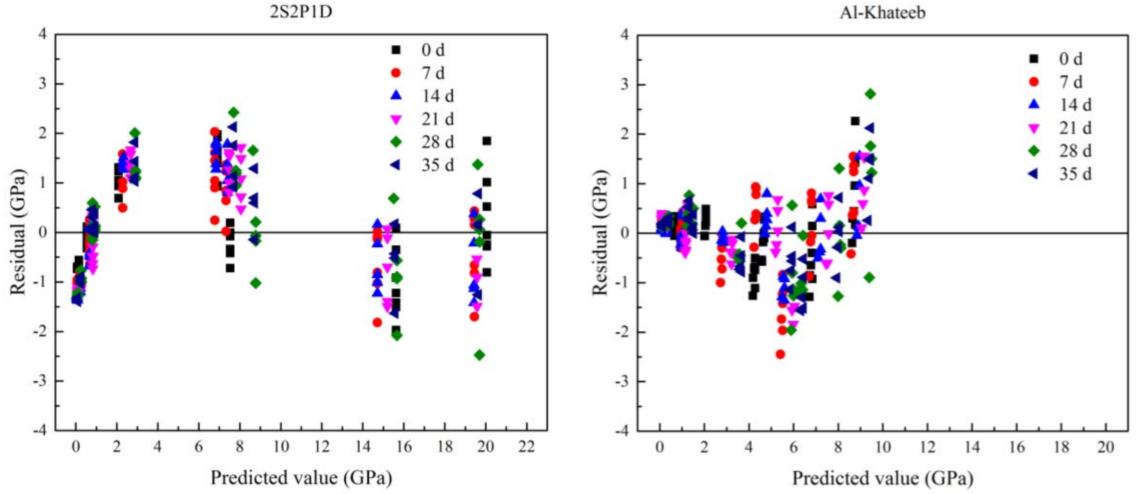

(e) (f)

Figure 6.6 The plots of residuals versus corresponding predicted values of (a) Witczak 1-37A, (b) Witczak 1-40D, (c) Original Hirsch, (d) Improved Hirsch, (e) 2S2P1D, and (f) Al-Khateeb models for WC mixture

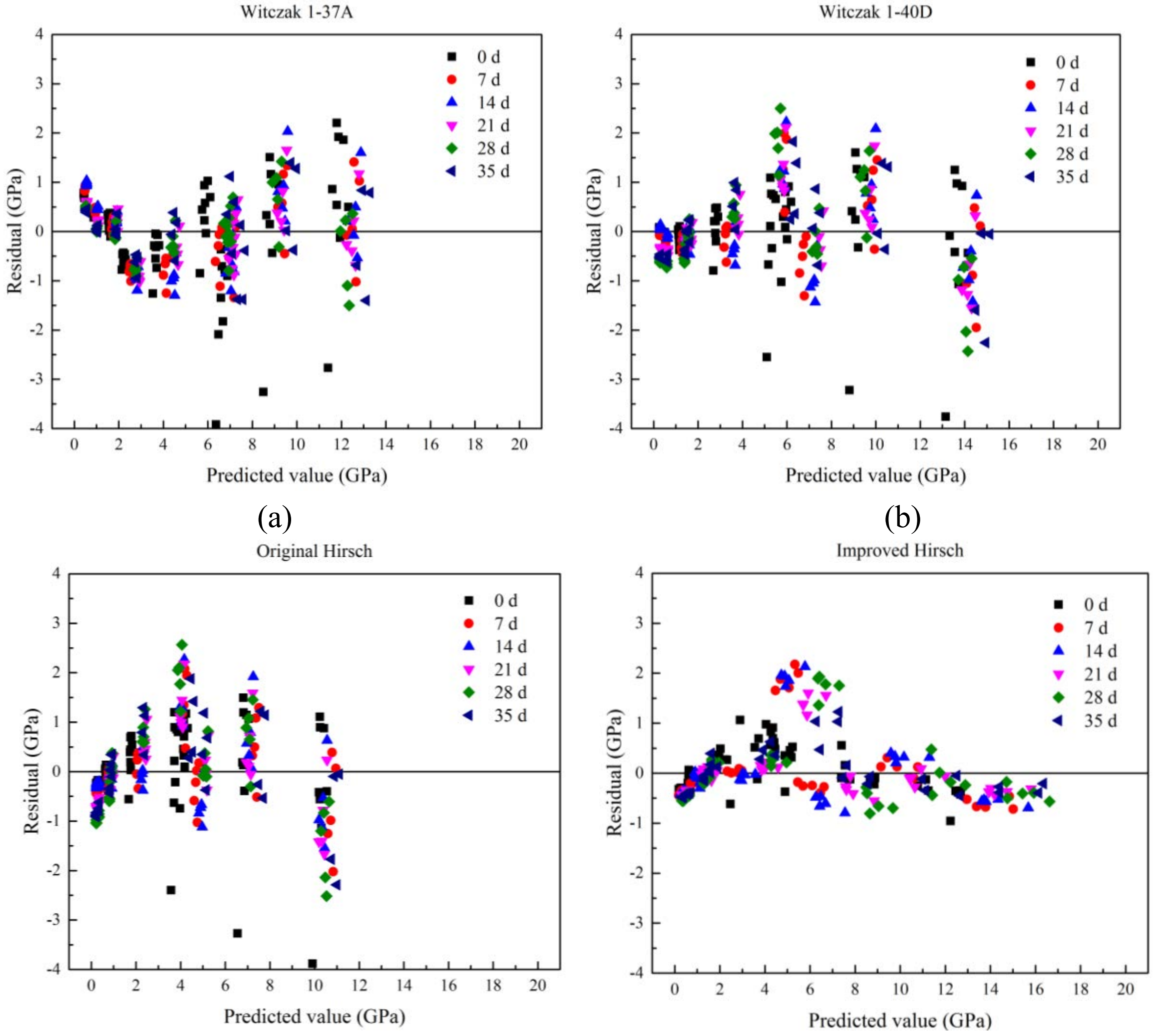

(a) (b)

(c) (d)

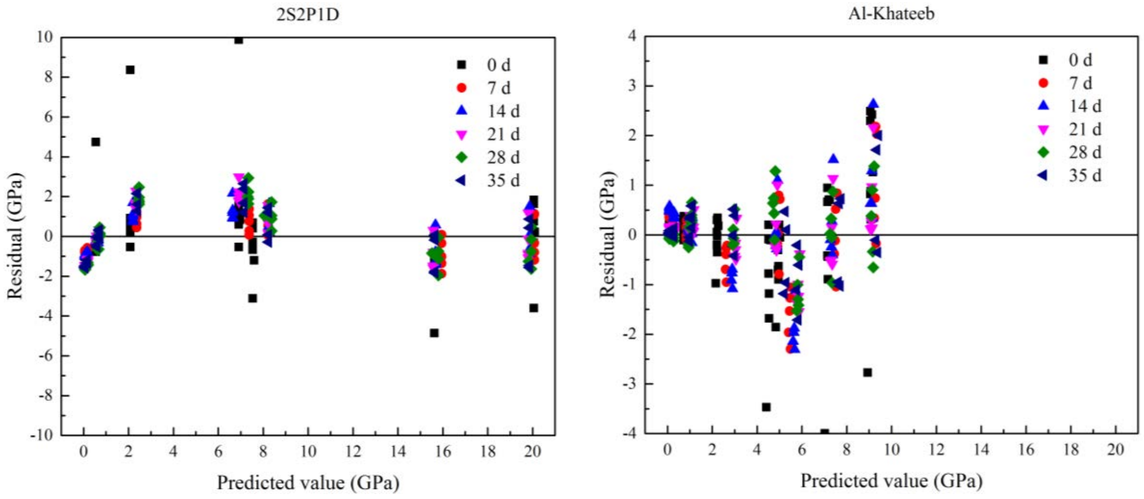

(e) (f)

Figure 6.7 The plots of residuals versus corresponding predicted values of (a) Witczak 1-37A, (b) Witczak 1-40D, (c) Original Hirsch, (d) Improved Hirsch, (e) 2S2P1D, and (f) Al-Khateeb models for BC mixture

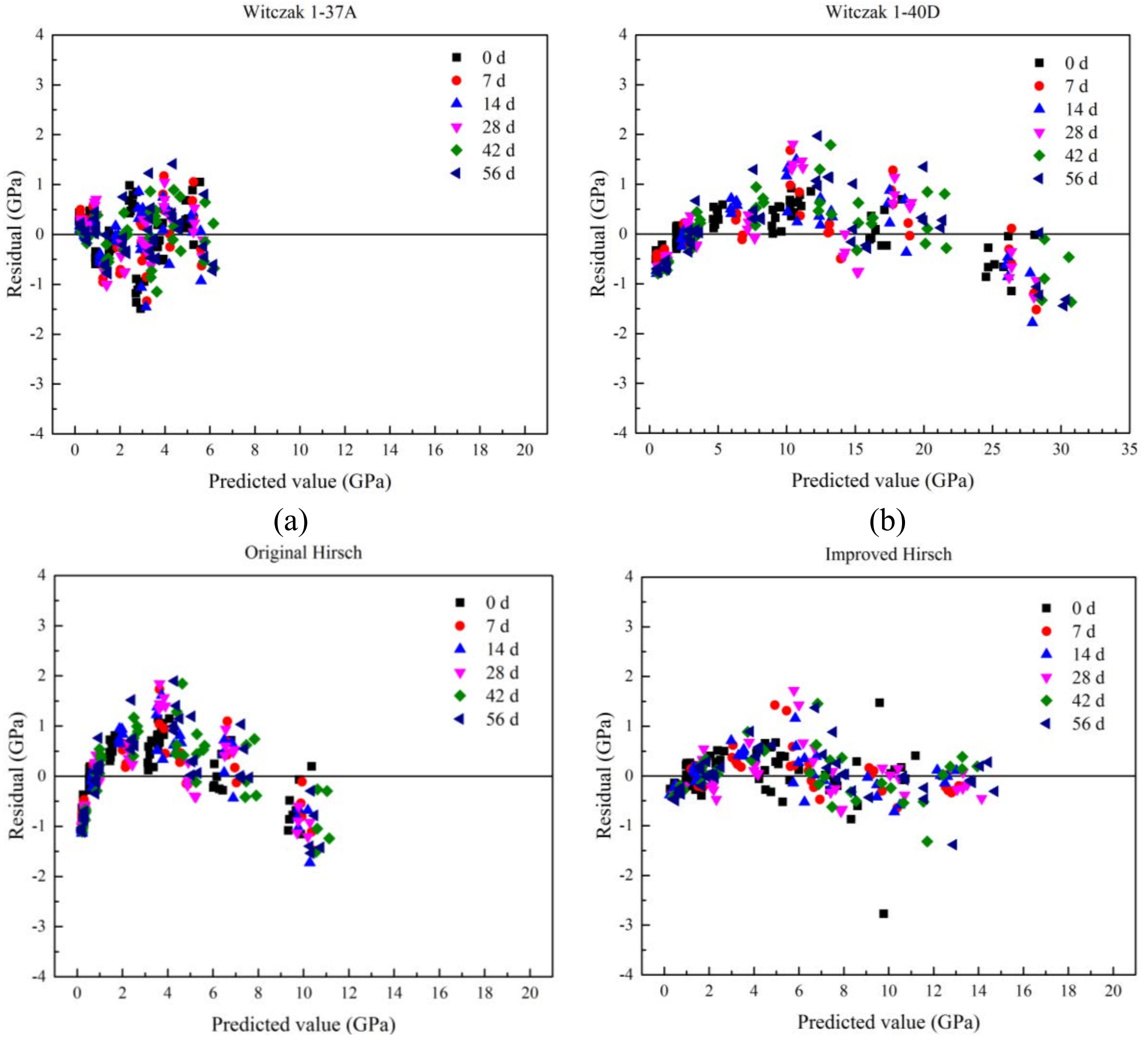

(a) (b)

(c) (d)

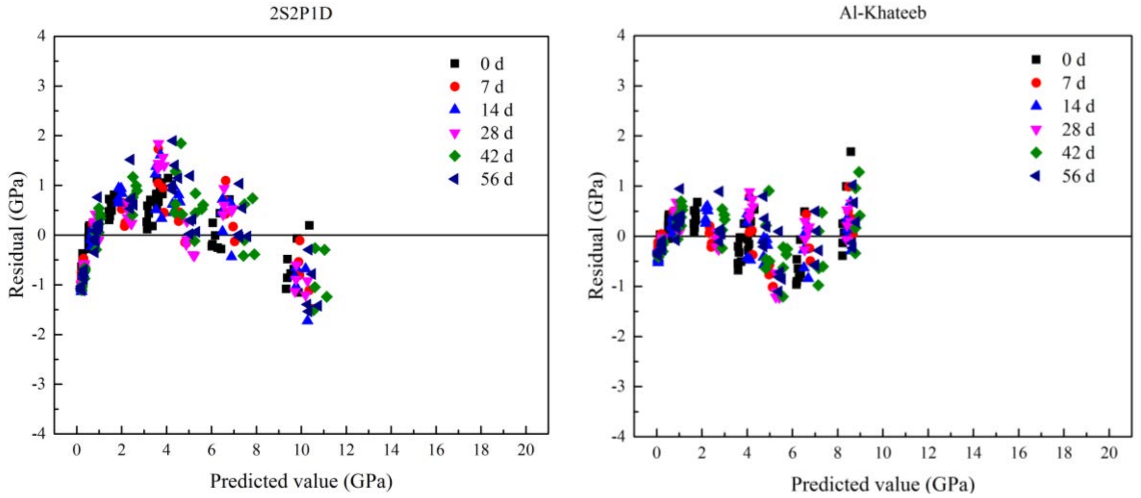

(e) (f)

Figure 6.8 The plots of residuals versus corresponding predicted values of (a) Witczak 1-37A, (b) Witczak 1-40D, (c) Original Hirsch, (d) Improved Hirsch, (e) 2S2P1D, and (f) Al-Khateeb models for SMA mixture

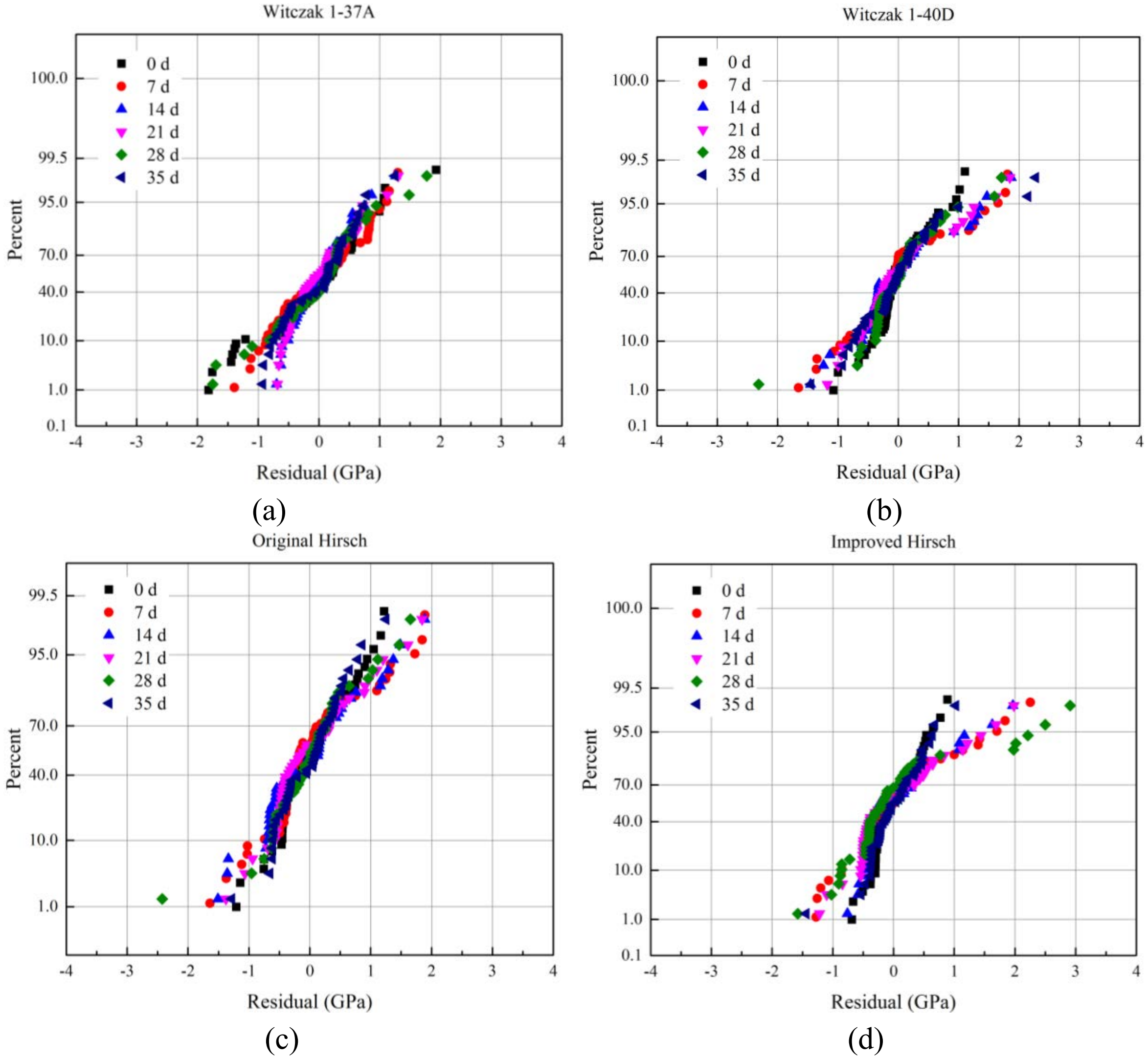

(a) (b)

(c) (d)

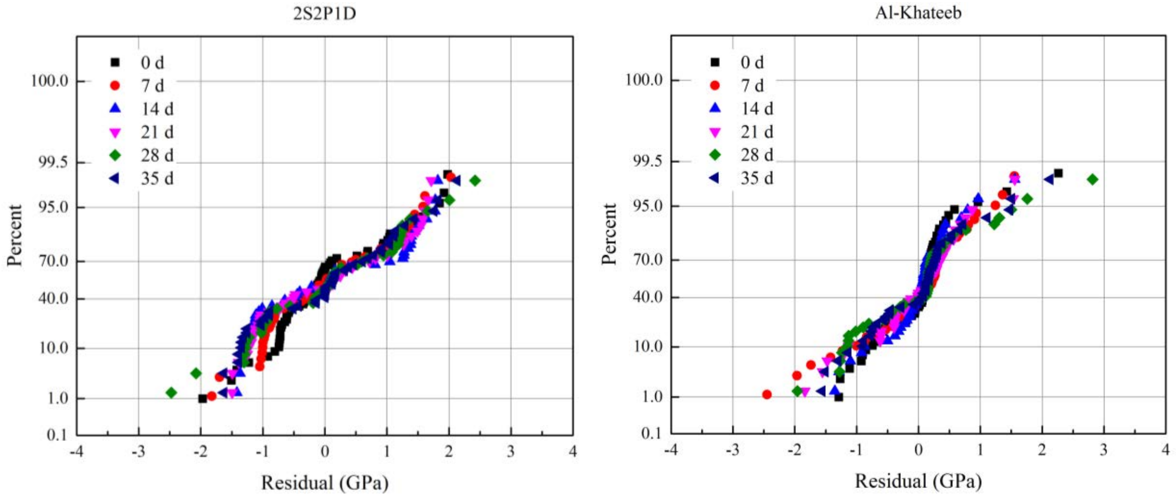

(e) (f)

Figure 6.9 The normal probability plot of residuals of (a) Witczak 1-37A, (b) Witczak 1-40D, (c) Original Hirsch, (d) Improved Hirsch, (e) 2S2P1D, and (f) Al-Khateeb models for WC mixture

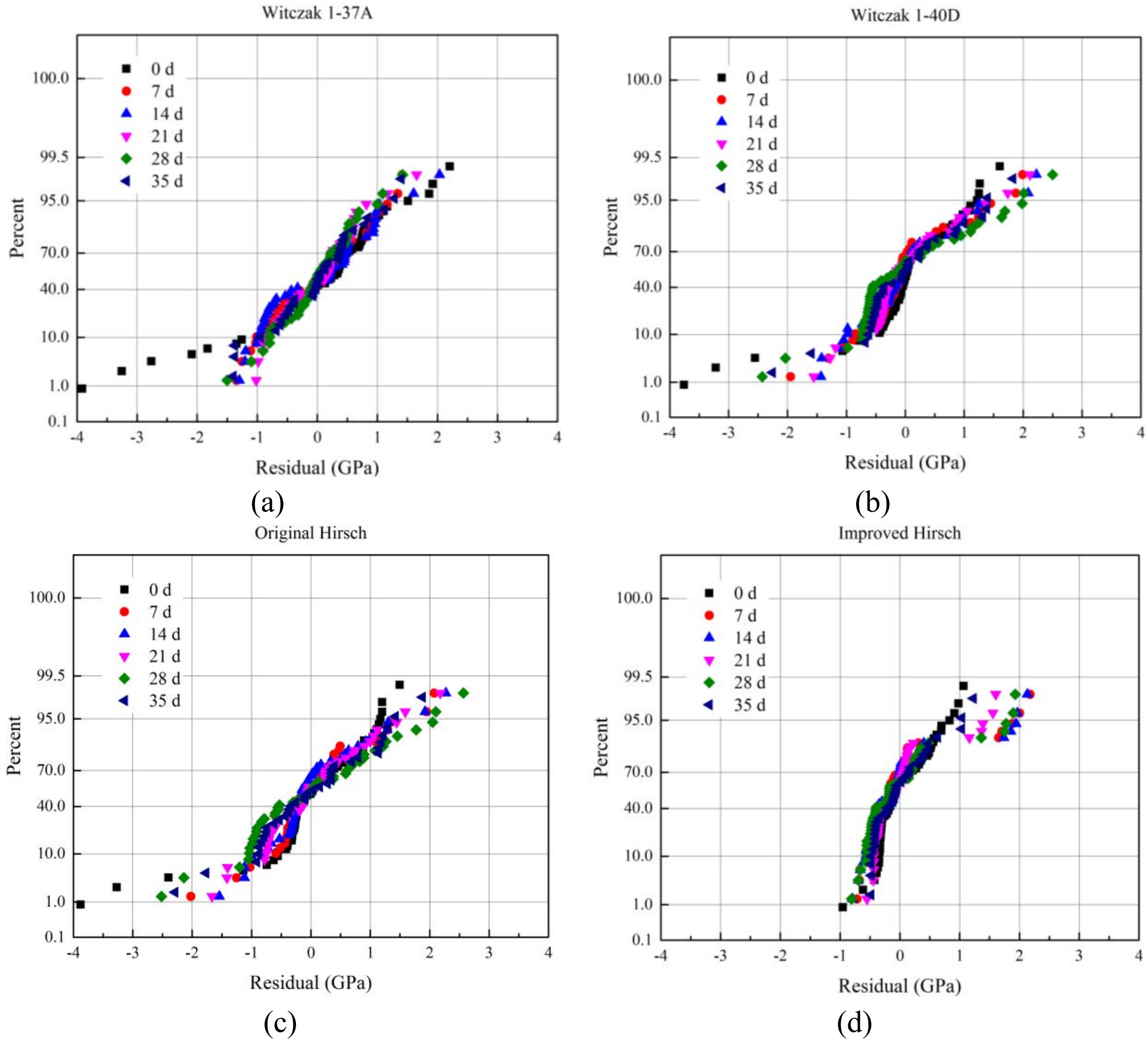

(c) (d)

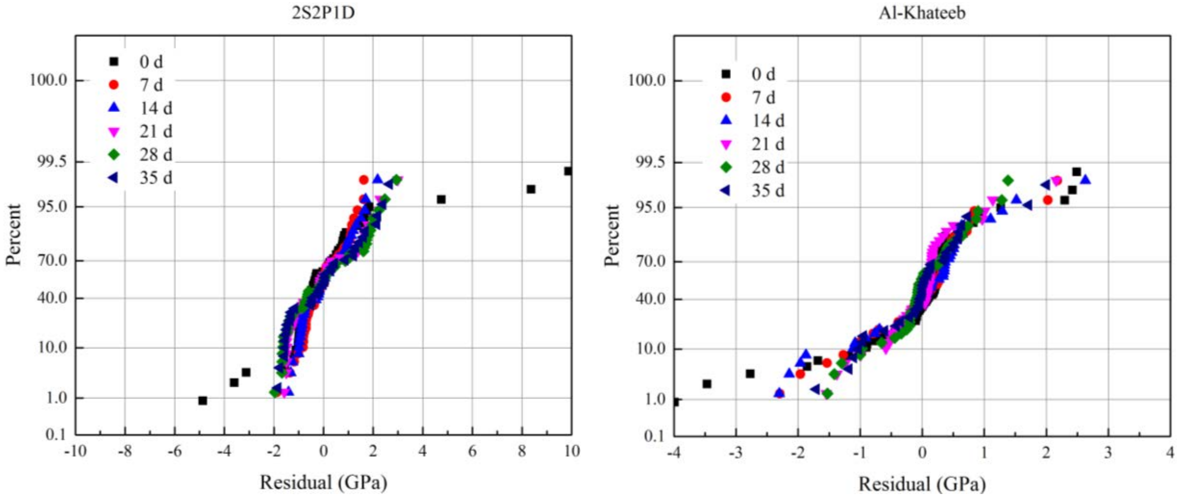

(e) (f)

Figure 6.10 The normal probability plot of residuals of (a) Witczak 1-37A, (b) Witczak 1-40D, (c) Original Hirsch, (d) Improved Hirsch, (e) 2S2P1D, and (f) Al-Khateeb models for BC mixture

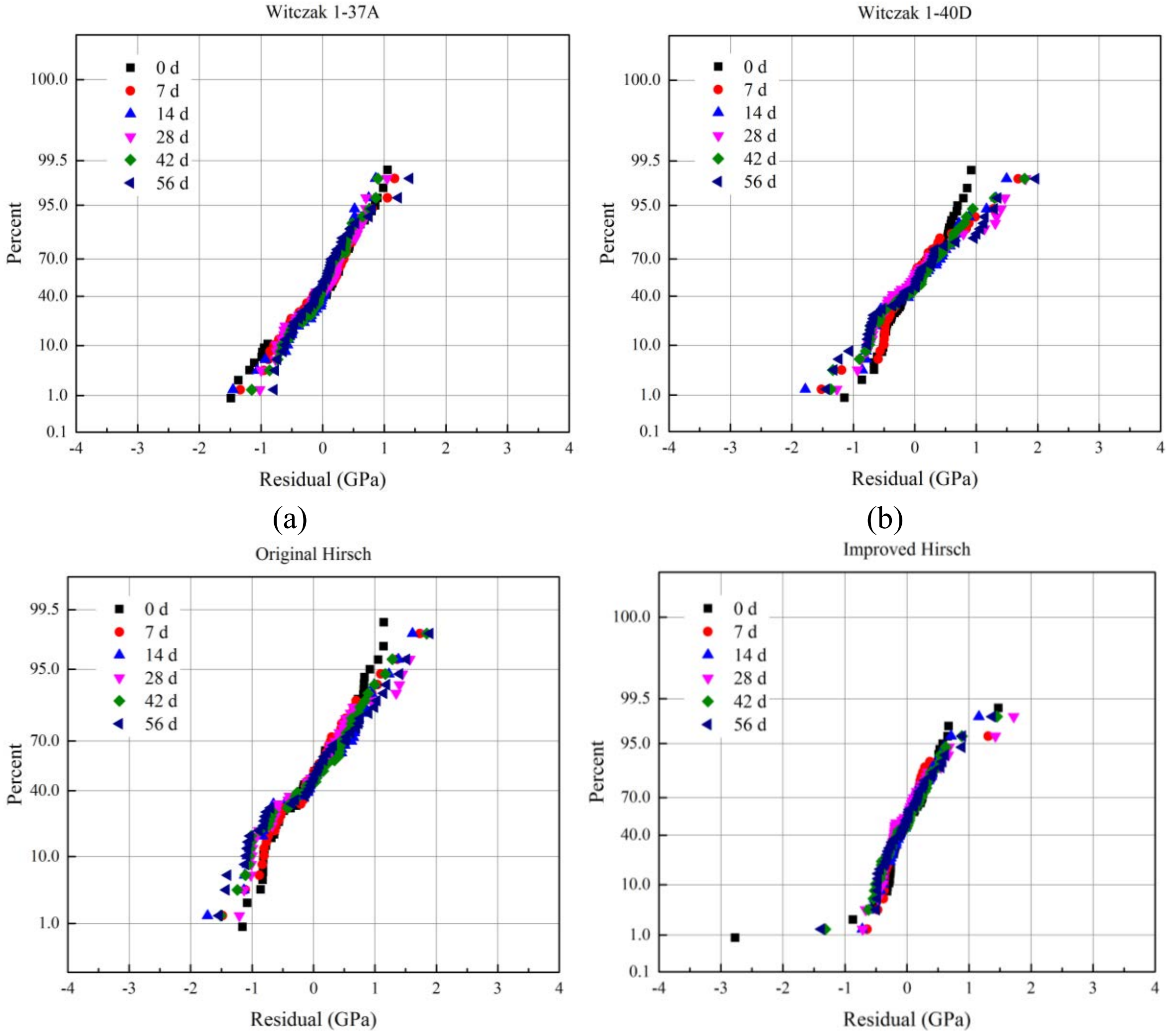

(a) (b)

(c) (d)

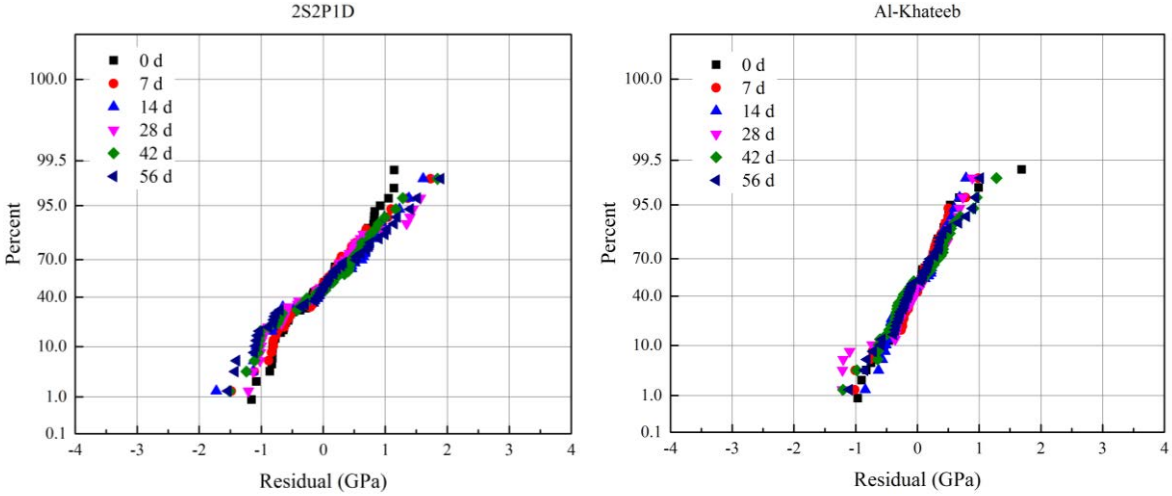

(e) (f)

Figure 6.11 The normal probability plot of residuals of (a) Witczak 1-37A, (b) Witczak 1-40D, (c) Original Hirsch, (d) Improved Hirsch, (e) 2S2P1D, and (f) Al-Khateeb models for SMA mixture

### 6.4.5 Bias of the predictive models

The slope, intercept and average error are three parameters to evaluate the model bias. Ideally, the slope, intercept and average error of a reliable model should be close to one, zero, and zero respectively. The deviation between the slope and one represents an overestimation or under prediction. Similarly, non-zero intercept and average error suggest that the predictions are overestimated or underpredicted. Figure 6.12 to 6.14 show the slopes, intercepts, and average errors of each model for WC, BC, SMA mixtures segregated by the aging states, respectively. As can be seen from these figures, the slopes of 2S2P1D model for the three mixture types at different aging levels were less than one, indicating that the model overestimates $|E^*|$ values. Witczak 1-40D model also exhibited the same trend for SMA mixture. Besides, the slopes of the other models were greater than one for three mixture types. The slopes of Al-Khateeb model were the highest in comparison with the other five models for WC, and BC mixtures. Witczak 1-37A also had the highest slope values for SMA mixture. On top of that, the slopes of Witczak 1-40D model were the closest to one for unaged WC and BC mixtures. For aged BC and SMA mixtures, the slopes of Improved Hirsch model were the closest to one. Also, the trends of the intercepts and average errors of the six predictive models were similar with those for WC and BC mixtures. The intercepts of Witczak 1-37A model were negative while most of the intercepts of the other five models were positive. The average errors of all models were negative except 2S2P1D model for WC and BC mixtures and Witczak 1-40D and 2S2P1D models for SMA mixture, indicating that most of the models underestimate $|E^{*}|$ values. The 2S2P1D model showed the highest intercept values and the least average errors for the three mixture types, indicating that the model significantly underpredicts $|E^{*}|$ values at high temperatures and overestimates them at other temperatures. It can also be seen that the slopes, intercepts, and average errors of the models exhibited the difference among the mixtures at different aging states. Improved Hirsch model showed the least difference in the slopes, intercepts, and average errors for the three specimens, indicating that the model is the least sensitivity to aging level compared with the other five models for the three types of asphalt mixtures blending with the base asphalt. Overall, Witczak 1-40D and Improved Hirsch models exhibited the highest accuracies in predicting $|E^{*}|$ values for unaged dense-graded (WC and BC), and SMA mixtures, respectively.

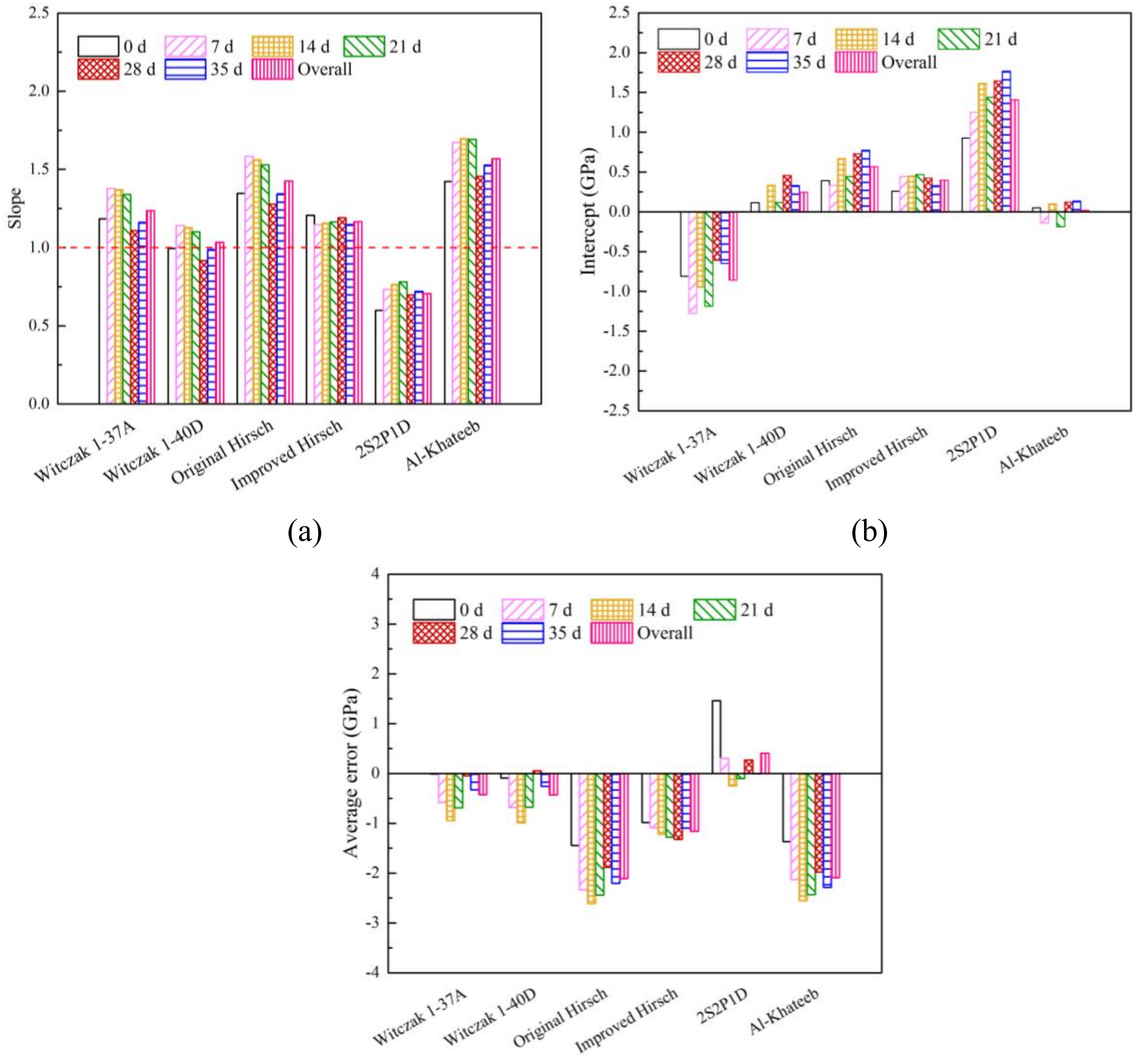

(a) (b)

(c)

Figure 6.12 The local and overall bias statistics for WC mixtures segregated by aging time: (a) Slope, (b) Intercept, and (c) Average error

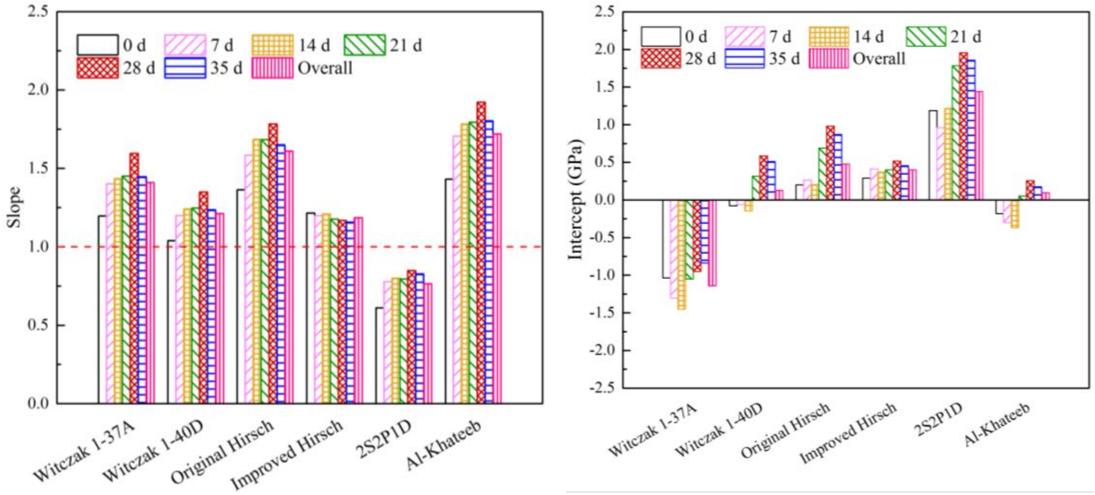

(a) (b)

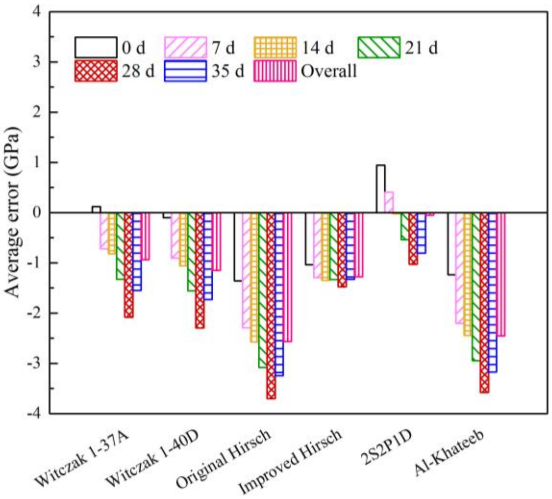

(c)

Figure 6.13 The local and overall bias statistics for BC mixtures segregated by aging time: (a) Slope, (b) Intercept, and (c) Average error

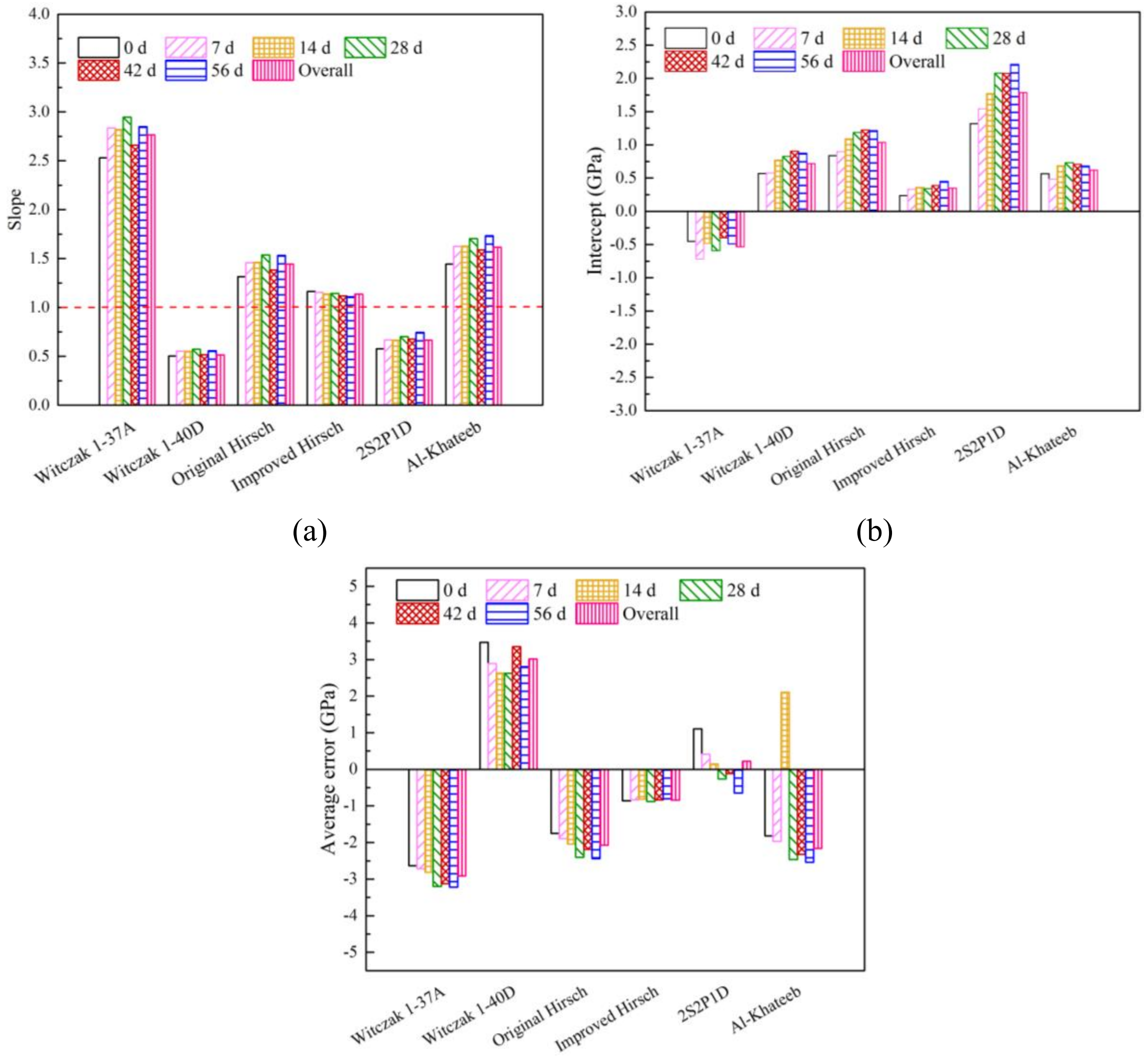

(a)

(b)

(c)

Figure 6.14 The local and overall bias statistics for SMA mixtures segregated by aging time: (a) Slope, (b) Intercept, and (c) Average error

### 6.4.6 Sensitivity analysis

Sensitivity analysis is a technique to evaluate the relationship between input and output parameters of a model [164]. Spearman's rank correlation coefficient was adopted to investigate the influence of input parameters on output parameters of a model [162, 165, 166]. Spearman's rank correlation coefficient ($\rho$) is a non-parametric method for evaluating the extent of correlation between the input and the output values, and it is independent of the relationship between two variables, which is calculated by using equation 6.18 [167].

$$\rho = 1 - \left(\frac{6\sum d_i^2}{n(n^2-1)}\right) \tag{6.18}$$

where $d_i$ is the difference in the ranks between the input and the output values in the same data pair, and $n$ is the number of simulations.

If the absolute value of ρ is close to one, the variable has the maximum effect on the oxygen diffusion coefficient; if $\rho$ is close to zero, the variable has the minimal effect. A positive $\rho$ indicates that a higher variable value leads to a higher oxygen diffusion coefficient, while a negative $\rho$ value means the opposite

In this study, A Tornado diagram was used as a pictorial illustration of the extent of the predicted $|E^*|$ values affected by its input parameters. Figures 6.15-6.17 show the Tornado plots of Spearman's rank correlation coefficients of the six models for WC, BC, and SMA mixtures, respectively. As can be seen from these figures, the binder properties inputs (i.e., $|G^*|$, $\delta$, and viscosity) were the most sensitivity in the prediction of $|E^*|$ values for the three mixture types. The high positive $\rho$ values of $|G^*|$ and viscosity for the models indicate the higher viscosity or $|G^*|$ values leads to higher predicted $|E^*|$ values of compacted asphalt mixtures and vice versa. The high negative $\rho$ values of $\delta$ of the binder for Witczak 1-40D model means as $\delta$ values of the binder decreases the predicted $|E^*|$ values of BC mixture increases. In addition, the inputs related to volumetric properties of mixtures (i.e., $V_a$, $VMA$, and $VFA$) had the minimal effect on the predictions of $|E^*|$ values for all six models except 2S2P1D model. In other words, the sensitivities of these models' predictions to $V_a$, $VMA$, and $VFA$ are insignificant. The $\rho$ values of frequency ($f$) in both Witczak models were positive and greater than $\rho$ values of volumetric properties of compacted asphalt mixtures, indicating that $f$ is positively correlated with predicted $|E^*|$ values though to a larger extent. Regarding 2S2P1D model, the $\rho$ value of characteristic time ($\tau$) was the highest followed by the pulsation ($\omega$), indicating that $\tau$ is the most sensitive in the prediction of $|E^*|$ values followed by $\omega$. It can also be seen that the aging did not have an obvious effect on the $\rho$ values of $|G^*|$, $\delta$, $V_a$, $VMA$, $VFA$, $\omega$, and $\tau$ for WC and BC mixtures. Furthermore, $\rho$ values of $V_a$, $VMA$, and $VFA$ of the SMA mixture, was changed from negative to positive or from positive to negative as the aging state of the mixture changed from unaged to aged. It indicates that these parameters of WC and BC mixtures are not sensitive to the aging levels and the aging has a slightly effect on these parameters of SMA mixture in predicting $|E^*|$ values. On top of these, the $\rho$ values of $\eta$ in Witczak 1-37A model for WC, BC, and SMA mixtures slightly decreased with increasing aging time, indicating that the aging reduces the predicted $|E^*|$ values. For Improved Hirsch model of the three mixture types, it is worth noting that the $\rho$ values of the peak-to-peak strain ($\varepsilon$) fluctuated with the increase of aging time and the most values were negative. It indicates that there is no a clear trend between aging levels and the $\rho$ values of $\varepsilon$.

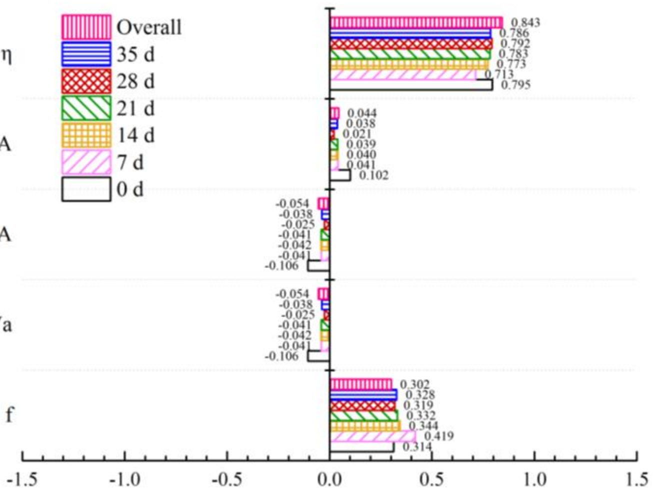
Overall
35 d
28 d
21 d
14 d
7 d
0 d
η
0.843
0.786
0.792
0.783
0.773
0.713
0.795
VFA
0.044
0.038
0.021
0.039
0.040
0.041
0.102
VMA
-0.054
-0.038
-0.025
-0.041
-0.042
-0.041
-0.106
Va
-0.054
-0.038
-0.025
-0.041
-0.042
-0.041
-0.106
f
0.302
0.328
0.319
0.332
0.344
0.419
0.314
-1.5
-1.0
-0.5
0.0
0.5
1.0
1.5

(a)

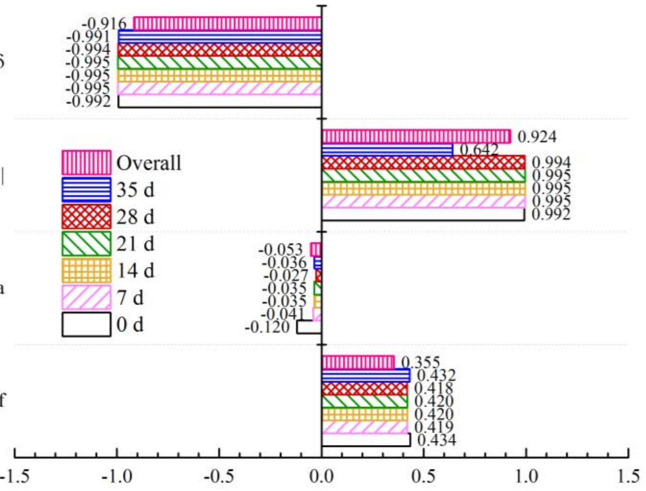
δ
-0.916
-0.991
-0.994
-0.995
-0.995
-0.995
-0.992
|G*|
0.924
0.642
0.994
0.995
0.995
0.995
0.992
Overall
35 d
28 d
21 d
14 d
7 d
0 d
Va
-0.053
-0.036
-0.027
-0.035
-0.035
-0.041
-0.120
f
0.355
0.432
0.418
0.420
0.420
0.419
0.434
-1.5
-1.0
-0.5
0.0
0.5
1.0
1.5

(b)

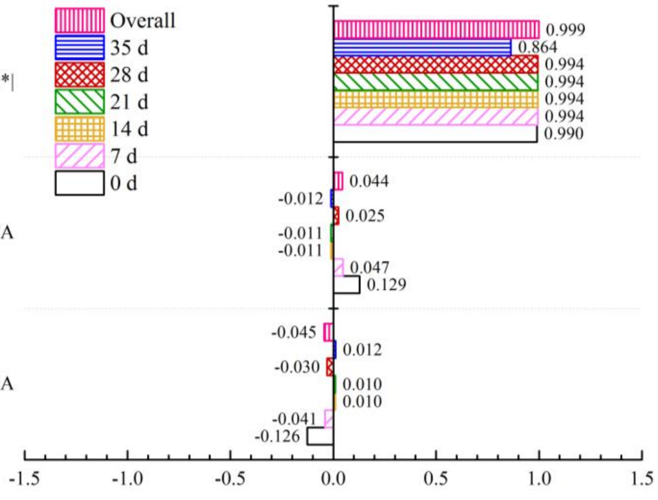
Overall
35 d
28 d
21 d
14 d
7 d
0 d
|G*|
0.999
0.864
0.994
0.994
0.994
0.994
0.990
VFA
0.044
-0.012
0.025
-0.011
-0.011
0.047
0.129
VMA
-0.045
0.012
-0.030
0.010
0.010
-0.041
-0.126
-1.5
-1.0
-0.5
0.0
0.5
1.0
1.5

(c)

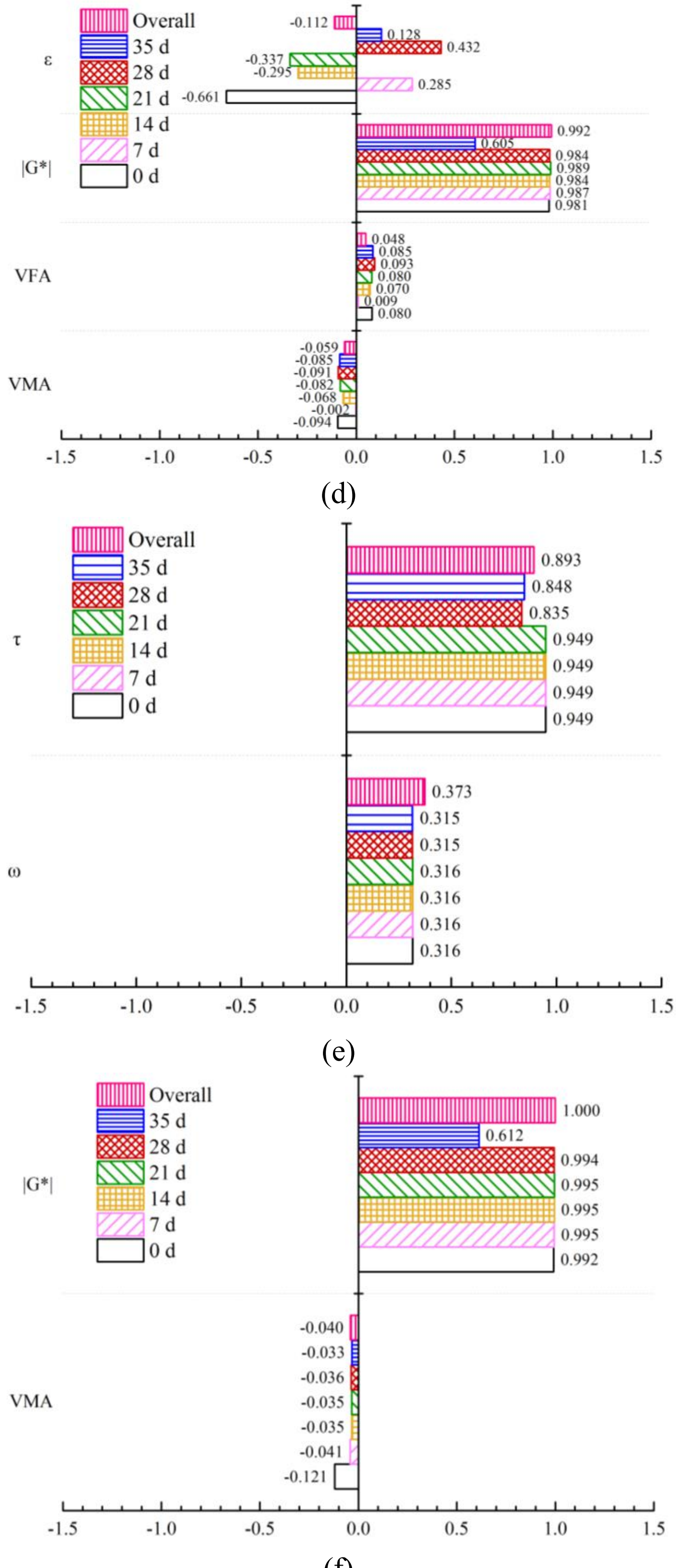

Figure 6.15 Tornado plots of Spearman’s rank correlation coefficient for WC mixture (a) Witczak 1-37A, (b) Witczak 1-40D, (c) Original Hirsch, (d) Improved Hirsch, (e) 2S2P1D, and (f) Al-Khateeb models

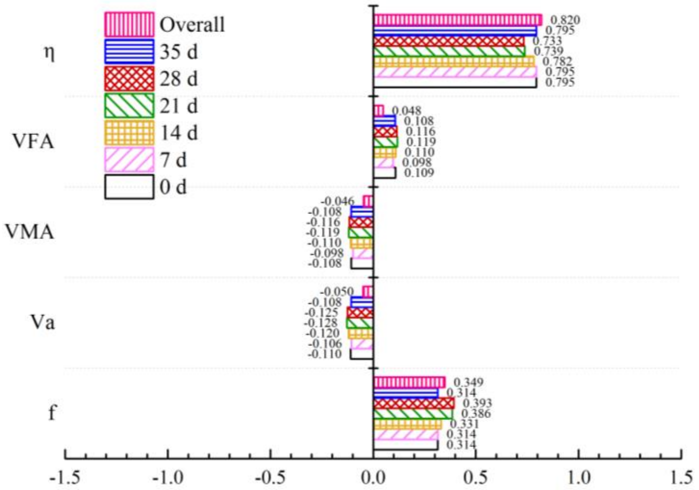
Overall
35 d
28 d
21 d
14 d
7 d
0 d
η
0.820
0.795
0.733
0.739
0.782
0.795
0.795
VFA
0.048
0.108
0.116
0.119
0.110
0.098
0.109
VMA
-0.046
-0.108
-0.116
-0.119
-0.110
-0.098
-0.108
Va
-0.050
-0.108
-0.125
-0.128
-0.120
-0.106
-0.110
f
0.349
0.314
0.393
0.386
0.331
0.314
0.314
-1.5
-1.0
-0.5
0.0
0.5
1.0
1.5

(a)

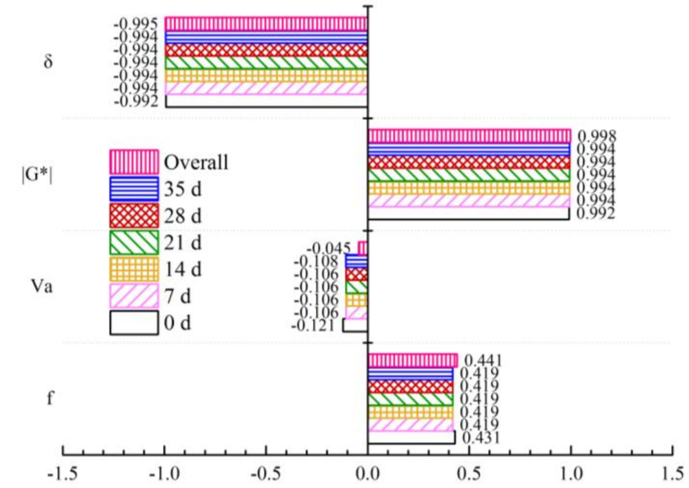
δ
-0.995
-0.994
-0.994
-0.994
-0.994
-0.994
-0.992
|G*|
0.998
0.994
0.994
0.994
0.994
0.994
0.992
Overall
35 d
28 d
21 d
14 d
7 d
0 d
Va
-0.045
-0.108
-0.106
-0.106
-0.106
-0.106
-0.121
f
0.441
0.419
0.419
0.419
0.419
0.419
0.431
-1.5
-1.0
-0.5
0.0
0.5
1.0
1.5

(b)

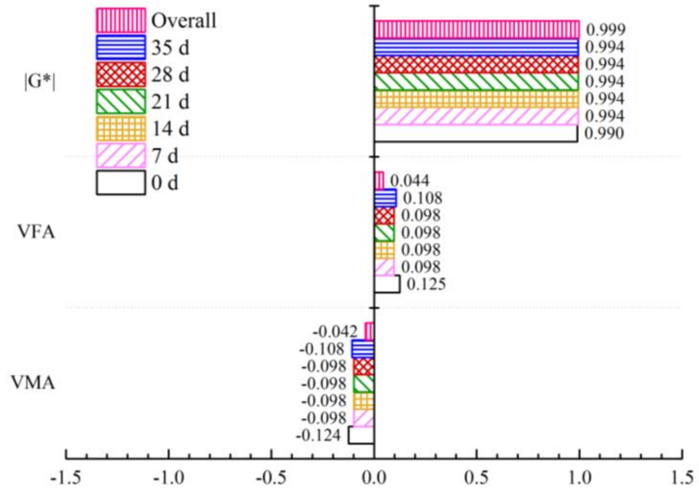
Overall
35 d
28 d
21 d
14 d
7 d
0 d
|G*|
0.999
0.994
0.994
0.994
0.994
0.994
0.990
VFA
0.044
0.108
0.098
0.098
0.098
0.098
0.125
VMA
-0.042
-0.108
-0.098
-0.098
-0.098
-0.098
-0.124
-1.5
-1.0
-0.5
0.0
0.5
1.0
1.5

(c)

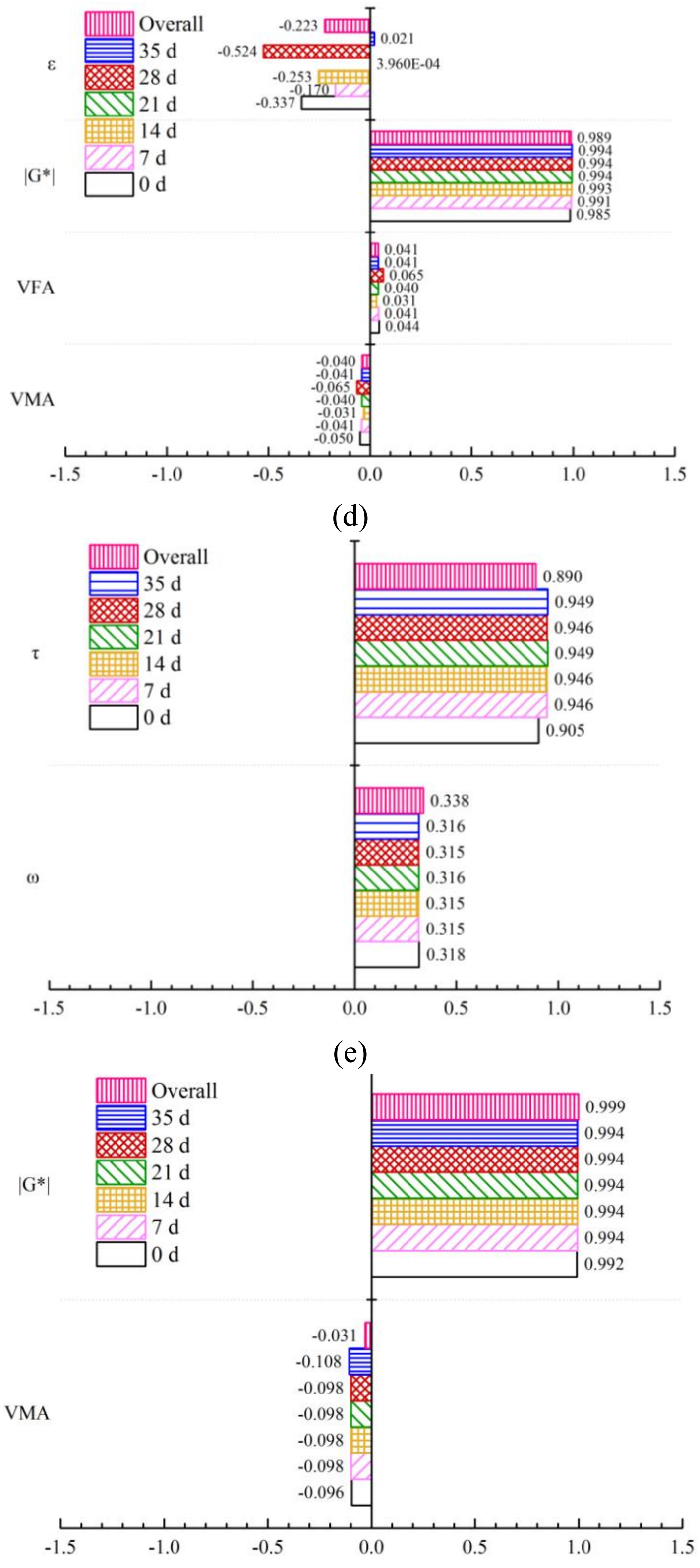

(d)

(e)

(f)

Figure 6.16 Tornado plots of Spearman's rank correlation coefficient for BC mixture (a) Witczak 1-37A, (b) Witczak 1-40D, (c) Original Hirsch, (d) Improved Hirsch, (e) 2S2P1D, and (f) Al-Khateeb models

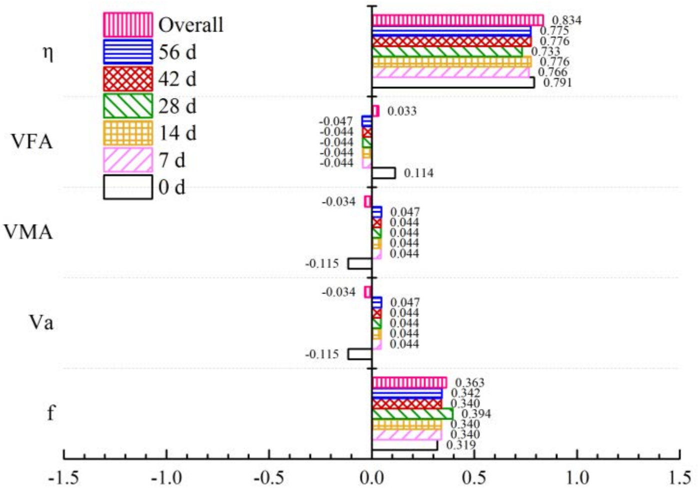
Overall
56 d
42 d
28 d
14 d
7 d
0 d
η
0.834
0.775
0.776
0.733
0.776
0.766
0.791
VFA
0.033
-0.047
-0.044
-0.044
-0.044
-0.044
0.114
VMA
-0.034
0.047
0.044
0.044
0.044
0.044
-0.115
Va
-0.034
0.047
0.044
0.044
0.044
0.044
-0.115
f
0.363
0.342
0.340
0.394
0.340
0.340
0.319
-1.5
-1.0
-0.5
0.0
0.5
1.0
1.5

(a)

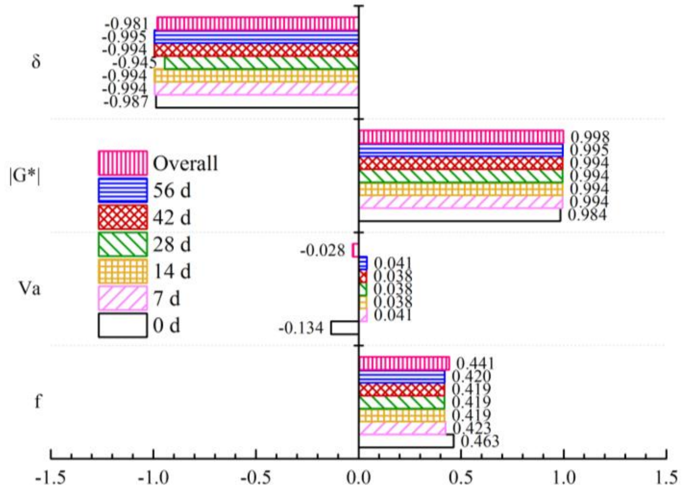
δ
-0.981
-0.995
-0.994
-0.945
-0.994
-0.994
-0.987
|G*|
0.998
0.995
0.994
0.994
0.994
0.994
0.984
Overall
56 d
42 d
28 d
14 d
7 d
0 d
Va
-0.028
0.041
0.038
0.038
0.038
0.041
-0.134
f
0.441
0.420
0.419
0.419
0.419
0.423
0.463
-1.5
-1.0
-0.5
0.0
0.5
1.0
1.5

(b)

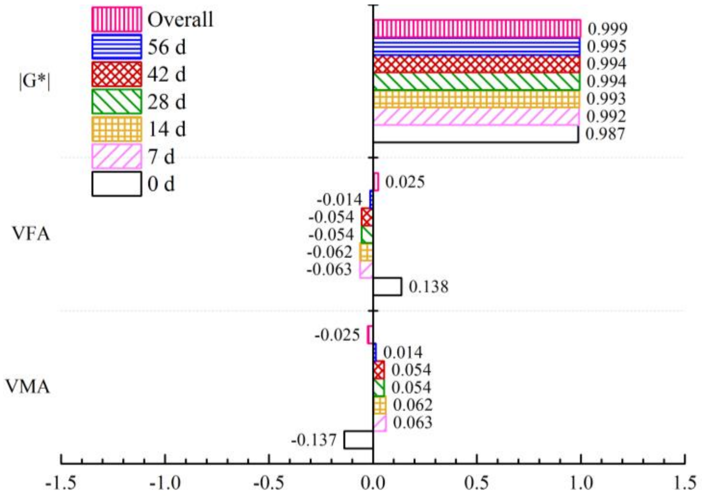
Overall
56 d
42 d
28 d
14 d
7 d
0 d
|G*|
0.999
0.995
0.994
0.994
0.993
0.992
0.987
VFA
0.025
-0.014
-0.054
-0.054
-0.062
-0.063
0.138
VMA
-0.025
0.014
0.054
0.054
0.062
0.063
-0.137
-1.5
-1.0
-0.5
0.0
0.5
1.0
1.5

(c)

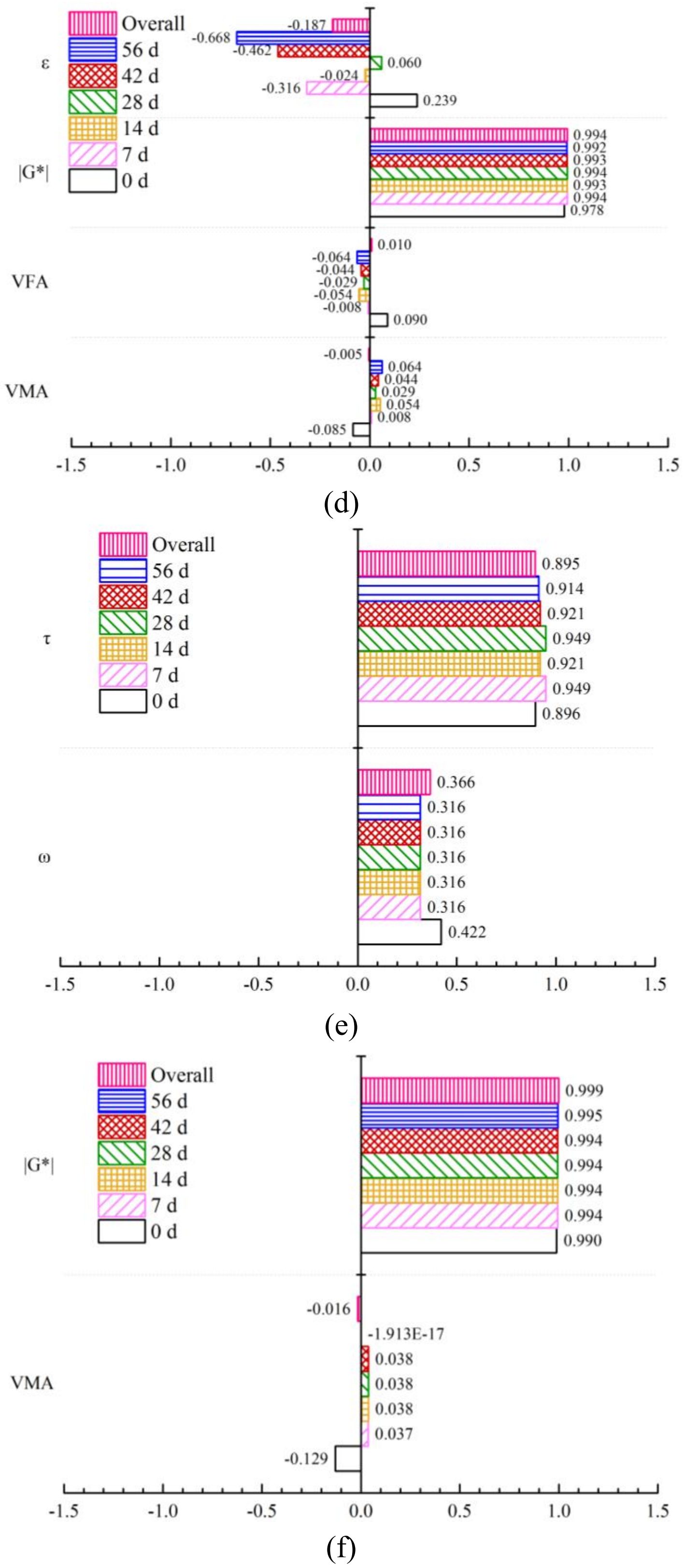

Figure 6.17 Tornado plots of Spearman's rank correlation coefficient for SMA mixture (a) Witczak 1-37A, (b) Witczak 1-40D, (c) Original Hirsch, (d) Improved Hirsch, (e) 2S2P1D, and (f) Al-Khateeb models

## 6.5 **Summary and conclusions**

In this chapter, $|E^*|$ values of the three types of asphalt mixtures blending with base asphalt (60/70 pen) were measured at different aging states in the laboratory. The effects of aging on the accuracies and sensitivities of six predictive models (Witczak 1-37A, Witczak 1-40D, Original Hirsch, Improved Hirsch, 2S2P1D, and Al-Khateeb) were then examined. The main conclusions can be succinctly drawn as follows.

(1) The $|E^*|$ values of compacted asphalt mixtures increase over aging time, and the increasing rates of $|E^*|$ values decrease with increasing aging time. Additionally, aggregate gradation shows an effect on the aging susceptibility of compacted asphalt mixtures.

(2) For WC and BC mixtures blending with the base asphalt, Witczak 1-40D performs a relatively high accuracy in predicting $|E^*|$ values compared with the other five models, especially for WC mixture. Besides, Witczak 1-37A model slightly overpredicts $|E^*|$ values at high temperatures and underestimates them at low temperatures. For SMA mixture blending with the base asphalt, Witczak 1-37A and 1-40D models substantially underpredict and overestimate $|E^*|$ values, respectively. On top of that, Original Hirsch, Improved Hirsch, and Al-Khateeb models underestimate $|E^*|$ values for the three mixture types over the whole temperature range. 2S2P1D model underpredicts $|E^*|$ values at high temperatures and overestimates them at the low temperatures for the three mixture types.

(3) For the three types of asphalt mixtures blending with the base asphalt, Improved Hirsch and 2S2P1D models are ranked as “Excellent” and “Good,” respectively. In

addition, the two Witczak models perform the better robustness for WC and BC mixtures (Grade E and G) than that for SMA mixture (Grade P and V). Finally, the best grade of Original Hirsch model is an “E” for WC mixture followed by BC and SMA mixtures classified as Grade F which is also the grade of the Al-Khateeb model for the three mixture types.

(4) For the three types of asphalt mixtures blending with the base asphalt, Improved Hirsch model exhibits the best robustness at different aging levels. Asphalt binder aging has an adverse effect on the robustnesses of Witczak 1-37A, Witczak 1-40D, Original Hirsch, and Al-Khateeb models and has a positive effect on that of the 2S2P1D model.

(5) For the three types of asphalt mixtures blending with the base asphalt at the same temperature, Witczak 1-37A, Witczak 1-40D, and Al-Khateeb models represent the better robustnesses for WC and BC mixtures than for SMA mixture. The robustnesses of the other three models are not sensitive to testing temperatures.

(6) For the levels of bias and error of the three types of asphalt mixtures blending with the base asphalt, Improved Hirsch model is the least sensitivity to aging level compared with the other five models. Additionally, Witczak 1-40D and Improved Hirsch models show the highest accuracies in predicting $|E^*|$ values for unaged WC and BC mixtures, and SMA mixtures at different aging states, respectively.

(7) The sensitivity analysis results indicate that the binder properties inputs (i.e., $|G^*|$, $\delta$, and $\eta$) are the most sensitive in the prediction of $|E^*|$ values for the three mixture types blending with the base asphalt. Additionally, the inputs related to the

volumetric properties of the three types of asphalt mixtures (i.e., $V_a$, $VMA$, and $VFA$) have the minimal effect on the predictions of $|E^*|$ values for all models except 2S2P1D model. For 2S2P1D model, τ is the most sensitive in predicting $|E^*|$ values followed by ω for the three mixture types blending with the base asphalt.

# CHAPTER 7. DEVELOPMENT OF A NEW APPROACH TO ASSESSING THE AGING SUSCEPTIBILITY OF COMPACTED ASPHALT MIXTURE

## 7.1 **Introduction**

The aging susceptibility of asphalt binder in asphalt pavement is essentially governed by pavement temperature and oxygen concentration in the pavement [14]. The oxygen concentration in asphalt pavement is dependent on oxygen diffusion and consumption coefficients of the asphalt pavement. For the oxygen diffusion and reaction in asphalt, researchers have developed different models to predict asphalt oxidation with time and position. The current aging models are developed related to the asphalt binder oxidation and can be classified into three categories: oxygen reaction rate models, oxygen diffusion models, and oxygen diffusion and consumption models. For oxygen reaction rate models, these models are developed according to Arrhenius's Equation [23, 25]. For oxygen diffusion and consumption models, the early diffusion models which do not consider the consumption of oxygen are developed using asphalt binder rather than asphalt mixture or pavement [109, 168]. Additionally, most of these models are not validated using the field oxidation data. Later, Glover's team makes modifications on the basis of the diffusion and reaction model proposed by Lunsford in the light of the actual air voids value obtained by using X-ray CT technique and field oxidation data [122, 169, 170]. However, oxygen diffusion coefficients obtained from these models are just parameters that oxygen diffuses into asphalt binder rather than the actual diffusion parameter that oxygen diffuses in the pavement. Therefore, it is also necessary to investigate the diffusion and reaction coefficient of asphalt pavement.

Compacted asphalt mixtures belong to one type of porous media. For the gaseous diffusion in porous media, it has been studied for many years. Buckingham firstly proposed a relationship between porosity of porous media and diffusion coefficient [171]. After that, several studies had been conducted to investigate the effect of the physical properties of soils, such as porosity, moisture, and particles size, on the diffusion coefficient of soil and proposed the different diffusion models [172-176]. Moreover, Sallam et al. designed a diffusion cell consisting of two air chambers separated by a soil chamber and verified these model under low air-filled porosities [177]. The diffusion model was calibrated to predict the diffusion well under the low air-filled porosity from 0.05 to 0.15. The two-chamber apparatus was then utilized to measure the gas diffusion in different types of materials by several researchers[178-181]. However, there is no published study to determine the oxygen diffusion coefficient in the pavement or compacted asphalt mixture.

To address the limits mentioned above, an apparatus to measure oxygen diffusion and consumption in compacted asphalt mixture was developed, and methods to compute oxygen diffusion coefficients and possible consumption rates of the asphalt mixtures were evaluated and compared. Based on our best knowledge, this is the first time that this approach is used to assess oxygen transport efficiency in the compacted asphalt mixture. The derived oxygen diffusion coefficients provide useful indications on the aging susceptibility of asphalt mixtures. The rest of the chapter is organized as follows. In section 7.2, the developed apparatus, as well as the computational methods, are introduced. In section 7.3, the experimental materials and methods are described. In section 7.4, examples of using the developed apparatus are illustrated, and the results are analyzed. In section 7.5, summary and conclusions are made. It is believed that the developed approach provides a convenient way to assess the aging susceptibility of asphalt mixtures, thereby contributing to the development of more durable asphalt mixture designs and quality control criteria in the future.

## 7.2 **The Measurement Equipment, Procedure, and Computational Methods**

### 7.2.1 The Measurement Equipment and Procedure

The concept of oxygen diffusion and consumption in asphalt mixture through the interconnected air paths is shown in Figure 7.1. Oxygen in the atmosphere enters asphalt pavement through the surface openings, or through the bottom openings if the air in pavement granular base or subbase has an oxygen level higher than that in the air inside of asphalt pavement. Oxygen diffuses rapidly into the interconnected air voids, but very slowly in asphalt binder and aggregate. As oxygen diffuses into asphalt binder, it reacts with some components in the asphalt. However, because the oxidative aging rate of asphalt binder at room temperature is slow and binder content is typically only about 4-6% of the total mixture by weight, the amount of consumed oxygen is believed to be small.

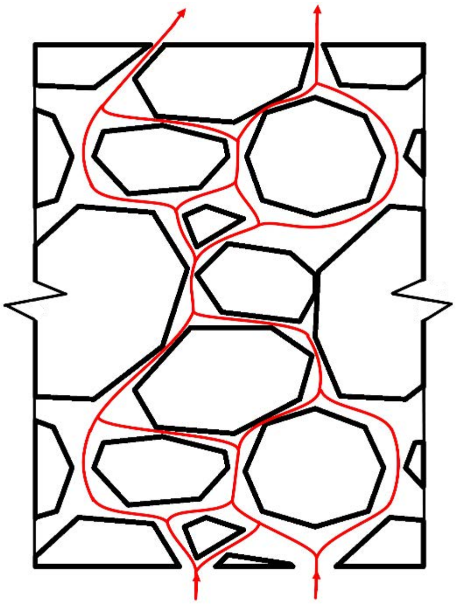

Figure 7.1 A schematic diagram of oxygen diffusion in compacted asphalt mixture

Gaseous diffusion in porous media has been extensively studied. Buckingham proposed a model between the porosity of porous media and diffusion coefficient [171]. Since then, several studies have been conducted to investigate the effect of the physical properties of soils, such as porosity, moisture, and particle size, on the diffusion coefficient of soil and proposed several diffusion models [172-176]. Sallam et al. designed a diffusion cell that consists of two air chambers separated by a soil sample chamber and then measured gas diffusion through soil at low air-filled porosity [177]. They found that the existing models result in high discrepancies between the estimated and measured values when the air-filled porosity is less than 0.30. The two-chamber apparatus was subsequently used to measure gaseous diffusion in different types of materials by several researchers [178-181]. To our best knowledge, there is no published study so far to determine the oxygen diffusion coefficient of compacted asphalt pavement samples.

In this study, a diffusion apparatus was developed as schematically presented in Figure 3.15. The diffusion system was then assembled as shown in Figure 7.2 The testing procedure for measuring oxygen diffusion and consumption was also developed, as summarized below.

(1) Prior to diffusion test, the oxygen analyzer needs to be calibrated in the free-flowing air and pure nitrogen.

(2) A compacted asphalt mixture specimen of 150 mm in diameter and about 60 mm in height is placed on a perforated plate.

(3) Solid Vaseline and an injection syringe are placed in an oven at 80°C. When the Vaseline becomes liquid, it is injected into the gap between the specimen and the chamber wall. The purpose is to prevent the flow of gas through the gap between the specimen and the chamber wall. Since the temperature of the specimen and tube is the same as room temperature, and the melting point of Vaseline is in the range of 45-60°C, the liquid Vaseline can transform into a solid state very quickly after being injected. The diffusion apparatus after being loaded with a specimen and sealed with Vaseline is shown in Figure 7.3.

(4) At the beginning of the test, all the air valves are opened to facilitate nitrogen to flow into the two reservoirs to expel oxygen in the apparatus and specimen until the oxygen concentration of the cells approaches to zero (In this study, it was found that the oxygen content was about 0.03% in the steady state).

(5) Four air valves in the reservoirs are then closed and monitored for a certain period (10 hours in this study, but the time can be shortened in future tests) to check whether the apparatus is well sealed.

(6) If the oxygen concentration is still close to zero after step (5), open the upper lid of the apparatus for 10 minutes to ensure the source reservoir is filled with air. After 10

minutes, the lid is closed, and oxygen will diffuse from the source chamber to receptor chamber due to oxygen concentration gradient between the two reservoirs.

(7) During the diffusion process, a data acquisition system is used to automatically record oxygen content until the oxygen concentration of the source reservoir is approximately equal to that of the receptor reservoir, except some asphalt mixture samples with extremely low diffusion coefficients.

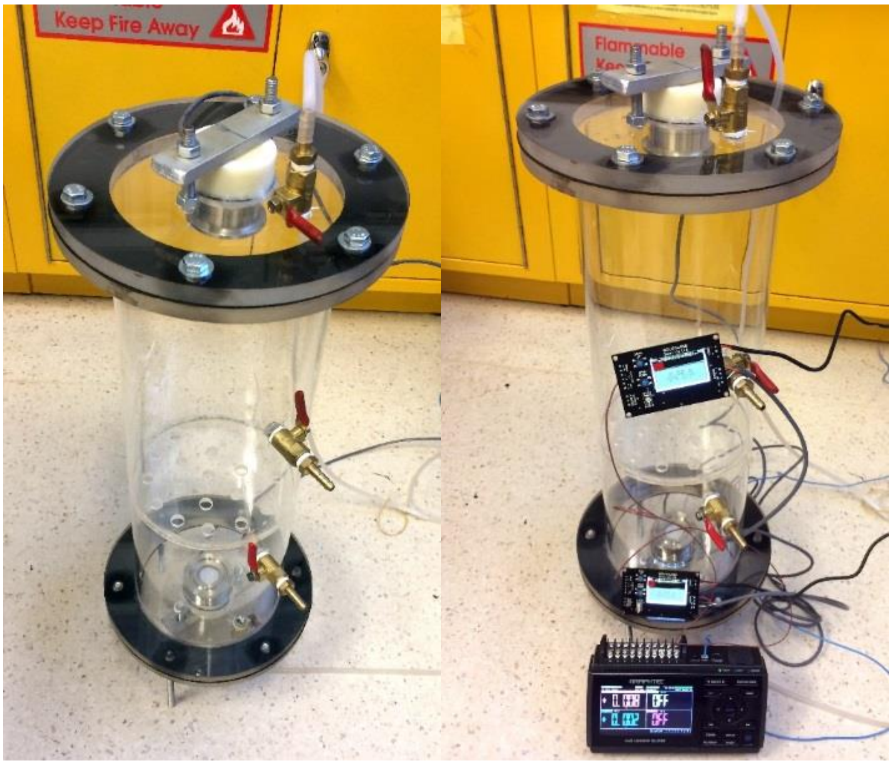

Figure 7.2 The customized diffusion test system with a data acquisition system

Figure 7.3 Part of the diffusion test system after being loaded with a specimen and sealed with Vaseline

### 7.2.2 Computation methods

For the two-chamber diffusion apparatus used in this study, the following conditions are assumed before analyzing the diffusion parameters:

(1) The oxygen diffusion coefficient $D_s$ of the compacted asphalt mixture ($-L \leq z \leq L$) is constant for each specimen (Note: All the dimensional information in the following equations and discussions is illustrated in Figure 7.4).

(2) The oxygen diffusion coefficient $D_g$ of the two-end chambers ($-(L+H) \leq z < -L$ and $L < z \leq L+M$) is constant.

(3) The oxygen concentration and gas flux $\partial C / \partial z$ are continuous at the interface ($z = \pm L$) between the compacted asphalt mixture and the gas chambers.

(4) Subjected to the assumptions above, equations for the two-chamber diffusion system

can be written as [177]:

In the two-end chambers: -(L+H) ≤ z < -L and L < z ≤ L+M

$$\frac{\partial C_g(z,t)}{\partial t} = D_g \frac{\partial^2 C_g(z,t)}{\partial z^2} \tag{7.1}$$

In the compacted asphalt mixture: $-L \leq z \leq L$

$$\frac{\partial C_s(z,t)}{\partial t} = D_s \frac{\partial^2 C_s(z,t)}{\partial z^2} - K_s \cdot C_s(z,t) \tag{7.2}$$

where $K_s$ is the oxygen cosumption coefficient of the compacted asphalt mixture, assumed to be a constant for each specimen.

If there is no oxygen consumption during the diffusion process or the oxygen consumption is negligible, Eq. (7.2) can be simplified as:

$$\frac{\partial C_s(z,t)}{\partial t} = D_s \frac{\partial^2 C_s(z,t)}{\partial z^2} \tag{7.3}$$

There is no gas flux at the two ends of the diffusion apparatus. Hence, the boundary condition can be expressed as:

$$\frac{\partial C_g(z,t)}{\partial z} = 0 \qquad \text{at } z = -(L+H) \text{ and } z = L+M \tag{7.4}$$

$$C_g(z,t) = C_s(z,t) \qquad \text{at } z = \pm L \tag{7.5}$$

$$-D_g \frac{\partial C_g(z,t)}{\partial z} = -D_s \frac{\partial C_s(z,t)}{\partial z} \qquad \text{at } z = \pm L \tag{7.6}$$

The initial conditions are set as

$$C(z,0) = C_0 \qquad -(L+H) \leq z < -L \tag{7.7}$$

$$C(z,0) = 0 \qquad -L \leq z \leq L \tag{7.8}$$

$$C(z,0) = 0 \qquad L < z \leq L+M \tag{7.9}$$

It is complicated to solve Eqs. (7.1) to (7.9) directly. Therefore, the system of equations is usually solved by an implicit finite difference method (FDM) or finite volume method (FVM). However, an analytical solution to determine the gaseous diffusion and consumption coefficients for a two-chamber diffusion system has been proposed by some researchers [125, 178, 181, 182]. In the analytical solution, the equations are solved by using Laplace transform or the separation of variables method under these boundary and initial conditions.

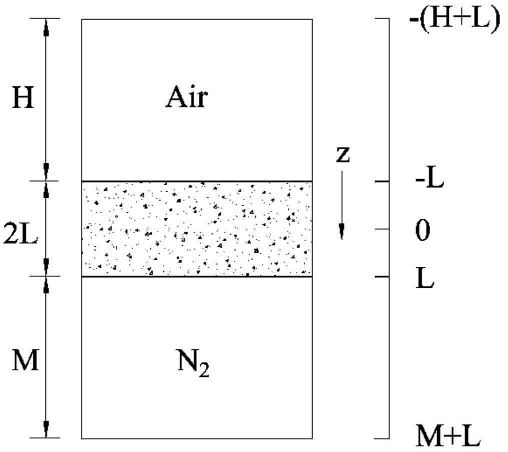

Figure 7.4 Dimensions of the two-chamber diffusion cell

7.2.2.1 Analytical solutions

*(1) Without the consideration of oxygen consumption in compacted asphalt mixture*

Since the oxidation rate of asphalt binder may become very slow at room temperature due to the inactivation of the polar aromatic fractions [10, 55], the oxygen consumption may be ignored when the diffusion test is conducted at room temperature. For a nonreactive diffusion test ($K_s = 0$) with the two-chamber apparatus, an analytical solution is given in a full form by Shair and Cohen [182] and is later simplified by Glauz and Rolston [183]. In their papers, the chamber dimensions were omittd and are given as:

$$\gamma = \frac{H}{M},\ \beta = \frac{H}{L\varepsilon},\ \tau = \frac{D_s t}{L^2 \varepsilon} \tag{7.10}$$

The analytical solution to Eq.(7.3) to (7.9) can be obtained by using Laplace transform. $D_s$ is optimized by making the calculated oxygen concentration to approximate the measured values at time *t*, using the Solver Tool in Excel.

$$\mathrm{C(z,t)} = C_{s0}\left[1/\left(1+\frac{1}{\gamma}+\frac{2}{\beta}\right)-\frac{A}{B}e^{-\alpha_1^2\tau}\right]-C_{r0} \tag{7.11}$$

where $C_{s0}$ is the initial oxygen concentration of the source chamber; $C_{r0}$ is the initial oxygen concentration of receptor chamber; $\alpha_1$, neglecting secondorder effects and oxygen concentration in the source chamber, is a function of $\beta$ and $\gamma$ [178]; A and B are the function of $\beta$, $\gamma$, and $\alpha_1$, and are given as:

$$\alpha_1 = \left[\frac{1}{2\beta}(1+\gamma) - \frac{1}{3\beta^2}(\gamma^2-\gamma+1) + \frac{2}{45\beta^3}(4\gamma^3-3\gamma^2-3\gamma+4)\right]^{1/2} \quad (7.12)$$

$$\mathrm{A} = -\frac{\gamma}{\beta^2} - \frac{\alpha_1^2}{\gamma} \quad (7.13)$$

$$\mathrm{B} = \alpha_1^4\frac{\beta}{\gamma} + \alpha_1^2\left(\frac{1}{\beta\gamma} + \frac{\gamma}{\beta} + \frac{1}{2\gamma} + \frac{1}{2}\right) + \frac{\gamma}{\beta^3} + \frac{\gamma}{2\beta^2} + \frac{1}{2\beta^2} \quad (7.14)$$

For oxygen concentration in the receptor chamber, Eq.(7.13) is replaced with

$$\mathrm{A} = \left[\alpha_1^4 + \frac{\gamma^2}{\beta^4} + (1+\gamma^2)\left(\frac{\alpha_1}{\beta}\right)^2\right]^{1/2} \quad (7.15)$$

After a sufficiently long time, a steady state condition can be researched. The concentration in both air chambers and the mixture will be then maintained at a constant level, as illustrated in Figure 7.5.

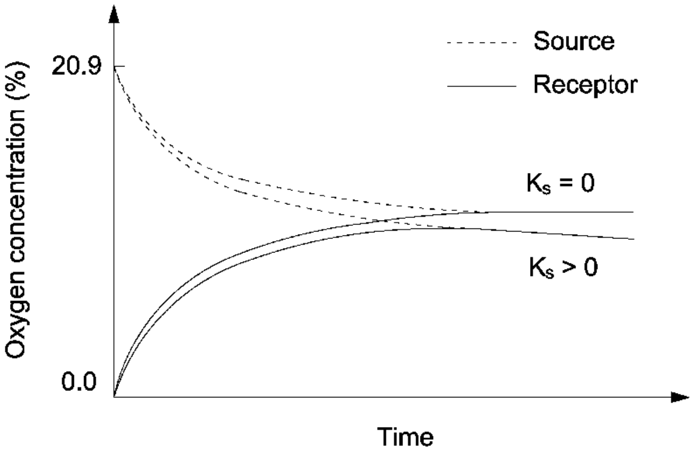

Figure 7.5 The schematic diagram of oxygen diffusion with and without oxygen consumption in source and receptor reservoirs

*(2) With oxygen consumption in compacted asphalt mixture*

If oxygen consumption in compacted asphalt mixture cannot be ignored, oxygen concentrations in both air chambers and the mixture specimen will initially reach a pseudo-steady state and then continuously decrease over time as oxygen is consumed, as shown in Figure 7.5.

For the diffusion process with a reaction rate coefficient $K_s$, Mbonimpa et al [181] provides a general solution of Eq.(7.2) for the same boundary conditions on the basis of Danckwerts' method [125]:

$$\mathrm{C(z,t)} = \mathrm{C}_{s0}\left[1-\frac{z}{L}-\frac{2}{\pi}\sum_{i=1}^{\infty}\frac{\sin(i\pi z/L)}{i}exp\left(-\left(\frac{i^2\pi^2}{L^2}D_s+K_s\right)t\right)- \frac{2K_s}{\pi}\sum_{i=1}^{\infty}\frac{\sin(i\pi z/L)}{i^2\pi^2D_s/L^2+K_s}\left\{1-exp\left[-\left(\frac{i^2\pi^2}{L^2}D_s+K_s\right)t\right]\right\}\right] \tag{7.16}$$

### 7.2.2.2 Numerical solution

FVM is a numerical method for solving partial differential equations. Since FVM was introduced into the field of computational fluid dynamics in the 1970s [184, 185], it has become very trendy in solving the convective diffusion problems due to its robustness, flexibility, and simple algorithmization [186]. The method, therefore, is widely adopted in many computational fluid dynamics programs [187].

To obtain a numerical solution for the three-layer diffusion system, a mesh is defined for each layer consisting of nodes $x_{i,j}$. For simplicity, it is assumed that each layer has $n$+1 equally-spaced nodes satisfying:

$$x_{i,j} = l_{i-1} + jh_i, \qquad i = 1,2,3, \quad j = 1,\ldots,\mathrm{n} \tag{7.17}$$

where $h_i = (l_i - l_{i-1})/n$, and $n$ is the number of divisions in each layer. Carr [188] utilizes a backward Euler discretization in time with time step $\tau$ and adopts $u_{i,j}^{(k)}$ as the numerical approximation to replace the value of $\mathrm{u}(x_{i,j}, t_k)$, where $t_k = k\tau$. Under the initial and boundary conditions listed above, the following finite volume scheme for the three-layer diffusion problem is derived:

First layer ($i$=1):

$$u_{1,0}^{(k+1)} - u_{1,0}^{(k)} = \frac{k_1\tau}{V_{1,0}}\left(\frac{u_{1,1}^{(k+1)} - u_{1,0}^{(k+1)}}{h_1}\right) \tag{7.18a}$$

$$u_{1,j}^{(k+1)} - u_{1,j}^{(k)} = \frac{k_1\tau}{V_{1,j}}\left(\frac{u_{1,j+1}^{(k+1)} - u_{1,j}^{(k+1)}}{h_1} - \frac{u_{1,j}^{(k+1)} - u_{1,j-1}^{(k+1)}}{h_1}\right), \quad j=1,\ldots,n-1 \tag{7.18b}$$

Middle layer ($i$=2):

$$u_{2,0}^{(k+1)} - u_{2,j}^{(k)} = \frac{\tau}{V_{1,n}+V_{2,0}}\left(k_2\frac{u_{2,1}^{(k+1)} - u_{2,0}^{(k+1)}}{h_2} - k_1\frac{u_{1,n}^{(k+1)} - u_{1,n-1}^{(k+1)}}{h_1}\right) \tag{7.18c}$$

$$u_{2,j}^{(k+1)} - u_{2,j}^{(k)} = \frac{k_2\tau}{V_{2,j}}\left(\frac{u_{2,j+1}^{(k+1)} - u_{2,j}^{(k+1)}}{h_2} - \frac{u_{2,j}^{(k+1)} - u_{2,j-1}^{(k+1)}}{h_2}\right), \quad j=1,\ldots,n-1 \tag{7.18d}$$

End layer ($i$=3):

$$u_{3,0}^{(k+1)} - u_{3,j}^{(k)} = \frac{\tau}{V_{2,n}+V_{3,0}}\left(k_3\frac{u_{3,1}^{(k+1)} - u_{3,0}^{(k+1)}}{h_3} - k_2\frac{u_{2,n}^{(k+1)} - u_{2,n-1}^{(k+1)}}{h_2}\right) \tag{7.18e}$$

$$u_{3,j}^{(k+1)} - u_{3,j}^{(k)} = \frac{k_3\tau}{V_{3,j}}\left(\frac{u_{3,j+1}^{(k+1)} - u_{3,j}^{(k+1)}}{h_3} - \frac{u_{3,j}^{(k+1)} - u_{3,j-1}^{(k+1)}}{h_3}\right), \quad j=1,\ldots,n-1 \tag{7.18f}$$

$$u_{3,n}^{(k+1)} - u_{3,n}^{(k)} = \frac{k_3\tau}{V_{3,n}}\left(-\frac{u_{3,n}^{(k+1)} - u_{3,n-1}^{(k+1)}}{h_3}\right) \tag{7.18g}$$

The equations for the three-layer diffusion system has been implemented through a MATLAB program, which is also published by Carr [188].

Both the numerical and analytical methods were used in this study to determine $D_s$ and $K_s$ values. Oxygen concentrations in the two reservoirs were predicted based on the predetermined $D_s$ and $K_s$ values. The predicted and measured oxygen concentrations were then used to make adjustments to $D_s$ and $K_s$ values until the "best-fit" was found. In general, $D_s$ and $K_s$ values are unique for the same specimens [181]. There are two key questions that remain to be answered:

(1) Is oxygen consumption noticeable during the diffusion test of compacted asphalt

mixture specimens?

(2) Do the numerical and analytical methods generate comparable results for the asphalt mixture specimens?

These questions were investigated and are presented in the following section.

## 7.3 **Material and specimen preparation**

Three types of HMA mixtures (WC, BC, and SMA) were prepared using non-modified asphalt binder (penetration grade 60/70) and granite aggregate. The gradations and volumetric properties of the mixtures are summarized in Table 6.1 and Table 7.1, respectively. For the SMA mixture, the hydrated lime content was 3% by mass of the total aggregate, and the cellulosic fiber content was 0.5% by mass of the total asphalt mixture. Prior to compaction, loose asphalt mixtures were short-term aged in a forced-draft oven for four hours at 135°C in accordance with AASHTO R30. The short-term aged samples were then compacted to a target air void using a Superpave® gyratory compactor.

Table 7.1 The volumetric properties of the mixtures and sample dimension

| Sample No. | Binder content (%) | $V_a$ (%) | VMA (%) | VFA (%) | Thickness (mm) |
|---|---|---|---|---|---|
| WC-1 | 5.4 | 9.4 | 20.9 | 55.2 | 59.3 |
| WC-2 | | 8.3 | 20.0 | 58.5 | 58.2 |
| WC-3 | | 6.1 | 18.1 | 66.0 | 56.8 |
| WC-4 | | 9.5 | 22.3 | 50.8 | 58.1 |
| WC-5 | | 11.6 | 25.4 | 43.0 | 60.7 |
| BC-1 | 5.0 | 3.1 | 13.7 | 77.3 | 60.4 |
| BC-2 | | 16.0 | 25.2 | 36.6 | 63.2 |
| BC-3 | | 13.6 | 23.1 | 41.0 | 61.5 |
| BC-4 | | 12.4 | 22.0 | 43.7 | 63.1 |
| BC-5 | | 11.8 | 21.5 | 45.0 | 62.3 |
| SMA-1 | 6.5 | 7.0 | 21.3 | 67.1 | 62.8 |
| SMA-2 | | 5.9 | 20.3 | 71.1 | 62.3 |
| SMA-3 | | 16.2 | 29.1 | 44.3 | 71.1 |
| SMA-4 | | 10.0 | 23.8 | 58.0 | 66.0 |
| SMA-5 | | 13.6 | 26.8 | 49.5 | 69.1 |

## 7.4 **The application of the developed methods**

### 7.4.1 Evaluation of oxygen consumption during the diffusion test

Oxygen is consumed in the oxidative aging of asphalt binder. However, due to the short period and low temperature, oxygen consumption may not be noticeable during the diffusion test. Because the equations to determine $D_S$ will be different with or without the consideration of oxygen consumption, this study first evaluated whether oxygen consumption is significant. If oxygen consumption is insignificant, oxygen concentrations in the source and receptor reservoirs will maintain at a constant level after the oxygen concentrations at the two reservoirs are balanced. Otherwise, the oxygen concentrations of the two reservoirs will firstly reach a pseudo-steady state and then continuously decrease over time as oxygen is consumed. In this study, several specimens were used to evaluate the significance of oxygen consumption and its possible impacts on the subsequent calculations. The measured results from one example specimen are shown in Figure 7.6. As can be seen in the figure, the oxygen concentrations of the source and receptor chambers firstly reached a steady state, and then stayed at an anpproxiamately constant value of 11.5% over time. Based on the data points after the approximate steady state, regression curves were developed for the measured oxygen concentration values at the two chambers. As shown in Figure 7.6, the slopes of the regression curves are both close to zero. Therefore, oxygen consumption during the test period can be safely ignored.

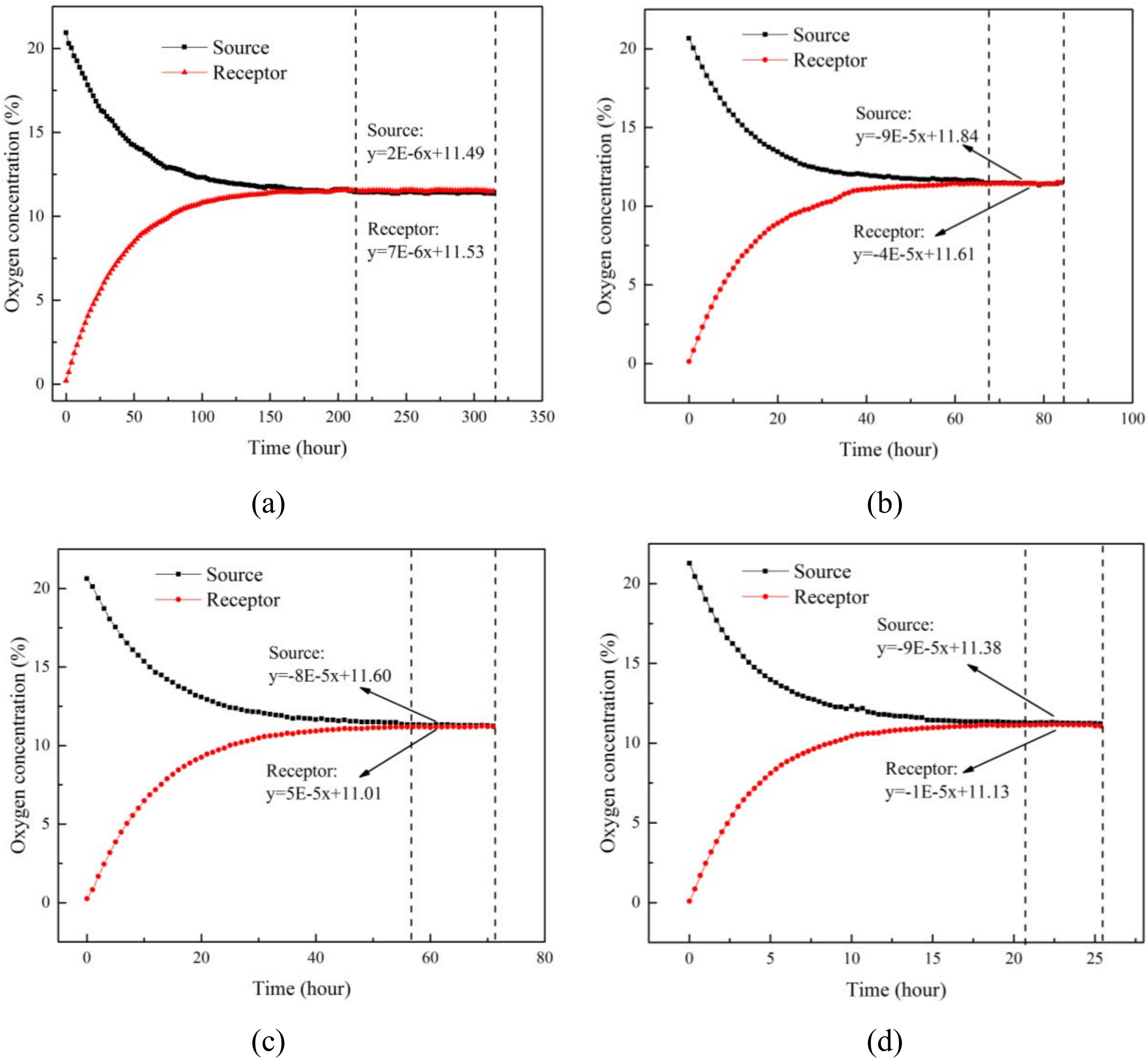

(a) (b)

(c) (d)

Figure 7.6 The oxygen concentration of source and receptor chambers over time for four specimens: (a) WC-2, (b) BC-2, (c) BC-3, and (d) SMA-3

### 7.4.2 Comparison of oxygen diffusion coefficients determined by different calculation methods

Without the consideration of oxygen consumption during the diffusion tests, the oxygen diffusion coefficients of specimens were calculated using the experimental data and the computational methods previously discussed. The experimental data suggest that oxygen concentration in the receptor reservoir initially increases at a relatively rapid rate, and then increases slowly (oxygen concentration in the source reservoir follows the opposite trend). To obtain the most accurate diffusion coefficients, ideally, the diffusion test may continue until the steady state has reached. However, the diffusion processes of the specimens were found to vary greatly. For some specimens, the diffusion process reached a steady state in a few days, while for some specimens, the diffusion could not arrive at a steady state even after several months! Because of the difficulty in obtaining the full data points till the steady state for those specimens with very slow diffusion rate, the $D_s$ values of such specimens were calculated using the data points before the steady state. For the same reason, the number of tested specimens was not large.

The calculated diffusion coefficients of the specimens are summarized in Table 7.2. Also shown in the table are the corresponding air void contents. The results indicate that the diffusion coefficients calculated by the two methods are very close. A paired-t-test was used to assess the difference between the two computational methods more rigorously. With a t-value of 2.13 and sample size of 15, there is no statistically significant difference between the numerical and analytical solutions. Therefore, both methods can be used to calculate the oxygen diffusion coefficients of the compacted asphalt mixture samples.

Table 7.2 The oxygen diffusion coefficient of three type of compacted asphalt mixture

| Sample No. | $D_s$ (cm$^2$/s) | | Air Voids |
|---|---|---|---|
| | Numerical solution | Analytical solution | (%) |
| WC-1 | 1.52E-03 | 1.50E-03 | 9.4 |
| WC-2 | 4.32E-04 | 4.30E-04 | 8.3 |
| WC-3 | 2.04E-04 | 2.06E-04 | 6.1 |
| WC-4 | 1.29E-03 | 1.27E-03 | 9.5 |
| WC-5 | 3.97E-03 | 3.75E-03 | 14.5 |
| BC-1 | 2.81E-06 | 2.76E-06 | 3.1 |
| BC-2 | 1.36E-03 | 1.37E-03 | 16.0 |
| BC-3 | 1.49E-03 | 1.47E-03 | 13.6 |
| BC-4 | 1.31E-03 | 1.28E-03 | 12.4 |
| BC-5 | 5.08E-04 | 5.09E-04 | 11.8 |
| SMA-1 | 7.32E-05 | 7.28E-05 | 7.0 |
| SMA-2 | 3.94E-05 | 3.94E-05 | 5.9 |
| SMA-3 | 5.08E-03 | 4.99E-03 | 16.2 |
| SMA-4 | 7.86E-04 | 7.73E-04 | 10.0 |
| SMA-5 | 3.15E-03 | 3.05E-03 | 13.6 |

To assess the overall accuracy of the calculated diffusion coefficients and the computation methods, the predicted and measured oxygen concentrations as a function of time are presented in Figure 7.7. The figure suggests that the predicted oxygen concentrations well match the measured values for all the specimens. Both the numerical solution and the analytical solution perform well, although the analytical solution seems slightly better. The comparison results suggest that it is feasible to calculate the oxygen diffusion coefficients of compacted asphalt mixture using the developed apparatus, test procedure, and existing computational methods. Hence, this study provides a new way to evaluate the oxygen transport efficiency of compacted asphalt mixtures.

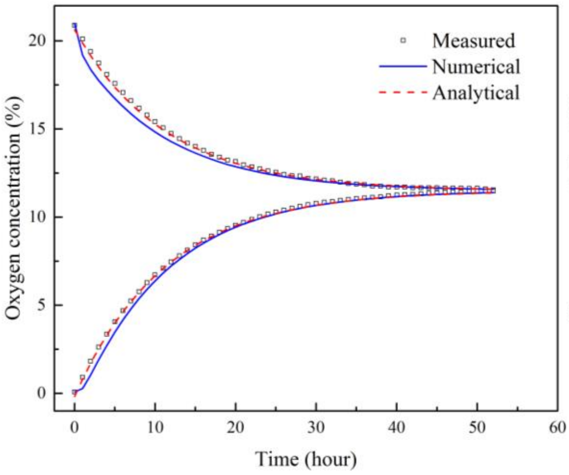
Measured
Numerical
Analytical
Oxygen concentration (%)
0
5
10
15
20
Time (hour)
0
10
20
30
40
50
60

(a)

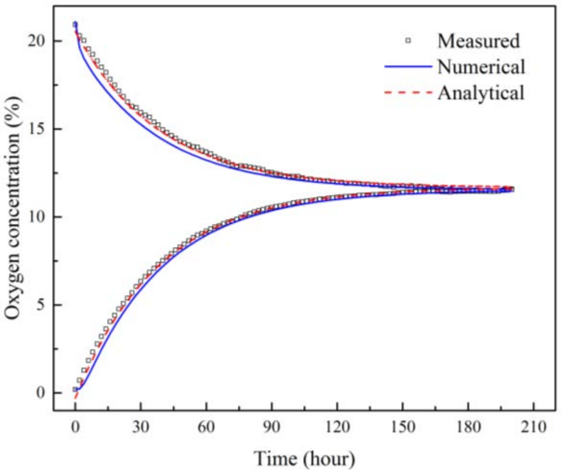
Measured
Numerical
Analytical
Oxygen concentration (%)
0
5
10
15
20
Time (hour)
0
30
60
90
120
150
180
210

(b)

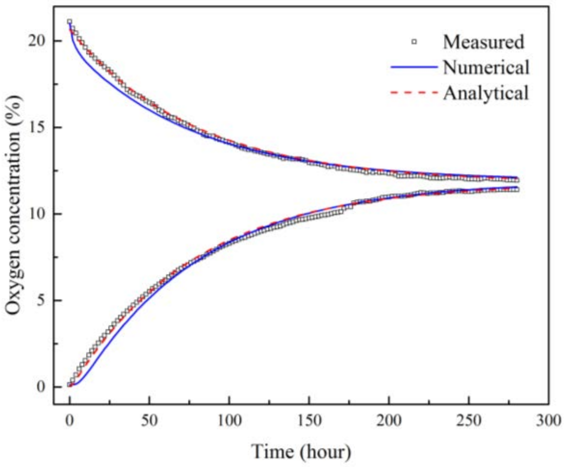
Measured
Numerical
Analytical
Oxygen concentration (%)
0
5
10
15
20
Time (hour)
0
50
100
150
200
250
300

(c)

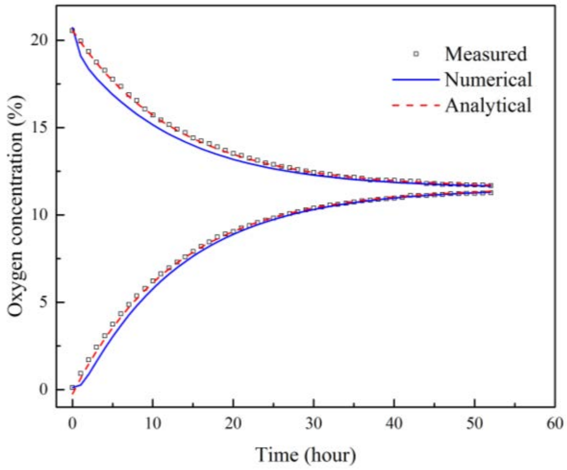
Measured
Numerical
Analytical
Oxygen concentration (%)
0
5
10
15
20
Time (hour)
0
10
20
30
40
50
60

(d)

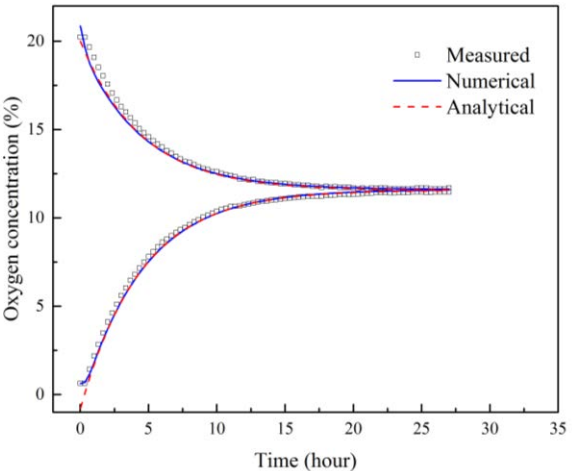
Measured
Numerical
Analytical
Oxygen concentration (%)
0
5
10
15
20
Time (hour)
0
5
10
15
20
25
30
35

(e)

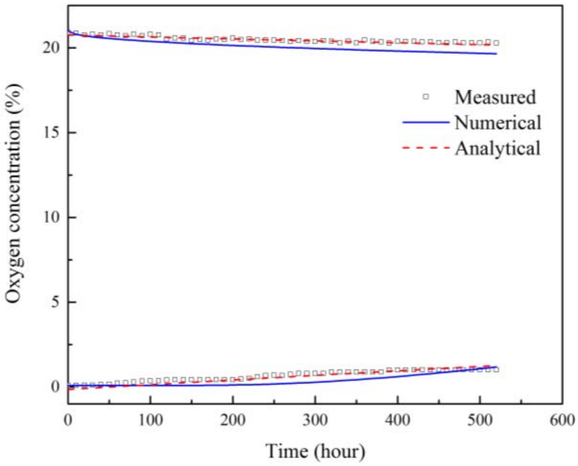
Measured
Numerical
Analytical
Oxygen concentration (%)
0
5
10
15
20
Time (hour)
0
100
200
300
400
500
600

(f)

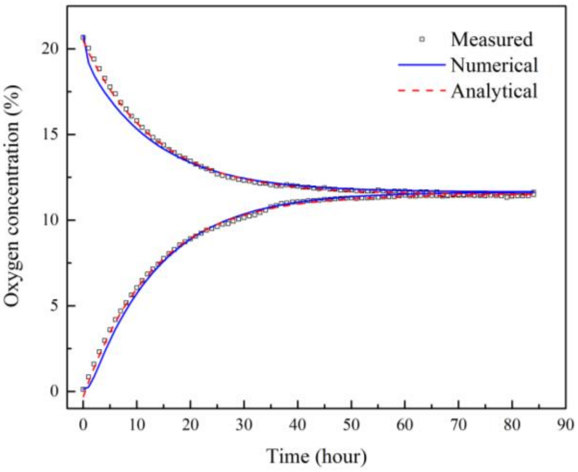
Measured
Numerical
Analytical
Oxygen concentration (%)
0
5
10
15
20
Time (hour)
0
10
20
30
40
50
60
70
80
90

(g)

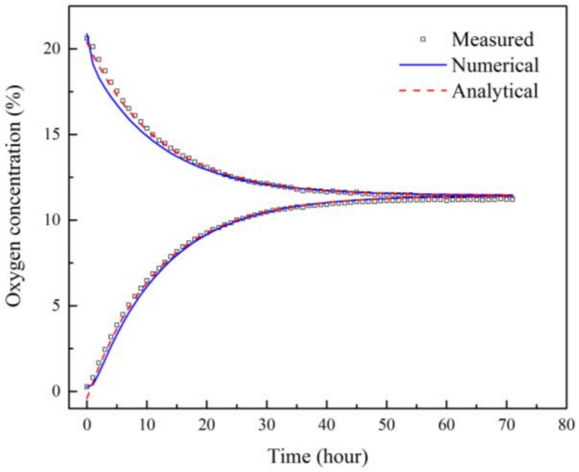
Measured
Numerical
Analytical
Oxygen concentration (%)
0
5
10
15
20
Time (hour)
0
10
20
30
40
50
60
70
80

(h)

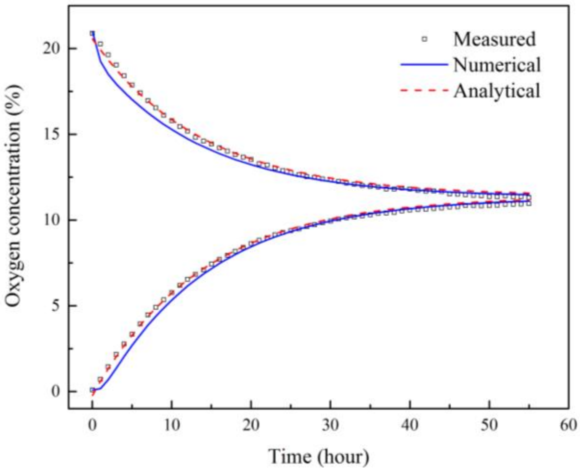
Measured
Numerical
Analytical
Oxygen concentration (%)
0
5
10
15
20
Time (hour)
0
10
20
30
40
50
60

(i)

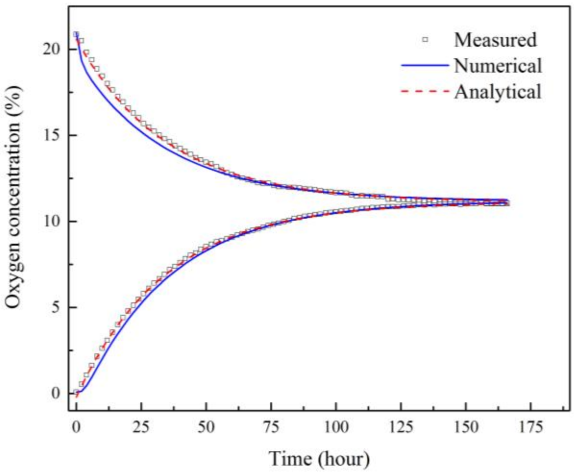
Measured
Numerical
Analytical
Oxygen concentration (%)
0
5
10
15
20
Time (hour)
0
25
50
75
100
125
150
175

(j)

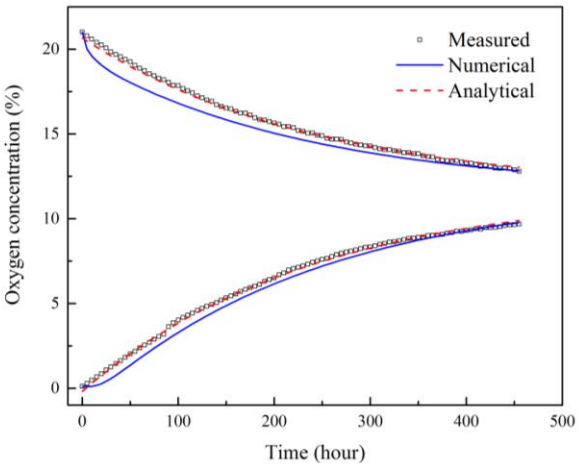
Measured
Numerical
Analytical
Oxygen concentration (%)
0
5
10
15
20
Time (hour)
0
100
200
300
400
500

(k)

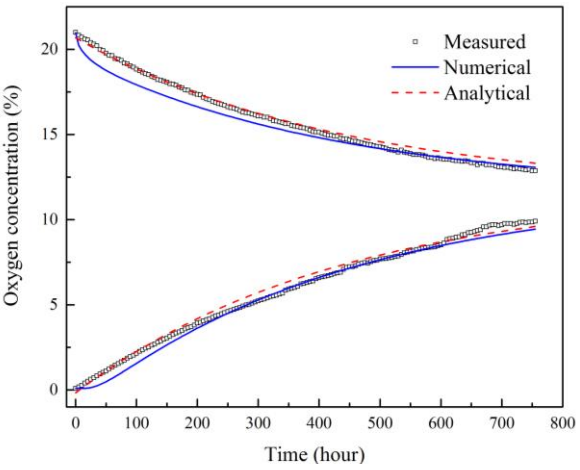
Measured
Numerical
Analytical
Oxygen concentration (%)
0
5
10
15
20
Time (hour)
0
100
200
300
400
500
600
700
800

(l)

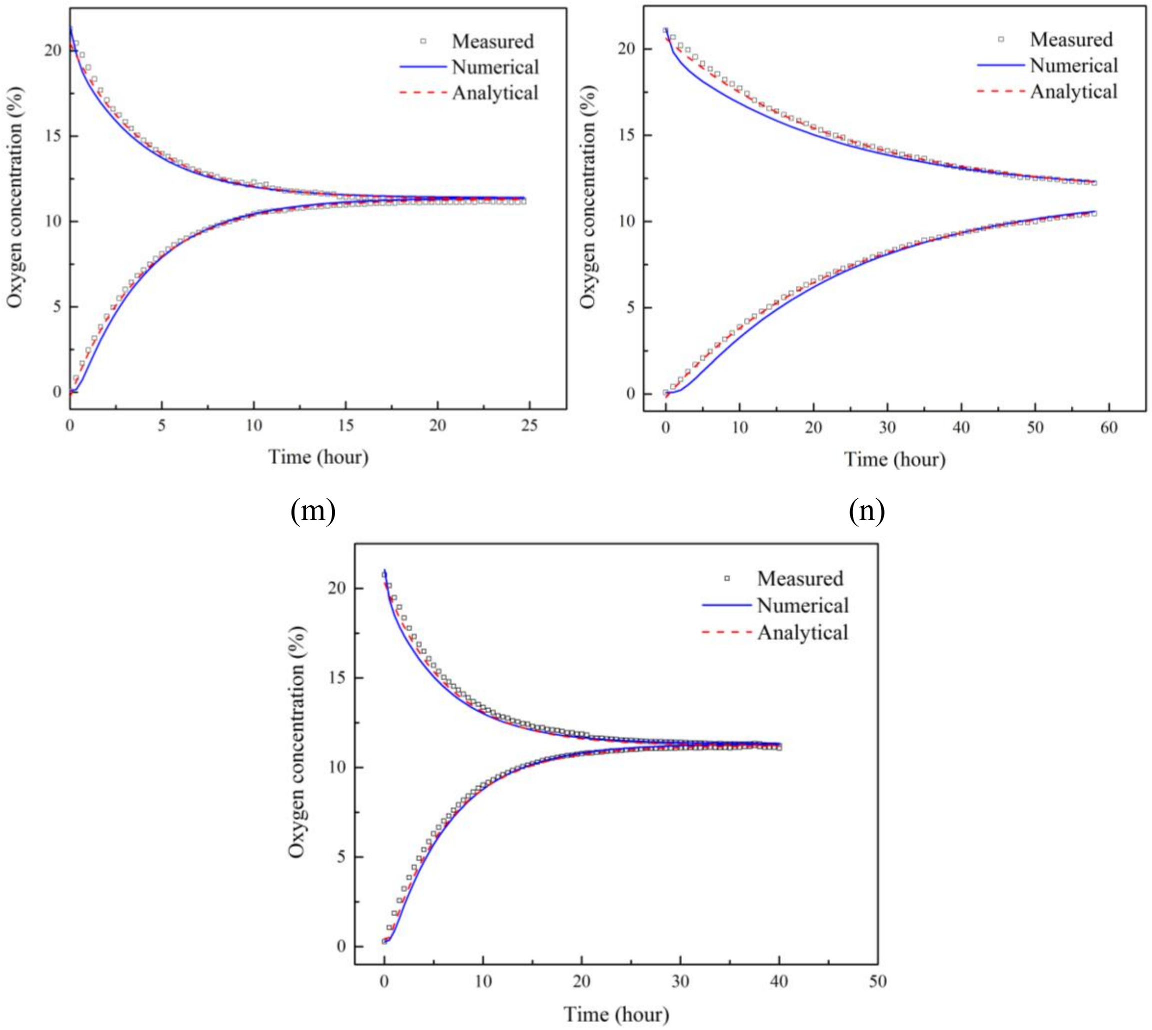

(m) (n)

(u)

Figure 7.7 Oxygen concentrations in the source and receptor chambers obtained by measurement, numerical solution, and analytical solution for: (a) WC-1, (b) WC-2, (c) WC-3, (d)WC-4, (e) WC-5, (f) BC-1, (g) BC-2, (h) BC-3, (i) BC-4, (j) BC-5, (k) SMA-1, (l) SMA-2, (m) SMA-3, (n) SMA-4, and (u) SMA-5.

### 7.4.3 Analysis of the differences in oxygen diffusion coefficients

Table 7.2 and Figure 7.7 indicate that the oxygen diffusion coefficients of the specimens are entirely different. For the same type of mix design, it appears that air void content is related to the diffusion coefficients. It also seems that mix design plays an important role in determining the oxygen diffusion coefficients. For example, the specimen SMA-1 has an air void content of 7%, which is greater than the air void content of the specimen WC-3. However, the diffusion coefficient of the specimen SMA-1 is less than three times of that for the specimen WC-3. Similarly, the diffusion coefficient of the specimen WC-1 is greater than those of specimen BC-2 and BC-3, although the latter ones have much higher air void content. Therefore, oxygen transport in asphalt mixtures is not only decided by the total air void, but also the characteristics of air void.

One specific air void characteristic that affects the oxygen diffusion coefficient of the asphalt mixture is the connectivity of the voids. The connected air void forms a path that facilitates oxygen diffusion. This may be observed from the CT images. Examples of the typical CT images of the WC and SMA mixtures are shown in Figure 7.8 and Figure 7.9, respectively. The figures indicate that air voids (black dots) in the WC mixture were smaller but were more evenly distributed as compared with those in the SMA mixtures. It appears that the smaller air voids in the WC mixture were more likely connected to each other, while the bigger ones in the SMA mixtures seemed more isolated. The connectivity of the air void is a major factor that affects oxygen diffusion in the asphalt mixture.

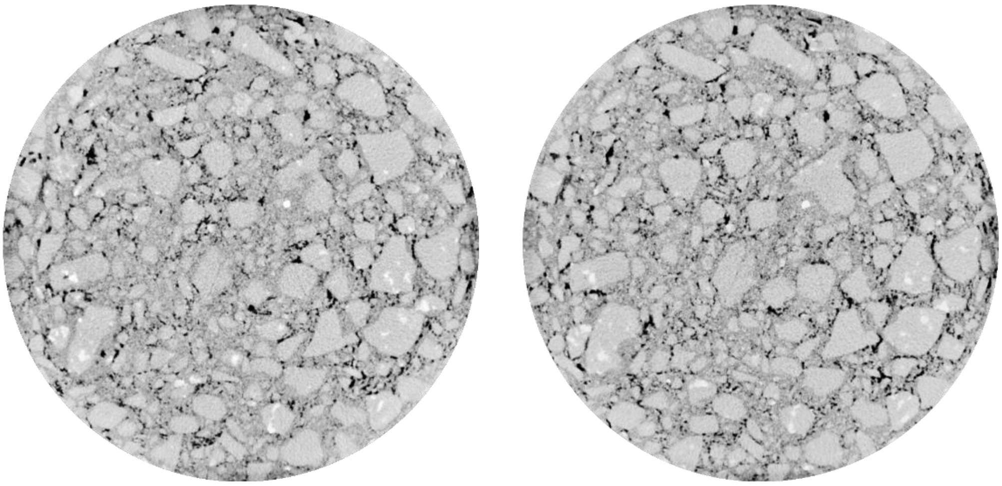

Figure 7.8 The CT images of WC mixture

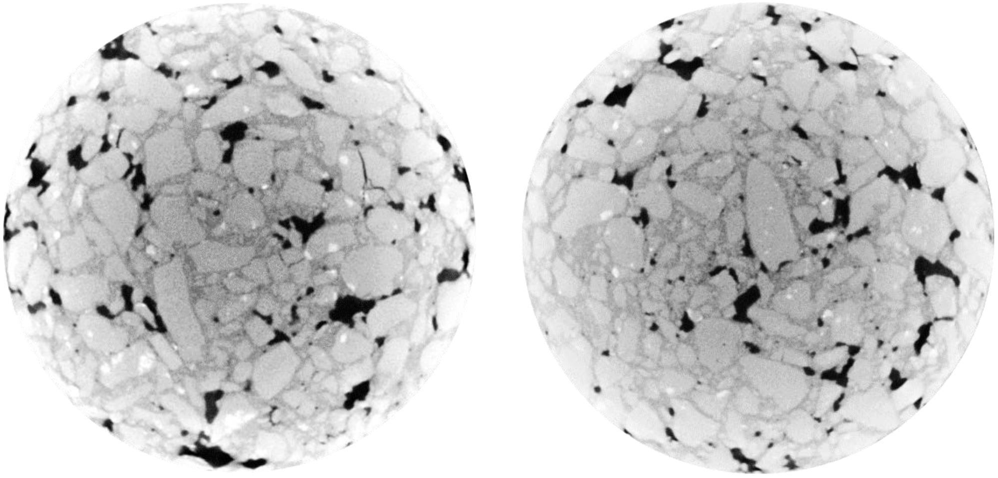

Figure 7.9 The CT images of SMA mixture

Due to the reasons mentioned in the introduction section, it is difficult to quantify the connectivity of air void directly. Therefore, attempts were made to evaluate the correlation between the commonly measured volumetric characteristics of the mixtures and the calculated diffusion coefficients. Spearman's rank correlation coefficient was adopted for this purpose. Spearman's rank correlation coefficient (ρ) is a non-parametric method for evaluating the extent of correlation between the rank values of two parameters when the relationship between two variables is monotonic [162, 165, 166], which is calculated by using Eq.(7.19) [167].

$$\rho = 1 - \left(\frac{6\sum d_i^2}{n(n^2-1)}\right) \tag{7.19}$$

where $d_i$ is the difference in the ranks between the input and the output values in the same data pair, and *n* is the number of simulations.

If the absolute value of $\rho$ is close to one, the variable has the maximum effect on the oxygen diffusion coefficient; if $\rho$ is close to zero, the variable has the minimal effect. A positive $\rho$ indicates that a higher variable value leads to a higher oxygen diffusion coefficient, while a negative $\rho$ value means the opposite. The examined volumetric characteristics include effective binder content ($P_{be}$), normal maximum aggregate size (NMAS), air voids ($V_a$), voids in the mineral aggregate (VMA), and voids filled asphalt (VFA). Because the thickness of the specimens varies slightly, it is also included for assessment. Figure 7.10 shows the Tornado plots of Spearman's rank correlation coefficients for the different variables. It can be seen that $V_a$, VMA, and $P_{be}$ have positive effects on the oxygen diffusion coefficient, indicating that as the increase of these variables likely lead to the increase of the oxygen diffusion coefficient. Conversely, NMAS, VFA, and thickness have negative $\rho$ values, incidating that the increase of these variables may cause the decrease of the diffusion coefficient. VMA, VFA, and $V_a$ apparently has the highest effect on the diffusion coefficient among the variables.

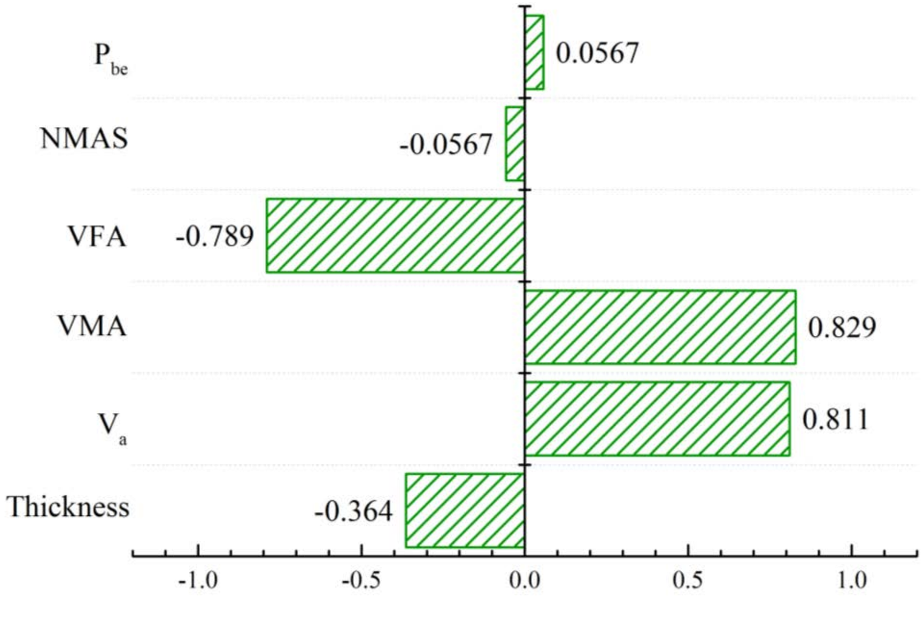

Figure 7.10 Tornado plots of Spearman's rank correlation coefficient

### 7.4.4 Implication of the oxygen diffusion coefficients of asphalt mixtures on pavement durability

The identified oxygen diffusion coefficients of asphalt mixtures can be potentially used in asphalt pavement design, mixture selection, and construction quality control. Load-induced pavement responses (e.g., tensile strains), pavement fatigue life and deformation are all dependent on the stiffness of asphalt binder, which is affected by its aging state [9]. The following equation can model the long-term age hardening (stiffness increase) of an asphalt binder [26].

$$r_n = HS \times r_{CA} \tag{7.20}$$

where $r_n$ is the long-term hardening rate of an asphalt binder, $HS$ is the hardening susceptibility of the binder, $r_{CA}$ is the growth rate of the carbonyl area in the infrared spectrum of the asphalt binder, representing the chemical changes in asphalt binder.

$$r_{CA} = \frac{\partial CA}{\partial t} = AP^{a}e^{-E/\mathrm{RT}} \tag{7.21}$$

where $A$, $E$, and $a$ are coefficients dependent on asphalt binder type, $R$ is the gas constant, $P$ is oxygen pressure, and $T$ is the absolute temperature. $E$ was also found to be a function of oxygen pressure [26].

Eq.(7.21) suggests that the oxygen pressure (concentration) and temperature are two external factors that determine the hardening rate of the asphalt binder in the asphalt mixture. Therefore, identification of oxygen concentration in the asphalt mixture and possible factors that affect the concentration is essential in understanding the long-term property evolution of the asphalt mixture.

To gain more understanding of oxygen concentration variations in asphalt pavement, oxygen concentration profiles of the specimens were created based on the previously determined diffusion coefficients. The schematic diagram for the numerical calculation of the profiles is shown in Figure 7.11, and the results are shown in Figure 7.12. In Figure 7.12, the area between the two red dashed lines represents the oxygen concentration inside of the compacted asphalt mixture, and the depth is defined according to Figure 7.11. Several observations can be made on the oxygen concentration profiles. Firstly, for the same specimen, the oxygen concentration gradient significantly affects the oxygen diffusion rate. The oxygen concentration gradient is initially high; therefore, the oxygen concentration in the source reservoir drops quickly. As the gradient is reduced, the oxygen concentration in the source reservoir decreases slowly. Secondly, the oxygen concentration in a specimen can be estimated by linear interpolation of the oxygen concentration levels at the two surfaces. Thirdly, the oxygen transport efficiency of the asphalt mixtures varies greatly. For the specimen SMA-3, the oxygen concentration in the source and receptor reservoirs is balanced in about 22 hours, while for the specimen BC-1 there was only a little drop in oxygen concentration in the source reservoir even after 520 hours.

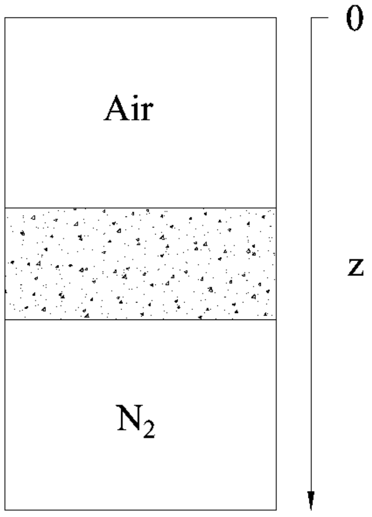

Figure 7.11 The schematic diagram of depth used in the numerical solution

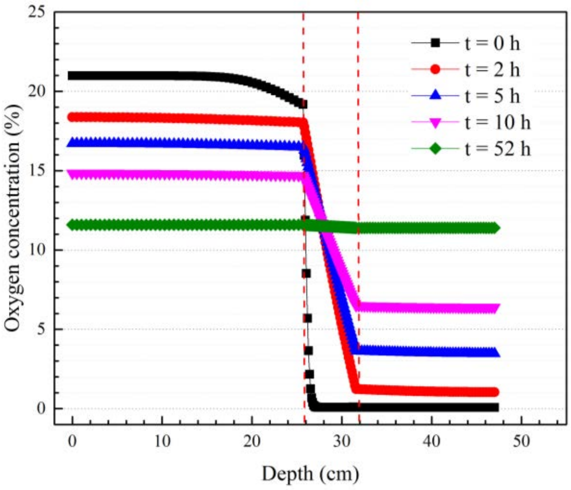
Oxygen concentration (%)
Depth (cm)
0
5
10
15
20
25
0
10
20
30
40
50
t = 0 h
t = 2 h
t = 5 h
t = 10 h
t = 52 h

(a)

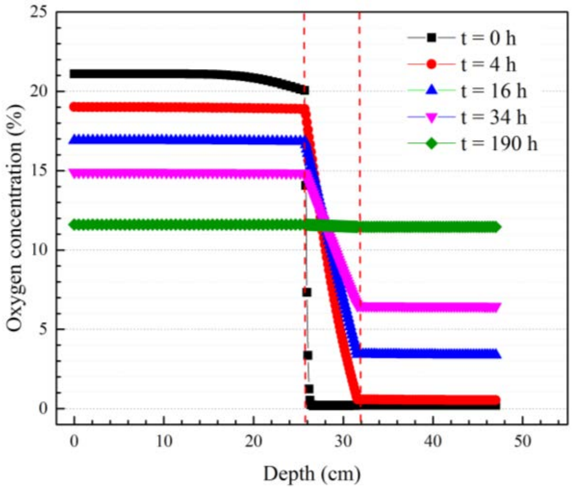
Oxygen concentration (%)
Depth (cm)
0
5
10
15
20
25
0
10
20
30
40
50
t = 0 h
t = 4 h
t = 16 h
t = 34 h
t = 190 h

(b)

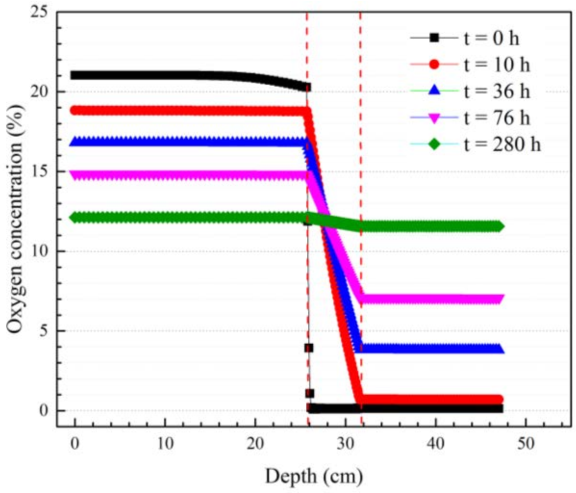
Oxygen concentration (%)
Depth (cm)
0
5
10
15
20
25
0
10
20
30
40
50
t = 0 h
t = 10 h
t = 36 h
t = 76 h
t = 280 h

(c)

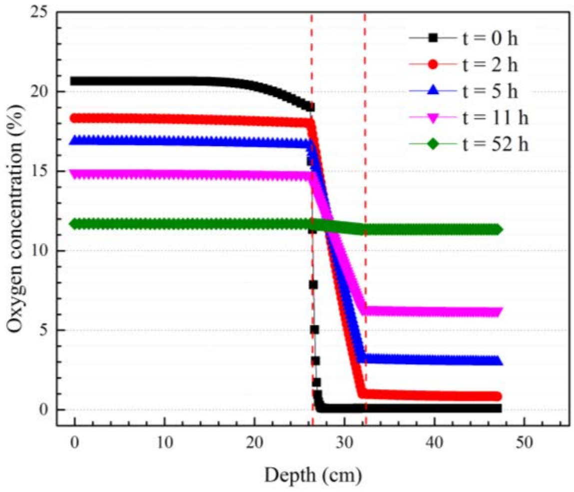
Oxygen concentration (%)
Depth (cm)
0
5
10
15
20
25
0
10
20
30
40
50
t = 0 h
t = 2 h
t = 5 h
t = 11 h
t = 52 h

(d)

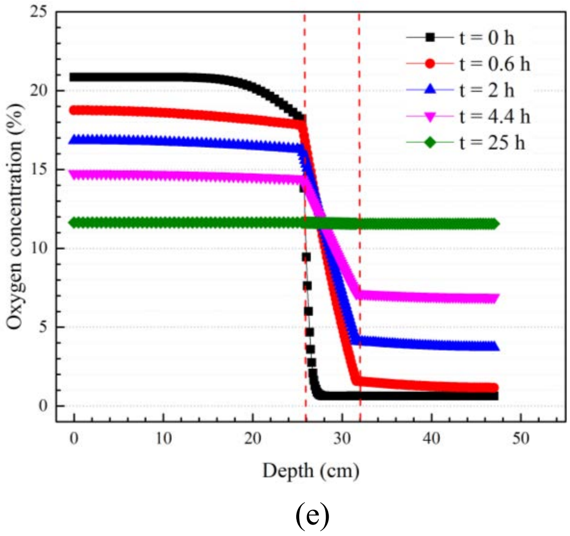
Oxygen concentration (%)
Depth (cm)
0
5
10
15
20
25
0
10
20
30
40
50
t = 0 h
t = 0.6 h
t = 2 h
t = 4.4 h
t = 25 h

(e)

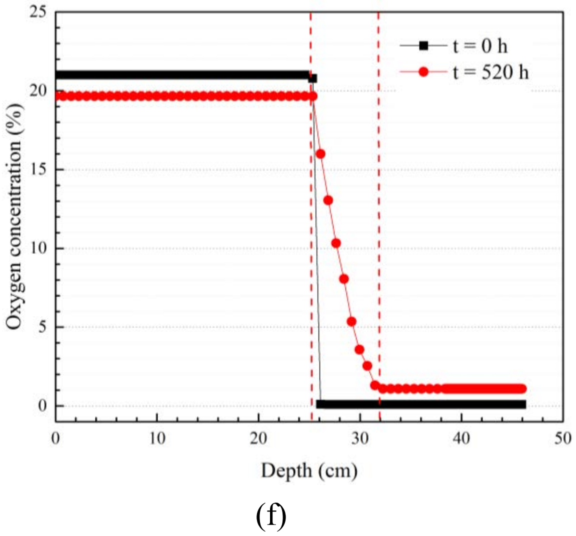
Oxygen concentration (%)
Depth (cm)
0
5
10
15
20
25
0
10
20
30
40
50
t = 0 h
t = 520 h

(f)

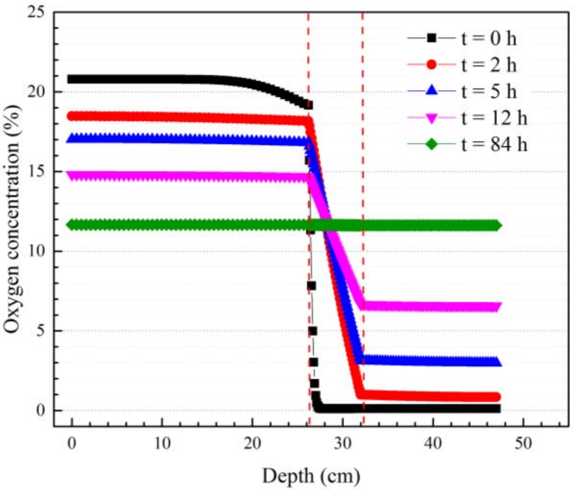

25
20
15
10
5
0
Oxygen concentration (%)
0
10
20
30
40
50
Depth (cm)
t = 0 h
t = 2 h
t = 5 h
t = 12 h
t = 84 h

(g)

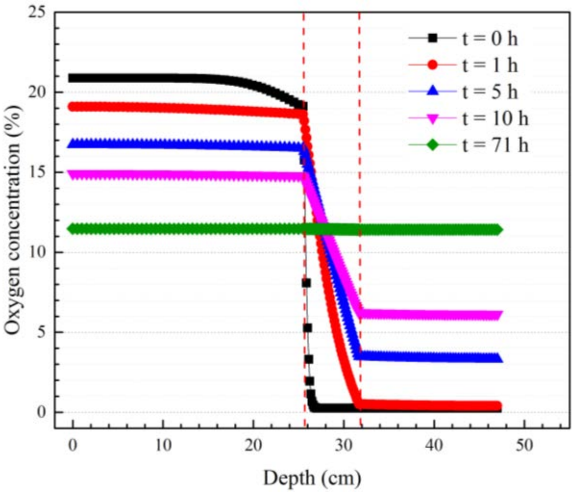

25
20
15
10
5
0
Oxygen concentration (%)
0
10
20
30
40
50
Depth (cm)
t = 0 h
t = 1 h
t = 5 h
t = 10 h
t = 71 h

(h)

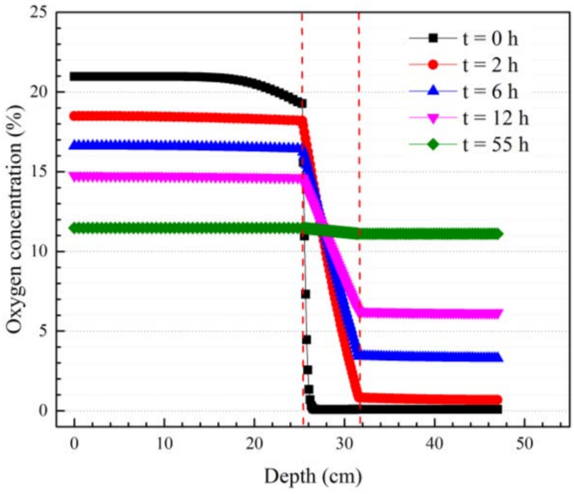

25
20
15
10
5
0
Oxygen concentration (%)
0
10
20
30
40
50
Depth (cm)
t = 0 h
t = 2 h
t = 6 h
t = 12 h
t = 55 h

(i)

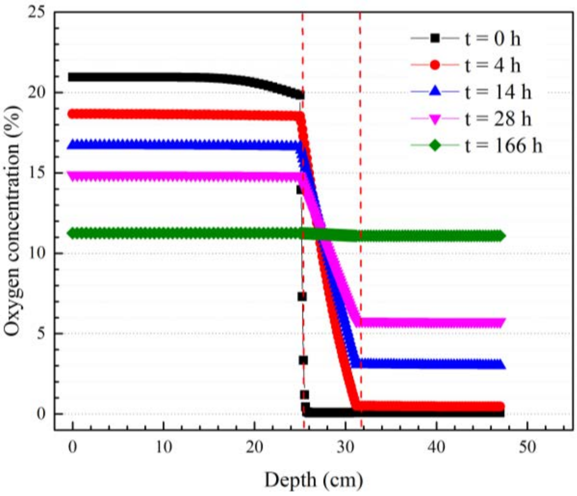

25
20
15
10
5
0
Oxygen concentration (%)
0
10
20
30
40
50
Depth (cm)
t = 0 h
t = 4 h
t = 14 h
t = 28 h
t = 166 h

(j)

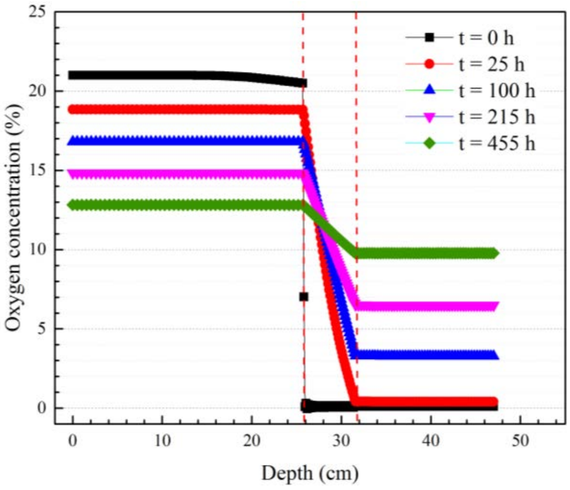

25
20
15
10
5
0
Oxygen concentration (%)
0
10
20
30
40
50
Depth (cm)
t = 0 h
t = 25 h
t = 100 h
t = 215 h
t = 455 h

(k)

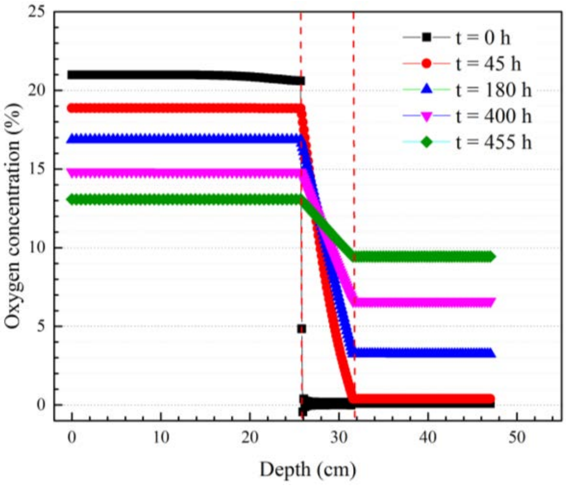

25
20
15
10
5
0
Oxygen concentration (%)
0
10
20
30
40
50
Depth (cm)
t = 0 h
t = 45 h
t = 180 h
t = 400 h
t = 455 h

(l)

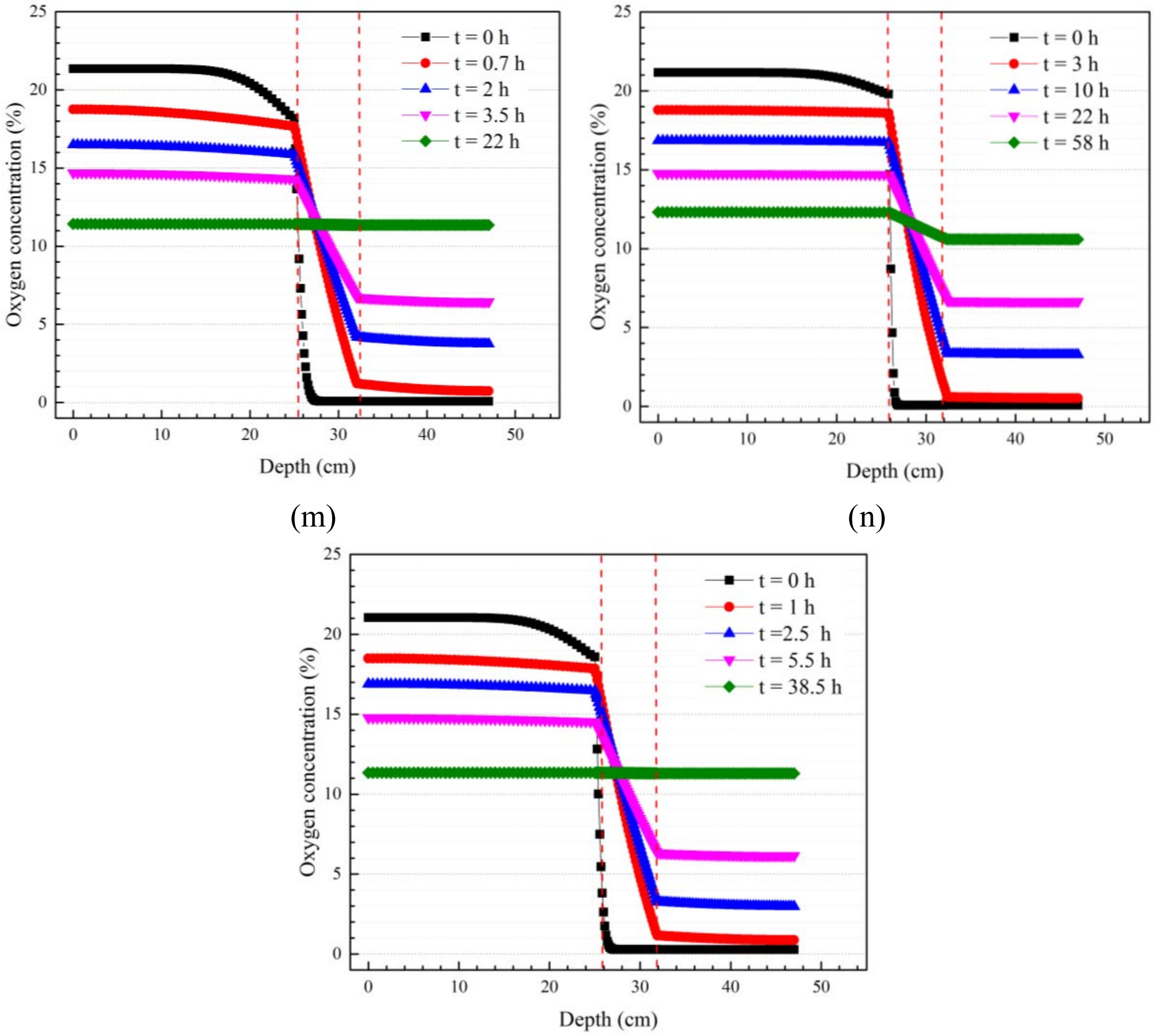

(m) (n)

(u)

Figure 7.12 Oxygen concentration profiles at different times for: (a) WC-1, (b) WC-2, (c) WC-3, (d)WC-4, (e) WC-5, (f) BC-1, (g) BC-2, (h) BC-3, (i) BC-4, (j) BC-5, (k) SMA-1, (l) SMA-2, (m) SMA-3, (n) SMA-4, and (u) SMA-5

The simulation results provide insights on the oxygen environment exposed by asphalt binders in actual pavements, where the surface is exposed to the atmosphere, and the bottom is exposed to air in granular base, subbase or subgrade. Because of the biological activities in subgrade soil, oxygen concentration at the bottom of the pavement is lower than that in the atmosphere [189]. In addition, rainwater that seeps into asphalt pavement not only blocks some air paths but also promotes biological oxygen consumption. Therefore, the oxygen content in the air of the asphalt mixture is likely to be lower than that in the atmosphere. This concentration gradient drives oxygen to diffuse from the air into the asphalt pavement. If a mix design with isolated air pockets is selected, or if the air voids can be controlled at a relatively low level for the same mix design, Figure 7.12 indicates that the oxygen diffusion may be greatly slowed. This will help make asphalt pavement more aging resistant, leading to improved durability. Therefore, the oxygen diffusion coefficient may serve as an indicator for the aging-related durability of the compacted asphalt mixture, which may be potentially used in asphalt mixture design and construction quality control.

### 7.4.5 Evaluation of three semi-empirical equations for predicting oxygen diffusion coefficient

Due to the limited number of specimens, a regression equation that relates the oxygen diffusion coefficients with the volumetric characteristics of the asphalt mixtures cannot be established. Semi-empirical models targeted at dry porous media (i.e., soil, sand and glass beads) have been developed in existing studies [190]. For instance, Penman (1940), Marshall (1959), and Millington (1959) proposed the following models, respectively [174, 175, 191]:

$$\frac{D_s}{D_0} = 0.66\varepsilon \tag{7.22}$$

$$\frac{D_s}{D_0} = \varepsilon^{3/2} \tag{7.23}$$

$$\frac{D_s}{D_0} = \varepsilon^{4/3} \tag{7.24}$$

where $D_0$ is the free diffusion coefficient in air; and $\varepsilon$ is the air-filled porosity which is defined as the ratio of air void volume of the sample to the total volume of the sample [192]. In this study, air voids in asphalt mixture is equivalent to the air-filled porosity.

Attempted were made to examine if the models above can provide a reasonable estimation of the diffusion coefficients of the asphalt mixture specimens. Results predicted by the models were compared with the measured values and are shown in Figure 7.13. It is evident that the three models significantly overpredict the oxygen diffusion coefficients in compacted asphalt mixture, although the Marshall model fits the data better than the others. Therefore, the existing diffusion coefficient models based on dry porous media are not applicable to asphalt mixtures. More volumetric characteristics may need to be included.

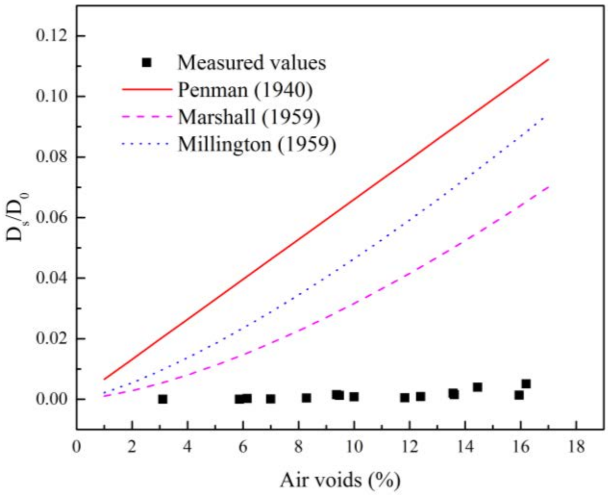

Figure 7.13 The diffusion coefficient ratio as a function of air voids predicted by three semi-empirical models

### 7.4.6 Development of a predicting model for predicting the oxygen diffusion coefficient of compacted asphalt mixture

Based on the previous results, $V_a$, VMA, and VFA have the greatest effect on the oxygen diffusion coefficient of the compacted asphalt mixture. Hence, a new oxygen diffusion coefficient model was assumed based on the three parameters, as presented in Eq. (7.25).

$$\log D_s = k_1 V_a^{k_2} VMA^{k_3}(k_4 VFA^2 + k_5 VFA + k_6) + k_7 \tag{7.25}$$

where $k_1$, …, $k_7$ are the regression parameters.

The optimization of the seven parameters was performed using the Solver function in Microsoft Excel® until the squared errors between the logarithm of the measured and predicted oxygen diffusion coefficients reached the minimum. The final seven parameters were determined to be -6.990E-05, -0.705, 1.668, 0.887, -75.019, 833.139, and -4.586, respectively. The comparisons between measured and predicted oxygen diffusion coefficient for three types of compacted asphalt mixture is plotted in Figure 7.14. The predicted oxygen diffusion coefficient shows a good match with the measured value. The $S_e/S_y$ and $R^2$ values were utilized to evaluate the goodness-of-fit of the predictive model. The detailed method is described in section 6.4.3. The two values of the new model are 0.20 and 0.96, respectively. The new model is rated as excellent according to the criteria for subjective classification of the goodness-of-fit statistics listed in Table 6.4.It indicates the new model has good prediction accuracy.

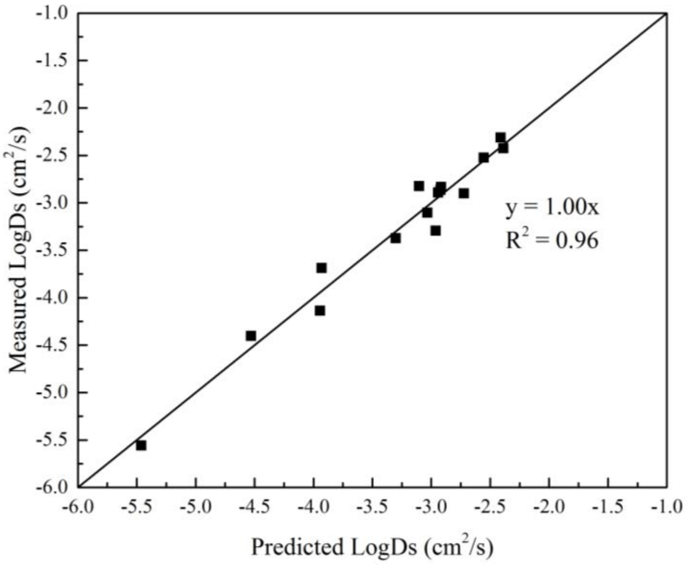

Figure 7.14 Measured and predicted oxygen diffusion coefficient

## 7.5 **Summary and conclusions**

The aging susceptibility of a compacted asphalt mixture is affected by the oxygen transport efficiency of the mixture, which can be assessed by its oxygen diffusion coefficient. In this chapter, a two-chamber apparatus was developed to measure the oxygen diffusion process of compacted asphalt mixture samples. Possible oxygen consumption during the diffusion test was evaluated. Both numerical and analytical methods were used to calculate the oxygen diffusion coefficients of samples prepared with different mixture designs and air voids (air void) content. The correlations between the oxygen diffusion coefficients and sample volumetric characteristics were examined. Based on the simulated oxygen concentration profiles, the oxygen environment exposed by asphalt binders in actual pavements and its implication on pavement durability were discussed. The accuracy of using existing semi-empirical equations to predict oxygen diffusion coefficients was also evaluated. The following conclusions are drawn from this study.

(1) It is feasible to use the developed apparatus and test procedure to measure the oxygen diffusion coefficients of the compacted asphalt mixture.

(2) Oxygen consumption during the diffusion test can be neglected at room temperature.

(3) The oxygen diffusion coefficients obtained from the numerical method is similar to those obtained from the analytical method, and the oxygen concentrations calculated by both methods match well with the actual observations.

(4) Oxygen diffusion coefficients of the tested samples vary greatly, depending on not only air voids content but also other volumetric characteristics.

(5) The oxygen diffusion coefficients of asphalt mixtures have significant implications on the oxygen contents at different depths of the asphalt pavements.

(6) The traditional models to predict the oxygen diffusion coefficients of dry porous media result in an overprediction of the diffusion coefficients for compacted asphalt mixture.

(7) The new predictive model of oxygen diffusion coefficient for compacted asphalt

mixture shows good prediction accuracy.

# CHAPTER 8. CONCLUSIONS AND RECOMMENDATIONS

This research aimed to determine a long-term aging method for compacted asphalt mixtures and then investigate the effect of aging on the rheological and chemical properties of recovered asphalt binders as well as $|E^*|$ values of compacted asphalt mixtures. The other aim of this research was to determine oxygen diffusion coefficients of compacted asphalt mixtures and then develop a predictive model for the oxygen diffusion coefficients based on the volumetric parameters of compacted asphalt mixtures.

To accomplish the two main aims, a customized autoclave was developed and used to simulate the long-term aging of compacted asphalt mixtures, and a two-chamber apparatus was developed to investigate the oxygen diffusion process of compacted asphalt mixtures. The major conclusions and limitations of this study are presented below, and recommendations are made for future work.

## 8.1 **Main conclusions**

The main conclusions can be drawn as follows:

(1) To safeguard the integrity of compacted asphalt mixtures during long-term aging simulation, they should be aged under ambient pressure at a temperature that is less than the softening point of asphalt binder. Pure oxygen may be used to accelerate the aging process. In this study, the long-term aging temperature was chosen to be 40˚C, which was lower than the softening point (46.2˚C) of the base asphalt (60/70 pen) used in the study.

(2) The new micro-sampling, and micro-extraction and recovery methods are reliable and efficient in extracting and recovering asphalt binders from compacted asphalt

mixtures. The methods only use a small amount of sample, and the process apparently does not heavily affect the properties of recovered asphalt binders.

(3) The oxidized chemical products (sulfoxides and ketones) and the dynamic viscosities of recovered asphalt binders increase rapidly in the initial stage of compacted asphalt mixture aging and then rise at a nearly constant rate. Moreover, sulfoxide is a major contributor to viscosity increase at 40ºC.

(4) The $|E^*|$ values of the three types of asphalt mixtures increase as the aging severity of asphalt binders increases. The increasing rates, however, decrease as the aging time increases. The increasing rates vary with the types of asphalt mixtures, indicating that aggregate gradation may affect the aging susceptibility of compacted asphalt mixtures.

(5) For the three types of asphalt mixtures with the base asphalt typically used in Hong Kong, the Improved Hirsch model exhibits the highest prediction accuracy, while the 2S2P1D model has the lowest predictive accuracy compared with the other five models.

(6) Regarding the robustness of the six predictive models for the three mixture types blending with the base asphalt, the Improved Hirsch model exhibits the greatest robustness. The Witczak 1-37A, Witczak 1-40D, and Al-Khateeb models have better robustness for the WC and BC mixtures than those for the SMA mixture, while there are no differences between WC and BC mixtures, and SMA mixture for the Original Hirsch and 2S2P1D models. Asphalt binder aging has an adverse effect on the robustnesses of Witczak 1-37A, Witczak 1-40D, Original Hirsch, and Al-Khateeb

models, while not heavily affecting the accuracy of the 2S2P1D model.

(7) The results of the sensitivity analysis indicate that the predicted $|E^*|$ values are the most sensitive to the binder properties (i.e., $|G^*|$, $\delta$, and $\eta$), and the least sensitive to the volumetric properties (i.e., $V_a$, $VMA$, and $VFA$) for the three mixture types tested in this study.

(8) It is feasible to use the customized apparatus and test procedure to determine the oxygen diffusion coefficients of the three types of asphalt mixtures. Oxygen consumption by the asphalt mixtures during the test process can be neglected at room temperature. The oxygen diffusion coefficients of compacted asphalt mixtures vary widely, depending on not only air void contents but also other volumetric characteristics.

(9) A predictive model of oxygen diffusion coefficient was developed based on the volumetric parameters of compacted asphalt mixtures. The model is proved to be accurate in predicting the diffusion coefficient.

## 8.2 **Limitations of this study**

For research topic 1, the entire aging period for each specimen type is very long since the capacity of the customized autoclave is limited and the aging temperature is low. Hence, the three types of asphalt mixtures were prepared with one type of asphalt binder to simulate the long-term aging. The six predictive models of $|E^*|$ values were then examined using the $|E^*|$ values of these mixutres at different aging states. The limited binder type and mixture types may affect the findings of the study, which are subject to further investigation.

For research topic 2, it is the first time in pavement field to determine the oxygen diffusion coefficients of compacted asphalt mixtures. There is no previous experience to follow; consequently, the overall progress is not as fast as that originally anticipated. Additionally, the diffusion test is also time-consuming for some specimens. Hence, the specimens were limited to the three types of asphalt mixtures were tested. The diffusion prediction model developed with these limited specimens need to be further calibrated using more specimens.

## 8.3 **Recommendations**

Some remaining research works may be conducted in the future.

(1) The results of research topic 1 were measured using one specimen size standard for $|E^*|$ test. It is assumed, also suggested in existing studies, that asphalt binder in this specimen is aged uniformly. Different specimen sizes may be considered in the future research efforts so that how specimen size affects both radial and vertical aging gradients of compacted asphalt mixtures may be examined [193].

(2) This dissertation adopted only one asphalt binder type (base asphalt, 60/70 pen) typically used in Hong Kong. Different combinations of polymer-modified asphalt binders and aggregate gradations may be used to simulate the long-term aging of compacted asphalt mixtures at temperatures lower than their softening points. Then, the binder type effect as a possible interactive factor may be evaluated.

(3) The oxygen diffusion test may be conducted by considering other possible influencing factors (e.g., types of asphalt binder, aggregate gradation temperature, pressure, moisture, crack, pavement structure), so that the oxygen diffusion coefficients may be predicted in more realistic conditions.

(4) Quantitative models may be developed to predict the aging susceptibility of asphalt binders in compacted asphalt mixtures, using the mixtures’ diffusion coefficients as a key predictor variable.

(5) Finally, a new aging model may be developed based on the oxygen diffusion and consumption coefficients of compacted asphalt mixtures and the environmental conditions inside of field pavements. This would help improve the aging prediction of asphalt pavements, leading to more accurate pavement design.

# REFERENCES

[1] R.J. Forbes, Notes on the history of ancient roads and their construction, Amsterdam: Nord-Hollandsche Uitgevers-mij1934.

[2] T.A.I.a. Eurobitume, The Bitumen Industry - A Global Perspective Production, chemistry, use, specification and occupational exposure, Brussels, Belgium; Lexington, KY, USA, 2015.

[3] R.C. Williams, J. Satrio, M. Rover, R.C. Brown, S. Teng, Utilization of fractionated bio oil in asphalt, The 88th annual meeting of the transportation research board, Washington, DC, 2009.

[4] Hong Kong Road Network, 2017. http://www.hyd.gov.hk/en/road_and_railway/existing/road_network/road.html. (Accessed 25/4/2017 2017).

[5] J.C. Petersen, Asphalt oxidation - An overview including a new model for oxidation proposing that physicochemical factors dominate the oxidation kinetics, Fuel science & technology international 11(1) (1993) 57-87.

[6] E.T. Hagos, The effect of aging on binder properties of porous asphalt concrete, TU Delft, Delft University of Technology, 2008.

[7] G.D. Airey, State of the Art Report on Ageing Test Methods for Bituminous Pavement Materials, International Journal of Pavement Engineering 4(3) (2003) 165-176.

[8] C.J. Glover, R. Han, X. Jin, N. Prapaitrakul, Y. Cui, A. Rose, J.J. Lawrence, M. Padigala, E. Arambula, E.S. Park, Evaluation of binder aging and its influence in aging of hot mix asphalt concrete: Technical report, Texas, 2014.

[9] C.J. Glover, A.E. Martin, A. Chowdhury, R. Han, N. Prapaitrakul, X. Jin, J. Lawrence, Evaluation of Binder Aging and Its Influence in Aging of Hot Mix Asphalt Concrete: Literature Review and Experimental Design, Research and Technology Implementation Office, Austin, Texas, 2009.

[10] J.C. Petersen, A review of the fundamentals of asphalt oxidation: chemical, physicochemical, physical property, and durability relationships, Transportation Research E-Circular (E-C140) (2009).

[11] M.W. Mirza, M. Witczak, Development of a Global Aging System for Short and Long Term Aging of Asphalt Cements (with Discussion), Journal of the Association of Asphalt Paving Technologists 64 (1995) 393-424.

[12] G. Martínez, B. Caicedo, Efecto de la radiación ultravioleta en el envejecimiento de ligantes y mezclas asfálticas, Ingeniería e Investigación 28(3) (2008) 5-12.

[13] N.A. Al-Azri, S.H. Jung, K.M. Lunsford, A. Ferry, J.A. Bullin, R.R. Davison, C.J. Glover, Binder oxidative aging in Texas pavements: hardening rates, hardening susceptibilities, and impact of pavement depth, Transport Res Rec (1962) (2006) 12-20.

[14] Y.H. Wang, Y. Wen, K.C. Zhao, D. Chong, A.S.T. Wong, Evolution and locational variation of asphalt binder aging in long-life hot-mix asphalt pavements, Construction and Building Materials 68(0) (2014) 172-182.

[15] Y.J. Sharew, Development of a laboratory ageing method for bitumen in porous asphalt, Civil Engineering, Delft University of Technology, Delft, The Netherlands, 2010.

[16] J. Petersen, P. Harnsberger, R. Robertson, Factors affecting the kinetics and mechanisms of asphalt oxidation and the relative effects of oxidation products on age hardening, American Chemical Society Division of Fuel Chemistry Preprints 41(4) (1996) 1232-1244.

[17] B.S. Underwood, 9-Multiscale modeling approach for asphalt concrete and its implications on oxidative aging, in: H.D. Benedetto (Ed.), Advances in Asphalt Materials, Woodhead Publishing, Oxford, 2015, pp. 273-302.

[18] R.K. Abu Al-Rub, M.K. Darabi, S.-M. Kim, D.N. Little, C.J. Glover, Mechanistic-based constitutive modeling of oxidative aging in aging-susceptible materials and its effect on the damage potential of asphalt concrete, Construction and Building Materials 41 (2013) 439-454.

[19] D.A. Anderson, R.F. Bonaquist, Investigation of short-term laboratory aging of neat and modified asphalt binders, Transportation Research Board, 2012.

[20] W. Van den bergh, The Effect of Ageing on the Fatigue and Healing Properties of Bituminous Mortars, Faculty of Civil Engineering and Geosciences, Delft University of Technology, Netherlands, 2011.

[21] L.S. Johansson, Bitumen ageing and hydrated lime, Infrastructure and Planning, Institutionen för infrastruktur och samhällsplanering, Viktoria Landgren, 1998.

[22] J.F. Branthaver, J. Petersen, R. Robertson, J. Duvall, S. Kim, P. Harnsberger, T. Mill, E. Ensley, F. Barbour, J. Scharbron, Binder characterization and evaluation. Volume 2: Chemistry, 1993.

[23] J.C. Petersen, J.F. Branthaver, R.E. Robertson, P.M. Harnsberger, J.J. Duvall, E.K. Ensley, Effects of physicochemical factors on asphalt oxidation kinetics, Transportation Research Record (1391) (1993).

[24] D.Y. Lee, R.J. Huang, Weathering of Asphalts as Characterized by Infrared Multiple Internal Reflection Spectra, Appl. Spectrosc. 27(6) (1973) 435-440.

[25] C. Lau, K. Lunsford, C. Glover, R. Davison, J. Bullin, Reaction rates and hardening susceptibilities as determined from pressure oxygen vessel aging of asphalts, Transportation research record (1342) (1992).

[26] L. Corbett, R. Merz, Asphalt binder hardening in the Michigan test road after 18 years of service, Transportation Research Record (544) (1975).

[27] F. Farcas, Etude d'une methode de simulation du vieillissement sur route des bitumes, Universit de Paris, Paris, 1996.

[28] D. Lesueur, The colloidal structure of bitumen: Consequences on the rheology and on the mechanisms of bitumen modification, Advances in colloid and interface science 145(1) (2009) 42-82.

[29] R.N. Hunter, S. Andy, J. Read, The shell bitumen handbook, Sixth ed., Thomas Telford, London, 2015.

[30] R.N. Traxler, Durability of asphalt cements (With discussion), Association of Asphalt Paving Technologists Proceedings, 1963.

[31] F. Farcas, Etude d" une méthode de simulation du vieillissement des bitumes sur route, LCPC, 1998.

[32] Chipperfield E.H., J.L. Duthie, R.B. Girdler, Asphalt characteristics in relation to road performance, Association of Asphalt Paving Technologists, Seattle, 1970.

[33] M. Zupanick, V. Baselice, Characterizing asphalt volatility, Transportation Research Record: Journal of the Transportation Research Board 1586(1) (1997) 1-9.

[34] C.A. Bell, Summary report on aging of asphalt-aggregate systems, 1989, p. 125.

[35] D.W. Christensen, D.A. Anderson, Interpretation of dynamic mechanical test data for paving grade asphalt cements (with discussion), Journal of the Association of Asphalt Paving Technologists 61 (1992) 67-116.

[36] C.A. Bell, D. Sosnovske, J.A. Wieder, Aging: binder validation, Strategic Highway Research Program, National Research Council, 1994, p. 81.

[37] T. Scholz, S. Brown, Effect of Mineral Aggregate on the Rheological Character of Bitumen, 1 st European Rheology Workshop–Eurobitume, 1995.

[38] B.O. Lerfald, Ageing and degradation of asphalt pavements on low-volume roads, Department of Road and Railway Engineering The Norwegian University of Science and Technology, Trondheim, 2000.

[39] C.E. Coombs, R.N. Traxler, Rheological Properties of Asphalts IV Observations Concerning the Anomalous Flow Characteristics of Air‐Blown Asphalts, Journal of Applied Physics 8(4) (1937) 291-296.

[40] I. Ishai, B. Brule, J. Vaniscote, G. Ramond, Some rheological and phsico-chemical aspects of long-term asphalt durability (With discussion), Association of Asphalt Paving Technologists Proc, 1988.

[41] I. Ishai, The Effects of Asphalt Composition on its Physical and durability Characteristics, Transportation Research Record (1996).

[42] J. Read, D. Whiteoak, The Shell Bitumen Handbook, Fifth ed., Thomas Telford, London, 2003.

[43] T. Mill, D. Tse, Oxidation and photooxidation of asphalts, American Chemical Society, 1990, pp. Medium: X; Size: Pages: 483-489.

[44] T. Davis, J. Petersen, An adaptation of inverse Gas Liquid Chromatography to asphalts studies, Analytical Chemistry 38 (1966) 1988-1990.

[45] J.C. Petersen, Chemical composition of asphalt as related to asphalt durability: state of the art, Transportation research record (999) (1984).

[46] J.C. Petersen, A dual, sequential mechanism for the oxidation of petroleum asphalts, Petroleum science and technology 16(9-10) (1998) 1023-1059.

[47] S.M. Dorrence, F.A. Barbour, J.C. Petersen, Direct Evidence of Ketones in Oxidized

Asphalts, Analytical Chemistry 46(14) (1974) 2242-2244.

[48] J.C. Petersen, S.M. Dorrence, M. Nazir, H. Plancher, F.A. Barbour, Oxidation of Sulfur-Compounds in Petroleum Residues-Reactivity-Structural Relationships Preprints, Div. Perto. Chem. 26(4) (1981) 898-906.

[49] L. Francken, A. Vanelstraete, A. Verhasselt, Long term ageing of pure and modified bitumen: Influence on the rheological properties and relation with the mechanical performance of asphalt mixtures, Eighth International Conference on Asphalt Pavements, Federal Highway Administration, 1997.

[50] E. Dickinson, J. Nicholas, S. Boas - Traube, Physical factors affecting the absorption of oxygen by thin films of bituminous road binders, Journal of Applied Chemistry 8(10) (1958) 673-687.

[51] C.P. Marais, Gap-graded Asphalt Surfacings - the South African Scene, Proc 2nd Conference on asphalt paving for Soutbern Africa, National Institute for Road Research, Pretoria, South Africa, 1974.

[52] H.E. Lubbers, Bitumen in de weg-en waterbouw, Nederlands Adviesbureau voor Bitumentoepassingen, NABIT, Gouda, 1985.

[53] D.A. Anderson, D.W. Christensen, H.U. Bahia, R. Dongre, M. Sharma, C.E. Antle, J. Button, Binder characterization and evaluation, volume 3: Physical characterization, Strategic Highway Research Program, National Research Council (1994).

[54] P.S. Kandhal, C.Y. Lynn, F. Parker, Characterization tests for mineral fillers related to performance of asphalt paving mixtures, Transportation Research Record: Journal of the Transportation Research Board 1638(1) (1998) 101-110.

[55] R.F. Coons, P.H. Wright, An investigation of the hardening of asphalt recovered from pavements of various ages, Georgia Institute of Technology, Georgia, 1965.

[56] C. Whiteoak, Fordyce, D, Asphalt workability: its measurement and how it can be modified, Shell Bitumen Review (64) (1989) 14-17.

[57] J.G. Cabrera, Performance and durability of bituminous materials, CRC Press, London, 2003.

[58] R. Griffin, T. Miles, C. Penther, Microfilm durability test for asphalt, Assoc Asphalt Paving Technol Proc., 1955.

[59] P.C. Blokker, H.v. Doorn, Durability of bitumen in theory and practice, Shell International Petroleum Company, London, 1959.

[60] W. Campen, J. Smith, L. Erickson, L. Mertz, The relationships between voids, surface area, film thickness and stability in bituminous paving mixtures, Proceedings of the Association of Asphalt Paving Technologists, 1959, pp. 149-178.

[61] V.A. Vallerga, R.M. White, K.S. Rostler, Changes in Fundamental Properties of Asphalts During Service in Pavements, Office of Research and Development, Bureau of Public Roads, Washington, DC, USA, 1970.

[62] L. Transportation Officials Advanced Asphalt Technologies, A Manual for Design of Hot Mix Asphalt with Commentary, Transportation Research Board, Washington, D.C., 2011.

[63] C.J. Glover, R.R. Davison, C.H. Domke, Y. Ruan, P. Juristyarini, D.B. Knorr, S.H. Jung, Development of a new method for assessing asphalt binder durability with field validation, Texas Transportation Institute, Texas A & M University System, 2005.

[64] W.J. Woo, E. Ofori-Abebresse, A. Chowdhury, J.M. Hilbrich, Z. Kraus, A.E. Martin, C.J. Glover, Polymer modified asphalt durability in pavements, Texas Department of Transportation, Research and Technology Implementation Office, Austin, Texas, 2007.

[65] Z. Su, Mineral Aggregates: Their Classification and Properties, Department of Research and Technology, Smid & Holland Services BV, Groningen, the Netherlands, 1996.

[66] A. Kavussi, R. Hicks, Properties of bituminous mixtures containing different fillers, Journal of the Association of Asphalt Paving Technologists 66 (1997).

[67] R. Gubler, Y. Liu, D.A. Anderson, M.N. Partl, Investigation of the system filler and asphalt binders by rheological means, Journal of Association of Asphalt Paving Technologists 68 (1999) 284-302.

[68] N. Shashidhar, S. Needham, B. Chollar, P. Romero, Prediction of the performance of mineral fillers in stone matrix asphalt, Journal of the Association of Asphalt Paving Technologists 68 (1999) 222-251.

[69] H. Bianchetto, R. Miró, F. Perez-Jimenez, A.H. Martínez, Effect of calcareous fillers on bituminous mix aging, Transportation Research Record: Journal of the Transportation Research Board 1998(1) (2007) 140-148.

[70] Y. Ruan, R.R. Davison, C.J. Glover, An Investigation of Asphalt Durability: Relationships Between Ductility and Rheological Properties for Unmodified Asphalts, Petroleum Science and Technology 21(1-2) (2003) 231-254.

[71] R. Clark, Practical results of asphalt hardening on pavement life, Association of Asphalt Paving Technologists, 1958, pp. 196-208.

[72] P.C. Doyle, Cracking characteristics of asphalt cement, Proc of Assoc of Asphalt Paving Technologists 27 (1958) 581-597.

[73] W.J. Halstead, The relation of asphalt ductility to pavement performance, Association of Asphalt Paving Technologists Proceedings, 1963.

[74] P. Kandhal, W. Koehler, Significant studies on asphalt durability:Pennsylvania experience (Discussion), Transportation Research Record (999) (1984).

[75] P.S. Kandhal, M.E. Wenger, Asphalt properties in relation to pavement performance, Transportation Research Record (544) (1975).

[76] L. Raad, S. Saboundjian, G. Minassian, Field aging effects on fatigue of asphalt concrete and asphalt-rubber concrete, Transportation Research Record: Journal of the Transportation Research Board 1767(1) (2001) 126-134.

[77] F.L. Roberts, P.S. Kandhal, E.R. Brown, D.-Y. Lee, T.W. Kennedy, Hot mix asphalt materials, mixture design and construction, NAPA Research and Education Foundation, Pennsylvania State, 1991.

[78] U. Isacsson, X. Lu, Laboratory investigation of polymer modified bitumen, Association of

asphalt pavement technologists (AAPT) 68 (1999) 35-63.

[79] S. Dessouky, C. Reyes, M. Ilias, D. Contreras, A.T. Papagiannakis, Effect of pre-heating duration and temperature conditioning on the rheological properties of bitumen, Construction and Building Materials 25(6) (2011) 2785-2792.

[80] H.U. Bahia, D. Hanson, M. Zeng, H. Zhai, M. Khatri, R. Anderson, Characterization of modified asphalt binders in Superpave mix design, Transportion Research Board Executive Committee, Washington, D.C., 2001.

[81] C.H. Domke, R.R. Davison, C.J. Glover, Effect of oxidation pressure on asphalt hardening susceptibility, Transportation Research Record: Journal of the Transportation Research Board 1661(1) (1999) 114-121.

[82] I. Yut, A. Zofka, Attenuated Total Reflection (ATR) Fourier Transform Infrared (FT-IR) Spectroscopy of Oxidized Polymer-Modified Bitumens, Appl. Spectrosc. 65(7) (2011) 765-770.

[83] J. Lamontagne, P. Dumas, V. Mouillet, J. Kister, Comparison by Fourier transform infrared (FTIR) spectroscopy of different ageing techniques: application to road bitumens, Fuel 80(4) (2001) 483-488.

[84] C.A. Bell, Y. Abwahab, M.E. Cristi, Selection of laboratory aging procedures for asphalt-aggregate mixtures, Strategic Highway Research Program, Washington, D.C., 1994.

[85] A. Kumar, W. Goetz, Asphalt hardening as affected by film thickness, voids and permeability in asphaltic mixtures, Association of Asphalt Paving Technologists Proc, 1977.

[86] J.T. Pauls, J. Welborn, Studies of the hardening properties of asphaltic materials, Assoc Asphalt Paving Technol Proc, 1952.

[87] H.L. Von Quintus, Asphalt-aggregate mixture analysis system, AAMAS, Transportation Research Board1991.

[88] T.V. Scholz, Durability of bituminous paving mixtures, University of Nottingham, 1995.

[89] H. Plancher, E. Green, J. Petersen, Reduction of Oxidative Hardening of Asphalts by Treatment with Hydrated Lime--A Mechanistic Study, Association of Asphalt Paving Technologists Proc, 1976.

[90] G.R. Kemp, N.H. Predoehl, A comparison of field and laboratory environments on asphalt durability, Association of Asphalt Paving Technologists Proceedings, 1981.

[91] F. Hugo, T.W. Kennedy, Surface cracking of asphalt mixtures in Southern Africa, University of Texas at Austin, 1984.

[92] M.R. Mugler, Die veränderung der Bitumeneigenschaften während der Verarbeitung und in Fertigen Belag, Route et Traffic, 1970.

[93] T.I.A. Gerber, W.J. Honiball, J.G.H. Dupreez, Spectroscopic Studies on the Interaction of the Antibiotic Lasalocid-a (X-537a) with Technetium(V) Ions in Chloroform, S Afr J Chem 41(3) (1988) 101-107.

[94] G. Van Gooswilligen, F.T. De Bats, T. Harrison, Quality of paving grade bitumen-a practical

approach in terms of functional tests, Proceedings of the fourth Eurobitume symposium, 1989, pp. 290-297.

[95] F. Hveem, E. Zube, J. Skog, Proposed new tests and specifications for paving grade asphalts, Association of Asphalt Paving Technologists Proceedings, 1963.

[96] O.-K. Kim, C. Bell, J. Wilson, G. Boyle, Effect of moisture and aging on asphalt pavement life, Part 2-Effect of aging, Oregon Department of Transportation, Salem, OR, 1986.

[97] H. Khalid, C. Walsh, Relating mix and binder fundamental properties of aged porous asphalt materials, 2nd Eurasphalt and Eurobitume Congress, Barcelona, Spain, 2000.

[98] H.C. Korsgaard, J. Blumensen, J. Sundahl, C. Gonzales, Accelerated ageing of asphalt in pressure ageing vessel, Euroasphalt & Eurobitume Congress Strasbourg, 1996.

[99] H. Khalid, A new approach for the accelerated ageing of porous asphalt mixtures, Proceedings of the ICE-Transport 153(3) (2002) 171-181.

[100] Y. Hachiya, K. Nomura, J. Shen, M. Partl, Accelerated aging tests for asphalt concretes, Sixth International RILEM Symposium on Performance Testing and Evaluation of Bituminous Materials, RILEM Publications SARL, 2003, pp. 133-140.

[101] C. De La Roche, M. Van de Ven, T. Gabet, V. Dubois, J. Grenfell, L. Porot, Development of a laboratory bituminous mixtures ageing protocol, Advanced Testing and Characterization of Bituminous Materials, Talor and Francis France, 2009, pp. 331-345.

[102] N. Piérard, A. Vanelstraete, Developing a test method for the accelerated ageing of bituminous mixtures in the laboratory, Advanced Testing and Characterization of Bituminous Materials (2009) 163-171.

[103] A. Verhasselt, A kinetic approach to the aging of bitumens, Asphaltenes and Asphalts, 2, Developments in petroleum science2000, pp. 475-497.

[104] G. Van Gooswilligen, H. Berger, F.T. De Bats, Oxidation of bitumens in various tests, 3rd Eurobitume Symposium, Hague, 1985, pp. 95-101.

[105] J. Knotnerus, Bitumen Durability - Measurement by Oxygen Absorption, Industrial & Engineering Chemistry Product Research and Development 11(4) (1972) 411-+.

[106] M. Liu, K.M. Lunsford, R.R. Davison, C.J. Glover, J.A. Bullin, The kinetics of carbonyl formation in asphalt, AIChE Journal 42(4) (1996) 1069-1076.

[107] P.R. Herrington, Effect of Concentration on the Rate of Reaction of Asphaltenes with Oxygen, Energy & Fuels 18(5) (2004) 1573-1577.

[108] W.P.V. Oort, Durability of Asphalt - It's Aging in the Dark, Industrial & Engineering Chemistry 48(7) (1956) 1196-1201.

[109] E. Dickinson, The diffusion controlled reaction of oxygen with films of bituminous binders, Australian Road Research 14(3) (1984).

[110] Y.A. Tuffour, I. Ishai, The diffusion model and asphalt age-hardening, Proc of Assoc of Asphalt Paving Technologists 59 (1990) 73-92.

[111] E. Dickinson, Prediction of the hardening of the bitumen in pavement surfacings by reaction

with atmospheric oxygen, Road Materials and Pavement Design 1(3) (2000) 255-279.

[112] P.R. Herrington, Diffusion and reaction of oxygen in bitumen films, Fuel 94(0) (2012) 86-92.

[113] K. Martin, R. Davison, C. Glover, J. Bullin, Asphalt aging in Texas roads and test sections, Transportation Research Record (1269) (1990) 9-19.

[114] R. Periasamy, The measurement of oxygen transport parameters for asphalt/aggregate and asphalt/glass systems using an electrodynamic balance, Fuel Science and Technology International 13(6) (1995) 699-711.

[115] R.B. Bird, W.E. Stewart, E.N. Lightfoot, Transport phenomena, Wiley1960.

[116] K.M. Lunsford, The effect of temperature and pressure on laboratory oxidized asphalt films with comparison to field aging, Texas A & M University, 1994.

[117] N. Prapaitrakul, Toward an improved model of asphalt binder oxidation in pavements, Texas A&M University, 2009.

[118] R. Han, Improvement to a transport model of asphalt binder oxidation in pavements: Pavement temperature modeling, oxygen diffusivity in asphalt binders and mastics, and pavement air void characterization, Texas A&M University, 2011.

[119] M. Liu, M.A. Ferry, R.R. Davison, C.J. Glover, J.A. Bullin, Oxygen Uptake As Correlated to Carbonyl Growth in Aged Asphalts and Asphalt Corbett Fractions, Industrial & Engineering Chemistry Research 37(12) (1998) 4669-4674.

[120] X. Jin, Asphalt oxidation kinetics and pavement oxidation modeling, Texas A&M University, 2012.

[121] N. Prapaitrakul, R. Han, X. Jin, C.J. Glover, A Transport Model of Asphalt Binder Oxidation in Pavements, Road Materials and Pavement Design 10(sup1) (2009) 95-113.

[122] R. Han, X. Jin, C.J. Glover, Oxygen Diffusivity in Asphalts and Mastics, Petroleum Science and Technology 31(15) (2013) 1563-1573.

[123] M. Aubertin, M. Mbonimpa, Diffusion of oxygen through a pulp and paper residue barrier: Discussion, Canadian geotechnical journal 38(3) (2001) 658-660.

[124] D. Hillel, Fundamentals of soil physics, Academic Press, Inc.(London) Ltd., New York, 1980.

[125] J. Crank, The mathematics of diffusion, 2nd ed., Clarendon Press, Oxford, U.K., 1975.

[126] N. Morian, E. Hajj, C. Glover, P. Sebaaly, Oxidative Aging of Asphalt Binders in Hot-Mix Asphalt Mixtures, Transportation Research Record: Journal of the Transportation Research Board 2207 (2011) 107-116.

[127] G. Rowe, S. Khoee, P. Blankenship, K. Mahboub, Evaluation of Aspects of E* Test by Using Hot-Mix Asphalt Specimens with Varying Void Contents, Transportation Research Record: Journal of the Transportation Research Board 2127 (2009) 164-172.

[128] J.C. Petersen, R. Glaser, Asphalt Oxidation Mechanisms and the Role of Oxidation Products on Age Hardening Revisited, Road Materials and Pavement Design 12(4) (2011) 795-819.

[129] J.C. Petersen, P.M. Harnsberger, Asphalt aging: dual oxidation mechanism and its interrelationships with asphalt composition and oxidative age hardening, Transportation Research Record: Journal of the Transportation Research Board 1638(1) (1998) 47-55.

[130] M. Farrar, C. Sui, S. Salmans, Q. Qin, Determining the low temperature rheological properties of asphalt binder using a dynamic shear rheometer (DSR), Fundamental Properties of Asphalts and Modified Asphalts III Product: FP 08, Western Research Institute, Laramie, Wyoming, 2015.

[131] C. Sui, M.J. Farrar, W.H. Tuminello, T.F. Turner, New technique for measuring low-temperature properties of asphalt binders with small amounts of material, Transportation Research Record, 2010, pp. 23-28.

[132] L. Bateman, K. Hargrave, Oxidation of organic sulphides. I. Interaction of cyclohexyl methyl sulphide with hydroperoxides in alcohols, Proceedings of the Royal Society of London A: Mathematical, Physical and Engineering Sciences, The Royal Society, 1954, pp. 389-398.

[133] R. Glaser, J. Schabron, T. Turner, J.-P. Planche, S. Salmans, J. Loveridge, Low-temperature oxidation kinetics of asphalt binders, Transportation Research Record: Journal of the Transportation Research Board (2370) (2013) 63-68.

[134] S. Obulareddy, Fundamental characterization of Louisiana HMA mixtures for the 2002 mechanistic-empirical design guide, Civil & Environmental Engineering, Louisiana State University, Baton Rouge, LA, 2006.

[135] B. Birgisson, G. Sholar, R. Roque, Evaluation of a predicted dynamic modulus for Florida mixtures, Journal of the Transportation Research Board 1929 (2005) 200-207.

[136] H. Azari, G. Al-Khateeb, A. Shenoy, N. Gibson, Comparison of Simple Performance Test| E*| of Accelerated Loading Facility Mixtures and Prediction| E*|: Use of NCHRP 1-37A and Witczak's New Equations, Washington, DC, 2007, pp. 1-9.

[137] D. Andrei, M. Witczak, M. Mirza, Development of a revised predictive model for the dynamic (complex) modulus of asphalt mixtures, Journal of the Transportation Research Board 1540 (1999) 15-23.

[138] M. Witczak, M. El-Basyouny, S. El-Badawy, Incorporation of the New (2005) E* Predictive Model in the MEPDG, NCHRP, 2007.

[139] D.W. Christensen, T. Pellinen, R.F. Bonaquist, Hirsch model for estimating the modulus of asphalt concrete, Asphalt Paving Technology: Association of Asphalt Paving Technologists-Proceedings of the Technical Sessions, 2003, pp. 97-121.

[140] D.W. Christensen, R. Bonaquist, Improved Hirsch model for estimating the modulus of hot-mix asphalt, Road Materials and Pavement Design 16(sup2) (2015) 254-274.

[141] F. Olard, H. Di Benedetto, General "2S2P1D" model and relation between the linear viscoelastic behaviours of bituminous binders and mixes, Road materials and pavement design 4(2) (2003) 185-224.

[142] G. Al-Khateeb, A. Shenoy, N. Gibson, T. Harman, A new simplistic model for dynamic

modulus predictions of asphalt paving mixtures, Journal of the Association of Asphalt Paving Technologists 75 (2006) 1-40.

[143] H. Ceylan, C.W. Schwartz, S. Kim, K. Gopalakrishnan, Accuracy of predictive models for dynamic modulus of hot-mix asphalt, Journal of Materials in Civil Engineering 21(6) (2009) 286-293.

[144] Y. Kim, M. King, M. Momen, Typical dynamic moduli values of hot mix asphalt in North Carolina and their prediction, Proceedings 84th annual meeting of the transportation research board, Transportation Research Board of the National Academies Washington, DC, 2005.

[145] N. Tran, K. Hall, Evaluating the predictive equation in determining dynamic moduli of typical asphalt mixtures used in Arkansas, Road Materials and Pavement Design (1) (2005) 1-17.

[146] R. Dongre, L. Myers, J. D'Angelo, C. Paugh, J. Gudimettla, Field Evaluation of Witczak and Hirsch Models for Predicting Dynamic Modulus of Hot-Mix Asphalt (With Discussion), Journal of the Association of Asphalt Paving Technologists 74 (2005).

[147] D. Singh, M. Zaman, S. Commuri, Evaluation of predictive models for estimating dynamic modulus of hot-mix asphalt in Oklahoma, Transportation Research Record: Journal of the Transportation Research Board (2210) (2011) 57-72.

[148] T.R. Clyne, X. Li, M.O. Marasteanu, E.L. Skok, Dynamic and resilient modulus of Mn/DOT asphalt mixtures, Minnesota Department of Transportation St. Paul, Minnesota 2003.

[149] C. Plati, K. Georgouli, A. Loizos, Asphalt concrete stiffness modulus estimation utilizing an algorithm approach, Airfield and Highway Pavement 2013: Sustainable and Efficient Pavements Transportation & Development Institute of ASCE, Los Angeles, California, 2013, pp. 1219-1228.

[150] G. Garcia, M. Thompson, HMA dynamic modulus predictive models (a review), Illinois Center for Transportation, Urbana, 2007, p. 95.

[151] F. Martinez, S. Angelone, Evaluation of different predictive dynamic modulus models of asphalt mixtures used in Argentina, Bearing Capacity of Roads, Railways and Airfields. 8th International Conference, Champaign, Illinois, 2009, p. 10.

[152] J. Shook, B. Kallas, N. McLeod, F. Finn, P. Pell, L. Krchma, R. Haas, K. Anderson, Factors influencing dynamic modulus of asphalt concrete, Association of Asphalt Paving Technologists Proc, Transportation Research Boad, Washington, D.C., 1969.

[153] O. Fonseca, M.W. Witczak, A prediction methodology for the dynamic modulus of in-place aged asphalt mixtures (with discussion), Journal of the Association of Asphalt Paving Technologists 65 (1996).

[154] W.P. Cox, E.H. Merz, Correlation of dynamic and steady flow viscosities, Journal of Polymer Science 28(118) (1958) 619-622.

[155] J. Bari, M.W. Witczak, Development of a new revised version of the Witczak E* predictive model for hot mix asphalt mixtures (with discussion), Journal of the Association of Asphalt Paving Technologists 75 (2006).

[156] T. Pellinen, A. Zofka, M. Marasteanu, N. Funk, Asphalt Mixture Stiffness Predictive Models (With Discussion), Journal of the Association of Asphalt Paving Technologists 76 (2007).

[157] M.S. Sakhaei Far, Development of New Dynamic Modulus (: E*:) Predictive Models for Hot Mix Asphalt Mixtures, North Carolina State University2011.

[158] M. NI, The 2S2P1D-An Excellent Linear Viscoelastic Model, UNIMAS e-Journal of Civil Engineering 1(2) (2010).

[159] H. Di Benedetto, F. Olard, C. Sauzéat, B. Delaporte, Linear viscoelastic behaviour of bituminous materials: From binders to mixes, Road Materials and Pavement Design 5(sup1) (2004) 163-202.

[160] Y.R. Kim, B. Underwood, M.S. Far, N. Jackson, J. Puccinelli, LTPP computed parameter: dynamic modulus, Federal Highway Administration, McLean, VA, 2011, p. 268.

[161] M.W. Witzcak, Simple performance test for superpave mix design, Transportation Research Board, Washington, D.C. , 2002.

[162] S. Yousefdoost, B. Vuong, I. Rickards, P. Armstrong, B. Sullivan, Evaluation of dynamic modulus predictive models for typical Australian asphalt mixes, AAPA International Flexible Pavements Conference, 15th, 2013, Brisbane, Queensland, Australia, 2013.

[163] M.M. Robbins, D.H. Timm, Evaluation of dynamic modulus predictive equations for southeastern United States asphalt mixtures, Journal of the Transportation Research Board 2210(2210) (2011) 122-129.

[164] A. Saltelli, K. Chan, E.M. Scott, Sensitivity Analysis: Gauging the Worth of Scientific Models, Wiley, New York, 2000.

[165] D. Vose, Quantitative risk analysis: a guide to Monte Carlo simulation modeling, Wiley New York, 1996.

[166] A.M. Abu Abdo, Sensitivity analysis of a new dynamic modulus (| E*|) model for asphalt mixtures, Road Materials and Pavement Design 13(3) (2012) 549-555.

[167] S. Thyagarajan, Improvements to strain computation and reliability analysis of flexible pavements in the mechanistic-empirical pavement design guide, Civil and Environmental Engineering, Washington State University, Washington, D.C, 2009.

[168] H. Fujita, Diffusion in polymer-diluent systems, Fortschritte Der Hochpolymeren-Forschung, Springer Berlin Heidelberg, 1961, pp. 1-47.

[169] X. Jin, R. Han, Y. Cui, C.J. Glover, Fast-Rate–Constant-Rate Oxidation Kinetics Model for Asphalt Binders, Industrial & Engineering Chemistry Research 50(23) (2011) 13373-13379.

[170] X. Jin, Y. Cui, C.J. Glover, Modeling Asphalt Oxidation in Pavement With Field Validation, Petroleum Science and Technology 31(13) (2013) 1398-1405.

[171] E. Buckingham, Contributions to our knowledge of the aeration of soils, in: B.o.s. U.S. Department of Agricultural (Ed.) Government printing office, Washington, D.C., 1904, p. 55.

[172] H. Burger, Das Leitvermögen verdünnter mischkristallfreier Legierungen, Physikalische

Zeitschrift 20(4) (1919) 73-75.

[173] J. Currie, Gaseous Diffusion in Porus Media Part 3-Wet Granular Materials, British Journal of Applied Physics 12(6) (1961) 275-281.

[174] T. Marshall, The diffusion of gases through porous media, European Journal of Soil Science 10(1) (1959) 79-82.

[175] H. Penman, Gas and vapour movements in the soil: I. The diffusion of vapours through porous solids, The Journal of Agricultural Science 30(03) (1940) 437-462.

[176] H. Penman, Gas and vapour movements in the soil: II. The diffusion of carbon dioxide through porous solids, The Journal of Agricultural Science 30(04) (1940) 570-581.

[177] A. Sallam, W. Jury, J. Letey, Measurement of gas diffusion coefficient under relatively low air-filled porosity, Soil Science Society of America Journal 48(1) (1984) 3-6.

[178] S.B. Jones, D. Or, G.E. Bingham, Gas Diffusion Measurement and Modeling in Coarse-Textured Porous Media, Vadose Zone Journal 2(4) (2003) 602-610.

[179] M. Aachib, M. Aubertin, M. Mbonimpa, Laboratory measurements and predictive equations for gas diffusion coefficient of unsaturated soils, 55th Canadian Geotechnical and 3rd Joint IAH-CNC and CGS Groundwater Specialty Conferences, Niagara Falls, Ontario, 2002, pp. 20-23.

[180] M. Aachib, M. Mbonimpa, M. Aubertin, Measurement and Prediction of the Oxygen Diffusion Coefficient in Unsaturated Media, with Applications to Soil Covers, Water, Air, and Soil Pollution 156(1) (2004) 163-193.

[181] M. Mbonimpa, M. Aubertin, M. Aachib, B. Bussière, Diffusion and consumption of oxygen in unsaturated cover materials, Canadian Geotechnical Journal 40(5) (2003) 916-932.

[182] F.H. Shair, D.S. Cohen, Transient ordinary and forced diffusion in a tube connecting stirred-tank end bulbs of finite size, Chemical Engineering Science 24(1) (1969) 39-48.

[183] R.D. Glauz, D.E. Rolston, Optimal Design of Two-Chamber, Gas Diffusion Cells, Soil Science Society of America Journal 53(6) (1989) 1619-1624.

[184] P.W. McDonald, The Computation of Transonic Flow Through Two-Dimensional Gas Turbine Cascades, International Gas Turbine Conference and Products Show, ASME, Houston, Texas, 1971, pp. 2-7.

[185] R. MacCormack, A. Paullay, Computational efficiency achieved by time splitting of finite difference operators, 10th Aerospace Sciences Meeting, American Institute of Aeronautin and Astronautics, San Diego, California, 1972, pp. 1-7.

[186] R. Eymard, T. Gallouët, R. Herbin, Finite volume methods, Handbook of numerical analysis 7 (2000) 713-1018.

[187] A. Shukla, A.K. Singh, P. Singh, A comparative study of finite volume method and finite difference method for convection-diffusion problem, American Journal of Computational and Applied Mathematics 1(2) (2011) 67-73.

[188] E.J. Carr, I.W. Turner, A semi-analytical solution for multilayer diffusion in a composite

medium consisting of a large number of layers, Applied Mathematical Modelling 40(15-16) (2016) 7034-7050.

[189] A. Fini, P. Frangi, E. Robbiani, F. Ferrini, Pervious vs. impervious pavements for sidewalks: effects on soil characteristics and physiology of two establishing urban tree species, 91st ISA Annual Conference, Orlando, Florida, 2015.

[190] P. Moldrup, T. Olesen, J. Gamst, P. Schjønning, T. Yamaguchi, D.E. Rolston, Predicting the Gas Diffusion Coefficient in Repacked Soil Water-Induced Linear Reduction Model, Soil Science Society of America Journal 64(5) (2000) 1588-1594.

[191] R. Millington, Gas diffusion in porous media, Science 130(3367) (1959) 100-102.

[192] L. Ruggieri, T. Gea, A. Artola, A. Sánchez, Air filled porosity measurements by air pycnometry in the composting process: A review and a correlation analysis, Bioresource Technology 100(10) (2009) 2655-2666.

[193] C.E. Zapata, W.N. Houston, Calibration and validation of the enhanced integrated climatic model for pavement design, Transportation Research Board, Washington, D.C., 2008, p. 72.